

UNCLASSIFIED

AD NUMBER

AD815267

LIMITATION CHANGES

TO:

Approved for public release; distribution is unlimited.

FROM:

Distribution authorized to U.S. Gov't. agencies and their contractors; Critical Technology; 01 MAR 1967. Other requests shall be referred to Air Force Office of Science Research, Bolling AFB, Washington, DC 20332. This document contains export-controlled technical data.

AUTHORITY

AFOSR ltr, 12 Nov 1971

THIS PAGE IS UNCLASSIFIED

The following notice applies to any unclassified (including originally classified and now declassified) technical reports released to "qualified U.S. contractors" under the provisions of DoD Directive 5230.25, Withholding of Unclassified Technical Data From Public Disclosure.

NOTICE TO ACCOMPANY THE DISSEMINATION OF EXPORT-CONTROLLED TECHNICAL DATA

- 1. Export of information contained herein, which includes, in some circumstances, release to foreign nationals within the United States, without first obtaining approval or license from the Department of State for items controlled by the International Traffic in Arms Regulations (ITAR), or the Department of Commerce for items controlled by the Export Administration Regulations (EAR), may constitute a violation of law.**
- 2. Under 22 U.S.C. 2778 the penalty for unlawful export of items or information controlled under the ITAR is up to ten years imprisonment, or a fine of \$1,000,000, or both. Under 50 U.S.C., Appendix 2410, the penalty for unlawful export of items or information controlled under the EAR is a fine of up to \$1,000,000, or five times the value of the exports, whichever is greater; or for an individual, imprisonment of up to 10 years, or a fine of up to \$250,000, or both.**
- 3. In accordance with your certification that establishes you as a "qualified U.S. Contractor", unauthorized dissemination of this information is prohibited and may result in disqualification as a qualified U.S. contractor, and may be considered in determining your eligibility for future contracts with the Department of Defense.**
- 4. The U.S. Government assumes no liability for direct patent infringement, or contributory patent infringement or misuse of technical data.**
- 5. The U.S. Government does not warrant the adequacy, accuracy, currency, or completeness of the technical data.**
- 6. The U.S. Government assumes no liability for loss, damage, or injury resulting from manufacture or use for any purpose of any product, article, system, or material involving reliance upon any or all technical data furnished in response to the request for technical data.**
- 7. If the technical data furnished by the Government will be used for commercial manufacturing or other profit potential, a license for such use may be necessary. Any payments made in support of the request for data do not include or involve any license rights.**
- 8. A copy of this notice shall be provided with any partial or complete reproduction of these data that are provided to qualified U.S. contractors.**

DESTRUCTION NOTICE

For classified documents, follow the procedure in DoD 5220.22-M, National Industrial Security Program, Operating Manual, Chapter 5, Section 7, or DoD 5200.1-R, Information Security Program Regulation, Chapter 6, Section 7. For unclassified, limited documents, destroy by any method that will prevent disclosure of contents or reconstruction of the document.

815 267

COLUMBIA UNIVERSITY

IN THE CITY OF NEW YORK

ELECTRONICS RESEARCH LABORATORIES

632 WEST 126th STREET
NEW YORK, NEW YORK 10027

March 1, 1967

WIDEBAND AMORPHOUS-SOLID DEBYE-SEARS LIGHT MODULATORS FOR ARRAY- ANTENNA PROCESSORS

TECHNICAL REPORT T-7/321

By

J. Minkoff

Prepared for

Director
Advanced Research Projects Agency
Washington, D.C. 20301

and

Electronics Division
Directorate of Engineering Sciences
Air Force Office of Scientific Research
Office of Aerospace Research
U.S. Air Force
Arlington, Virginia 22209

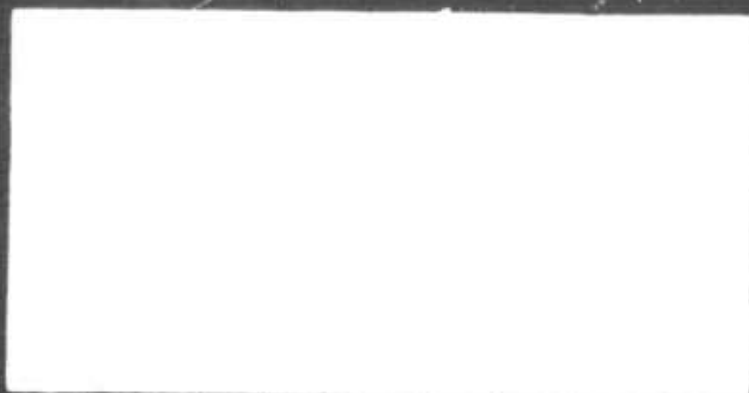
Contract No. AF 49(638)-1478
ARPA Order No. 279



STATEMENT #2 UNCLASSIFIED

This document is subject to special export controls and each transmittal to foreign governments or foreign nationals may be made only with prior approval of AFOSR.

*Attn: Electronics Div.
Arlington, Va, 22209*



**BEST
AVAILABLE COPY**

ABSTRACT

The use of fused-silica Debye-Sears light modulators in electro-optical array-antenna processing is investigated theoretically and experimentally, with the result that a significant gain in signal-processing capacity, over that which can be achieved with liquid light-modulators, is shown to be possible. It is shown that fused-silica light-modulators would enable electro-optical processors to be applied to square arrays consisting of more than 30,000 elements receiving signals with bandwidths in excess of 150 MHz.

The operation of the fused-silica light-modulator in the neighborhood of 80 MHz is investigated. Transfer characteristics between electrical excitation and spatial modulation of light wave front are found to be linear, first-order light-intensity distributions are measured and found to be nearly ideal, and measurements of bandpass characteristics show that light-modulator bandwidths which are 50 per cent of resonant transducer frequency are easily achieved. The effects of internal refraction on the electro-optical processor are determined. For any given set of operating conditions, a unique lower bound on transducer depth is established which minimizes these effects. The effects of cross coupling on closely spaced light-modulator channels are also investigated experimentally and results are found to be consistent with evaluations of signal-processing capacity.

Large aperture-bandwidth array-antenna processing is shown to result in non-separable optical transmission functions for which the diffraction patterns are determined here for the first time. Evaluation is also made of signal to noise degradation which would occur in this case. It is shown that this degradation would not be a limiting factor in the electro-optical processor.

COLUMBIA UNIVERSITY—ELECTRONICS RESEARCH LABORATORIES

AUTHORIZATION

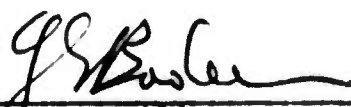
The research described in this report was performed at the Electronics Research Laboratories of Columbia University. This report was prepared by J. Minkoff.

This project is directed by the Advanced Research Projects Agency of the Department of Defense and is administered by the Air Force Office of Scientific Research under Contract AF 49(638)-1478.

Submitted by:

Approved by:

L. Lambert
Assistant Director



For L. W. O'Neill
Professor of Electrical
Engineering
Director

TABLE OF CONTENTS

	<u>Page</u>
ABSTRACT	
1. INTRODUCTION AND SUMMARY	1
1.1 INTRODUCTION	1
1.2 RESEARCH OBJECTIVES AND RESULTS	1
1.3 INVESTIGATIONS AND CONTRIBUTIONS	1
2. REVIEW OF ELECTRO-OPTICAL SIGNAL PROCESSING FOR ARRAY ANTENNAS	6
2.1 THE ELECTRO-OPTICAL CONFIGURATION	6
2.2 LINEAR ARRAY ANTENNA: SPATIAL MULTI- PLEXING	13
2.3 LINEAR ARRAY ANTENNA: TIME MULTIPLEXING	19
2.4 PLANAR ARRAY ANTENNA	24
3. LITERATURE SEARCH	29
3.1 ELECTRO-OPTICAL AND ELECTRONIC PROCESS- ING FOR ARRAY ANTENNAS	29
3.2 LIMITATIONS ON ELECTRO-OPTICAL ARRAY ANTENNA PROCESSING	30
3.2.1 Acoustic Attenuation	31
3.2.2 Internal Refraction	32
3.2.3 Transducer Limitations	33
3.2.4 Ultrasonic-Beam Broadening and Cross-Channel Coupling	33
3.3 ULTRASONIC DIFFRACTION OF LIGHT IN SOLID MEDIA	34
3.3.1 Birefringence and Light Polariza- tion	35
3.3.2 Shear and Compression Modes	36
3.4 LARGE APERTURE-BANDWIDTH ARRAY-ANTENNA PROCESSING	36

TABLE OF CONTENTS (CONT'D.)

	<u>Page</u>
4. ULTRASONIC DIFFRACTION OF LIGHT IN AMORPHOUS SOLID MEDIA	38
4.1 BEHAVIOR OF ELECTROMAGNETIC PLANE WAVES IN HOMOGENEOUS ANISOTROPIC MEDIA	39
4.2 STRESS AND STRAIN BIREFRINGENCE: THE STRAIN-OPTIC CONSTANTS	41
4.3 RELATIONSHIP BETWEEN PIEZOELECTRIC-TRANSDUCER VIBRATION AND SPATIAL VARIATION OF INDEX OF REFRACTION FOR AMORPHOUS MEDIA	44
4.3.1 Transverse Vibrations Along Optic Axis	44
4.3.2 Transverse Vibrations Normal to Optic Axis	46
4.3.3 Longitudinal Vibrations	54
4.4 OPTIMUM LIGHT POLARIZATION AS A FUNCTION OF MODE OF PROPAGATION	57
4.4.1 Shear Mode	60
4.4.2 Compression Mode	61
4.5 SUMMARY AND COMPARISON OF TRANSFER CHARACTERISTICS	62
5. OPTIMIZATION OF DESIGN OF ELECTRO-OPTICAL ARRAY-ANTENNA PROCESSOR USING FUSED-SILICA LIGHT-MODULATOR MEDIUM	65
5.1 SIGNAL-PROCESSING CAPACITY AND APERTURE-BANDWIDTH PRODUCT	66
5.2 LIMITATIONS ON SIGNAL-PROCESSING CAPACITY	68
5.2.1 Acoustic Attenuation	68
5.2.2 Internal Refraction	69
5.2.3 Limitations Imposed by Ultrasonic Transducer	84
5.2.4 Limitations Imposed by Ultrasonic-Beam Broadening and Cross-Channel Coupling	86

TABLE OF CONTENTS (CONT'D.)

	<u>Page</u>
5.3 MAXIMIZATION OF SIGNAL-PROCESSING CAPACITY: TRANSDUCER LIMITED	89
5.4 MAXIMIZATION OF SIGNAL-PROCESSING CAPACITY: FUSED-SILICA MEDIUM	94
5.5 SUMMARY AND CONCLUSIONS	98
6. LIGHT-DIFFRACTION PATTERNS PRODUCED BY NON- SEPARABLE OPTICAL TRANSMISSION FUNCTIONS	100
6.1 LINEAR ARRAY: SPATIAL MULTIPLEXING	101
6.1.1 Interpretation of Diffraction Patterns: Large and Small Aperture-Bandwidth Linear Arrays	115
6.2 LINEAR ARRAY: TIME MULTIPLEXING	120
6.3 PLANAR ARRAY ANTENNA	127
6.3.1 Interpretation of Diffraction Patterns: Large and Small Aper- ture-Bandwidth Planar Arrays	138
6.4 SIGNAL TO NOISE DEGRADATION IN LARGE APERTURE-BANDWIDTH ELECTRO-OPTICAL ARRAY-ANTENNA PROCESSORS	141
6.4.1 Light Diffraction by Random Signals	143
6.4.2 Evaluation of Signal to Noise Degradation	160
6.5 SUMMARY AND CONCLUSIONS	167
7. EXPERIMENTAL INVESTIGATIONS	169
7.1 DESCRIPTION OF MEASUREMENT APPARATUS	170
7.2 BASIC SYSTEM MEASUREMENTS	181

COLUMBIA UNIVERSITY—ELECTRONICS RESEARCH LABORATORIES

TABLE OF CONTENTS (CONT'D.)

	<u>Page</u>
7.2.1 Measurement of Light-Intensity Distribution in Image Plane	181
7.2.2 Measurements Using Schlieren Techniques	189
7.3 ULTRASONIC LIGHT-DIFFRACTION EXPERIMENTS IN AN AMORPHOUS SOLID MEDIUM	196
7.3.1 Elimination of Standing Waves	196
7.3.2 Measurement of Transfer Charac- teristics	203
7.3.3 First-Order Diffraction Patterns Obtained with Fused-Silica Light Modulator	206
7.4 FUSED-SILICA LIGHT-MODULATOR EXPERIMENTS RELATED TO EVALUATION OF SIGNAL-PRO- CESSING CAPACITY	213
7.4.1 Measurement of Light-Modulator Bandwidth	213
7.4.2 Internal-Refractive Effects: Determination of Lower Bound on Transducer Depth	214
7.4.3 Experimental Studies of Ultra- sonic-Beam Broadening and Cross-Channel Coupling	218
7.5 SUMMARY AND CONCLUSIONS OF EXPERIMENTAL WORK	227
APPENDIX A BEHAVIOR OF ELECTROMAGNETIC PLANE WAVES IN HOMOGENEOUS ANISOTROPIC MEDIA	229
APPENDIX B THE PHOTOELASTIC MATRIX FOR AMOR- PHOUS MEDIA	242
APPENDIX C DETERMINATION OF $R(u,v)$: BAND- LIMITED CASE	252
APPENDIX D OPTIMIZATION OF DESIGN OF FUSED- SILICA LIGHT MODULATOR: SUMMARY OF RESULTS	257
REFERENCES	265

LIST OF FIGURES

<u>Figure No.</u>	<u>Title</u>	<u>Page</u>
2.1-1	Schematic Diagram of Coherent Optical Configuration	7
2.1-2	Single-Channel Debye-Sears Light Modulator	10
2.2-1	Linear Array Showing Delayed Pulse Amplitudes	14
2.2-2	N-Channel Debye-Sears Light Modulator	16
2.2-3	N Spatially-Multiplexed Linear-Array Signals: Small Aperture-Bandwidth Product	18
2.3-1	Time Multiplexing: Linear Array	20
2.3-2	Sequence of Time-Multiplexed Pulses in Single-Channel Debye-Sears Light Modulator	23
2.4-1	Planar Array with Incident Plane Wave	25
2.4-2	Time Multiplexing Signals from p^{th} Column of Planar Array	26
2.4-3	N Spatially-Multiplexed Sequences of M Time-Multiplexed Signals: Small Aperture-Bandwidth Planar Array	28
4.3-1	Elementary Light-Modulator Configuration	45
4.3.2-1	Diagram Showing Effect of Shear Strain on Ellipsoid of Wave Normals	49
4.3.3-1	Diagram Showing Effect of Compressional Strain on Ellipsoid of Wave Normals	55
4.3.3-2	Photoelastic Interpretation of Ultrasonic Diffraction in Liquids	58

LIST OF FIGURES (CONT'D.)

<u>Figure No.</u>	<u>Title</u>	<u>Page</u>
5.2.1-1	Acoustic-Loss Characteristics for Various Solids (Lamb, Redwood, Shteinshleifer, 1959)	70
5.2.1-2	Effects of Acoustic Attenuation on Diffraction Patterns (Lambert 1965)	71
5.2.2-1	Effect of Refractive-Index Variation on Direction of Light Wave Front	72
5.2.2-2	Trajectories of Rays Across Ultrasonic Beam: Normal Light Incidence	74
5.2.2-3	Transducer Depth (L) vs γ for Shear Mode	82
5.2.2-4	Transducer Depth (L) vs γ for Compression Mode	83
5.2.4-1	Ultrasonic Diffraction in a Spatially-Multiplexed Debye-Sears Light Modulator	88
6.1-1	Linear Array Showing Delayed Pulse Amplitudes	102
6.1-2	N-Channel Debye-Sears Light Modulator	105
6.1-3	N Spatially-Multiplexed Linear-Array Signals: Large Aperture-Bandwidth Product	107
6.1-4	graph of $\left \frac{\sin \pi N(\beta v - A)}{\sin \pi(\beta v - A)} \right $	111
6.1-5	graph of $\left \frac{\sin \pi N(\beta v - \beta \Delta u - \gamma)}{\sin \pi(\beta v - \beta \Delta u - \gamma)} \right $	113
6.1-6	Positive First-Order Light Intensity: Spatially-Multiplexed Large Aperture-Bandwidth Linear Array (N Elements)	114

LIST OF FIGURES (CONT'D.)

<u>Figure No.</u>	<u>Title</u>	<u>Page</u>
6.1-7	Null Patterns and Location of Peak Intensities: Large and Small Aperture-Bandwidth Spatially-Multiplexed Linear Arrays	119
6.2-1	Time Multiplexing: Linear Array	121
6.2-2	Sequence of Time-Multiplexed Pulses in Single-Channel Debye-Sears Light Modulator	123
6.2-3	graph of $\left \frac{\sin \pi N(u d_s + \gamma)}{\sin \pi (\pi d_s + \gamma)} \right $	126
6.2-4	Diffraction Pattern: Time-Multiplexed Linear Array (N Elements)	128
6.3-1	Planar Array with Incident Plane Wave	129
6.3-2	Time Multiplexing Signals from p^{th} Column of Planar Array	131
6.3-3	N Spatially-Multiplexed Sequences of M Time-Multiplexed Signals: Large Aperture-Bandwidth Planar Array	134
6.3-4	Positive First-Order Peak Light Intensity: Large Aperture-Bandwidth Planar Array	137
6.3.1-1	Null Patterns and Location of Peak Intensities: Large and Small Aperture-Bandwidth Planar Arrays	142
6.4.1-1	Diagram for Evaluation of an Integral	158
6.4.1-2	Diagram for Evaluation of an Integral	159

LIST OF FIGURES (CONT'D.)

<u>Figure No.</u>	<u>Title</u>	<u>page</u>
7.1-1	Schematic Diagram of Coherent Optical System	171
7.1-2	Coherent Optical System	172
7.1-3	T-Support for Optical Table and Damp- ing Mounts	173
7.1-4	Spreader-Lens Assembly	174
7.1-5	Collimation of Laser Beam	176
7.1-6	Details of Collimated Light Region	177
7.1-7	xy-Stage: Scanning-Mechanism Details	179
7.1-8	Scanning-Mechanism Assembly	180
7.2.1-1	Schematic Representation of Fine Struc- ture for Ideal Zero-Order Light Dis- tribution	182
7.2.1-2	Schematic Diagram of Apparatus for Measuring Spatial Light-Intensity Distribution	183
7.2.1-3	Output Focal-Plane Light Intensity Distribution Along x_1 Coordinate with 3" \times 3" Aperture	184
7.2.1-4	Output Focal-Plane Light-Intensity Distribution Along y_1 Coordinate with 2" \times 2" Aperture	185
7.2.1-5	Ideal Zero-Order Light-Intensity Dis- tribution for Aperture of Length D (Scan Along u Axis)	187
7.2.1-6	Scattered Light Level of Optical System	188

LIST OF FIGURES (CONT'D.)

<u>Figure No.</u>	<u>Title</u>	<u>Page</u>
7.2.2-1	Schlieren Configuration	190
7.2.2-2	First-Order Diffraction Fringes for Ultrasonic Wave with Arbitrary Direction of Propagation	192
7.2.2-3	Operation of Wedge	193
7.2.2-4	Diffraction Pattern Caused by Incident Wave and First Two Reflections from 36 deg Wedge	194
7.2.2-5	Schlieren Photograph of Incident Beam and Observable Reflections from 36 deg Wedge	195
7.3-1	Experimental Solid Light Modulator	197
7.3-2	Electrical Connector for Back Electrode	198
7.3.1-1	Schlieren Photographs of Reflections from 36 deg Wedge Showing Effects of Silver Paint Absorber	201
7.3.1-2	Photograph of First-Order Diffraction Pattern Showing Absence of Reflections from Observation Region	202
7.3.2-1	System for Measuring Diffracted Light Intensity	205
7.3.2-2	Peak Phase Modulation vs Peak Input Voltage for a Fused-Silica Light Modulator Employing Shear-Mode Transducer	207
7.3.2-3	Peak Phase Modulation vs Peak Input Voltage for a Fused-Silica Light Modulator Employing Compression-Mode Transducer	208

COLUMBIA UNIVERSITY—ELECTRONICS RESEARCH LABORATORIES

LIST OF FIGURES (CONT'D.)

<u>Figure No.</u>	<u>Title</u>	<u>Page</u>
7.3.3-1	Positive First-Order Light Intensity	211
7.3.3-2	Zero-Order Light Intensity	212
7.4.1-1	Bandpass Characteristics of Fused-Silica Light Modulator Employing Ultrasonic Shear Mode	215
7.4.1-2	Bandpass Characteristics of Fused-Silica Light Modulator Employing Ultrasonic Compression Mode	216
7.4.2-1	Normalized Effective Phase Modulator vs Transducer Depth	219
7.4.3-1	Schlieren Photographic Study Showing Extent of Beam Broadening	221
7.4.3-2	Shear-Mode Transducer: Schlieren Photo- graphic Study of Cross Coupling	223
7.4.3-3	Compression-Mode Transducer: Schlieren Photographic Study of Cross Coupling	224
7.4.3-4	Shear-Mode Transducer: Schlieren Photo- graphic Study of Cross Coupling	225
7.4.3-5	Compression-Mode Transducer: Schlieren Photographic Study of Cross Coupling	226

I. INTRODUCTION

1.1 RESEARCH OBJECTIVES AND RESULTS

The object of the research for this thesis has been to investigate the operation of wideband fused-silica Debye-Sears light modulators and to consider their application to electro-optical array-antenna processing.

The use of liquid Debye-Sears light modulators in electro-optical array antenna processing has already been investigated. Electro-optical processors using liquid media have been synthesized, and it has been shown that this method of array-antenna processing results in significant advantages over purely electronic signal processing schemes employing phase shifting networks or delay lines. The reason for considering the use of fused silica is that, because of its lower acoustic attenuation, this medium will permit operation at significantly higher frequencies than are possible in liquids. For a given optical aperture size, the capacity of this electro-optical array-antenna processor is limited by the high-frequency capability of the Debye-Sears light modulator, and it will be shown that the use of fused silica would permit electro-optical processors to be applied to array antennas with aperture-bandwidth products more than ten times larger than those which could be processed with the use of liquids.

1.2 INVESTIGATIONS AND CONTRIBUTIONS

This conclusion, concerning the increase in processing capacity which could be obtained with the use of fused silica, has been drawn from the following theoretical and experimental results.

COLUMBIA UNIVERSITY—ELECTRONICS RESEARCH LABORATORIES

1. The transfer characteristics, relating electrical excitation with the resulting spatial phase modulation of the light wave front, were derived for a general amorphous-solid Debye-Sears light modulator for both shear and compression modes. The derivations included the effect of the light polarization on the operation of the light modulator which must be considered because of stress birefringence. This result exhibits the differences between solid and liquid light modulators, since in liquids only compression waves are possible and the operation is independent of the light polarization. The relevant experiments in this case were concerned with verifying that, for both modes of sonic propagation, the relationship between electrical excitation and phase modulation is linear.

2. First-order light intensity distributions resulting from diffraction of light by ultrasonic waves in fused silica were measured and found to be nearly ideal. Since degradations in optical quality resulting from imperfections such as residual internal stresses and surface irregularities will cause distortion in diffraction patterns, these measurements also serve to establish the general feasibility of the use of fused silica in electro-optical processing.

3. Light-modulator bandwidths were measured for both shear and compression modes. It was found that light-modulator bandwidths which are 50 per cent of the resonant ultrasonic transducer frequency can be obtained in fused silica without additional transducer loading.

4. The effect of internal refraction was considered. For any given set of operating conditions a unique lower bound on transducer depth was established, theoretically, for minimizing this effect. This result was verified experimentally.

5. Experiments related to the necessary transducer spacing in a multi-channel light-modulator configuration were performed. The results were found to be consistent with evaluations of processing capacity.

On the basis of these theoretical and experimental results, the design of the electro-optical array-antenna processor using a fused-silica light modulator was optimized with regard to maximizing the processing capacity. The analysis assumed a square planar array and a maximum optical aperture width of 6 in.

Two separate cases were considered. In the first, the use of piezoelectric quartz crystal transducers was assumed for which an improvement of a factor of 10 in processing capacity over that which could be obtained with liquids was shown to be possible. In this case the improvement was limited by the maximum transducer frequency and did not represent the limits which could be achieved with the fused-silica medium.

A second case was considered in which the transducer limitations were removed. It was found that, ideally, an improvement of a factor of 30 would represent the maximum which could be achieved with this medium. In this analysis the maximum frequency was in the neighborhood of 550 MHz which, although no experiments were performed, would theoretically be possible with the use of evaporated thin film transducers.

In the optimization of the design of the light modulator it was necessary to consider the relationship between processing capacity and the mode of ultrasonic propagation. It was found that:

6. For any fixed frequency the mode with the lower sonic velocity will result in a greater processing capacity. However, although the sonic velocity of compression waves is greater than that of shear waves, the compression mode will permit operation at significantly higher frequencies. It was found in fact that the extent of the difference in high-frequency capability for the two modes was such that a larger processing capacity could be obtained with the use of compression waves. Thus in this application the compression mode is optimal.

It was also necessary to consider the problem of the extraction of information in this electro-optical processor under large aperture-bandwidth conditions. With regard to the specific results:

7. A non-separable complex optical transmission function was shown to occur under large aperture-bandwidth conditions. The diffraction patterns which would occur in this case were determined and their proper interpretation, with regard to the extraction of angle information, was established.

8. A degradation in peak signal-to-noise ratio was shown to occur in large aperture-bandwidth processing. This degradation was evaluated by first deriving a mathematical model describing the light intensity patterns produced by random ultrasonic disturbances. It was found that this model was consistent with the operation of the electro-op-

tical processor as a spectrum analyzer. On the basis of this analysis the degradation of peak signal-to-noise ratio was evaluated. It was found that this degradation would not be a limiting factor for either the planar-array or the time-multiplexed linear-array configurations; the use of spatial multiplexing in linear-array processing however could introduce significant degradation in the large aperture-bandwidth case.

In all cases, the results concerning applications to electro-optical processing of array antennas considered a processor configuration which has already been established for the electro-optical processors which have been synthesized. For reference purposes therefore, it was necessary to include some previously established results. The sections which contain such material, which does not represent original contributions of this research, will be indicated in the introductions to the chapters in which they appear. It is also noted that Appendices A and B do not present new results but are included for completeness.

The following two chapters present a review of electro-optical array-antenna processing and the results of a literature search of the topics relevant to this research. In Chap. 4 the transfer characteristics of fused-silica light modulators are derived. The optimization of the design of the electro-optical array-antenna processor and the evaluation of its processing capacity is dealt with in Chap. 5. A summary of these results in concise form, presenting relationships between the important system parameters, is also included as a special appendix (D). Chapter 6 deals with the extraction of information in large aperture-bandwidth electro-optical array-antenna processing, and representative examples of the experimental data which were obtained in this research are presented in Chap. 7.

2. REVIEW OF ELECTRO-OPTICAL PROCESSING FOR ARRAY ANTENNAS

This section presents a review of the electro-optical processors employing Debye-Sears light modulators (Debye and Sears 1932) which have been synthesized (Lambert 1965). Included is a description of the basic electro-optical configuration and the necessary modifications which have been developed to provide for signal processing of array antennas (Lambert, Arm, Ainette 1965).

2.1 THE ELECTRO OPTICAL CONFIGURATION

The electro-optical processors for array antennas which have been synthesized make use of the Debye-Sears effect in a liquid. In the Debye-Sears effect a beam of light is spatially phase modulated by an ultrasonic disturbance in a transparent medium. In this application, by means of the spatial-multiplexing and time-multiplexing processes, an ensemble of ultrasonic signals is formed in the Debye-Sears light modulator which is located in the object plane of a coherent optical configuration (Fig. 2.1-1). Thus the ultrasonic signal ensemble serves as the complex optical transmission function (Chentham 1954, Cutrona 1960) of the coherent configuration and, for a light source producing a plane wave of constant amplitude over the optical aperture, the light distribution in the image plane is given by (Born and Wolf 1964):

$$G'(u,v) = K \int \int_{x,y} T(x,y) e^{j\varphi(x,y)} e^{-j2\pi ux} e^{-j2\pi vy} dx dy \quad (2.1-1)$$

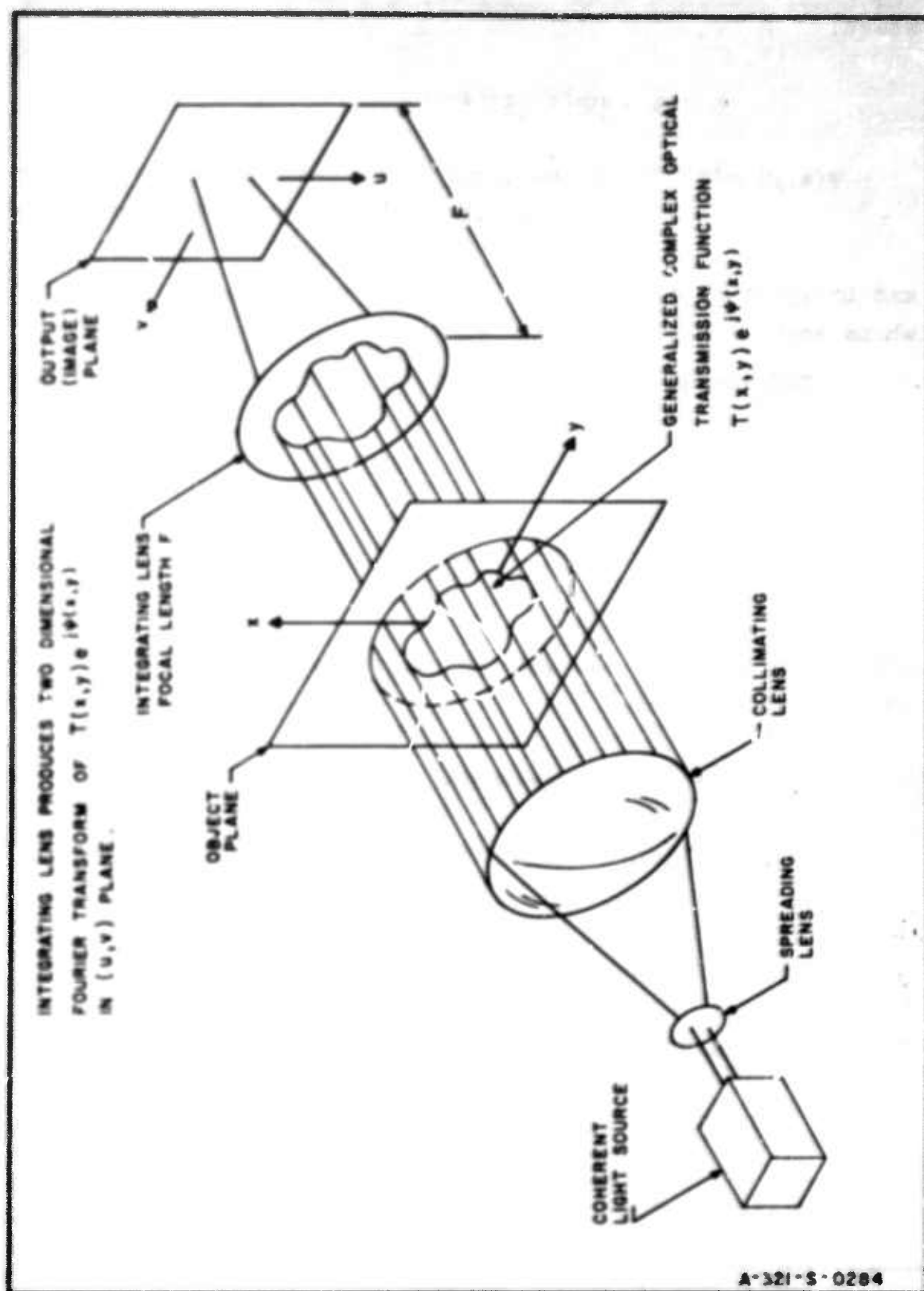


FIG 2.1-1 SCHEMATIC DIAGRAM OF COHERENT OPTICAL CONFIGURATION.

where:

K = a complex constant

$T(x,y) e^{j\psi(x,y)}$ = the complex optical transmission function formed by the ultrasonic signals,

and integration is performed over the entire optical aperture, whose spatial variables are x and y .

The output variables in the image plane are given by:

$$u = \frac{x_1}{\lambda F}$$

$$v = \frac{y_1}{\lambda F}$$

where x_1 and y_1 are spatial variables with the same units as x and y , and:

λ = light wavelength

F = focal length of integrating lens

It is sometimes convenient to include the optical aperture dimensions in the amplitude of the transmission function, $T(x,y)$. In addition, it will be seen that the relative spatial light distribution, which can be defined as:

$$G(u,v) = \frac{G'(u,v)}{K}$$

is the quantity of interest in this method of signal processing.

Thus, Eq. 2.1-1 can also be written :

$$G(u,v) = \frac{G'(u,v)}{K} = \int_{-\infty}^{\infty} \int_{-\infty}^{\infty} T(x,y) e^{j\psi(x,y)} e^{-j2\pi ux} e^{-j2\pi vy} dx dy \quad (2.1-2)$$

Consider a single channel liquid light modulator (Fig. 2.1-2). The piezoelectric transducer, which has been cut to vibrate in the longitudinal (compressional) mode, will, when excited by an electrical signal, generate a traveling pressure wave in the liquid medium with characteristic speed S . For a sinusoidal input of frequency f_i it can be shown (Raman and Nath 1936, Phariseau 1956) that the pressure wave will cause spatial perturbations of refractive index so that, at some instant of time, the index of refraction $n(x)$ can be written:

$$n(x) = n_0 - \bar{n} \sin 2\pi \frac{f_i x}{S} \quad (2.1-3)$$

where:

n_0 = equilibrium value of index of refraction

$\bar{n} = kV_m$

V_m = peak voltage of electrical signal at ultrasonic transducer

k = constant

In this electro-optical processor conditions are such that, to a first approximation, a ray of light normal to the surface of the light modulator will experience a uniform index of refraction in propagating through the medium (Raman

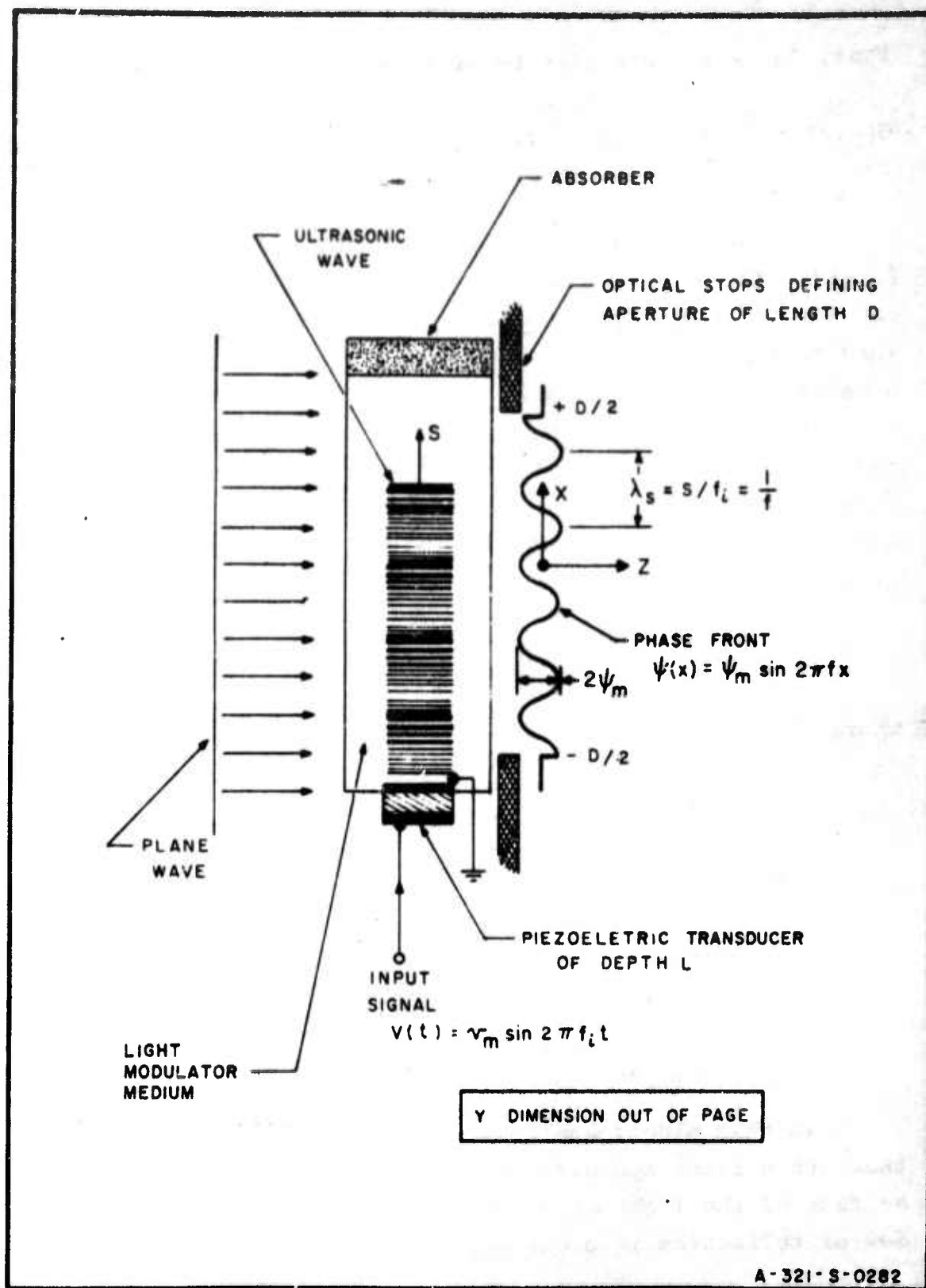


FIG. 2.1-2 SINGLE-CHANNEL DEBYE-SEARS LIGHT MODULATOR

and Nath 1936). Thus in this case, if the incident light is a plane wave, the emerging wave front will have a sinusoidal spatial phase variation with the peak phase deviation given by (Raman and Nath 1936):

$$\psi_m = \frac{2\pi n L}{\lambda}$$

and

λ = light wavelength,

L = length of light path,
(depth of ultrasonic transducer)

It is seen therefore that for an aperture of length D (dimension in the direction of sonic propagation) and width b , the complex transmission function at some instant of time is:

$$T(x,y) e^{j\psi(x,y)} = \text{rect}\left(\frac{x}{D}\right) e^{j\psi_m \sin 2\pi f x} \text{rect}\left(\frac{y}{b}\right) \quad (2.1-4)$$

where

$$\text{rect}\left(\frac{z}{A}\right) = \begin{cases} 1 & |z| < \frac{A}{2} \\ 0 & \text{otherwise} \end{cases}$$

$$f = \frac{f_i}{s} = \text{spatial frequency (cycles per meter)}$$

Now in this electro-optical processor measurement of the light distribution is done by means of photodetectors. Therefore the output light intensity, $|G(u,v)|^2$, is actually what is observed. In addition, the relationship:

$Df \gg 1$ will always hold. Hence, making use of the identity:

$$e^{j\psi_m \sin 2\pi f x} = \sum_{p=-\infty}^{\infty} J_p(\psi_m) e^{j2\pi p f x}$$

where $J_p(\psi_m)$ is the p^{th} order Bessel function with argument ψ_m , it is easily shown that:

$$|G(u, v)|^2 = \left(\frac{b \sin \pi b v}{\pi b v} \right)^2 \sum_{p=-\infty}^{\infty} \left(J_p(\psi_m) \frac{D \sin \pi D(u - pf)}{\pi D(u - pf)} \right)^2 \quad (2.1-5)$$

Thus the sinusoidal phase modulation of the light wave front gives rise to an infinite number of positive and negative diffraction fringes. It will be seen however that only the first-order light intensity is of interest and, in fact, it is desirable to suppress all higher orders. Considering the function $J_p(\psi_m)$, it is well known that for small ψ_m , $J_q(\psi_m) \approx \frac{\psi_m^q}{2^q q!}$, and therefore: $J_0 \approx 1$, $J_1 \approx \frac{\psi_m}{2}$, $J_2 \approx \frac{\psi_m^2}{8}$ etc. Hence, using this relationship, it has been shown (Lambert 1962) that if $\psi_m \leq .2$ all diffraction orders for $p > 1$ can be neglected and the relative output light intensity becomes:

$$\begin{aligned} |G(u, v)|^2 &= \left(\frac{b \sin \pi b v}{\pi b v} \right)^2 \left(\frac{D \sin \pi D u}{\pi D u} \right)^2 \\ &+ \left(\frac{b \sin \pi b v}{\pi b v} \right)^2 \frac{\psi_m^2}{4} \left[\left(\frac{D \sin \pi D(u-f)}{\pi D(u-f)} \right)^2 + \left(\frac{D \sin \pi D(u+f)}{\pi D(u+f)} \right)^2 \right] \end{aligned} \quad (2.1-6)$$

For small z , $e^{jz} \approx 1 + jz$. Thus, because of the constraint ($\psi_m < .2$) on peak phase deviation, Eq. 2.1-4 can be written:

$$T(x,y) e^{j\psi(x,y)} = \text{rect}\left(\frac{x}{D}\right) \text{rect}\left(\frac{y}{b}\right) \left[1 + \frac{\psi_m}{2} \begin{pmatrix} e^{j2\pi fx} & -e^{-j2\pi fx} \end{pmatrix} \right] \quad (2.1-7)$$

and the positive first order light intensity, $|G_1(u,v)|^2$, which in this case is

$$|G_1(u,v)|^2 = \frac{\psi_m^2}{4} \left(\frac{b \sin \pi bv}{\pi bv} \right)^2 \left(\frac{D \sin \pi D(u-f)}{\pi D(u-f)} \right)^2, \quad (2.1-8)$$

is seen to result from a complex optical transmission function given by:

$$T_1(x,y) e^{j\psi_1(x,y)} = \frac{\psi_m}{2} \text{rect}\left(\frac{x}{D}\right) e^{j2\pi fx} \text{rect}\left(\frac{y}{b}\right) \quad (2.1-9)$$

2.2 LINEAR ARRAY ANTENNA: SPATIAL MULTIPLEXING

A plane wave incident at an angle θ on a linear array antenna whose elements are separated by a distance δ will cause signals to appear at the antenna-element outputs with incremental time delay between adjacent outputs given by (Fig. 2.2-1):

$$\Delta\tau = \frac{\delta \sin \theta}{c}$$

where c = the velocity of electromagnetic propagation, and angle information is contained in the incremental time delay $\Delta\tau$. For a signal of duration T , if the aperture bandwidth product is small then:

$$T \gg N |\Delta\tau|_{\max} \quad (2.2-1)$$

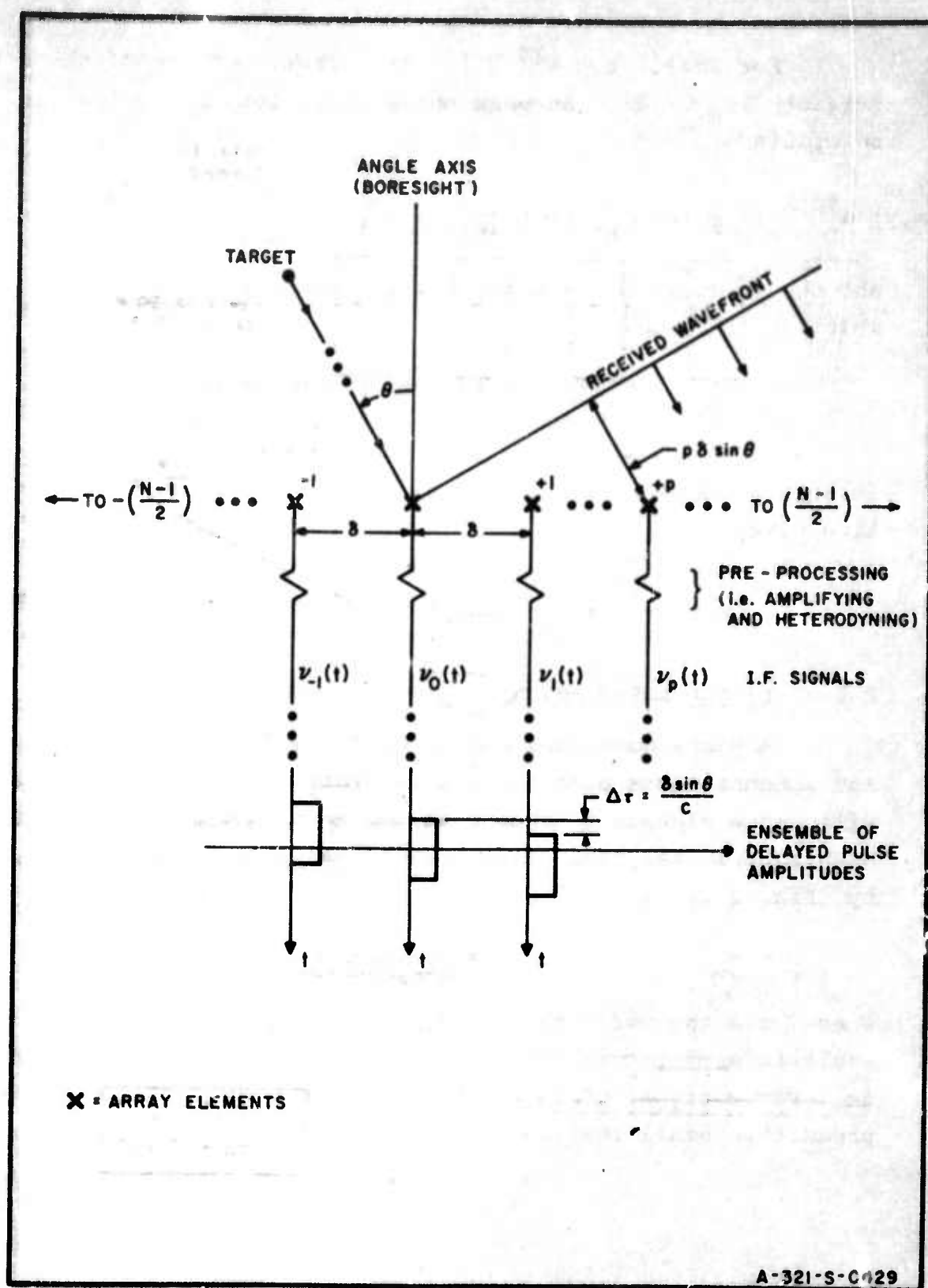


FIG. 2.2-1 LINEAR ARRAY SHOWING DELAYED PULSE AMPLITUDES

where N is the number of elements in the array. Under these conditions, the displacement in pulse amplitudes can be ignored to a good approximation (Lambert, Arm, Aimetie 1965, Lambert 1965), and the angle information can be considered to be contained in the incremental phase shift between adjacent carriers which is given by:

$$\Delta\phi = 2\pi f_r \Delta\tau \quad (2.2-2)$$

where:

$$f_r = \text{carrier frequency of received signal} = f_c + f_d$$

$$f_c = \text{carrier frequency of transmitted signal}$$

$$f_d = \text{Doppler frequency}$$

After amplification and heterodyning, these signals are used to excite the piezoelectric transducers of an N-channel Debye-Sears light modulator (Fig. 2.2-2) which is located in the aperture of a coherent optical configuration (Fig. 2.1-1).

In the light modulator the spatial frequency of the ultrasonic signals is:

$$f = \frac{f_i}{S} \quad (\text{cycles per meter})$$

where

$$f_i = \text{frequency of electrical signals} \\ \text{exciting piezoelectric transducers}$$

$$S = \text{sonic velocity}$$

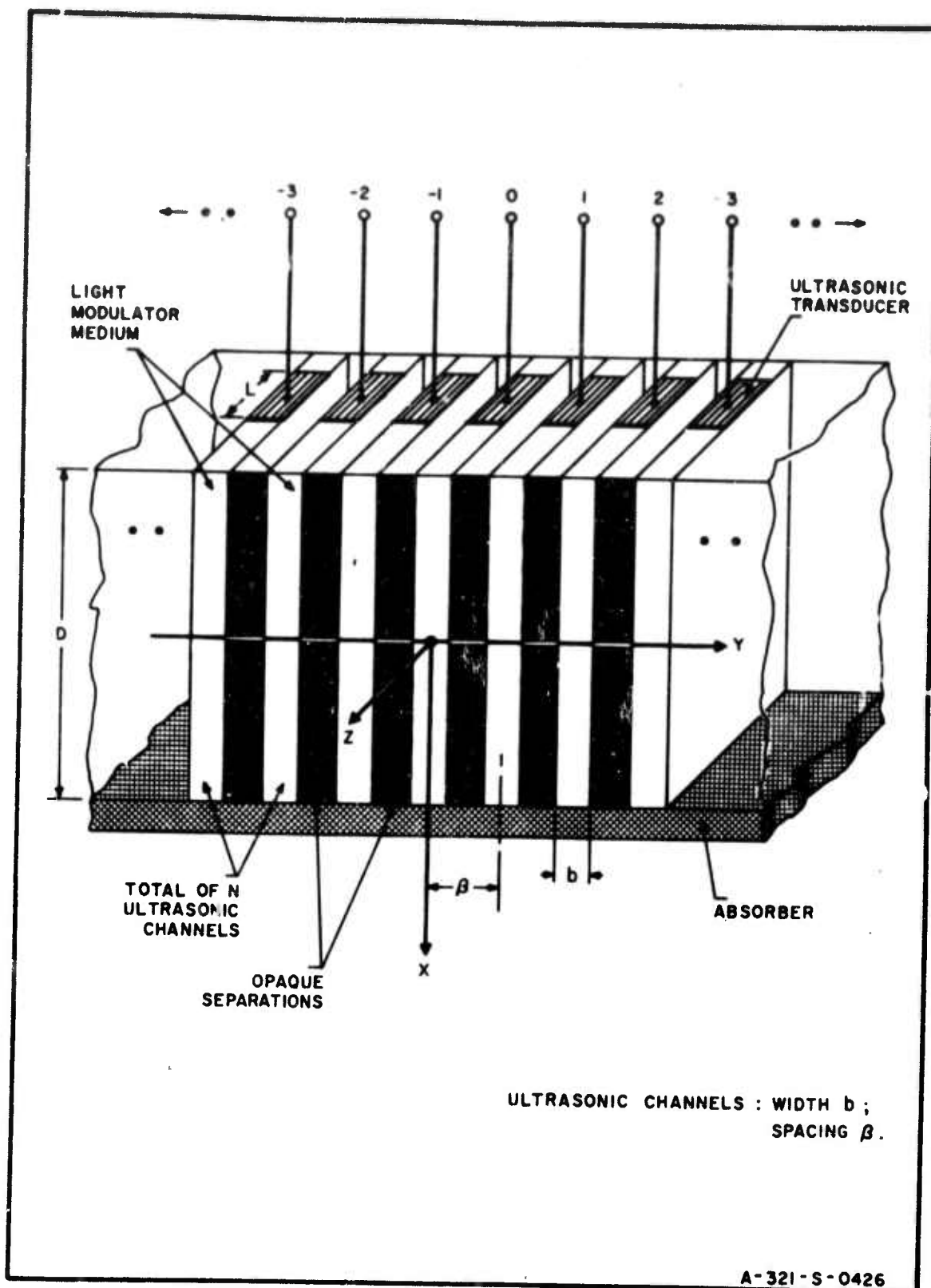


FIG. 2.2-2 N - CHANNEL DEBYE - SEARS LIGHT MODULATOR

and

$$f_i = f_o + f_d$$

f_o = intermediate frequency.

Since the incremental displacement in pulse amplitudes is ignored in this approximation, the N spatially multiplexed signals can be assumed, at some instant of time, to appear as shown in Fig. 2.2-3. It is seen that the ultrasonic signals are assumed to be aligned, and form a rectangular pattern in the light modulator whose length, given by

$$D = ST,$$

is equal to the ultrasonic pulse length. Note that since the quantity $\Delta\phi$ undergoes no change in heterodyning, the phase increment between adjacent ultrasonic signals is given by Eq. (2.2-2).

As shown in the previous section, the ensemble of ultrasonic signals imposes a spatial phase modulation on the wave front of the incident light. The resulting positive first order light intensity can be shown to be:

$$|G_1(u,v)|^2 = \frac{\psi_m^2}{4} \left(\frac{b \sin \pi bv}{\pi bv} \right)^2 \left(\frac{\sin \pi N(\beta v - \frac{\Delta\phi}{2\pi})}{\sin \pi(\beta v - \frac{\Delta\phi}{2\pi})} \right)^2 \left(\frac{D \sin \pi D(u-f)}{\pi D(u-f)} \right)^2 \quad (2.2-3)$$

The function $\left(\frac{b \sin \pi bv}{\pi bv} \right)^2$ imposes a negligible amplitude weighting on the first order intensity and can be ignored (Lambert 1965).

Thus it is seen that the information concerning

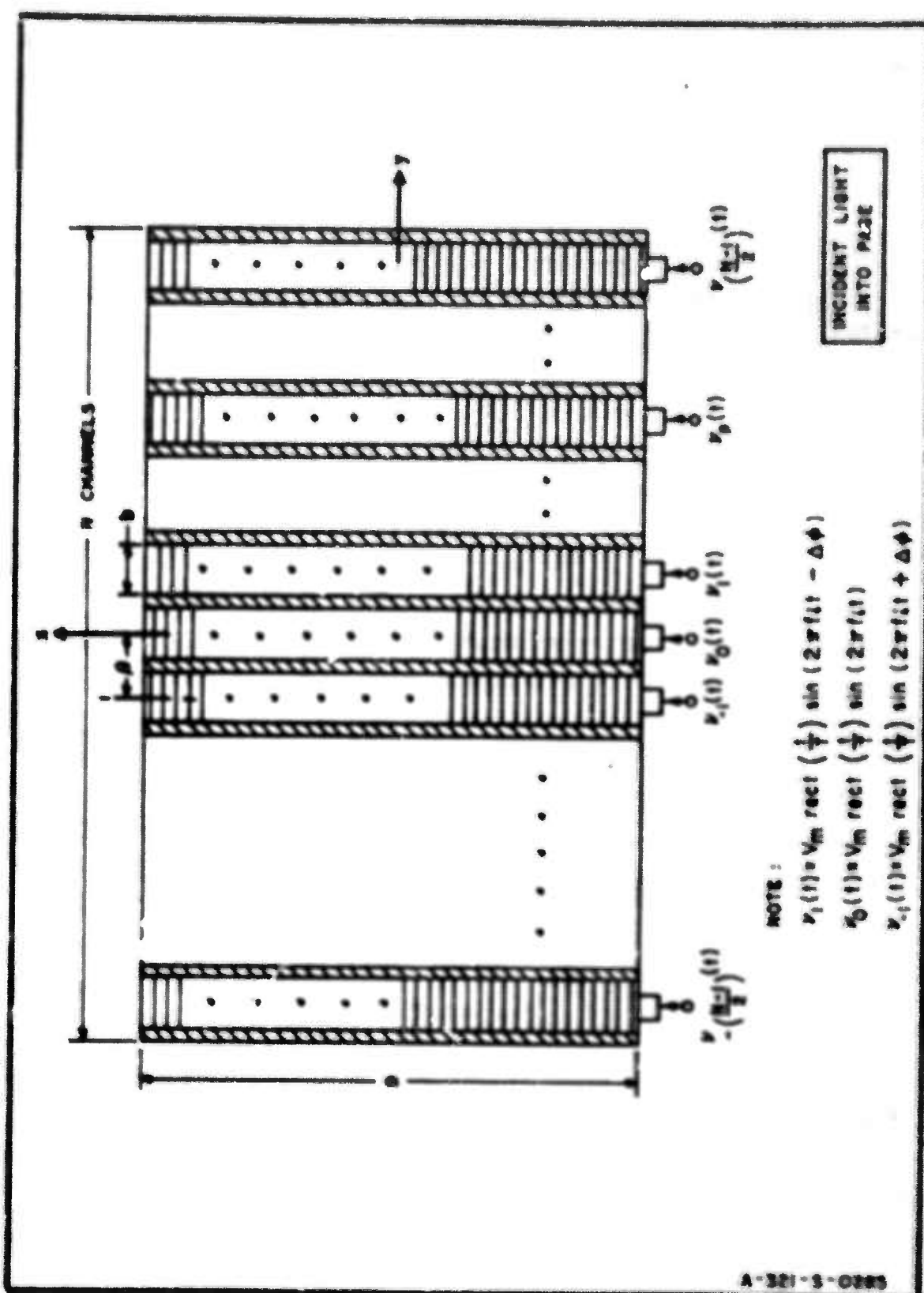


FIG. 2.2-3 N SPATIALLY-MULTIPLEXED LINEAR-ARRAY SIGNALS : SMALL APERTURE-BANDWIDTH PRODUCT

Doppler shift and angle of arrival of the electromagnetic energy at the array antenna is transformed into the location of peak first-order light intensity which occurs in the image plane at the point:

$$u = f$$

$$v = \frac{\Delta f}{2\pi\beta}$$

The actual measurement procedures in this case, as well as for the time-multiplexed linear array and the planar array, will be dealt with in more detail in Chap. 6 which considers the extraction of angle information under large and small aperture-bandwidth conditions.

2.3 LINEAR ARRAY ANTENNA: TIME MULTIPLEXING

A second method of electro-optical processing of linear-array signals involves time multiplexing the antenna-element outputs and then passing the resulting time sequence into a single-channel light modulator.

The time-multiplexing procedure is diagrammed in Fig. 2.3-1. Each antenna output is passed through a fixed delay element, the delay for the n^{th} element, T_n , being such that:

$$T_{n+1} - T_n = T_D \quad (2.3-1)$$

where T_D is fixed.

The quantity T_D is the time separation between any two adjacent pulses for a boresight signal. Hence, if the pulse duration is T , it is necessary to choose the

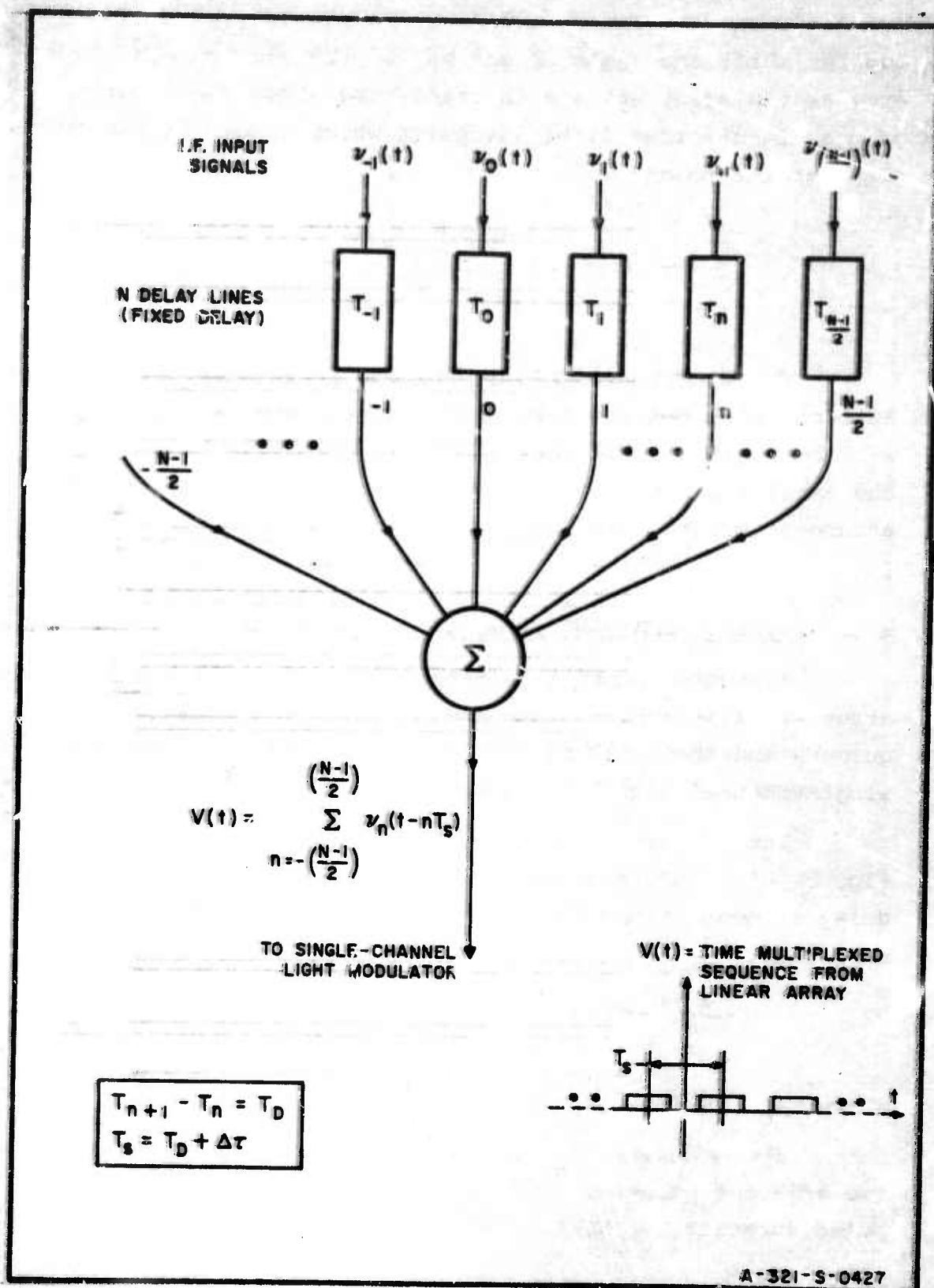


FIG. 2.3-1 TIME MULTIPLEXING: LINEAR ARRAY

delay time such that

$$T_D \geq \tau + |\Delta\tau|_{\max} \quad (2.3-2)$$

where

$$|\Delta\tau|_{\max} = \frac{\delta \sin |\theta|_{\max}}{c} \quad (2.3-3)$$

and $|\theta|_{\max}$ is the maximum off-boresight angle that the antenna is required to cover.

In general, for some arbitrary value of θ , the time separation, T_s , between adjacent antenna outputs will be given by:

$$T_s = T_D + \Delta\tau \quad (2.3-4)$$

As in Sec. 2.2, the signals are assumed to be heterodyned to an intermediate frequency and, after time multiplexing, the input to the light modulator can be shown to be of the form:

$$v(t) = \sum_{n=-\left(\frac{N-1}{2}\right)}^{n=+\left(\frac{N-1}{2}\right)} v_n(t) \quad (2.3-5)$$

where

$$v_n(t) = v_o(t - nT_s - n\gamma) \quad (2.3-6)$$

$$\gamma = (f_c - f_o) \Delta\tau$$

and, at some instant of time, the ultrasonic pulses in the light modulator will appear as shown in Fig. (2.3-2) in which the separation between ultrasonic signals is:

$$d_s = ST_s$$

and the ultrasonic signal length is:

$$d = ST.$$

In a manner similar to that of Sec. 2.2, the resulting first-order light intensity in the image plane can be shown to be:

$$|G_1(u, v)|^2 = \frac{\psi_m^2}{4} \left(\frac{b \sin \pi b v}{\pi b v} \right)^2 \left(\frac{d \sin \pi d(u-f)}{\pi d(u-f)} \right)^2 \left(\frac{\sin \pi N(u d_s + \gamma)}{\sin \pi(u d_s + \gamma)} \right)^2 \quad (2.3-7)$$

Note that in this case since Doppler information is contained in the peak of the amplitude-weighting function:

$$\left(\frac{d \sin \pi d(u-f)}{\pi d(u-f)} \right)^2$$

it cannot be recovered because peak first-order intensity is determined by

$$\left(\frac{\sin \pi N(u d_s + \gamma)}{\sin \pi(u d_s + \gamma)} \right)^2$$

independent of any Doppler shift. Thus only angle information can be obtained from the time-multiplexed linear-array configuration.

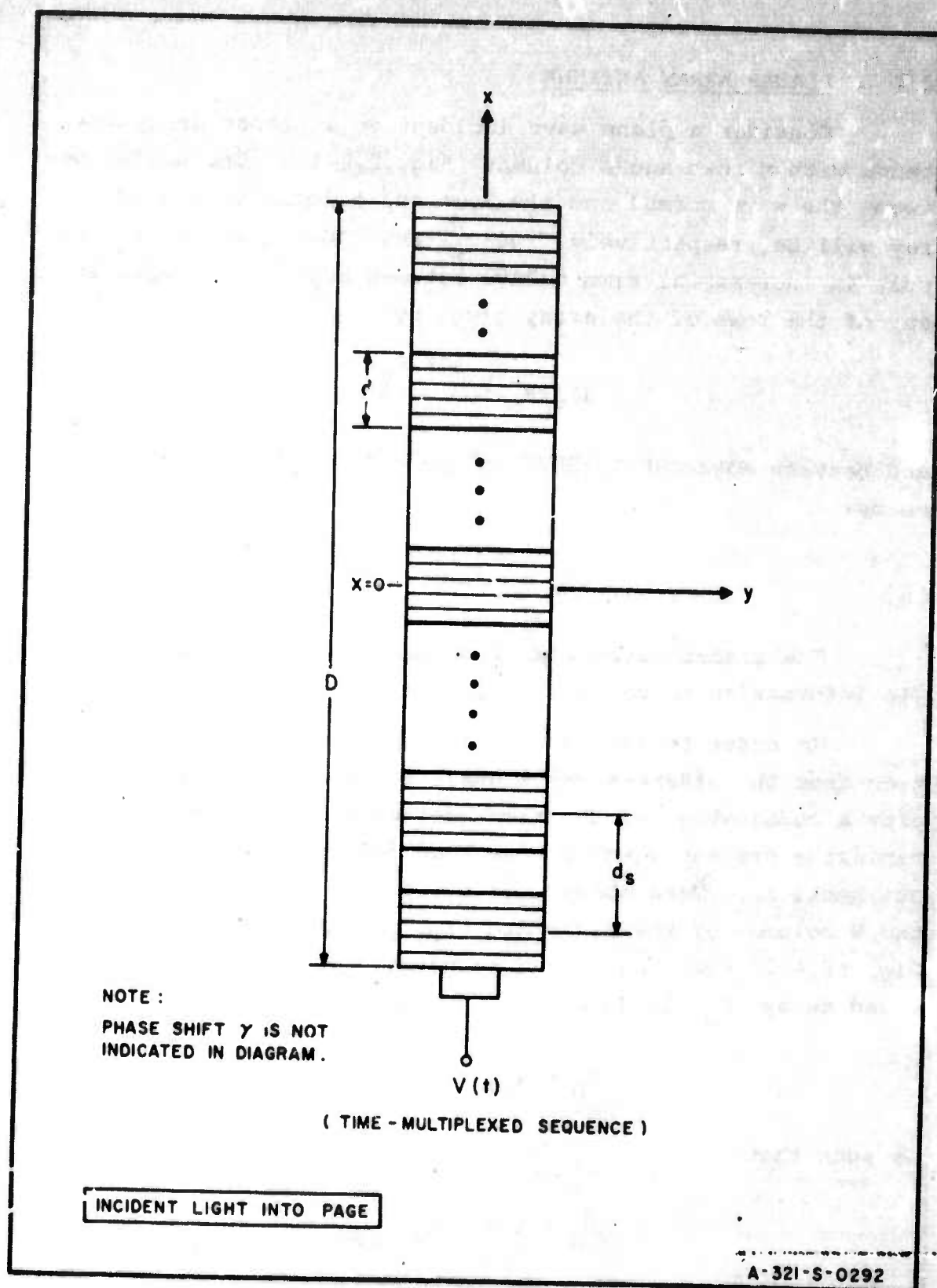


FIG. 2.3-2 SEQUENCE OF TIME-MULTIPLEXED PULSES IN SINGLE-CHANNEL DEBYE-SEARS LIGHT MODULATOR

2.4 PLANAR ARRAY ANTENNA

Consider a plane wave incident on a planar array antenna with M rows and N columns (Fig. 2.4-1). The angles between the wave normal and the rows and columns of the array will be, respectively, $90-\theta_y$ and $90-\theta_x$, which will result in incremental time delays between adjacent outputs in any of the rows of the array given by:

$$\Delta\tau_y = \frac{\delta_y \sin \theta_y}{c} \quad (2.4-1)$$

and between adjacent outputs in the columns of the array given by:

$$\Delta\tau_x = \frac{\delta_x \sin \theta_x}{c} \quad (2.4-2)$$

The planar array therefore permits two-dimensional angle information to be extracted from the incident wave.

In order to form a complex optical transmission function from the planar-array signals it is now necessary to employ a combination of the time-multiplexing and spatial-multiplexing processes which have been described in the previous sections. More specifically, the M signals from each of the N columns of the array are time multiplexed as shown in Fig. (2.4-2) such that, in a manner similar to Sec. 2.3, the fixed delay T_D given by:

$$T_D = T_{n+1} - T_n \quad (2.4-3)$$

is such that

$$T_D > T + |\Delta\tau_x|_{\max} \quad (2.4-4)$$

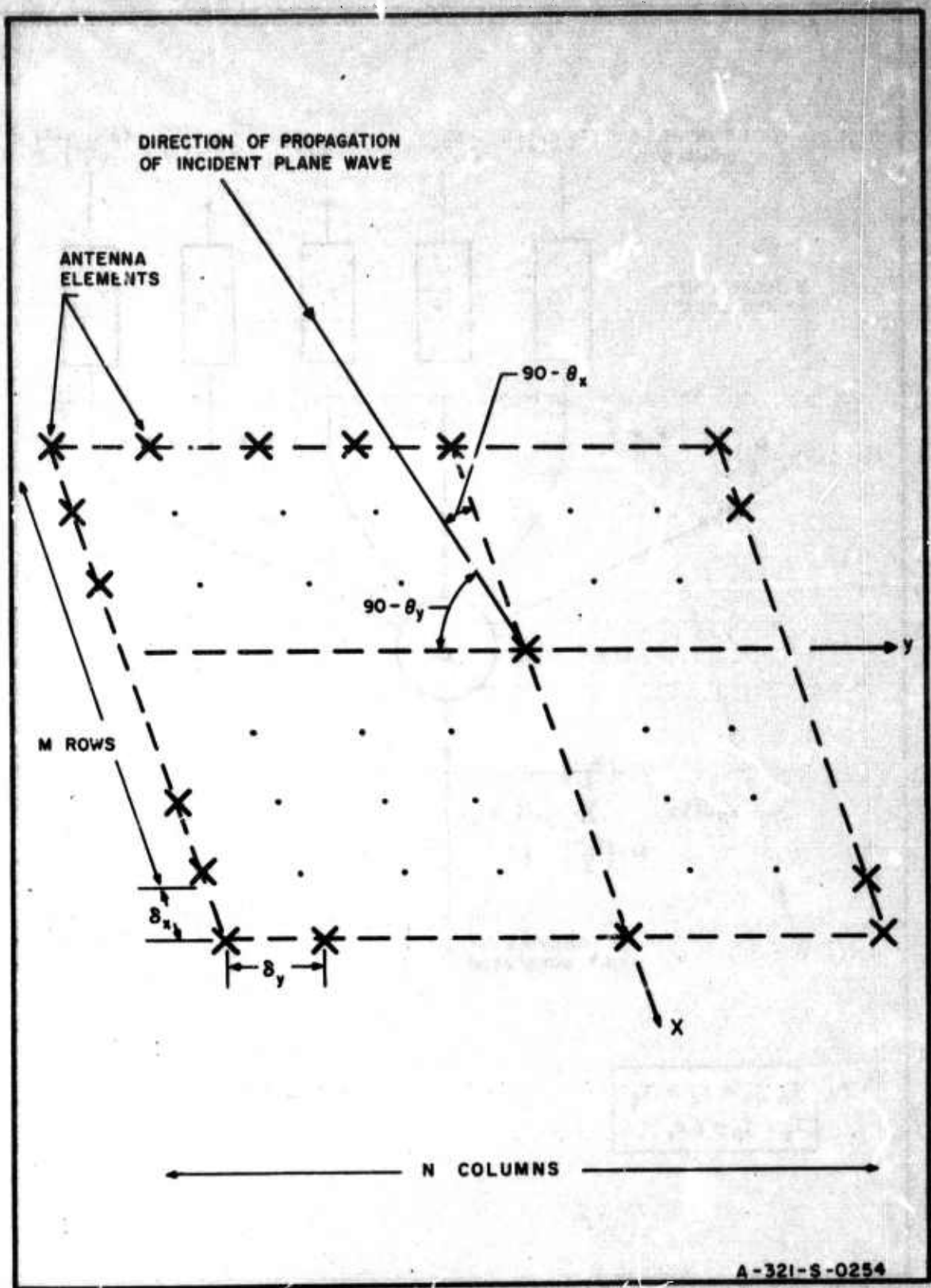
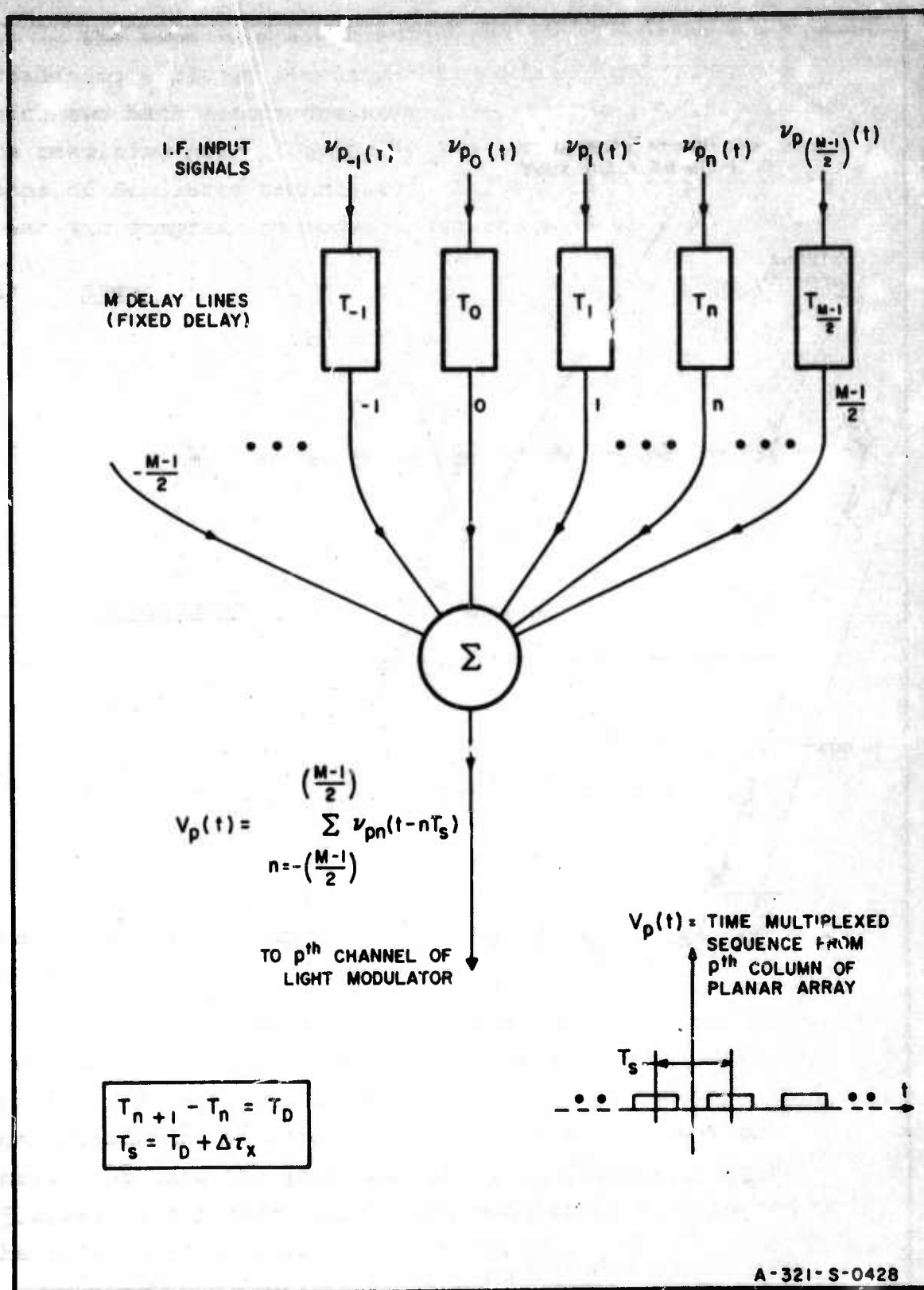


FIG. 2.4-1 PLANAR ARRAY WITH INCIDENT PLANE WAVE

FIG. 2.4-2 TIME MULTIPLEXING SIGNALS FROM p^{th} COLUMN OF PLANAR ARRAY

and the time separation between pulses is:

$$T_s = T_D + \Delta\tau_x$$

Hence, after amplification and heterodyning, the output of the p^{th} column of array elements is a time function which can be written:

$$v_p(t) = \sum_{n=-(\frac{M-1}{2})}^{(\frac{M-1}{2})} v_{pn}(t)$$

and which serves the input to the p^{th} channel of the N -channel light modulator. In this way the complex transmission function consists of N spatially-multiplexed sequences of M time-multiplexed signals. As in Sec. 2-2, the aperture-bandwidth product is assumed to be small enough so that incremental displacements of pulse amplitudes between signals in any row of the array can be ignored. Thus, for any row of the array, the amplitudes of the corresponding ultrasonic signals are aligned across the width of the optical aperture (Fig. 2.4-3) and the signal ensemble is rectangular.

The resulting light-diffraction pattern for this configuration has been determined and it has been shown that two-dimensional angle information can be obtained from the location of peak first-order light intensity.

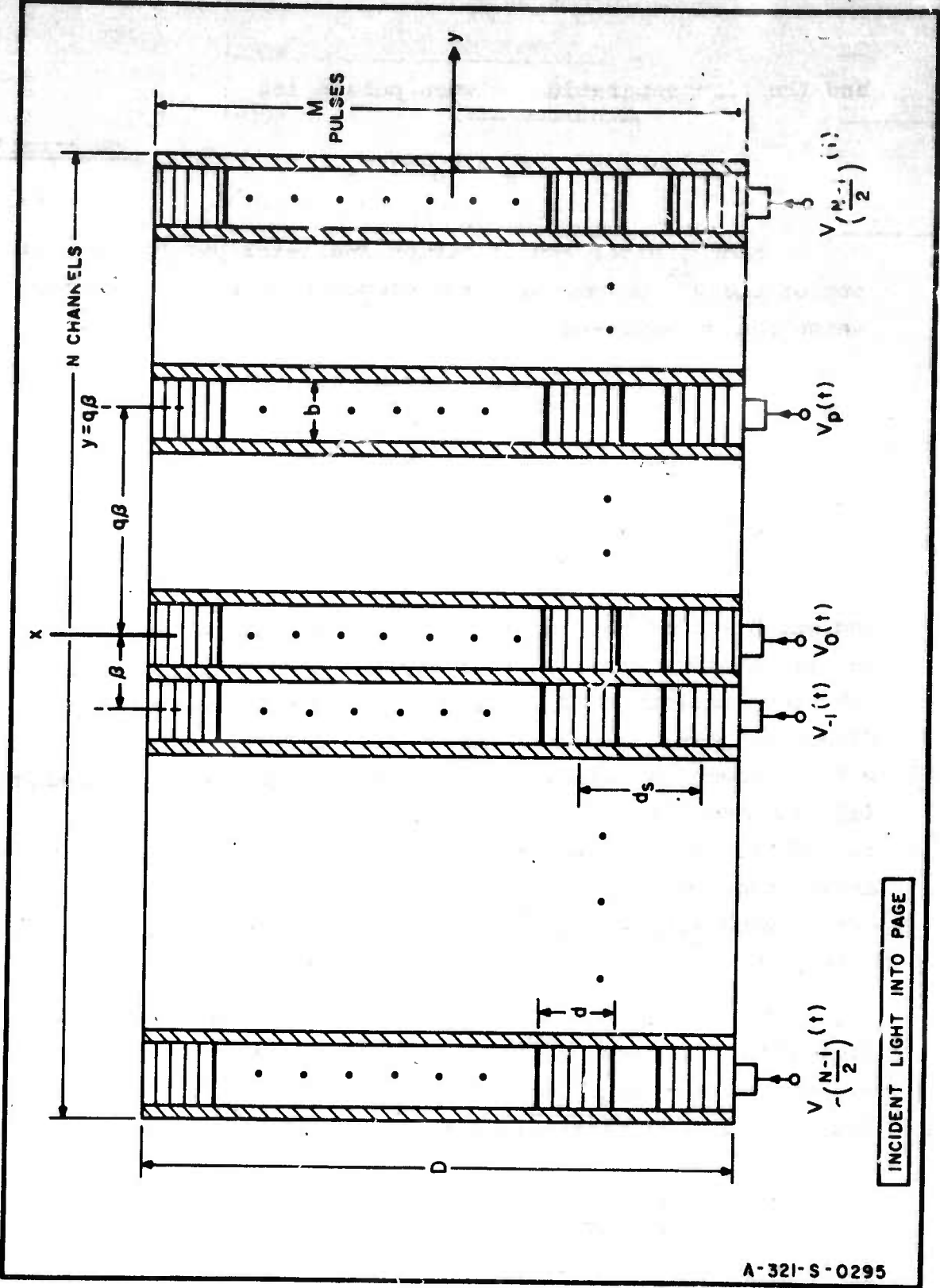


FIG. 2.4-3 N SPATIALLY-MULTIPLEXED SEQUENCES OF M TIME-MULTIPLEXED SIGNALS : SMALL APERTURE-BANDWIDTH PLANAR ARRAY

3. LITERATURE SEARCH

3.1 ELECTRO-OPTICAL AND ELECTRONIC PROCESSING FOR ARRAY ANTENNAS

Because the array antenna is a stationary structure in which the beam is steered electronically, it can produce a narrow beam, capable of high angular resolution, which can rapidly observe large volumes of the sky (Allen 1962). It is seen that a mechanically-steered dish with the same capability would need to possess a huge inertial mass and, at the same time, high maneuverability. Thus the array antenna is at present of great engineering interest (Allen 1965, Kraus 1958).

Although electronic scanning permits the antenna beam direction to be changed very rapidly there are also requirements which make it necessary for the antenna to form multiple beams to provide for simultaneous coverage of many angle resolution cells (Allen 1962). Under these conditions it is necessary to employ many sets of phase-shifting networks, each set having its own incremental phase shift corresponding to a given angle-resolution cell, which permit the antenna to be pointed in many directions simultaneously (Schnitkin 1960, 1961). It is easily shown however that, for an angle resolution of one degree,* approximately 10^6 phase-shifting networks would be necessary in order to provide for ± 60 deg angular coverage. In addition, purely electronic signal-processing schemes may become more complex under large-aperture bandwidth conditions in which case it becomes necessary to employ delay lines rather than phase-shifting networks (Allen 1964, Sklar 1960, Payne 1964).

* There are at present requirements calling for much narrower beamwidths than this (Allen 1964).

One approach to this problem (Lambert 1965) which appears to be a method of realizing the potential of the array antenna without necessitating signal-processing methods of too great complexity employs a coherent electro-optical configuration (Cutrona 1960). The mathematical relationship between the light distribution in the object and image planes of the coherent optical configuration (Cutrona 1960, Born and Wolf 1964) is identical to that which relates the signals at the elements of an array antenna to the resulting far-field radiation pattern (Schelkunoff 1949, Silver 1949). This relationship is made use of in the electro-optical processor for array antennas, which produces an optical analog of the antenna pattern and is capable therefore of forming, simultaneously, a continuum of all possible antenna beams without introducing angle-quantizing error (Allen 1959) which normally results from the use of phase-shifting networks.

As a result of the research which has been applied to electro-optical signal processing, electro-optical processors for array antennas have been synthesized (Lambert, Arm, Almette 1965) and it has been shown that a single electro-optical processor would be realistically capable of processing an array antenna in which the equivalent electronic processor would require approximately 200,000,000 phase shifting networks.

3.2 LIMITATIONS ON ELECTRO-OPTICAL ARRAY-ANTENNA PROCESSING

In the electro-optical array-antenna processor, the signals at the outputs of the antenna elements are combined by means of time multiplexing and spatial multiplexing to form a complex optical transmission function (Cutrona 1960, Cheatham 1964) consisting of ultrasonic signals in the De-

bye-Sears light modulator. On the assumption that the transformation from electrical to acoustic energy is linear, the ensemble of ultrasonic signals in the light modulator is an exact replica of the electric signals which appeared at the antenna elements.

The signal-processing capacity of the electro-optical processor has been defined in terms of the maximum number of antenna elements and the maximum bandwidth signal which can be processed. Large bandwidth and high-frequency operation are, however, interrelated for these signal processors. It has been shown (Liben 1960, Mason 1948) that it is possible to maintain an acoustic bandwidth in the Debye-Sears light modulator that is approximately 50 per cent of the ultrasonic signal frequency by properly matching the piezoelectric crystal to its load. In addition to the bandwidth, it has also been shown that the maximum number of antenna elements which can be processed will also depend on frequency. Thus it is necessary to consider the factors which limit high-frequency operation in Debye-Sears light modulators.

3.2.1 ACOUSTIC ATTENUATION

The amplitude of an ultrasonic wave will undergo an exponential attenuation in propagation (Parthasarathy 1954, 1957, Klein 1963) and the amount of decay will depend upon the characteristic acoustic attenuation of the medium. This quantity is generally frequency dependent and, in liquids, has been found (Richardson and Tait 1957, McSkimin 1957) to be proportional to the square of the ultrasonic frequency for any given value of temperature. Aside from the actual loss in ultrasonic energy, the exponential decay in a light modulator has been found (Gopal 1963, Lambert 1965) to cause a

broadening of the observed diffraction fringes. Since angle information is contained in the optical diffraction pattern, the net result of acoustic attenuation is to degrade angular resolution. Hence, operation at excessively high frequencies will destroy the signal processor's ability to determine angle information satisfactorily.

3.2.2 INTERNAL REFRACTION

The theory of Raman and Nath (Raman and Nath 1936 (I)) assumes that a ray of light normal to the surface of the Debye-Sears light modulator experiences a uniform index of refraction in propagating through the ultrasonic disturbance. This assumption is actually an approximation since the light rays in regions of relatively low refractive index tend to be bent towards regions where the index of refraction is greater. It has been found (Willard 1949, Lucas and Biquard 1932) that the effect will become more severe with an increase in the frequency of electrical excitation, strength of the ultrasonic disturbance, and the depth of the acoustic wave (dimension along direction of light propagation).

Exact mathematical solutions of internal-refraction effects on light-diffraction patterns have been obtained (Bhatia and Noble 1953, Mertens 1950, Phariseau 1959) and all serve to extend the theory of Raman and Nath. In addition to the above solutions, a first-order theory of Rao and Murty (Rao and Murty 1958) which, while not applicable under conditions of abnormal diffraction (Willard 1949), serves to predict the effects of internal refraction on the positive and negative first-order fringes under certain specific conditions. It has been shown (Rao and Murty 1958) that the more extensive

treatments (Bhatia and Noble 1953) reduce to the solution of Rao and Murty if these conditions are assumed, and it is possible that this theory may be especially applicable to this research since the operating conditions in these electro-optical processors are such that the assumptions of Rao and Murty are valid. At present, in the electro-optical processors which have been synthesized, internal-refraction effects are negligible (Hargrove and Achyutha: 1965).

3.2.3 TRANSDUCER LIMITATIONS

The thickness of a piezoelectric quartz crystal is inversely proportional to its resonant frequency (Mason 1948). As a result present fabrication techniques limit the high frequency of light modulators employing piezoelectric quartz crystals to approximately 300 MHz.* It is possible that this limitation may be extended in the future to approximately 1000 MHz with the use of evaporated thin-film transducers (Foster 1965, DeKlerk and Kelly 1965).

3.2.4 ULTRASONIC BEAM BROADENING AND CROSS-CHANNEL COUPLING

In addition to frequency limitations it is evident that the signal-processing capacity of the electro-optical array-antenna processor will also be limited by the aperture size. At present lens-fabrication techniques limit the largest possible aperture dimension to 6 inches. Thus, in order to maximize the signal-processing capacity, it is necessary to be able to fit as many light-modulator channels as possible into a given aperture size. In this case the limiting factors are cross talk due to ultrasonic diffraction,

* Private communication with Valpey Co.

and electromechanical cross coupling between adjacent transducers. With regard to ultrasonic diffraction, it has been shown (Vigoreux 1951, Seki 1956, Freedman 1962) that, for longitudinal (compression) waves, ultrasonic propagation follows the same laws as electromagnetic propagation in space. Thus the ultrasonic beam passes through a Fresnel region, in which it is approximately collimated, and into the Fraunhofer region where spreading takes place. It has been shown (Lambert 1965) that, in considering these effects, satisfactory criteria for determining the minimum transducer width and interelectrode spacing can be obtained in order to maximize the number of light-modulator channels which may be fitted into a given optical aperture.

3.3 ULTRASONIC DIFFRACTION OF LIGHT IN SOLID MEDIA

The electro-optical array-antenna processors which have been synthesized employ a liquid light-modulator medium and in this case it has been found that the high-frequency limitation is imposed by acoustic attenuation. Thus, in order to extend the signal-processing capacity, it is necessary to employ a light-modulator medium with a lower acoustic loss. This leads to consideration of solid light modulators since, although acoustic absorption in solids will also increase with frequency (Lamb, Redwood, Shteinshleifer 1959), the loss in many solids has been found (ibid) to be significantly lower than that of the optimal liquid medium.

The particular solid chosen for this research was fused silica. In addition to its low acoustic loss (Lamb, Redwood, Shteinschleifer 1959, Mason 1964), fused silica has been used extensively in the manufacture of acoustic delay lines and is known to be a suitable medium for ultrasonic propagation

(Hammond 1962, Mason 1964). Its bandwidth properties have been investigated and it has been found (Konig, Lambert, Schilling 1961) that acoustic bandwidths which are 50 per cent of the resonant transducer frequency are relatively easily obtained. Finally, it is especially suitable as a light-modulator medium because it is a transparent substance which can be polished to a high degree of optical flatness.

The operation of light modulators using solid media is, however, considerably more complicated than it is for a liquid. In a liquid, spatial phase modulation of a light wave front can be explained directly in terms of ultrasonic pressure variations which have been shown (Raman 1936, Phariseau 1956) to be proportional to the input electrical excitation. In a solid, however, it is necessary to consider how the mechanical vibrations generated by the ultrasonic transducer will alter the material's dielectric structure. This in turn can be related to spatial variation of refractive index by means of the theory of photoelasticity (Mueller 1935, 1938, Coker and Filon 1957). Thus the transfer characteristics of the fused-silica light modulator will be obtained by combining photoelastic theory (ibid) with the electromechanical coupling characteristics of piezoelectric quartz transducers.

In addition to the mechanics of electro-acoustic transfer, the use of a solid light modulator necessitates a number of considerations which do not arise with the use of liquids. These will be discussed below.

3.3.1 BIREFRINGENCE AND LIGHT POLARIZATION

A solid subjected to a mechanical stress becomes birefringent, that is, the index of refraction becomes a

function of the polarization of the incident light (Neumann 1841, Hargrove and Achyuthan 1965). It will be necessary, therefore, to determine the effects of this phenomenon on electro-optical processing, particularly with regard to the transfer between input electrical excitation and the phase deviation of the light wave front.

3.3.2 SHEAR AND COMPRESSION MODES

One of the characteristics which distinguishes liquids from solids is the ability of a solid to support shear; thus diffraction of light in a fused-silica light modulator can be accomplished by transverse as well as longitudinal ultrasonic waves (Schaefer and Bergman 1934, Hiedemann 1935, McSkimin 1962). The sonic velocity and acoustic attenuation for these two modes of propagation in fused silica, as well as in all amorphous solids, are not the same and, as a result, it can be shown that the frequency-limiting characteristics of solid light modulators is a function of the ultrasonic mode. Thus, in considering the use of a fused-silica light modulator, it will be necessary to determine how the signal-processing capacity of the electro-optical array-antenna processor can be maximized with regard to the mode of ultrasonic propagation.

3.4 LARGE APERTURE - BANDWIDTH ARRAY-ANTENNA PROCESSING

Consider a linear array antenna used for reception. As the aperture-bandwidth product becomes large the duration of the received signal becomes comparable to the time necessary for electromagnetic energy to traverse the antenna aperture. This condition will cause problems to arise in electronic as well as electro-optical processing. In electronic

COLUMBIA UNIVERSITY—ELECTRONICS RESEARCH LABORATORIES

processing under these conditions it has been shown that the more commonly used methods which employ phase-shifting networks (Ogg 1961, Allen 1964) will result in a degradation of signal-to-noise ratio (Sklar 1961), and the use of true time delay elements becomes necessary.

The equivalent problem in electro-optical processing concerns extraction of the desired angle information as well as signal to noise ratio degradation. It has been shown (Lambert 1965) that when the aperture bandwidth product is not large the complex transmission function is separable in terms of the spatial variables in the optical aperture. The diffraction patterns obtained in this case have been determined and it has been shown that angle information can be extracted from the light distribution in the image plane. When the aperture-bandwidth product is large, however, the transmission function will be a non-separable function and the resulting light-diffraction patterns produced under these conditions have not been determined. Thus, aside from evaluating the signal-to-noise degradation, it will also be necessary to determine the image-plane light distribution produced by nonseparable transmission functions in order to provide for proper interpretation of the diffraction patterns produced under large aperture-bandwidth conditions.

4. ULTRASONIC DIFFRACTION OF LIGHT IN AMORPHOUS SOLID MEDIA

Ultrasonic diffraction results from a spatial phase modulation which is imposed on a light wavefront when it passes through a transparent medium in which there is an ultrasonic disturbance. The phase modulation occurs because the ultrasonic waves, which are generated by exciting a piezoelectric transducer suitably placed with respect to the light-modulator medium, can cause a spatial variation in the index of refraction of the medium.

In a liquid the propagation of an ultrasonic disturbance can be accomplished only by means of compression waves since an ideal liquid cannot support shear; hence the variations in index of refraction can be thought of as resulting directly from the accompanying spatial variations in liquid density. The process is more complicated in a solid, however, since both shear and compression waves are possible; further, it will be seen that the way in which the ultrasonic disturbance alters the solid's dielectric structure will necessitate consideration of the polarization of the incident light.

The expressions representing the transfer from electrical excitation of the piezoelectric transducer to variations of index of refraction will be derived for amorphous solids using the theory of photoelasticity. It will be shown that, if the ultrasonic transducer is excited by a sinusoid of amplitude V_m and frequency f_1 , then, for ultrasonic propagation in the x direction, the index of refraction at some instant of time can be written:

$$n(x) = n_0 - \bar{n} \sin 2\pi f_1 x \quad (4-1)$$

where

$$\bar{n} = kV_m$$

$$k = \text{constant}$$

$$n_0 = \text{equilibrium value of refractive index}$$

$$f = \frac{f_i}{S} = \text{spatial frequency (cycles per meter)}$$

$$S = \text{velocity of ultrasonic propagation}$$

It will also be shown that the behavior of liquids as light-modulator media can be explained in terms of a degenerate case of these results.

4.1 BEHAVIOR OF ELECTROMAGNETIC PLANE WAVES IN HOMOGENEOUS ANISOTROPIC MEDIA

The behavior of light in an optically anisotropic medium, such as a crystal, can be described in terms of the vector components of the electromagnetic wave. In Appendix A it is shown that:

(i) In a crystal there is an orthogonal set of principal dielectric axes and three principal dielectric constants:

$$\epsilon_x, \epsilon_y \text{ and } \epsilon_z$$

(ii) For a given energy density $w = 2w_e$, where w_e = electric energy density, at each point in the crystal the \vec{D} field of the propagating electromagnetic wave will obey the relationship:

$$\frac{D_x^2}{\epsilon_x} + \frac{D_y^2}{\epsilon_y} + \frac{D_z^2}{\epsilon_z} = 8\pi w_e$$

where x , y and z are the principal dielectric axes.

(iii) This relationship for the \vec{D} field defines the "ellipsoid of wave normals":

$$\frac{x^2}{\epsilon_x} + \frac{y^2}{\epsilon_y} + \frac{z^2}{\epsilon_z} = 1$$

in the coordinate system defined by the principal axes. When light propagates through the crystal it is in general split into two separate beams. For a given crystal, the velocity and polarization characteristics of these two beams are functions of the direction of the unit wave normal (the unit vector perpendicular to the wave front), and can be described, exactly, in terms of the following geometrical construction:

Through the origin construct a plane parallel to the wave front (perpendicular to the unit wave normal). The intersection of this plane with the ellipsoid of wave normals is an ellipse \mathcal{E} . Each of the two beams will be linearly polarized with mutually perpendicular directions of polarization along the major and minor axes of \mathcal{E} , and with velocities of propagation which are inversely proportional to the lengths of the semi-major and minor axes. More precisely, the lengths of the semi-major and minor axes, r' and r'' are given by:

$$r' = \frac{n'}{\sqrt{\mu}}, \quad r'' = \frac{n''}{\sqrt{\mu}}$$

where n' and n'' are the indices of refraction for light linearly polarized along the major and minor axes and μ is the magnetic permeability.

It will be seen that, in a solid, phase modulation of a light beam is accomplished by causing the shape of \mathcal{E} to vary with the spatial variable along the direction of ultrasonic propagation.

4.2 STRESS AND STRAIN BIREFRINGENCE: THE STRAIN-OPTIC CONSTANTS

The ultrasonic wave in the solid results in the occurrence of a system of strains (and proportional stresses). The relationship between these strains (stresses) and the shape and orientation of the ellipsoid of wave normals will be dealt with in this section. Thus, for a given direction of light propagation, the shape and orientation of \mathcal{E} will be a function of the ultrasonic disturbance, and therefore of the piezoelectric vibrations.

* * *

The theory of photoelasticity (Mueller 1935, 1938, Coker and Filon 1957) assumes that the ellipsoid of wave normals for a transparent solid, given by:

$$\frac{x^2}{\epsilon_x} + \frac{y^2}{\epsilon_y} + \frac{z^2}{\epsilon_z} = 1,$$

is transformed, when the solid is subjected to mechanical stresses, into a different ellipsoid given by:

$$a_{xx}x^2 + a_{yy}y^2 + a_{zz}z^2 + 2a_{yz}yz + 2a_{xz}xz + 2a_{xy}xy = 1 \quad (4.2-1)$$

For the purposes of obtaining these two quadratic forms, the dielectric tensors for the unstressed and stressed case may be represented symbolically in matrix form as follows:

$$\begin{bmatrix} \frac{1}{\epsilon_x} & 0 & 0 \\ 0 & \frac{1}{\epsilon_y} & 0 \\ 0 & 0 & \frac{1}{\epsilon_z} \end{bmatrix}$$

unstressed

$$\begin{bmatrix} a_{xx} & a_{xy} & a_{xz} \\ a_{xy} & a_{yy} & a_{yz} \\ a_{xz} & a_{yz} & a_{zz} \end{bmatrix}$$

stressed

It is further assumed in photoelastic theory that the changes in the dielectric tensor are linear functions of the strains (stresses). This assumption is expressed in the following set of linear relationships:

$$\begin{aligned}
 a_{xx} - \frac{1}{\epsilon_x} &= p_{11} S_{xx} + p_{12} S_{yy} + p_{13} S_{zz} + p_{14} S_{yz} + p_{15} S_{xz} + p_{16} S_{xy} \\
 a_{yy} - \frac{1}{\epsilon_y} &= p_{21} S_{xx} + p_{22} S_{yy} + p_{23} S_{zz} + p_{24} S_{yz} + p_{25} S_{xz} + p_{26} S_{xy} \\
 a_{zz} - \frac{1}{\epsilon_z} &= p_{31} S_{xx} + p_{32} S_{yy} + p_{33} S_{zz} + p_{34} S_{yz} + p_{35} S_{xz} + p_{36} S_{xy} \\
 a_{yz} &= p_{41} S_{xx} + p_{42} S_{yy} + p_{43} S_{zz} + p_{44} S_{yz} + p_{45} S_{xz} + p_{46} S_{xy} \\
 a_{xz} &= p_{51} S_{xx} + p_{52} S_{yy} + p_{53} S_{zz} + p_{54} S_{yz} + p_{55} S_{xz} + p_{56} S_{xy} \\
 a_{xy} &= p_{61} S_{xx} + p_{62} S_{yy} + p_{63} S_{zz} + p_{64} S_{yz} + p_{65} S_{xz} + p_{66} S_{xy}
 \end{aligned}
 \tag{4.2-2}$$

where the p_{ij} 's are referred to as the strain-optic constants (Hargrove and Achyuthan 1965), and the strain component S_{ij} ($= S_{ji}$ $i, j = x, y, z$) is a measure of the displacement in the j th direction of the i th face of an infinitesimal cube. An equivalent set of equations may be written in terms of the stress-optic constants q_{ij} and the stresses T_{ij} . The p_{ij} 's (and q_{ij} 's) are physical constants depending on the material. Thus, by the geometrical construction described in the beginning of this section (rule (iii)), velocity and polarization of light in a stressed transparent medium may be determined, since the ellipsoid of wave normals resulting from the strains (Eq. (4.2-1)) is completely determined by Eqs. (4.2-2).

COLUMBIA UNIVERSITY—ELECTRONICS RESEARCH LABORATORIES

These equations (Eq. (4.2-2)) become simplified if the medium under consideration exhibits symmetries in its crystal-line structure. In particular, in the case of a cubic system which has three equivalent principal axes and is therefore optically isotropic (i.e., $\epsilon_x = \epsilon_y = \epsilon_z = \epsilon$), the array of strain-optic constants considered as a matrix $P = [p_{ij}]$ becomes (see Appendix B):

$$P = \begin{bmatrix} p_{11} & p_{12} & p_{12} & 0 & 0 & 0 \\ p_{12} & p_{11} & p_{12} & 0 & 0 & 0 \\ p_{12} & p_{12} & p_{11} & 0 & 0 & 0 \\ 0 & 0 & 0 & p_{44} & 0 & 0 \\ 0 & 0 & 0 & 0 & p_{44} & 0 \\ 0 & 0 & 0 & 0 & 0 & p_{44} \end{bmatrix}$$

In most crystals $\mu \approx 1$ and the index of refraction for a cubic system will be a constant given by:

$$n_o = \sqrt{\mu\epsilon} \approx \sqrt{\epsilon}$$

Thus Eqs. (4.2-2) become:

$$\begin{aligned} a_{xx} - \frac{1}{n_o^2} &= p_{11} s_{xx} + p_{12} s_{yy} + p_{12} s_{zz} \\ a_{yy} - \frac{1}{n_o^2} &= p_{12} s_{xx} + p_{11} s_{yy} + p_{12} s_{zz} \\ a_{zz} - \frac{1}{n_o^2} &= p_{12} s_{xx} + p_{12} s_{yy} + p_{11} s_{zz} \end{aligned} \quad (4.2-3)$$

$$a_{yz} = p_{44} S_{yz}$$

$$a_{xz} = p_{44} S_{xz}$$

$$a_{xy} = p_{44} S_{xy} \quad (4.2-3)$$

In addition, if the material is amorphous (i.e., fused silica, most glasses) it is found that:

$$p_{44} = \frac{p_{11} - p_{12}}{2} \quad (\text{Appendix B}).$$

4.3 RELATIONSHIP BETWEEN PIEZOELECTRIC TRANSDUCER VIBRATION AND SPATIAL VARIATION OF INDEX OF REFRACTION FOR AMORPHOUS MEDIA

The relationship between the voltage applied at the piezoelectric transducer and spatial variation of index of refraction will be derived in this section for normal light incidence. It will be seen that either longitudinal or transverse vibrations of the transducer will cause these variations, and that, for the transverse mode, only one direction of vibration need be considered.

The configuration shown in Fig. 4.3-1 will apply to the three cases which will be considered. For all cases the incident light will be assumed to be traveling along the z (optic) axis, perpendicular to the xy plane.

4.3.1 TRANSVERSE VIBRATIONS ALONG OPTIC AXIS

In this case the only nonzero strain component is S_{xz} . Eqs. (4.2-3) become:

$$a_{xx} = \frac{1}{n_o^2}, \quad a_{yy} = \frac{1}{n_o^2}, \quad a_{zz} = \frac{1}{n_o^2}, \quad a_{xz} = p_{44} S_{xz}$$

$$\begin{aligned}
 a_{yz} &= p_{44} s_{yz} \\
 a_{xz} &= p_{44} s_{xz} \\
 a_{xy} &= p_{44} s_{xy}
 \end{aligned}
 \tag{4.2-3}$$

In addition, if the material is amorphous (i.e., fused silica, most glasses) it is found that:

$$p_{44} = \frac{p_{11} - p_{12}}{2} \quad (\text{Appendix B}).$$

4.3 RELATIONSHIP BETWEEN PIEZOELECTRIC TRANSDUCER VIBRATION AND SPATIAL VARIATION OF INDEX OF REFRACTION FOR AMORPHOUS MEDIA

The relationship between the voltage applied at the piezoelectric transducer and spatial variation of index of refraction will be derived in this section for normal light incidence. It will be seen that either longitudinal or transverse vibrations of the transducer will cause these variations, and that, for the transverse mode, only one direction of vibration need be considered.

The configuration shown in Fig. 4.3-1 will apply to the three cases which will be considered. For all cases the incident light will be assumed to be traveling along the z (optic) axis, perpendicular to the xy plane.

4.3.1 TRANSVERSE VIBRATIONS ALONG OPTIC AXIS

In this case the only nonzero strain component is s_{xz} . Eqs. (4.2-3) become:

$$a_{xx} = \frac{1}{n_o^2}, \quad a_{yy} = \frac{1}{n_o^2}, \quad a_{zz} = \frac{1}{n_o^2}, \quad a_{xz} = p_{44} s_{xz}$$

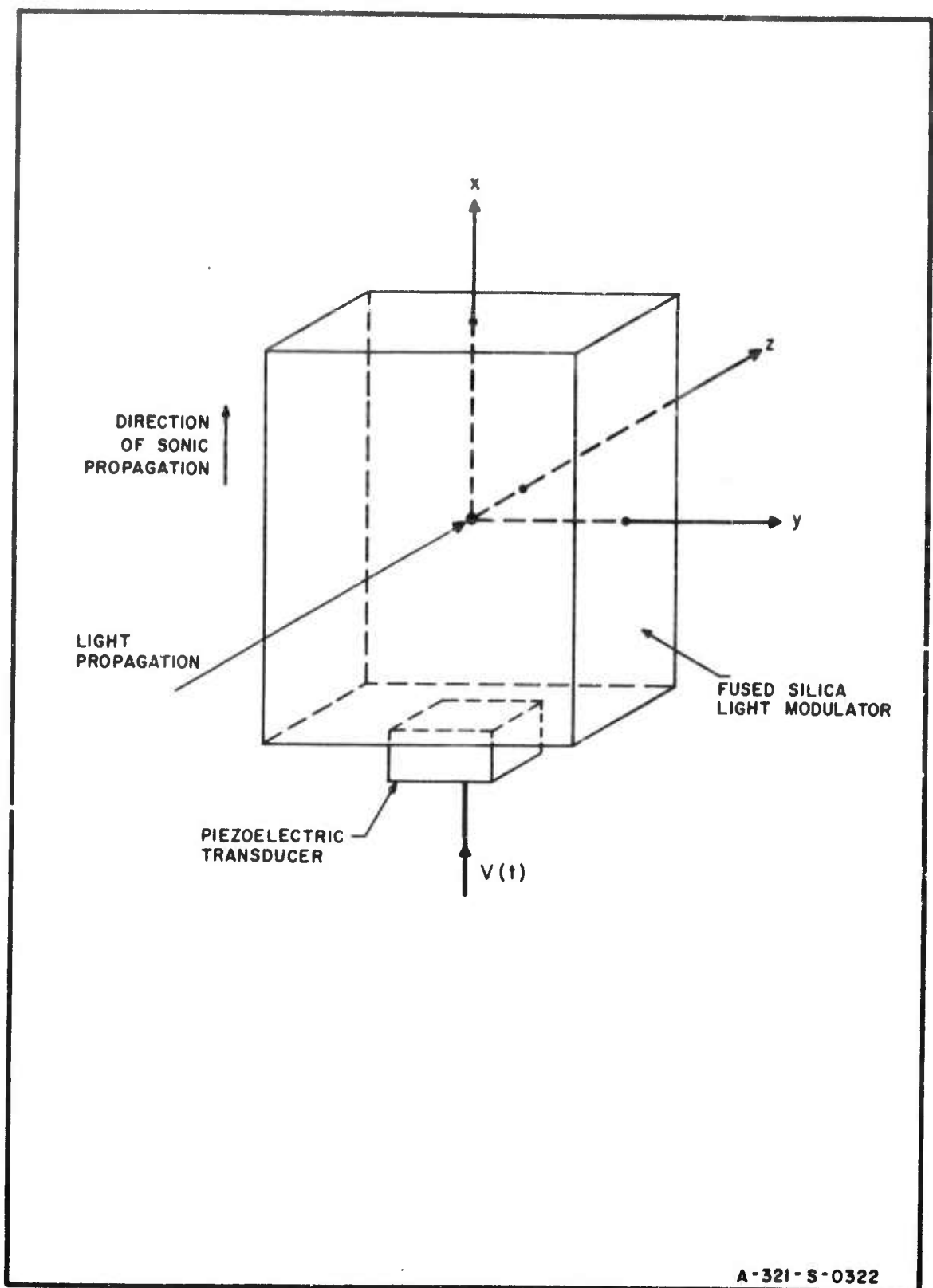


FIG. 4.3-1 ELEMENTARY LIGHT-MODULATOR CONFIGURATION

and the ellipsoid of wave normals is:

$$\frac{x^2}{n_o^2} + \frac{y^2}{n_o^2} + \frac{z^2}{n_o^2} + 2p_{44} S_{xz} xz = 1$$

The plane through the origin perpendicular to the unit wave normal is defined by $z = 0$. Hence, by rule (iii) of Sec. 4, the ellipse \mathcal{E} becomes:

$$\frac{x^2}{n_o^2} + \frac{y^2}{n_o^2} = 1$$

It is seen that \mathcal{E} has degenerated into a circle of radius n_o independent of S_{xz} , and the index of refraction is therefore a constant, independent of x , for light propagating in this direction. Thus transverse vibrations parallel to the direction of light propagation have no effect.

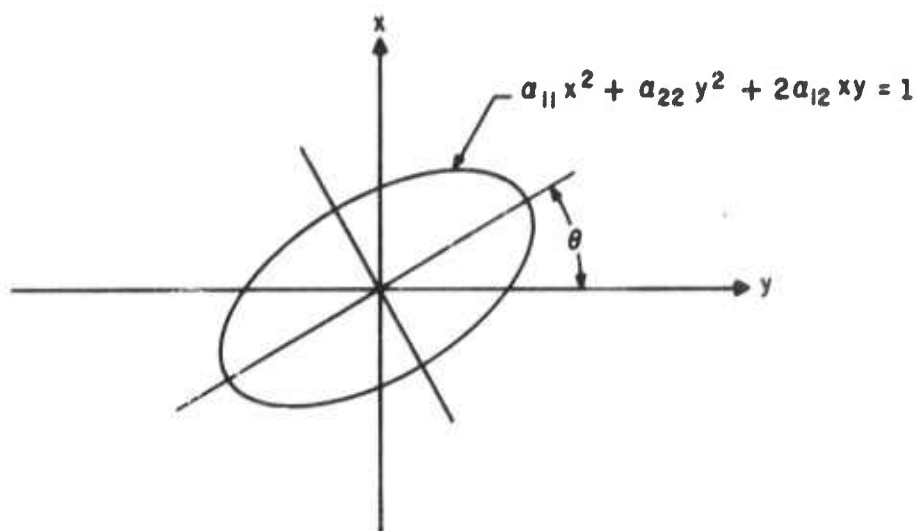
4.3.2 TRANSVERSE VIBRATIONS NORMAL TO OPTIC AXIS

The nonzero shear-strain component is now S_{xy} ; the ellipsoid of wave normals is:

$$\frac{x^2}{n_o^2} + \frac{y^2}{n_o^2} + \frac{z^2}{n_o^2} + 2p_{44} S_{xy} xy = 1$$

and setting $z = 0$ gives the ellipse \mathcal{E} :

$$\frac{x^2}{n_o^2} + \frac{y^2}{n_o^2} + 2p_{44} S_{xy} xy = 1$$



It is easily shown that, in general, an ellipse of the form

$$a_{11}x^2 + a_{22}y^2 + 2a_{12}xy = 1$$

is inclined to the y axis at an angle θ defined by:

$$\tan 2\theta = \frac{2a_{12}}{a_{22} - a_{11}}$$

In this case,

$$a_{11} = \frac{1}{n_o^2}, \quad a_{22} = \frac{1}{n_o^2}, \quad a_{12} = p_{44} s_{xy}$$

and

$$\theta = 45^\circ \quad \text{for } s_{xy} > 0$$

$$\theta = -45^\circ \quad \text{for } s_{xy} < 0$$

independent of the magnitude of S_{xy} ; thus, for transverse vibrations, the semi-major and minor axes of \mathcal{E} will always be inclined at either plus or minus 45° to the y axis.

The voltage exciting the piezoelectric transducer is assumed to be sinusoidal. Hence, because of the direction of the transducer vibrations, a sinusoidal ultrasonic traveling wave, in the shear mode, propagates in the x direction. At a given instant of time, therefore, the wave shape is a sinusoid, and infinitesimally thin layers of the medium are displaced in the $\pm y$ direction from their rest position, causing a corresponding sinusoidal variation with x of the shear strain, S_{xy} , as shown. In Fig. (4.3.2-1) it is shown that:

(i) Because of the variations in $S_{xy}(x)$, the shape of \mathcal{E} , which can be written as $\mathcal{E}(x)$, will vary proportionately.

(ii) Since the index of refraction for light polarized at plus or minus 45° to the y axis varies with x as does the length of the corresponding axis of $\mathcal{E}(x)$, then, by rule (iii) of Sec. 4, the index of refraction variation is also proportional to $S_{xy}(x)$.

(iii) If $n_1(x)$ and $n_2(x)$ are the indices of refraction for light polarized at plus and minus 45° respectively, then $n_1(x)$ and $n_2(x)$ exhibit variations about n_0 , and $n_1(x)$ is 180° out of phase with $n_2(x)$.

In order to establish these conclusions more precisely, consider $\mathcal{E}(x)$ for some value of x at a given instant of time as shown in the following sketch:

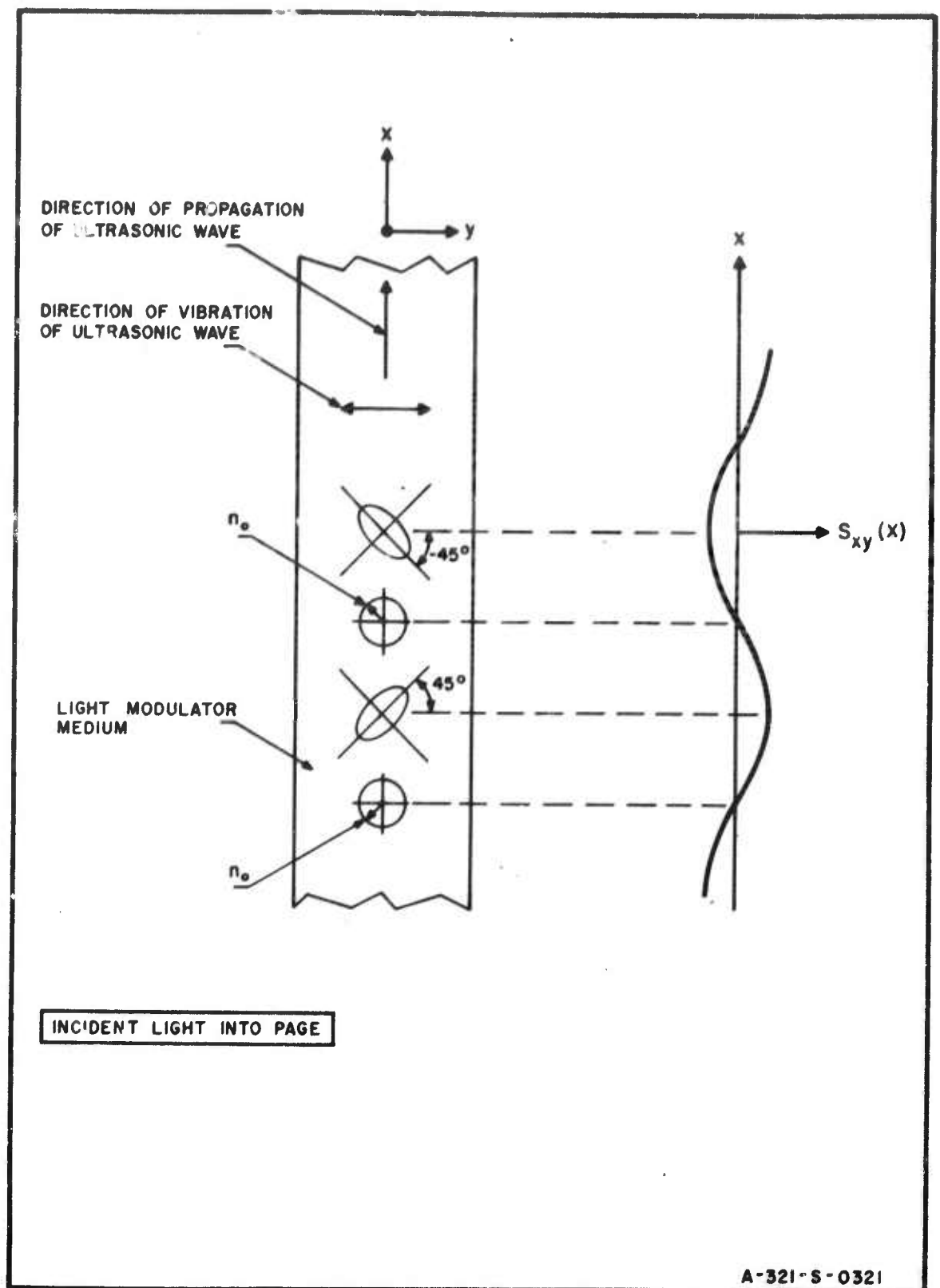
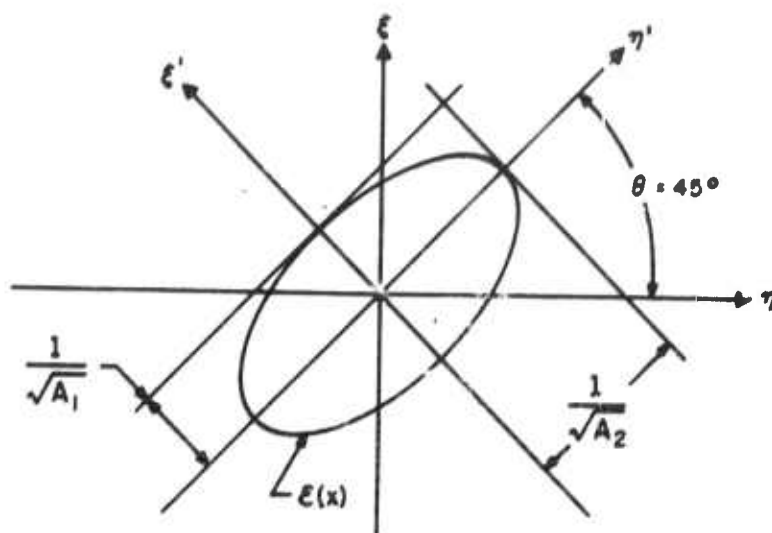


FIG. 4.3.2 -1 DIAGRAM SHOWING EFFECT OF SHEAR STRAIN ON ELLIPSOID OF WAVE NORMALS



Variables other than x and y (e.g., ξ and η) are now used in the graph of the ellipse, since $\mathcal{E}(x)$, in which x is now a parameter, serves only as a geometrical description of index of refraction for each point x , but does not actually occupy physical space in the light modulator (x, y plane). The ξ and η axes are assumed parallel to the x and y axes respectively.

In general, $\mathcal{E}(x)$ can be written as:

$$a_{11}\xi^2 + a_{22}\eta^2 + 2a_{12}\xi\eta = 1$$

In the (ξ', η') coordinates, the equation of the ellipse will contain no cross term, and will be of the form: $A_1\xi'^2 + A_2\eta'^2 = 1$. In order to determine A_1 and A_2 use the linear transformations:

$$\xi' = b_{11}\xi + b_{12}\eta \quad \xi = b_{11}\xi' + b_{21}\eta'$$

$$\eta' = b_{21}\xi + b_{22}\eta \quad \eta = b_{12}\xi' + b_{22}\eta'$$

where

$$b_{11} = b_{22} = \cos \theta$$

$$b_{21} = -b_{12} = \sin \theta$$

Substituting ξ' for ξ and η' for η in the equation:

$$a_{11}\xi^2 + a_{22}\eta^2 + 2a_{12}\xi\eta = 1,$$

and equating coefficients gives:

$$A_1 = a_{11}b_{11}^2 + a_{22}b_{12}^2 + 2a_{12}b_{11}b_{12}$$

$$A_2 = a_{11}b_{21}^2 + a_{22}b_{22}^2 + 2a_{12}b_{21}b_{22}$$

$$0 = 2a_{11}b_{11}b_{21} + 2a_{22}b_{12}b_{22} + 2a_{12}[b_{11}b_{22} + b_{12}b_{21}]$$

In this example:

$$b_{11} = b_{22} = b_{21} = -b_{12} = \frac{1}{\sqrt{2}}$$

$$a_{11} = a_{22} = \frac{1}{n_0^2}$$

$$a_{12} = p_{44}S_{xy}$$

Thus as a function of x :

$$A_1(x) = \frac{1}{n_o^2} - p_{44} S_{xy}(x)$$

$$A_2(x) = \frac{1}{n_o^2} + p_{44} S_{xy}(x) \quad (4.3.2-1)$$

and it is seen that the shape of $\mathcal{E}(x)$ will vary with $S_{xy}(x)$.

But for light polarized at plus or minus 45 deg, the indices of refraction $n_1(x)$ and $n_2(x)$ are given by (rule (iii) and Appendix A):

$$n_1(x) = \frac{1}{\sqrt{A_2(x)}} \quad \text{for } +45^\circ$$

$$n_2(x) = \frac{1}{\sqrt{A_1(x)}} \quad \text{for } -45^\circ$$

Then from Eq. (4.3.2-1):

$$\frac{1}{n_o^2} - \frac{1}{n_1^2(x)} = -p_{44} S_{xy}(x) \quad \text{for light polarized at } +45^\circ$$

$$\frac{1}{n_o^2} - \frac{1}{n_2^2(x)} = p_{44} S_{xy}(x) \quad \text{for light polarized at } -45^\circ$$

Now let $n_1(x) = n_o - \bar{n}_1(x)$, and $n_2(x) = n_o - \bar{n}_2(x)$, where n_o is constant and $\bar{n}_1(x)$ and $\bar{n}_2(x)$ represent small perturbations of index of refraction with magnitudes given by:

$|\bar{n}_1(x)|_{\max} = \bar{n}_1$, $|\bar{n}_2(x)|_{\max} = \bar{n}_2$. Since $n_o \gg (\bar{n}_1, \bar{n}_2)$ then:

$$\frac{1}{n_1^2(x)} = \frac{1}{n_o^2} \left(\frac{1}{1 - \frac{\bar{n}_1(x)}{n_o}} \right)^2 \approx \frac{1}{n_o^2} \left(1 + 2 \frac{\bar{n}_1(x)}{n_o} \right)$$

$$\frac{1}{n_2^2(x)} = \frac{1}{n_o^2} \left(\frac{1}{1 - \frac{\bar{n}_2(x)}{n_o}} \right)^2 \approx \frac{1}{n_o^2} \left(1 + 2 \frac{\bar{n}_2(x)}{n_o} \right)$$

and

$$\bar{n}_1(x) = \frac{n_o^3 p}{2} s_{xy}(x) = -\bar{n}_2(x)$$

hence

$$n_1(x) = n_o - n_o^3 \frac{p}{2} s_{xy}(x) \quad (4.3.2-2)$$

$$n_2(x) = n_o + n_o^3 \frac{p}{2} s_{xy}(x)$$

This appears to be a general result with sinusoidal $s_{xy}(x)$ being a particular case.

$n_1(x)$ and $n_2(x)$ can now be expressed in terms of the transducer voltage. The shear strain can be written (Sokolnikoff 1956):

$$s_{xy}(x) = \frac{1}{\mu} T_{xy}(x)$$

where

$$T_{xy}(x) = \text{shear stress}$$

$$\mu = \text{modulus of rigidity}$$

In the sinusoidal case, $T_{xy}(x) = |T_{xy}|_{\max} \sin 2\pi fx$ where f is the spatial frequency (cycles per meter). But the maximum shear stress, $|T_{xy}|_{\max}$, can be shown to be directly proportional to the amplitude of the voltage at the transducer (Arm, Konig, Lambert, Weissman 1962). Thus (at a given instant of time):

$$(n_1(x), n_2(x)) = n_0 + \frac{n_0^3 p_{44}}{2} \frac{1}{\mu} k_s v_m \sin 2\pi f x$$

where k_s is the electromechanical coupling coefficient of the ultrasonic shear transducer. This expression is seen to be of the same form as Eq. (4-1) with:

$$\bar{n}_1 = \frac{n_0^3 p_{44}}{2} \frac{1}{\mu} k_s v_m = -\bar{n}_2 \quad (4.3.2-3)$$

4.3.3 LONGITUDINAL VIBRATIONS

In this case the transducer vibrates, piston-like, along the x axis which produces a compression wave. Under the assumption that a plane wave is generated, the only non-zero strain component is S_{xx} and Eq. (4.2-3) thus becomes:

$$a_{xx} = p_{11} S_{xx} + \frac{1}{n_0^2}, \quad a_{yy} = p_{12} S_{xx} + \frac{1}{n_0^2}, \quad a_{zz} = p_{12} S_{xx} + \frac{1}{n_0^2}$$

The ellipsoid of wave normals is:

$$\left(p_{11} S_{xx} + \frac{1}{n_0^2}\right) x^2 + \left(p_{12} S_{xx} + \frac{1}{n_0^2}\right) y^2 + \left(p_{12} S_{xx} + \frac{1}{n_0^2}\right) z^2 = 1$$

and the ellipse \mathcal{E} becomes:

$$\left(p_{11} S_{xx} + \frac{1}{n_0^2}\right) x^2 + \left(p_{12} S_{xx} + \frac{1}{n_0^2}\right) y^2 = 1 \quad (4.3.3-1)$$

It is seen that the major and minor axes of \mathcal{E} are now always aligned with either the x or y axis and the corresponding indices of refraction will apply to vertically and horizontally polarized light. Fig. 4.3.3-1 shows the variations of \mathcal{E} with S_{xx} (assuming that $p_{11} > p_{12}$).

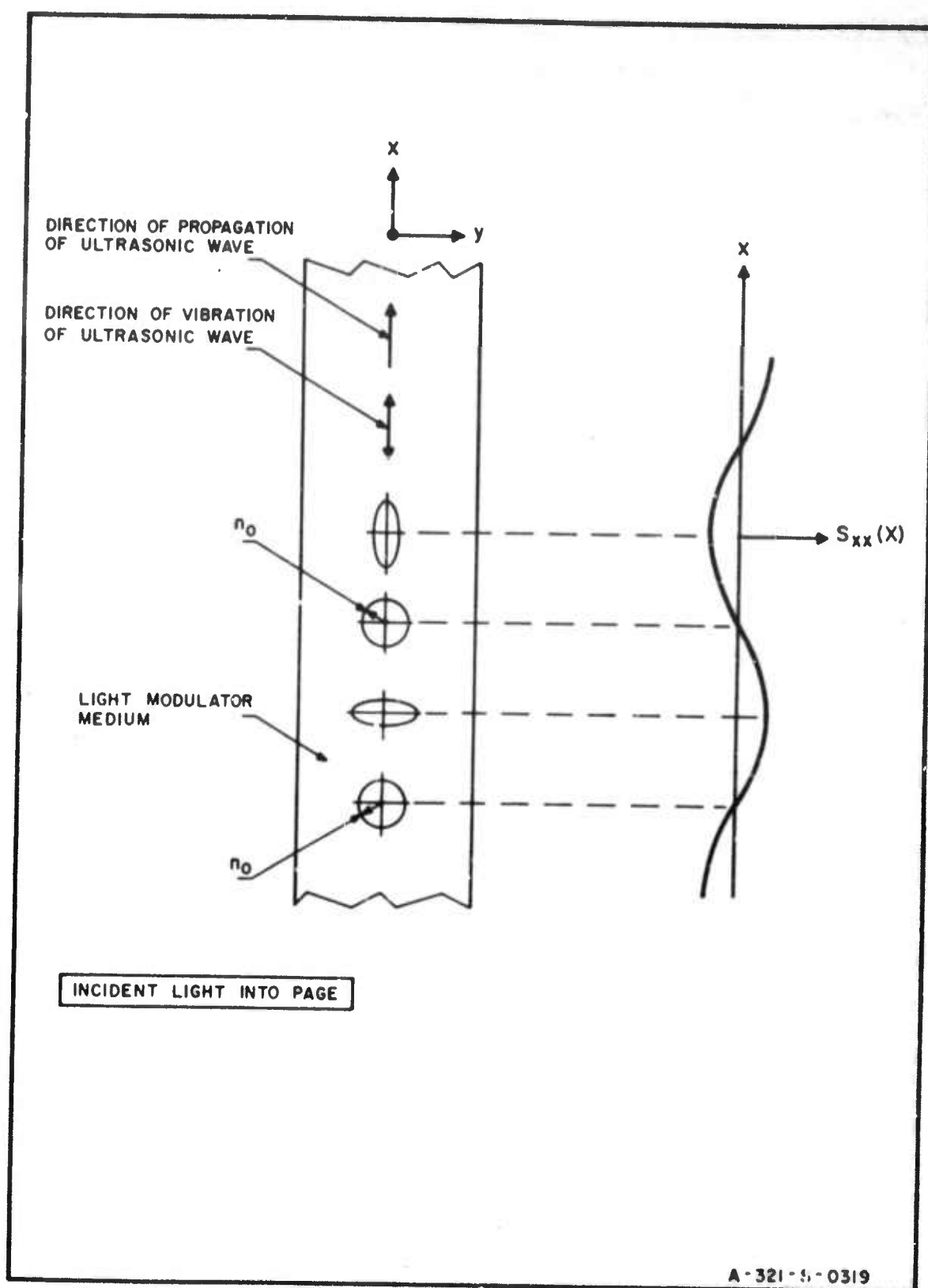


FIG. 4.3.3 -1 DIAGRAM SHOWING EFFECT OF COMPRESSIONAL STRAIN ON ELLIPSOID OF WAVE NORMALS

COLUMBIA UNIVERSITY—ELECTRONICS RESEARCH LABORATORIES

If $n_1(x)$ and $n_2(x)$ are the indices of refraction for vertically and horizontally polarized light then, as before (Eq. 4.3.2-1 et. seq.):

$$\begin{aligned}\frac{1}{n_o^2} - \frac{1}{n_1^2(x)} &= -p_{11} s_{xx}(x) \\ \frac{1}{n_o^2} - \frac{1}{n_2^2(x)} &= -p_{12} s_{xx}(x)\end{aligned}\tag{4.3.3-2}$$

and

$$\begin{aligned}n_1(x) &= n_o - \frac{n_o^3 p_{11} s_{xx}(x)}{2} \\ n_2(x) &= n_o - \frac{n_o^3 p_{12} s_{xx}(x)}{2}\end{aligned}\tag{4.3.3-3}$$

In this case, under the assumption that the ultrasonic propagation is accomplished by plane waves,

$$s_{xx}(x) = \frac{1}{C} T_{xx}(x)$$

where

$$C = B + \frac{4}{3} \mu, \quad B = \text{bulk modulus}, \quad \mu = \text{modulus of rigidity}$$

Thus for a sinusoidal excitation:

$$\begin{aligned}n_1(x) &= n_o - \frac{n_o^3 p_{11}}{2C} k_c v_m \sin 2\pi f x \\ n_2(x) &= n_o - \frac{n_o^3 p_{12}}{2C} k_c v_m \sin 2\pi f x\end{aligned}\tag{4.3.3-4}$$

where k_c is the electromechanical coupling coefficient of the compression transducer.

COLUMBIA UNIVERSITY—ELECTRONICS RESEARCH LABORATORIES

A photoelastic interpretation of ultrasonic diffraction in a liquid for longitudinal transducer vibrations now follows directly.

The fact that transverse vibrations of the piezoelectric transducer have no effect on the index of refraction of a liquid can be demonstrated by setting p_{44} equal to zero (see Eq. (4.3.2-2)). Since a liquid is an amorphous medium, and $p_{44} = \frac{p_{11} - p_{12}}{2}$, it follows that $p_{11} = p_{12}$. Hence from Eq. (4.3.3 1) for longitudinal vibrations:

$$\left(p_{11}S_{xx} + \frac{1}{n_o^2}\right)x^2 + \left(p_{11}S_{xx} + \frac{1}{n_o^2}\right)y^2 = 1$$

Thus, for liquids, $\mathcal{E}(x)$ degenerates into a circle whose radius varies with $S_{xx}(x)$. For each value of x the corresponding circle can be looked at as a degenerate form of an ellipse with infinitely many major and minor axes. Hence it follows from rule (iii) of Sec. 4 that all polarizations of the incident light are equally affected by ultrasonic diffraction in liquids. This interpretation is symbolized in Fig. 4.3.3-2.

4.4 OPTIMUM LIGHT POLARIZATION AS A FUNCTION OF MODE OF PROPAGATION

It is shown in Appendix B that in amorphous media the relationship: $p_{44} = \frac{p_{11} - p_{12}}{2}$ holds. These strain-optic constants are usually expressed in terms of Neumann's p, q constants (Mueller 1937, Neumann 1841) where:

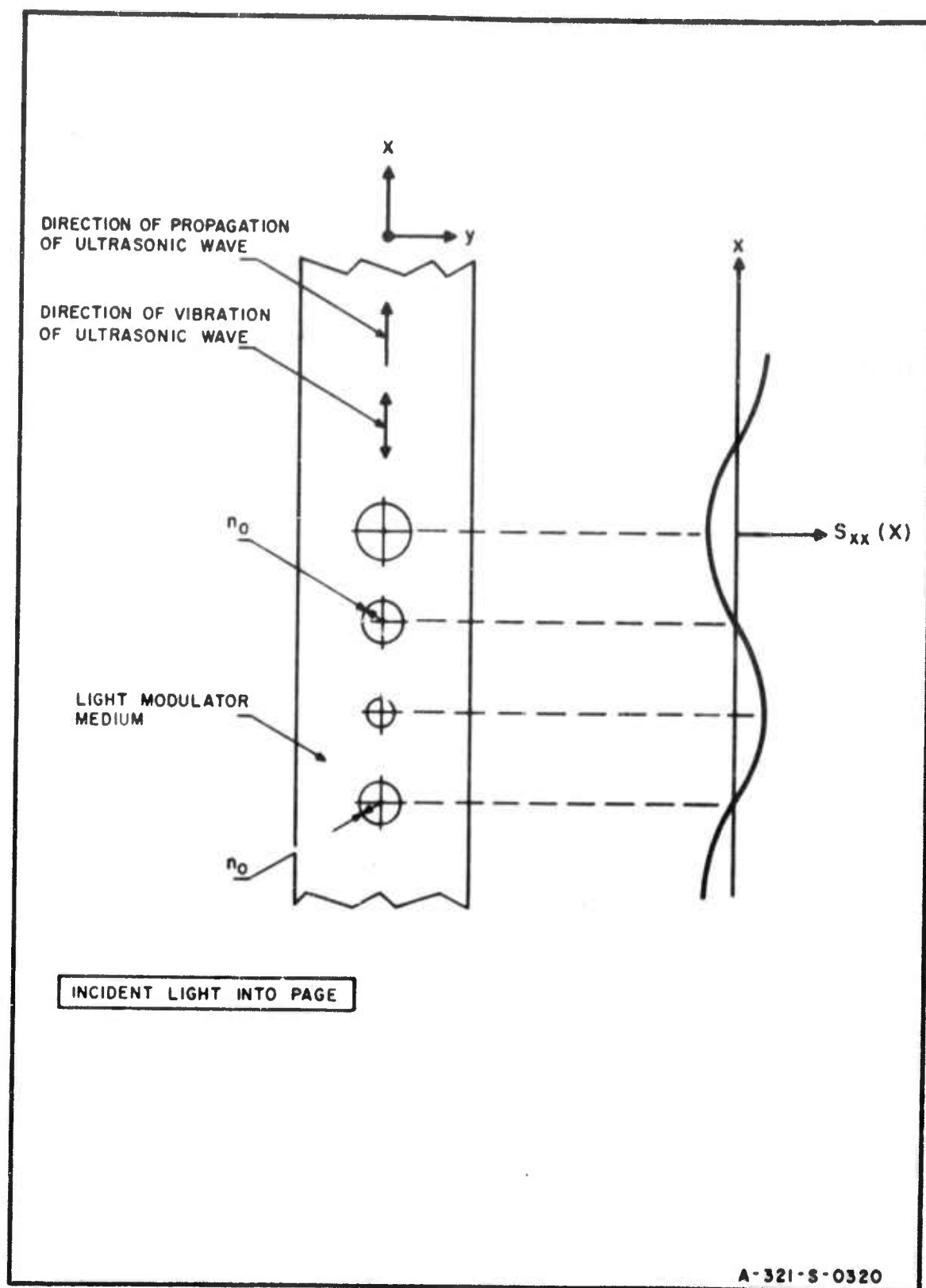


FIG. 4.3.3-2 PHOTOELASTIC INTERPRETATION OF ULTRASONIC DIFFRACTION IN LIQUIDS

COLUMBIA UNIVERSITY—ELECTRONICS RESEARCH LABORATORIES

$$p_{11} = \frac{2q}{n_o}$$

$$p_{12} = \frac{2p}{n_o}$$

$$p_{44} = \frac{q-p}{n_o}$$

Thus, in the case of sinusoidal excitation, the expressions for index of refraction become:

(i) Shear mode:

$$n_1(x) = n_o - \frac{n_o^2(q-p)}{2} \frac{1}{\mu} k_s V_m \sin 2\pi f x - \text{light polarized at } 45^\circ$$

$$n_2(x) = n_o + \frac{n_o^2(q-p)}{2} \frac{1}{\mu} k_s V_m \sin 2\pi f x - \text{light polarized at } -45^\circ$$

(4.4-1)

(ii) Compression mode:

$$n_1(x) = n_o - \frac{n_o^2 q}{C} k_c V_m \sin 2\pi f x - \text{light polarized along } x \text{ axis}$$

$$n_2(x) = n_o - \frac{n_o^2 p}{C} k_c V_m \sin 2\pi f x - \text{light polarized along } y \text{ axis}$$

(4.4-2)

It has been shown (Raman and Nath 1936) that the relative peak first-order light amplitude in the image plane of the electro-optical processor is equal to $\frac{\pi \bar{n} L}{\lambda}$, where:

\bar{n} = maximum variation of refractive index

L = length of light path in light modulator
(depth of transducer)

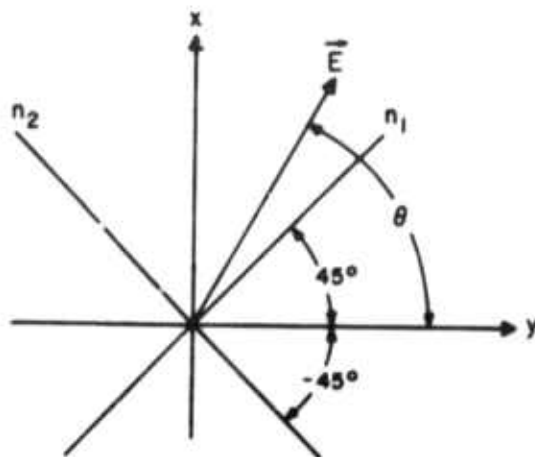
λ = light wavelength

COLUMBIA UNIVERSITY—ELECTRONICS RESEARCH LABORATORIES

Now consider the effect of light polarization on the peak first-order light amplitude. Since the coherent light sources used in the electro-optical processor produce linearly polarized light (Fox and Li 1961, Schachter 1964), this will be assumed to be the case with the angle of polarization arbitrary.

4.4.1 SHEAR MODE

Consider a beam of linearly polarized light whose electric field vector \vec{E} is inclined at an arbitrary angle θ as shown



let:

\vec{i} = unit vector in x direction

\vec{j} = unit vector in y direction

$$|\vec{E}| = 1$$

The components along $\pm 45^\circ$ will be, respectively, $\cos(\theta - \frac{\pi}{4})$ and $\sin(\theta - \frac{\pi}{4})$ which can be written vectorially as:

$$\vec{E}_1 = \frac{1}{\sqrt{2}} \cos(\theta - \frac{\pi}{4}) (\vec{i} + \vec{j})$$

$$\vec{E}_2 = \frac{1}{\sqrt{2}} \sin(\theta - \frac{\pi}{4}) (\vec{i} - \vec{j})$$

Since $\bar{n}_1 = -\bar{n}_2$ (Eq. (4.3.2-3)), the first order electric field amplitude (written vectorially) will be (Raman and Nath 1936):

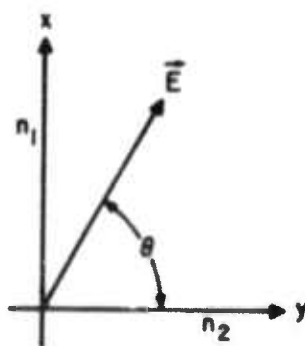
$$\begin{aligned} & \frac{\pi L}{\lambda} \cos(\theta - \frac{\pi}{4}) \frac{\bar{n}_1}{\sqrt{2}} (\vec{i} + \vec{j}) - \frac{\pi L}{\lambda} \sin(\theta - \frac{\pi}{4}) \frac{\bar{n}_1}{\sqrt{2}} (\vec{i} - \vec{j}) \\ &= \frac{\pi L}{\lambda} \frac{\bar{n}_1}{\sqrt{2}} \left(\frac{2}{\sqrt{2}} \cos \theta \vec{i} + \frac{2}{\sqrt{2}} \sin \theta \vec{j} \right) \end{aligned}$$

and the first order amplitude is $\frac{\pi L \bar{n}_1}{\lambda}$ which is identical to that which would be obtained with $\pm 45^\circ$ polarization. Note, however, that the polarization of the electric field at the output has been rotated to the angle $(90 - \theta)$.

Thus the angle of polarization has no significant effect on a light modulator operating in the transverse mode.

4.4.2 COMPRESSION MODE

In this case:



$$\vec{E}_1 = \sin \theta \vec{i}$$

COLUMBIA UNIVERSITY—ELECTRONICS RESEARCH LABORATORIES

$$\vec{E}_2 = \cos \theta \vec{j}$$

and from Eq. 4.4-2

$$\bar{n}_1 = \frac{q}{p} \bar{n}_2$$

Thus the first order electric field amplitude (written vectorially) is:

$$\frac{\pi L}{\lambda} [\bar{n}_1 \sin \theta \vec{i} + \bar{n}_2 \cos \theta \vec{j}] = \frac{\pi L \bar{n}_2}{\lambda} \left[\frac{q}{p} \sin \theta \vec{i} + \cos \theta \vec{j} \right]$$

and it is evident that, in order to maximize the peak first order light amplitude, then:

$$\frac{q}{p} > 1 \implies \text{let } \theta = \frac{\pi}{2}$$

$$\frac{q}{p} < 1 \implies \text{let } \theta = 0$$

Note that, as pointed out in Sec. 4.3.3. in an amorphous solid p cannot be equal to q .

Although p and q will vary with the composition of the medium and the light wavelength (Primak and Post 1959), it will generally be true (ibid) that, in fused silica, $p > q$. Thus the light polarization should be normal to the direction of ultrasonic propagation when longitudinal waves are used.

4.5 SUMMARY AND COMPARISON OF TRANSFER CHARACTERISTICS

The most important result of the preceding sections is that:

$$\psi_m = KV_m \quad (K = \text{constant}) \quad (4.5-1)$$

for both the shear and compression modes and independent of the angle of polarization. That is, because of the linear relationship between electrical excitation and phase modulation, it would be possible to generate in the light modulator a complex transmission function consisting of ultrasonic signals, which is an exact replica of the electrical signals which appeared at the outputs of the antenna elements. Thus it is seen that, theoretically, fused-silica light modulators employing piezoelectric ultrasonic transducers can be used in electro-optical array-antenna processing. Experiments relevant to this result will be dealt with in Chap. 7.

To summarize the specific results of this chapter, it has been shown that the relationship between the amplitude of the electrical input to a fused-silica light modulator, V_m , and the resulting peak phase deviation of the light wave front, ψ_m , is given by:

(i) Shear Mode

$$\psi_m = \frac{\pi L n_o^2 |p - q|}{\lambda} \frac{1}{u} k_s V_m \quad (4.5-2)$$

independent of polarization angle

(ii) Compression Mode

$$\psi_m = \frac{2\pi L n_o^2 p}{\lambda C} k_c \left(\sqrt{\left(\frac{q}{p} \sin \theta\right)^2 + \cos^2 \theta} \right) V_m \quad (4.5-3)$$

for arbitrary polarization angle θ

COLUMBIA UNIVERSITY—ELECTRONICS RESEARCH LABORATORIES

where:

L = depth of ultrasonic transducer

n_0 = equilibrium value of refractive index

p = Neumann's p constant

q = Neumann's q constant

$$C = B + \frac{4}{3} \mu$$

B = bulk modulus

μ = modulus of rigidity

k_s = electromechanical coupling coefficient
of shear transducer

k_c = electromechanical coupling coefficient
of compression transducer

λ = wavelength of incident light

5. OPTIMIZATION OF DESIGN OF ELECTRO-OPTICAL ARRAY-ANTENNA
PROCESSOR USING FUSED-SILICA LIGHT-MODULATOR MEDIUM

In this chapter the design of the array antenna processor using a fused-silica Debye-Sears light modulator will be optimized and the processing capacity evaluated. This problem has already been considered for liquid media (Lambert 1965). The differences which occur with the use of solids arise from the possibility of significantly higher frequencies and the use of the shear as well as the compression mode of sonic propagation. Other factors however, which must be considered for liquids as well as solids, make it possible to use a number of results which have already been established. These will be presented, briefly, for reference purposes in Secs. 5.1, 5.2.1, 5.2.3, and 5.2.4. The remaining sections (5.2.2, 5.3 and 5.4) present original results of this research. One of the limiting factors not considered in Sec. 5.2 is the size of the optical aperture. This is of course limited by the maximum size lenses which are available and a realistic constraint on the largest possible aperture width (or length) would be 6 in. (ibid).

In this analysis it will be assumed that the processor is to be applied to a planar array antenna. In order to avoid the unrealistic situation in which an apparent increase in aperture-bandwidth capability is achieved at the expense of a highly asymmetrical antenna configuration, the number of rows in the array will be constrained to be equal to the number of columns. It will be seen that, using present methods of converting electric to ultrasonic

energy, a fused-silica light modulator operating in the compression mode could enable the electro-optical processor to be applied to array antennas with aperture-bandwidth products ten times as large as those which can be processed at present; the use of more advanced ultrasonic transducers which are currently in the developmental stage (Foster 1965, Dekker and Kelly 1965) could effect a further increase in processing capacity. A concise summary of the results of this chapter and the relationships between the important system parameters will be presented in Appendix D.

5.1 SIGNAL-PROCESSING CAPACITY AND APERTURE-BANDWIDTH PRODUCT

Consider a planar array with its elements in M rows and N columns and with a spacing between adjacent elements in any of the rows or columns equal to a half-wavelength of the transmitted signal carrier. Then, if the bandwidth of the signal is B , the aperture-bandwidth product (ABP) would be given by:

$$ABP = \frac{M}{2} \times \frac{N}{2} \times B$$

The signal-processing capacity (P) for the electro-optical array processor has been defined (Lambert 1965) in terms of the maximum number of antenna elements and the maximum bandwidth signal which can be processed. That is:

$$P = M \times N \times B \quad (5.1-1)$$

thus when, as is generally the case (Skolnick 1962), the array has a half-wavelength spacing between elements, the signal-processing capacity is proportional to the aperture-bandwidth product.

Let:

D = optical aperture length

W = optical aperture width

S = sonic velocity

f_i = frequency of electrical signal
exciting transducers

T = signal duration

The acoustic bandwidth of the light modulator can be maintained at 50 per cent of the resonant transducer frequency if the transducer is properly matched and bonded to the light-modulator medium. Thus assume the light-modulator bandwidth to be:

$$B = \frac{f_i}{2} \quad (5.1-2)$$

and, if it is further assumed that the signals under consideration are those for which $BT \approx 1$, the following relationships can be shown (Lambert 1965) to hold:

$$N = \frac{W}{2} \sqrt{\frac{f_i}{DS}} \quad (5.1-3)$$

$$M = \frac{Df_i}{2S} \quad (5.1-4)$$

and the maximum signal-processing capacity becomes:

$$P = M \times N \times B = \frac{W\sqrt{D}}{8} \frac{f_i^{3/2}}{S^{3/2}} \quad (5.1-5)$$

Hence P increases with frequency.

In fused silica the velocity of propagation of longitudinal waves is greater than that of transverse waves which, from Eq. (5.1-5), appears to favor the shear mode. It will be seen however that processing capacity can in fact be maximized by the compression mode, since it will permit operation at significantly higher frequencies.

Equation (5.1-5) will be used in Secs. 5.3 and 5.4 to evaluate the signal-processing capacity of fused-silica light modulators. It is seen that the relevant experimental investigations, which are necessary in order to justify the use of this expression for fused-silica light modulators, are related to Eq. (5.1-3), which determines the maximum number of light-modulator channels for a given aperture size, and the light-modulator bandwidth which is assumed in the derivation of Eq. (5.1-5) to be 50 per cent of the resonant transducer frequency.

5.2 LIMITATIONS ON SIGNAL-PROCESSING CAPACITY

5.2.1 ACOUSTIC ATTENUATION

The amplitude of a sinusoidal ultrasonic wave will undergo an exponential attenuation as it propagates (Mason 1964). That is, if propagation is in the x direction and the amplitude at $x = 0$ is $A(0)$, then the amplitude at some value $x_0 > 0$ will be:

$$A(x_0) = A(0) e^{-\alpha x_0}$$

The constant α is referred to as the acoustic attenuation of the medium in units of nepers per cm. An expression for acoustic attenuation of longitudinal waves in fused silica (in units of decibels per cm) is given by (Mason 1964):

$$A(\text{db cm}) = 3 \times 10^{-4} f + 1.9 \times 10^{-5} f^2 \quad (f \text{ in MHz})$$

(5.2.1-1)

Transverse waves have not been as carefully measured but the loss appears to be the same for the same signal duration (ibid). However, since the velocity of transverse waves in fused silica is about 63 per cent of the velocity of longitudinal waves, then the path length for transverse waves will also be shorter by this same amount; hence α for transverse waves is greater than it is for longitudinal waves in this medium.

Another source of data of this kind (Lamb, Redwood and Shteinshleifer, 1959; see Fig. 5.2.1-1) shows that, in the case of longitudinal waves above 100 MHz, the linear term becomes negligible and acoustic attenuation is approximately proportional to frequency squared in this range.

Acoustic attenuation has been shown (Lambert 1965) to cause an attenuation in peak first order intensity as well as a deterioration in the structure of the diffraction pattern. The important parameter in this case has been shown (ibid) to be the acoustic attenuation factor, a , defined as:

$$a = \frac{\alpha D}{2}$$

The effect of acoustic attenuation on the diffraction patterns is shown in Fig. 5.2.1-2.

5.2.2 INTERNAL REFRACTION

Consider a small section of the wave front of a light beam in a medium with a spatially-varying index of refraction (Fig. 5.2.2-1). Let $n(r)$ increase with decreasing r .

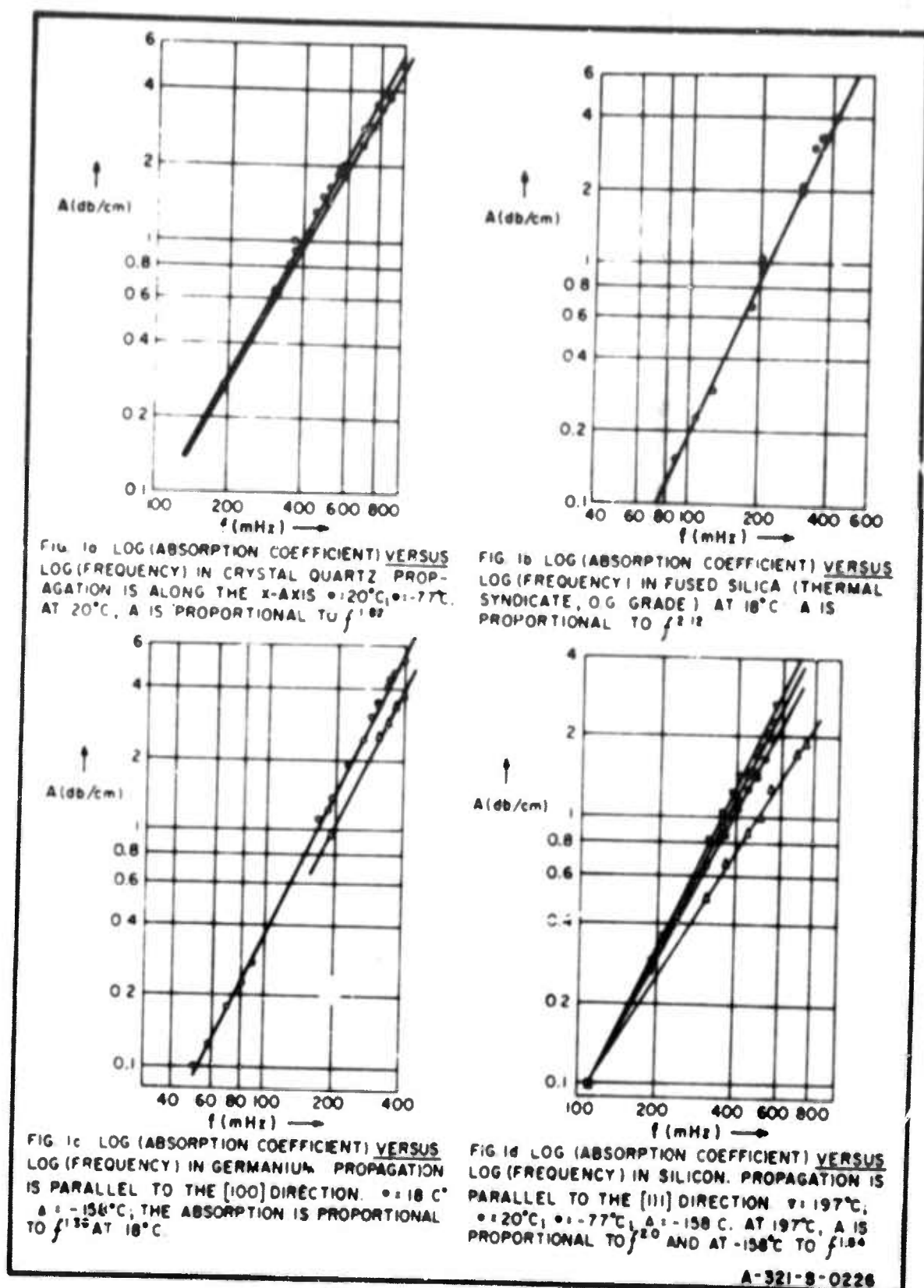


FIG. 5.2.1-1 ACOUSTIC-LOSS CHARACTERISTICS FOR COMPRESSION MODE IN VARIOUS SOLIDS
(LAMB, REDWOOD, SHTEINSHLEIFER, 1959)

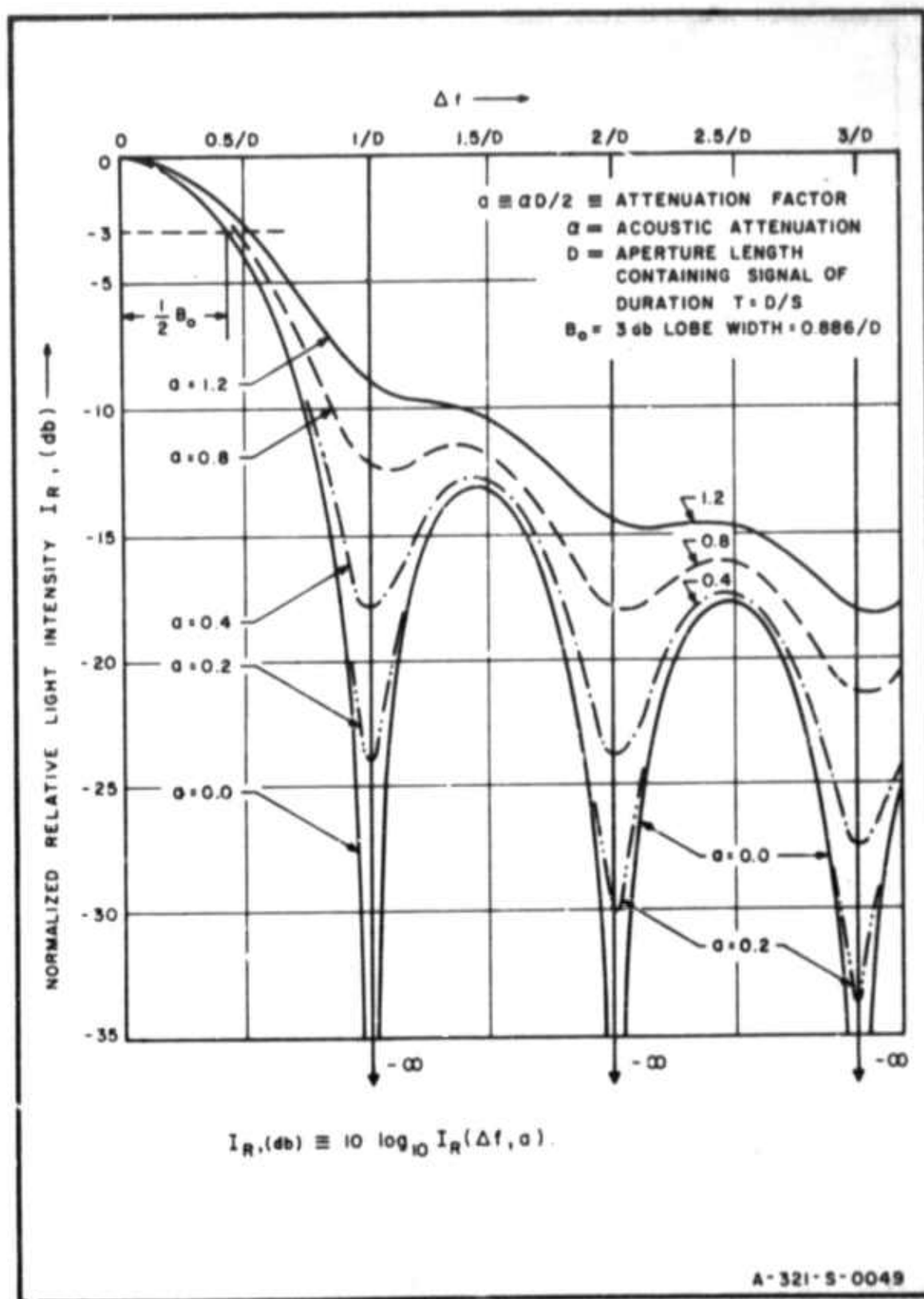


FIG. 5.2.1-2 EFFECTS OF ACOUSTIC ATTENUATION ON DIFFRACTION PATTERNS
(LAMBERT, 1965)

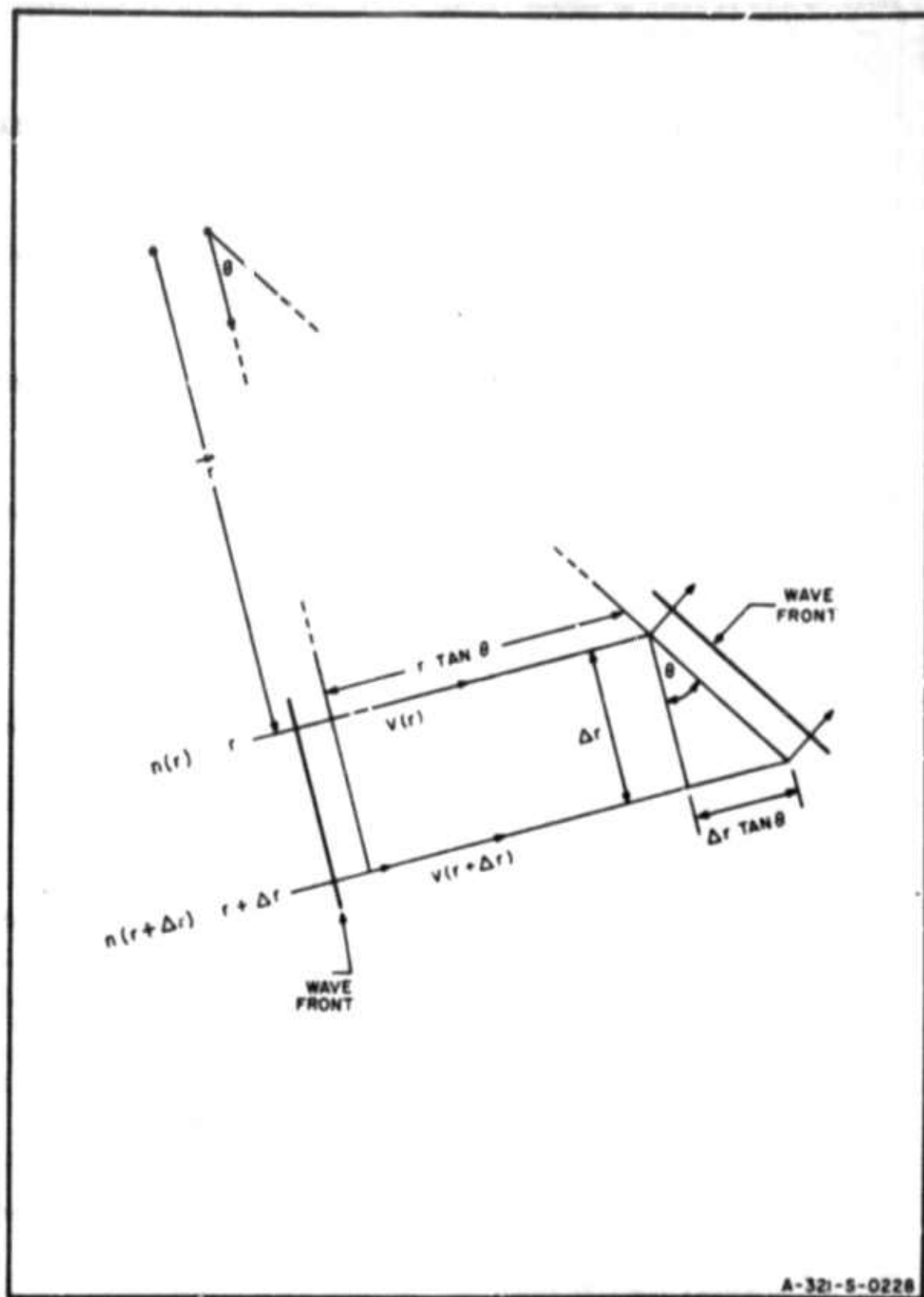


FIG. 5.2.2-1 EFFECT OF REFRACTIVE INDEX VARIATION ON DIRECTION OF LIGHT WAVE FRONT

The ray at the point r will have a velocity $v(r) = c/n(r)$. Since $n(r)$, the index of refraction at the point r , is assumed to be greater than $n(r + \Delta r)$, then $v(r + \Delta r) > v(r)$, and, in some time Δt , the ray at $r + \Delta r$ will traverse a greater distance than the ray at r which results in a change of direction of the wave front as shown. Thus the unit wave normal, perpendicular to the portion of the wave front under consideration, will have a certain trajectory as the light passes through the medium as shown in Fig. 5.2.2-2a. To determine this trajectory observe that in some time Δt :

$$v(r + \Delta r)\Delta t - v(r)\Delta t = \Delta r \tan \theta$$

but

$$\tan \theta = \frac{v(r)}{r} \Delta t$$

hence

$$\frac{v(r + \Delta r) - v(r)}{\Delta r} = \frac{v(r)}{r}$$

Now

$$v(r) = \frac{c}{n(r)}$$

and

$$\lim_{\Delta r \rightarrow 0} \frac{v(r + \Delta r) - v(r)}{\Delta r} = \frac{\partial v(r)}{\partial r} = c \frac{\partial}{\partial r} \left(\frac{1}{n(r)} \right)$$

hence in the limit

$$\frac{1}{r} = n \frac{\partial}{\partial r} \left(\frac{1}{n} \right) = -\frac{1}{n} \frac{\partial n}{\partial r} \quad (5.2.2-1)$$

Note that $\partial n / \partial r$, the partial derivative of n in the direction of increasing r , is negative in this example by

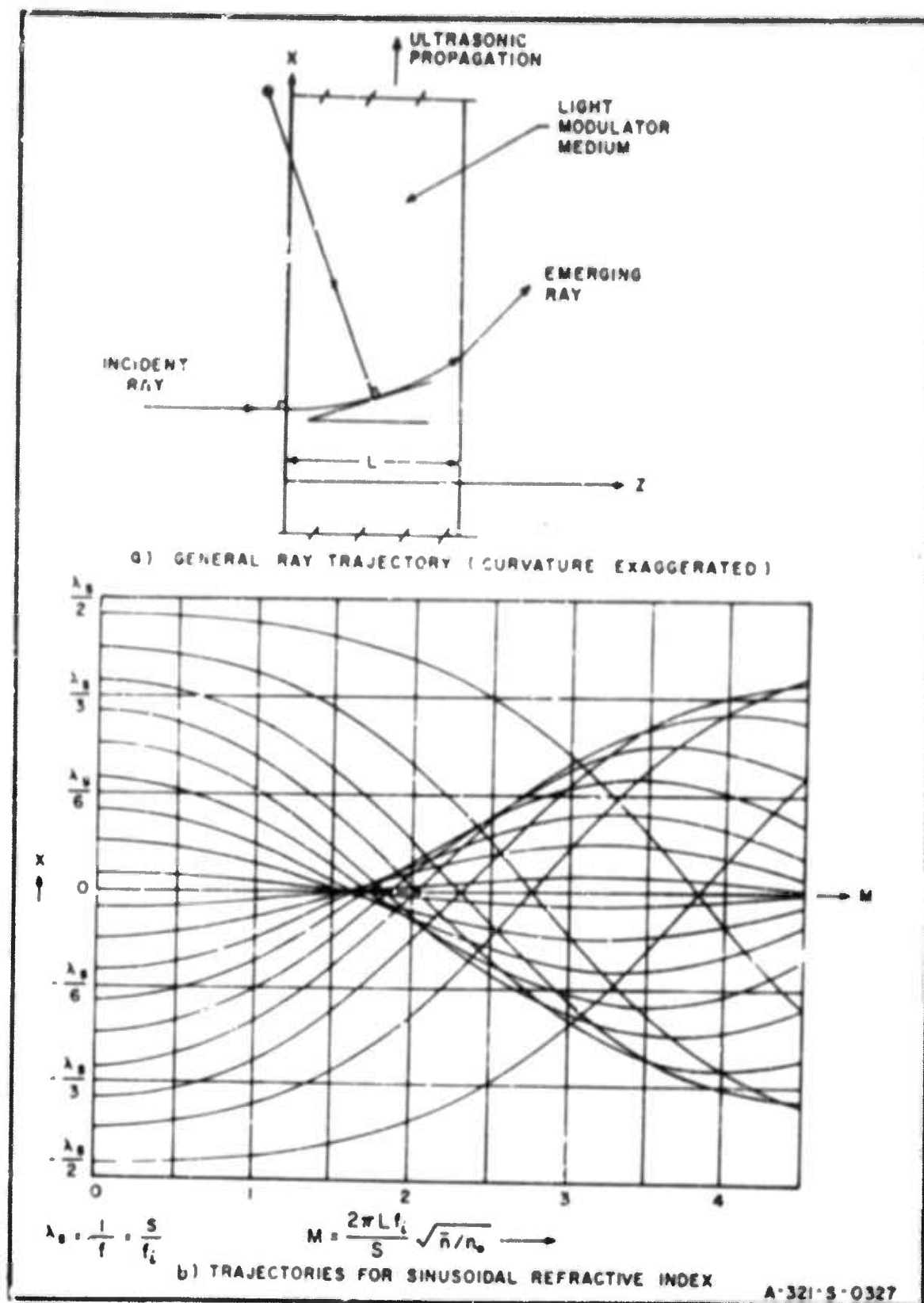


FIG. 5.2 2-2 TRAJECTORIES OF RAYS ACROSS ULTRASONIC BEAM: NORMAL LIGHT INCIDENCE

definition. Thus the curvature of the trajectory, $1/r$, is positive as shown.

This expression can now be used to obtain a differential equation for the ray trajectory in the medium, since in general:

$$\frac{1}{r} = \frac{\frac{d^2x}{dz^2}}{\left[1 + \left(\frac{dx}{dz}\right)^2\right]^{3/2}} \quad (5.2.2-2)$$

and from which it can be shown that:

$$\frac{d^2x}{dz^2} = \frac{1}{n} \frac{\partial n}{\partial x} \left[1 + \left(\frac{dx}{dz}\right)^2\right] \quad (5.2.2-3)$$

This nonlinear differential equation has been solved by Lucas and Biquard (Lucas and Biquard 1932), and the light-ray trajectories have been determined for refractive index of the form:

$$n(x) = n_0 + \bar{n} \cos 2\pi f x \quad (5.2.2-4)$$

Because of this form of the index of refraction, the results are directly applicable to the electro-optical processor under consideration. The trajectories arising from Eq. (5.2.2-3) are plotted in Fig. 5.2.2-2b as a function of the parameter M , given by:

$$M = \frac{2\pi f_1 L}{s} \sqrt{\frac{\bar{n}}{n_0}} \quad (5.2.2-5)$$

Consider the effects of these ray trajectories. It is seen that as M approaches $\frac{\pi}{2}$ the light rays will become increasingly clustered about the points $x = 0, \pm \frac{1}{f}, \pm \frac{2}{f}$ etc.

thus internal refraction tends to impose periodic amplitude modulation on the incident light. The point at which the ray trajectories first intersect is at $M = \frac{\pi}{2}$ which defines the point at which "abnormal diffraction" (Willard 1949, Bhavagantam and Rao 1946, 1947, 1948) occurs. This refers to the fact that the theory of Raman and Nath ("normal diffraction") is not valid* when $M > \frac{\pi}{2}$ since the ultrasonic disturbance can no longer be treated as a pure phase grating (Willard 1949).

Under these conditions the diffracted light distribution can be obtained by applying Maxwell's equations. A number of solutions have been obtained (Mertens 1950, Bhatia and Noble 1953, Phariseau 1959) and it has been found that the diffracted light intensity in the case of significant amplitude modulation can be determined for oblique as well as normal light incidence.

Raman-Nath theory can however be used to determine the diffraction patterns if the amplitude modulation is not too severe. It is evident that, when the ultrasonic disturbance can be treated as a phase grating, the value of peak phase deviation, ϕ_m , will be dependent on the difference in optical path lengths between a ray entering the light modulator at a point where $n(x)$ is a maximum and a ray entering where $n(x)$ has its minimum value. But although a ray entering at the point $x = 0$ (Fig. 5.2.2-2b) will pass straight through, the light rays entering the light modulator in regions of lower refractive index will, because of their curved paths, experience greater optical path lengths than if their paths were not curved. Raman-

* Willard's criterion

COLUMBIA UNIVERSITY—ELECTRONICS RESEARCH LABORATORIES

Nath theory is based on the approximation that the paths of all the rays are straight. Thus, to a first approximation, it is to be expected that the effect of internal refraction is to cause a decrease in peak phase deviation, and therefore an attenuation of the resulting first-order light intensity.

This result has been established by Rao and Murty (Rao and Murty 1958). It has been shown under the assumptions:

$$(i) \quad \psi_m < 1 \quad (5.2.2-6)$$

(ii) The incident light is normal to the direction of ultrasonic propagation

$$(iii) \quad \frac{n_o \bar{n} s^2}{\lambda^2 f_i^2} < < 1$$

where

\bar{n} = maximum perturbation of refractive index

n_o = equilibrium value of refractive index

λ = light wavelength

L = depth of ultrasonic beam

s = velocity of propagation of ultrasonic wave

that internal-refraction effects will cause the first-order intensity to be attenuated by the factor:

$$\left(\frac{\sin \frac{\pi \lambda L f_i^2}{2 n_o s^2}}{\frac{\pi \lambda L f_i^2}{2 n_o s^2}} \right)^2 \quad (5.2.2-7)$$

That is, if the ideal peak first-order intensity is:

$$I_1 = k \frac{\psi_m^2}{4}$$

where k = constant

then, under the above assumptions, internal-refraction effects will result in a first-order light intensity given by:*

$$I_{1r} = k \frac{\psi_m^2}{4} \left(\frac{\sin \gamma}{\gamma} \right)^2 \quad (5.2.2-8)$$

where

$$\gamma = \frac{\pi \lambda L f_1^2}{2 n_o s^2} \quad (5.2.2-9)$$

The assumptions of Rao and Murty, however, are consistent with the operating conditions of the electro-optical array-antenna processor (Lambert 1965). Thus it should be possible to use Raman-Nath theory to predict the diffraction patterns, and to take account of internal-refraction effects in electro-optical processing by including the attenuation-factor $\frac{\sin \gamma}{\gamma}$.

In considering the conditions under which Raman-Nath theory must be modified because of internal-refraction effects, it is seen from Eqs. (5.2.2-5) and (5.2.2-7) that, regardless of the frequency, these effects will always be negligible if the transducer depth, L , is made small enough. The question now arises, "How small must this dimension be?" In order to answer this question, consider the attenuating

* It has been shown in fact (Rao and Murty 1958) that the more general solution of Bhatia and Noble reduces to the solution of Rao and Murty if the above assumptions are valid.

COLUMBIA UNIVERSITY—ELECTRONICS RESEARCH LABORATORIES

effects of internal refraction on the peak phase deviation and define the effective phase modulation, $\bar{\psi}_m$, as:

$$\bar{\psi}_m = \frac{\sin \gamma}{\gamma} \psi_m \quad (5.2.2-10)$$

where:

$$\psi_m = \frac{2\pi n L}{\lambda}$$

Now although the attenuation due to internal refraction decreases with a decrease in L , there is also a decrease in phase modulation ψ_m . Thus there should be some value of L such that $\sin \gamma/\gamma$ and ψ_m combine to yield a maximum effective phase modulation $\bar{\psi}_m$. In order to find this value of L take $d\bar{\psi}_m/dL = 0$. Hence:

$$\frac{d}{dL}(\bar{\psi}_m) = 0 = \frac{2\pi n}{\lambda} \frac{\sin \gamma}{\gamma} + \frac{2\pi n L}{\lambda} \left[\frac{\cos \gamma}{\gamma} - \frac{\sin \gamma}{\gamma^2} \right] \frac{d\gamma}{dL} = 0$$

But

$$L \frac{d\gamma}{dL} = \gamma$$

Thus for maximum $\bar{\psi}_m$ we obtain:

$$\cos \gamma = 0 \implies \gamma = \frac{\pi}{2}, \frac{3\pi}{2}, \text{ etc.}$$

Since $\gamma > \pi$ would carry the factor $\sin \gamma/\gamma$ out of its main lobe and into the side-lobe region, the only satisfactory solution is $\gamma = \pi/2$.

Hence

$$\frac{\pi \lambda L f_1^2}{2n_0 s^2} = \frac{\pi}{2}$$

and

$$L_{\text{opt}} = \frac{n_o s^2}{\lambda f_i^2} \quad (5.2.2-11)$$

Thus L_{opt} is the smallest value of transducer depth which would be made necessary by internal-refraction considerations.

It is necessary to consider this result with regard to the restrictions imposed by Willard's criterion and by the assumptions of Rao and Murty. With regard to Willard's criterion, we must have:

$$M = \frac{2\pi L f_i}{s} \sqrt{\frac{\bar{n}}{n_o}} < \frac{\pi}{2} \quad (5.2.2-12)$$

But

$$\psi_m = \frac{2\pi \bar{n} L}{\lambda}$$

Thus, if

$$L = \frac{n_o s^2}{\lambda f_i^2},$$

then

$$\bar{n} = \frac{\psi_m}{2\pi} \frac{\lambda^2 f_i^2}{n_o s^2},$$

and substituting these values of L and \bar{n} into Eq. (5.2.2-12) results in:

$$\psi_m < \frac{\pi}{8} = 0.39 \quad (5.2.2-13)$$

COLUMBIA UNIVERSITY—ELECTRONICS RESEARCH LABORATORIES

This is consistent with established practice since it is generally desirable to restrict the phase modulation to $\psi_m \leq 0.2$.

With regard to the restriction,

$$\frac{n_o \bar{n} S^2}{\lambda^2 f_i^2} \ll 1 ,$$

let the phase modulation have its maximum value of $\pi/8$. Then, if

$$L = \frac{n_o S^2}{\lambda f_i^2} ,$$

then

$$\bar{n} = \frac{\lambda^2 f_i^2}{16 n_o S^2}$$

and

$$\frac{n_o \bar{n} S^2}{\lambda^2 f_i^2} = \frac{1}{16} \ll 1$$

It should therefore be possible to operate with this value of ultrasonic-beam depth (Eq. (5.2.2-11)) provided the necessary restriction on ψ_m as shown by Eq. (5.2.2-13) is adhered to. Note that the optimal value of L results from $\gamma = \pi/2$. Hence in this case the operation will be such that the internal-refraction attenuation factor will always have the value $2/\pi$.

In order to give an approximate idea of the effects of internal refraction Figs. 5.2.2-3 and 5.2.2-4 are included. Each figure presents a plot of L vs γ , with f_i as a parameter, according to the relationship:

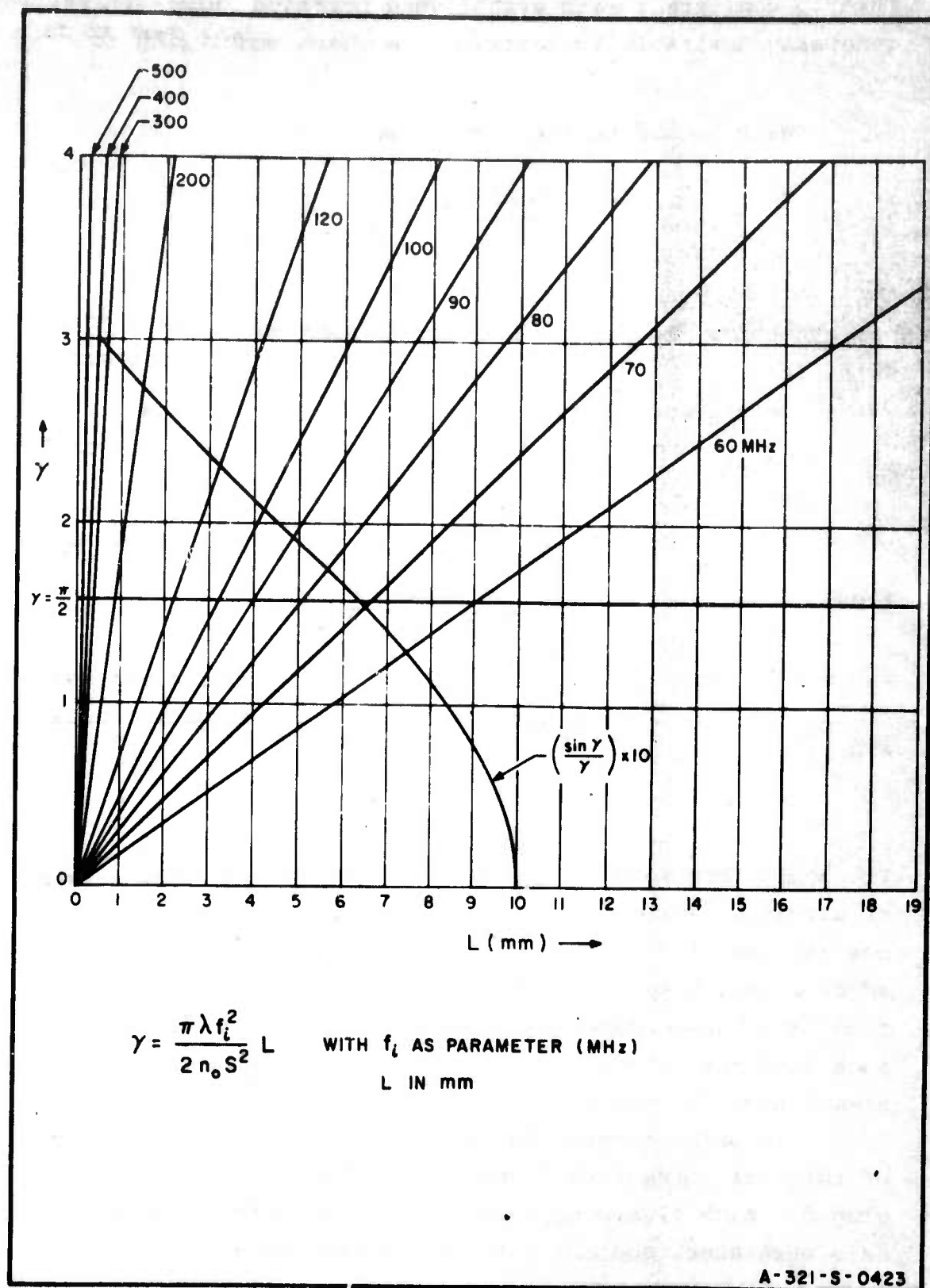


FIG. 5.2.2-3 TRANSDUCER DEPTH (L) vs. γ FOR SHEAR MODE

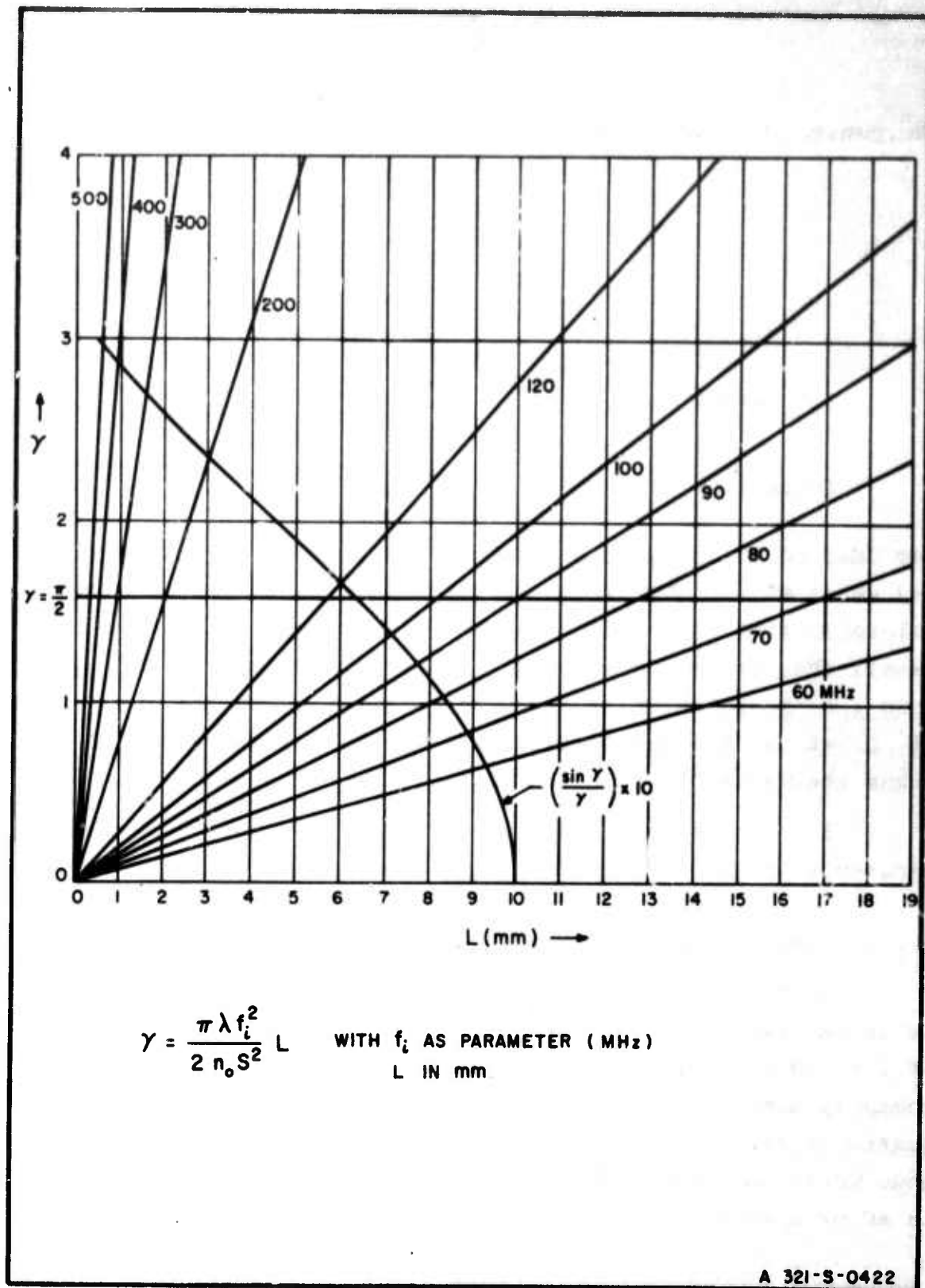


FIG. 5.2.2-4 TRANSDUCER DEPTH (L) vs. γ FOR COMPRESSION MODE

COLUMBIA UNIVERSITY—ELECTRONICS RESEARCH LABORATORIES

$$\gamma = \frac{\pi \lambda f_1^2}{2n_0 S^2} L$$

The nominal values of the parameters have been assumed to be;

$$n_0 = 1.46$$

$$\lambda = 6328 \times 10^{-10} \text{ m}$$

$$S \Big|_{\text{shear mode}} = 3760 \text{ m/sec}$$

$$S \Big|_{\text{compression mode}} = 5968 \text{ m/sec}$$

Included on the abscissa with L is $\frac{\sin \gamma}{\gamma}$; thus for any value of L and f_1 the corresponding amount of internal-refraction attenuation can be determined. In addition, recall that operation with L_{opt} corresponds to $\gamma = \pi/2$. Thus the intersection of the line $\gamma = \pi/2$ with the graph of L vs γ for any particular value of the parameter f_1 gives the value of L_{opt} for that value of frequency.

It is necessary that these results be investigated experimentally, and this will be dealt with in Chap. 7.

5.2.3 LIMITATIONS IMPOSED BY ULTRASONIC TRANSDUCER

In order to operate the Debye-Sears light modulator it is necessary to transform electrical signals into mechanical vibrations of the light-modulator medium. The most commonly used ultrasonic transducers employ piezoelectric quartz crystals. In a fused-silica light modulator a shear mode would be generated by a piezoelectric transducer using an AC or a Y-cut quartz crystal, and a compression-mode

COLUMBIA UNIVERSITY—ELECTRONICS RESEARCH LABORATORIES

transducer would use an X-cut crystal. The well-known relationship between crystal thickness and resonant frequency are:

$$d = \frac{2.85}{f_o} \quad \text{X-cut} \quad (5.2.3-1)$$

$$d = \frac{1.92}{f_o} \quad \text{Y-cut} \quad (5.2.3-2)$$

$$d = \frac{1.64}{f_o} \quad \text{AC-cut} \quad (5.2.3-3)$$

where

d = crystal thickness (mm)

f_o = resonant frequency (MHz)

Thus the factors which limit high-frequency piezoelectric quartz transducers are concerned with the extremely small dimensions which are necessary. At present,* thicknesses of the order of .0095 mm are possible, and the corresponding frequencies for the shear and compression modes are:

(i) Compression mode

$$f_o = 300 \text{ MHz (X-cut)}$$

(ii) Shear mode

$$f_o = 200 \text{ MHz (Y-cut)}$$

$$f_o = 175 \text{ MHz (AC-cut)}$$

These quantities will be used in Sec. 5.3 in evaluating the processing capacity of fused-silica light modulator employing piezoelectric quartz transducers.

* Private communication from Valpey Co.

In addition to these methods, the conversion of electric to ultrasonic energy has also been accomplished (Foster 1965, DeKlerk and Kelly 1965) by means of evaporated thin-film transducers. Although these methods are at present in the developmental stage, it appears that frequencies as high as 1000 MHz would be feasible; possible gains in signal-processing capacity for the electro-optical array-antenna processor using evaporated thin-film transducers will be considered in Sec. 5.4.

5.2.4 LIMITATIONS IMPOSED BY ULTRASONIC BEAM BROADENING AND CROSS-CHANNEL COUPLING

The expression for the maximum number of light-modulator channels, N , which may be fitted into a given aperture size is (Eq. 5.1-3);

$$N = \frac{W}{2} \sqrt{\frac{f_i}{DS}} \quad (5.2.4-1)$$

where

W = aperture width

D = aperture length (dimension along direction of sonic propagation)

f_i = input electrical frequency

S = velocity of ultrasonic propagation

In the derivation of this relationship (Lambert 1965) the limiting factors have been shown to be the electromechanical coupling between adjacent transducers, and cross talk between adjacent ultrasonic channels due to broadening of the ultra-

COLUMBIA UNIVERSITY—ELECTRONICS RESEARCH LABORATORIES

sonic beam in propagation (Freedman 1962, Mason 1964). The beam spreading results from the fact that a propagating ultrasonic wave undergoes diffraction in a manner analogous to an electromagnetic wave in space. Calculations based on the assumption of longitudinal waves show that there is a Fresnel region for which the wave is essentially plane and in which the beam is collimated. For a transducer of width b , this region is approximately given by (Freedman 1962):

$$x \leq .25 \frac{b^2}{\lambda_s} \quad (5.2.4-2)$$

where:

x = direction of sonic propagation

λ_s = sonic wavelength = $\frac{1}{f}$

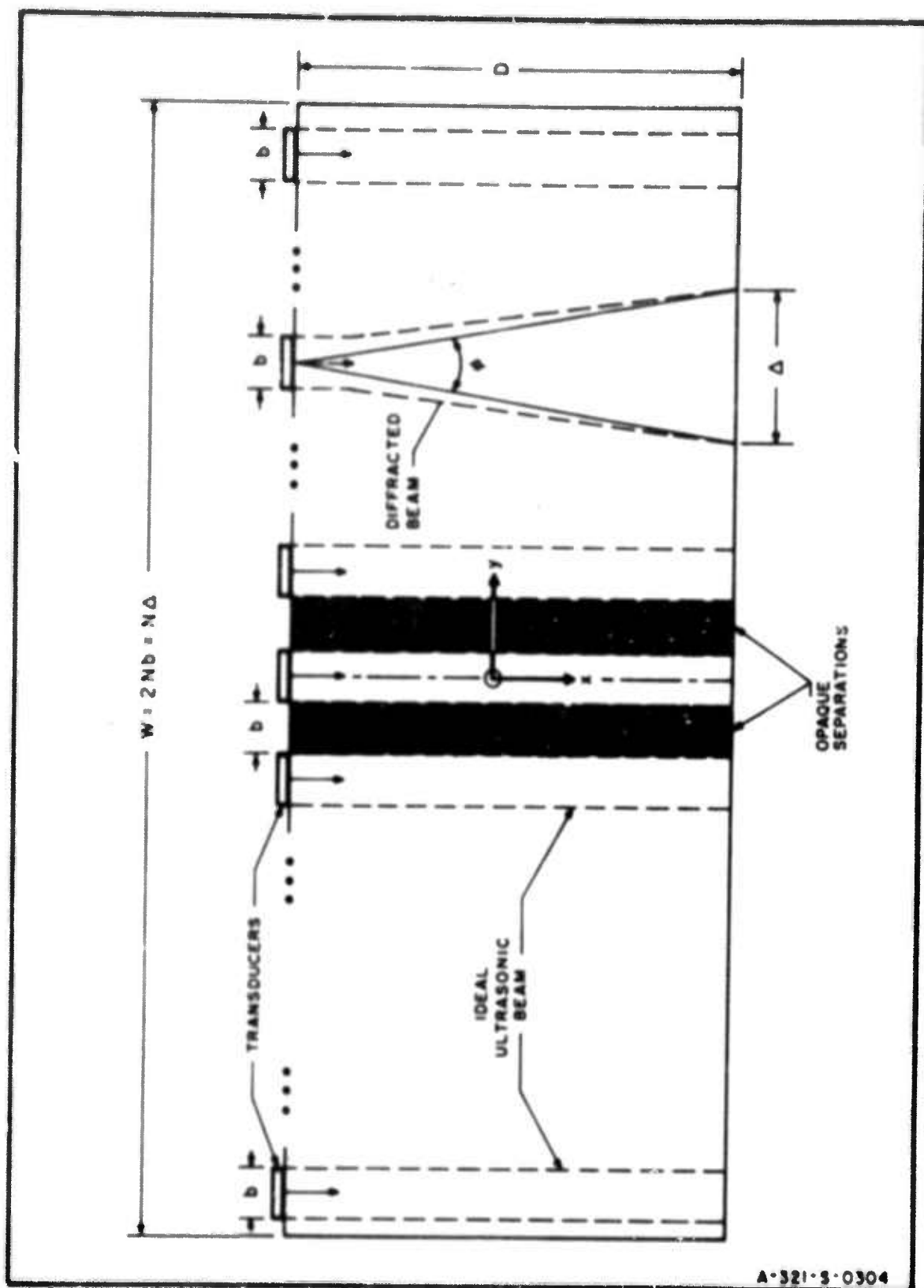
f = ultrasonic spatial frequency
(cycles per meter)

Beyond this distance the ultrasonic energy spreads out at an angle ϕ determined by the equation (Mason 1964):

$$\sin\left(\frac{\phi}{2}\right) = \frac{\lambda_s}{b}$$

which results in a spreading width, Δ (Fig. 5.2.4-1). In order to eliminate "cross-talk" the maximum number of channels has been constrained to be (Lambert 1965):

$$N \leq \frac{W}{\Delta} \quad (5.2.4-3)$$



A-321-S-0304

FIG. 5.2.4-1 ULTRASONIC DIFFRACTION IN A SPATIALLY-MULTIPLEXED DEBYE-SEARS LIGHT MODULATOR

COLUMBIA UNIVERSITY—ELECTRONICS RESEARCH LABORATORIES

where W is the aperture width.

Because of electromechanical cross-channel coupling, it was found (ibid) that the adjacent channels should be spaced by one transducer width. Thus:

$$N = \frac{W}{2b} \quad (5.2.4-4)$$

and Eq. (5.2.4-1) follows from Eqs. (5.2.4-3) and (5.2.4-4).

It is easily shown that Eqs. (5.2.4-1) and (5.2.4-4) are equivalent to:

$$D = \frac{b^2}{\lambda_s} \quad (5.2.4-5)$$

Thus some spreading of the ultrasonic beam can be tolerated since the spacing of adjacent channels will eliminate cross-talk.

Evaluation of signal-processing capacity is dependent upon Eq. (5.2.4-1). Although the equation is known to be valid for liquid light modulators, it will be necessary to verify this relationship, experimentally, for the fused-silica light modulator.

5.3 MAXIMIZATION OF SIGNAL-PROCESSING CAPACITY: TRANSDUCER LIMITED

The maximum value of signal-processing capacity for a fused-silica light modulator using piezoelectric quartz transducers will be obtained in this section and compared

COLUMBIA UNIVERSITY—ELECTRONICS RESEARCH LABORATORIES

with the values which can be obtained with the optimal liquid light modulator. For the reasons given in the introduction to this chapter the number of rows in the array will be constrained to be equal to the number of columns, and the maximum aperture width will be assumed to be 6 in.

From Eqs. (5.1-3) and (5.1-4) it is easily shown that:

$$M = N \implies W = D^{3/2} \left(\frac{f_i}{S} \right)^{1/2}$$

$$\text{and } D = W^{2/3} \left(\frac{S}{f_i} \right)^{1/3} \quad (5.3-1)$$

We now consider acoustic-attenuation effects.

$$\text{let: } \begin{array}{l} S | \\ \text{shear} \end{array} = 3760 \text{ m/sec}$$

$$\begin{array}{l} S | \\ \text{comp.} \end{array} = 5968 \text{ m/sec} \quad (5.3-2)$$

From Sec. 5.2.3 (using the Y-cut shear transducer):

$$\begin{array}{l} f_i | \\ \text{shear} \end{array} = 200 \text{ MHz}$$

$$\begin{array}{l} f_i | \\ \text{comp.} \end{array} = 300 \text{ MHz} \quad (5.3-3)$$

Thus for an aperture 6 in. wide:

$$W = 6(2.54) \times 10^{-2} = .1524 \text{ m.}$$

and (Eq. 5.3-1):

$$E \Big|_{\text{shear}} = .750 \text{ cm}$$

$$D \Big|_{\text{comp.}} = .775 \text{ cm} \quad (5.3-4)$$

Note that W rather than D is the limiting aperture dimension.

It has been reported (Mason 1964) that the acoustic attenuation for the shear and compression modes is approximately the same for the same signal duration. Thus let:

$$\alpha \Big|_{\text{shear}} = \frac{5968}{3760} \alpha \Big|_{\text{comp.}} \quad (5.3-5)$$

where α is the acoustic attenuation in nepiers per cm. Thus Eq. (5.2.1-1) becomes approximately:

$$\alpha \Big|_{\text{shear}} = 13.80 \times 10^{-2} \text{ nepiers/cm}$$

$$\alpha \Big|_{\text{comp.}} = 19.80 \times 10^{-2} \text{ nepiers/cm}$$

In evaluating acoustic-attenuation effects, the parameter $a = \frac{\alpha D}{2}$ is of interest. Thus:

$$a \Big|_{\text{shear}} = \frac{(.138)(.75)}{2} = .052$$

$$a \Big|_{\text{comp.}} = \frac{(.198)(.775)}{2} = .077$$

and from Fig. 5.2.1-2 it is seen that, for either mode, acoustic attenuation will be a negligible factor.

Now consider the signal-processing capacity, P , for the two modes. Recall that (Eq. 5.1-5):

$$P = \frac{W\sqrt{D}}{8} \left(\frac{f_1^5}{s^3} \right)^{1/2} \quad (5.3-6)$$

and since (Eq. 5.3-1):

$$D = W^{2/3} \left(\frac{s}{f_1} \right)^{1/3} \quad (5.3-7)$$

then for a given value of W :

$$P = \frac{W^{4/3}}{8} \left(\frac{f_1^7}{s^4} \right)^{1/3} \quad (5.3-8)$$

Let

$$f_s = f_1 \quad \text{for shear mode}$$

$$f_c = f_1 \quad \text{for compression mode}$$

$$\text{Then} \quad P_c = \left(\frac{f_c}{f_s} \right)^{7/3} \left(\frac{s_s}{s_c} \right)^{4/3} P_s \quad (5.3-9)$$

and finally, using Eqs. (5.3-2) and (5.3-3):

$$P_c \approx 1.4 P_s \quad (5.3-10)$$

Thus although the sonic velocity of the compression mode is greater than that of the shear mode, it nevertheless

COLUMBIA UNIVERSITY—ELECTRONICS RESEARCH LABORATORIES

provides for a greater processing capacity and is therefore optimal. This will be discussed further in Sec. 5.5.

Now consider the optimal liquid light modulator medium. This has been shown (Lambert 1965) to be distilled water. A realistic maximum frequency for this medium is (ibid) 50 MHz, which implies a bandwidth of 25 MHz if the transducer is properly loaded. The sonic velocity in distilled water is approximately 1500 m/sec, and if P_w is the maximum processing capacity for a distilled-water light modulator then, using the optimal mode of propagation:

$$P_c = \left(\frac{300}{50}\right)^{7/3} \left(\frac{1500}{5968}\right)^{4/3} P_w \approx 10P_w$$

Thus the processing capacity can be increased by a factor of ten with the use of a fused-silica light modulator and piezoelectric quartz transducers. Using Eq. 5.1-4 or 5.1-3, it is easily seen that:

$$M = N \approx 185 \quad \text{antenna elements}$$

and, for this operating frequency, the bandwidth of the piezoelectric quartz transducer bonded to the fused-silica light modulator would be, without any additional transducer loading:

$$B = 150 \text{ MHz}$$

Finally, the transducer width in this configuration would be:

$$b = .4 \text{ mm}$$

and, from Fig. 5.2.2-4, the smallest value of transducer depth which would be made necessary by internal-refraction effects is approximately:

$$L = 1 \text{ mm}$$

5.4 MAXIMIZATION OF SIGNAL-PROCESSING CAPACITY: FUSED-SILICA MEDIUM

In Sec. 5.2.2 it has been shown that internal-refraction effects can be made negligible by reducing the transducer depth, and the smallest depth which would be necessary has been found to be:

$$L_{\text{opt}} = \frac{n_o s^2}{\lambda f_i^2} \quad (5.4-1)$$

In this section a second criterion for the minimum transducer depth is now introduced. This is that the transducer depth can be made no smaller than its width. It can be seen from Eqs. (5.2.4-2) and (5.2.4-5) that if the transducer depth were made any smaller, then in addition to the effects of beam spreading in terms of the variable y (Fig. 5.2.4-1), which can cause cross-talk between adjacent channels, it would also be necessary to consider the spreading of the ultrasonic beam in terms of the variable z (Fig. 2.1-2), which defines the direction of light propagation.

Thus, using this criterion, and applying the constraints mentioned at the beginning of Sec. 5.3 (i.e., $M=N$ and $W=6$ in.) the signal-processing capacity of the fused-silica light modulator will be evaluated. It will be seen that the frequency range in this case will necessitate the use of evaporated thin-film ultrasonic transducers. Although not yet proven experimentally, it will be assumed that the transfer characteristics are linear, and that light-modulator bandwidths of the order of 50 per cent of the resonant transducer frequency are possible.

COLUMBIA UNIVERSITY—ELECTRONICS RESEARCH LABORATORIES

In this case let:

$$L = \frac{n_o s^2}{\lambda f_i^2}$$

and since (Eqs. 5.2.4-4 and 5.2.4-1):

$$b = \frac{W}{2N} = \sqrt{\frac{SD}{f_i}}$$

then:

$$b = L \Rightarrow D = \left(\frac{n_o}{\lambda}\right)^2 \left(\frac{s}{f_i}\right)^3$$

But:

$$M = N \Rightarrow D = W^{2/3} \left(\frac{s}{f_i}\right)^{1/3}$$

thus:

$$f_i = \frac{s}{W^{1/4}} \left(\frac{n_o}{\lambda}\right)^{3/4} \quad (5.4-1)$$

and using the values:

$$W = (6)(2.54 \times 10^{-2}) = .1524 \text{ m}$$

$$\lambda = 6328 \times 10^{-10} \text{ m}$$

$$n_o = 1.46$$

equation 5.4-1 becomes:

$$f_i = 9.45 \times 10^4 \text{ s} \quad (5.4-2)$$

Now using the values:

$$\left. \begin{array}{l} s \\ \text{shear} \end{array} \right| = 3760 \text{ m/sec}$$

$$\left. \begin{array}{l} s \\ \text{comp.} \end{array} \right| = 5968 \text{ m/sec} \quad (5.4-3)$$

COLUMBIA UNIVERSITY—ELECTRONICS RESEARCH LABORATORIES

it is seen that:

$$f_s = f_i \Big|_{\text{shear}} = 356 \text{ MHz}$$

$$f_c = f_i \Big|_{\text{comp.}} = 564 \text{ MHz} \quad (5.4-4)$$

which could be achieved with the use of evaporated thin-film transducers (Foster 1965).

We now consider acoustic-attenuation effects.

Since:

$$D = W^{2/3} \left(\frac{S}{f_i} \right)^{1/3}$$

and, for both the shear and compression modes:

$$\frac{S}{f_i} = \frac{1}{9.45 \times 10^4}$$

then the aperture length, D , will be the same for both cases. Thus for a 6 in. aperture width:

$$D = .632 \text{ cm}$$

In Sec. 5.3 it has been shown that the acoustic attenuation will be:

$$\alpha \Big|_{\text{shear}} = 3.45 \times 10^{-6} f_i^2 \text{ napiers/cm}$$

$$\alpha \Big|_{\text{comp.}} = 2.20 \times 10^{-6} f_i^2 \text{ napiers/cm}$$

thus

$$\alpha \Big|_{\text{shear}} = .444 \text{ napiers/cm}$$

$$\alpha \Big|_{\text{comp.}} = .697 \text{ nepiers/cm}$$

and the attenuation factor $a = \frac{\alpha D}{2}$ is:

$$a \Big|_{\text{shear}} = .155$$

$$a \Big|_{\text{comp.}} = .220$$

It can be shown (Lambert 1965) that for values of the attenuation factor such that $a < .32$ the first minimum will be at least 20 db below the peak and the broadening of the main lobe will not be greater than 1.5 per cent. Thus the values obtained for "a" in this case, while not negligible, do not represent a serious degradation in the structure of the diffraction pattern.

In determining the processing capacity of the two modes, it is seen that since (Eq. 5.1-4):

$$M = N = \frac{D}{2} \frac{f_i}{S} \quad (5.4-5)$$

then for either mode the maximum-size antenna will be the same. The processing capacity however is given by:

$$P = M \times N \times B$$

and therefore:

$$P_c = \frac{f_c}{f_s} P_s \approx 1.6 P_s$$

Thus, as in the previous section, the compression mode is optimal because it permits operation at higher frequencies.

In comparing this configuration with the optimal liquid light modulator we have, for any aperture width W :

$$P_c = \left(\frac{564}{50}\right)^{7/3} \left(\frac{1500}{5968}\right)^{4/3} \approx 30P_w$$

In this case the antenna size is (Eq 5.4-5)

$$M = N \approx 290 \text{ elements}$$

and, assuming a 50 per cent bandwidth:

$$B \approx 250 \text{ MHz}$$

Finally, the transducer dimensions would be:

$$b = L \approx .3 \text{ mm}$$

5.5 SUMMARY AND CONCLUSIONS

The purpose of this section has been to optimize the design of an electro-optical array-antenna processor using a fused-silica light modulator, and then to compare the resulting signal-processing capacity with that which could be obtained with the optimum liquid light-modulator medium.

One of the major considerations in the fused-silica light modulator concerns the optimum mode of propagation. It has been shown that, in spite of the fact that signal-processing capacity (Eq. 5.3-8) will decrease with an increase in sonic velocity, the compression mode, which propagates at a higher velocity than does the shear mode, is consistently optimal. The reason for this is that in both Sec. 5.3 and 5.4 the compression mode permits operation at significantly higher frequencies. Thus, because of the exponential relationship between P , S , and f_1 (Eq. 5.3-8),

the high-frequency capability of the compression mode more than makes up for its greater sonic velocity.

With regard to the comparison between solid and liquid media, it has been shown in Sec. 5.3 that, using piezoelectric quartz-crystal transducers, electro-optical processors using fused-silica light modulators could be applied to array antennas with aperture-bandwidth products ten-times as large as those which could be processed by means of liquid light modulators. In considering the values of the acoustic-attenuation factor and the minimum transducer depth which have been obtained for this configuration, it appears that these results do not represent the absolute limits; that is, higher frequencies, and therefore greater processing capacities, would still be possible in fused-silica light modulators before the restrictions imposed by acoustic attenuation and internal refraction would be felt.

In Sec. 5.4 the limits imposed on high-frequency operation by the ultrasonic transducer have been removed, and these results seem to represent the limit in processing capacity which could be obtained with this light-modulator medium. In this case it has been shown that the signal-processing capacity could be increased by a factor of 30 over that which could be obtained with liquid light modulators.

6. LIGHT DIFFRACTION PATTERNS PRODUCED BY NON-SEPARABLE
OPTICAL TRANSMISSION FUNCTIONS

It has been shown that, under small aperture-bandwidth conditions, the complex optical transmission function of the electro-optical processor will be separable in terms of the spatial variables in the optical aperture. The resulting light diffraction patterns have been obtained for this case. It will be seen however that in the large aperture-bandwidth case the transmission function becomes non-separable, for which a mathematical representation of the resulting light distribution in the image plane has, as yet, not been determined. It is the purpose of this chapter therefore to determine the effects of non separability on the output light distribution and thereby extend the applicability of the existing processor configuration to the large aperture bandwidth case. Thus, although the following sections deal with signal processing concepts which have already been established (i.e., time multiplexing, spatial multiplexing; see Sec. 2), the results, with one exception, represent original contributions of this research. The exception mentioned refers to Sec. 6.2. This section is included because of the subsequent necessity of considering the details of the time-multiplexing process.

It will also be shown that a degradation in peak signal-to-noise ratio will occur in the large aperture-bandwidth case. A mathematical model describing the light intensity in the image plane, when the input to the light

modulator consists of samples of a random process, will be derived. This model will then be used to evaluate the signal-to-noise degradation. On the basis of these results it will be shown that a significant degradation will occur only in the case of the spatially-multiplexed linear array, and that, in the case of the time-multiplexed linear array and the planar array, the degradation will be negligible.

In this chapter the light-modulator medium is unspecified, but it is assumed that the results of Chap. 2 will apply. Thus for liquids this assumption is seen to be valid, and, on the basis of Chs. 4 and 5, it will be valid, theoretically, for fused silica as well. Experimental verification of these assumptions will be dealt with in Chap. 7.

6.1 LINEAR ARRAY: SPATIAL MULTIPLEXING

A plane wave of unit amplitude and duration T incident at an angle θ on a linear array antenna whose elements are separated by a distance δ will cause signals to appear at the outputs of the antenna elements with incremental time delay between adjacent outputs given by (Fig. 6.1-1):

$$\Delta\tau = \frac{\delta \sin \theta}{c} \quad (6.1-1)$$

where c = velocity of electromagnetic propagation

Hence information concerning angle of arrival is contained in the incremental time delay $\Delta\tau$.

It is assumed that the carrier frequency of the received signal includes a Doppler shift f_d . Thus if the transmitted frequency is f_c , the received signal frequency

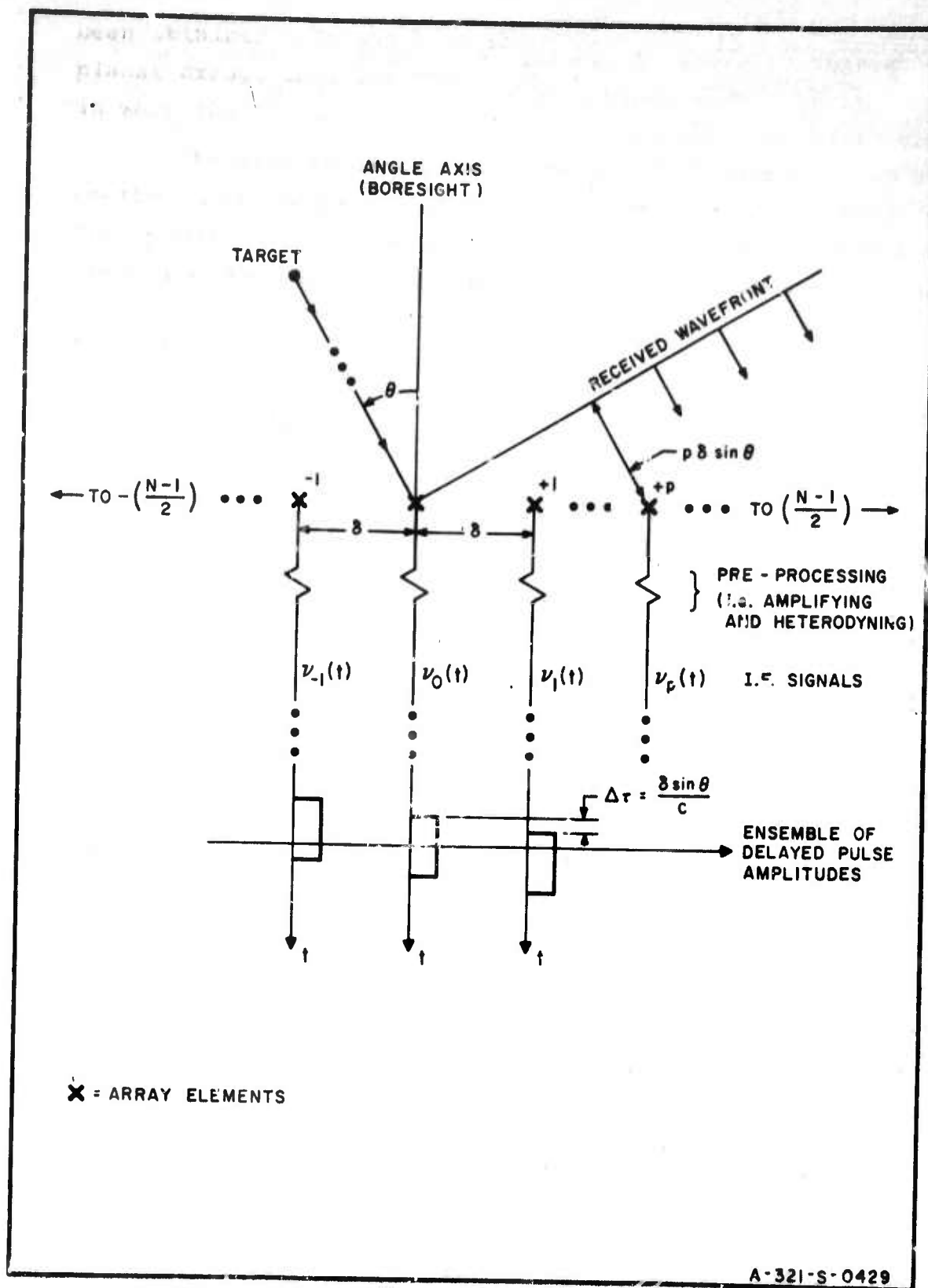


FIG. 6.1-1 LINEAR ARRAY SHOWING DELAYED PULSE AMPLITUDES

COLUMBIA UNIVERSITY—ELECTRONICS RESEARCH LABORATORIES

will be: $f_c + f_d$, and the output of the zeroth antenna element can be written as:

$$P_T(t) \sin 2\pi f_r t \quad (6.1-2)$$

where $P_T(t)$ is a unit amplitude time function of duration T . The output of the p^{th} antenna element will be:

$$P_T(t - p\Delta\tau) \sin 2\pi f_r(t - p\Delta\tau) \quad (6.1-3)$$

if however the antenna aperture bandwidth product is small, then:

$$T \gg N |\Delta\tau|_{\max} \quad (6.1-4)$$

and the delay in the signal envelopes can be neglected (Lambert, Arm, Airmette 1965). Thus the output of the p^{th} element can be written in approximate form as:

$$P_T(t) \sin 2\pi f_r(t - p\Delta\tau) \quad (6.1-5)$$

and it is seen that the angle information is now contained in the incremental phase shift between adjacent outputs which is given by:

$$\Delta\phi = 2\pi f_r \Delta\tau \quad (6.1-6)$$

The diffraction patterns resulting from spatially multiplexed signals of the form of Eq. (6.1-5) have been obtained and the results are presented in Chap. 2. It is seen however that, when the aperture bandwidth product is large, Eq. (6.1-4) will not hold and the approximation of Eq. (6.1-5) will no longer be valid. Thus under large aper-

ture bandwidth conditions it will be necessary to determine the diffraction patterns which are obtained when the relative displacement in signal envelopes is taken into account

* * *

In the spatial-multiplexing process, N antenna outputs serve as separate inputs to an N -channel Debye-Sears light modulator (Fig. 6.1-2). It is assumed, however, that before being spatially multiplexed the signals are pre-processed in order to increase their amplitudes and to reduce their carrier frequency. Realizing that heterodyning to a frequency f_o consists of first multiplying the signal by a coherent local oscillator signal of the form $\sin 2\pi(f_c - f_o)t$, and then taking the difference frequency component by filtering, it can be shown that the input to the p^{th} light-modulator channel after amplification and heterodyning will be a signal of the form:

$$V_m P_T(t - p\Delta\tau) \sin 2\pi(f_i t - p\Delta\tau f_r) \quad (6.1-7)$$

where:

f_i = input frequency = $f_o + f_d$

f_o = intermediate frequency

V_m = peak voltage amplitude for all values
of index p

and, for convenience, Eq. (6.1-7) can be re-written as:

$$\begin{aligned} & V_m P_T(t - p\Delta\tau) \sin 2\pi[f_i(t - p\Delta\tau) - p\Delta\tau(f_r - f_i)] \\ & = V_m P_T(t - p\Delta\tau) \sin 2\pi[f_i(t - p\Delta\tau) - p\gamma] \end{aligned} \quad (6.1-8)$$

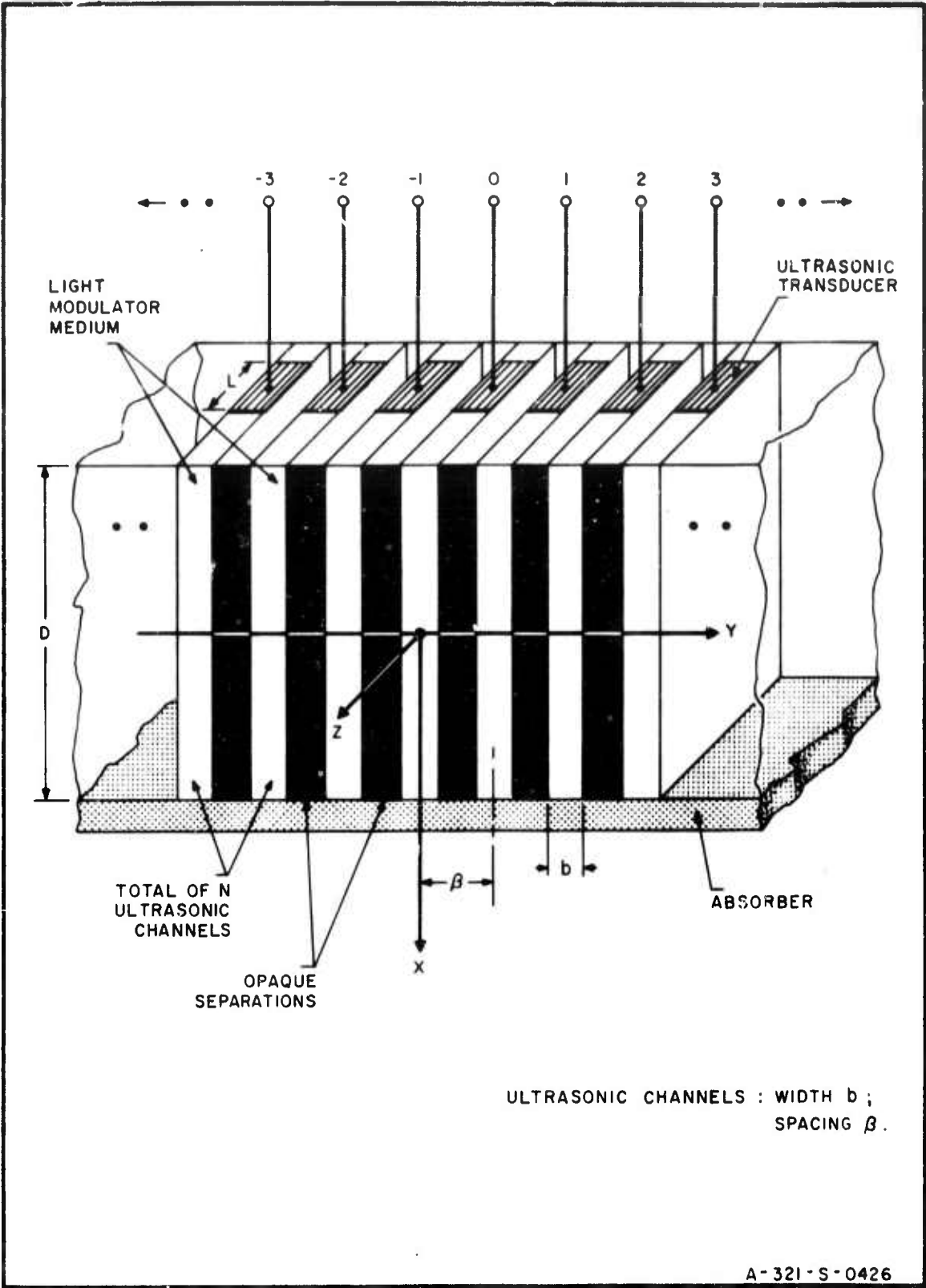


FIG 6.1-2 N - CHANNEL DEBYE - SEARS LIGHT MODULATOR

COLUMBIA UNIVERSITY—ELECTRONICS RESEARCH LABORATORIES

where:

$$\gamma = (f_r - f_i)\Delta\tau = (f_c - f_o)\Delta\tau$$

Now an input to the Debye-Sears light modulator of the form:

$$\sin 2\pi f_1 t$$

will be transformed into an ultrasonic traveling wave of the form:

$$\sin 2\pi f_1 \left(t - \frac{x}{s}\right)$$

where:

s = ultrasonic velocity of propagation

Thus the electrical signal (Eq. (6.1-8)) will, at some instant of time, result in an ultrasonic signal of the form:

$$P_d(x + p\Delta x) \sin 2\pi[f(x + p\Delta x) + p\gamma] \quad (6.1-9)$$

where $P_d(x)$ is a unit amplitude spatial function of length d ,

$$d = sT$$

$$f = \frac{f_1}{s} \text{ (spatial frequency)}$$

$$\Delta x = s\Delta\tau$$

and, at some instant of time, the ensemble of ultrasonic signals in the Debye-Sears light modulator will appear as shown in Fig. 6.1-3. It is seen that the pulse envelopes are skewed across the light modulator along a line described by the equation:

$$x = -\Lambda y \quad (6.1-10)$$

and the incremental displacement between adjacent ultrasonic signals is given by:

$$\Delta x = S\Delta\tau = \Lambda\beta \quad (6.1-11)$$

Thus, using Eqs. (2.1-4), (2.1-7), and (2.1-9), it is seen that the contribution to the positive first order light amplitude in the image plane from the channel located at $y=p\beta$ (Eq. 6.1-9) will be:

$$\bar{g}_p(u,v) = \frac{\psi_m}{2} \int_{x=-p\Lambda\beta-\frac{d}{2}}^{-p\Lambda\beta+\frac{d}{2}} \int_{y=p\beta-\frac{b}{2}}^{p\beta+\frac{b}{2}} e^{j2\pi[f(x+p\Lambda\beta)+py]} e^{-j2\pi ux} e^{-j2\pi vy} dx dy \quad (6.1-12)$$

Let $\xi = x + p\Lambda\beta$, $\eta = y - p\beta$ and:

$$\bar{g}_p(u,v) = \frac{\psi_m}{2} e^{-j2\pi p(\beta v - \beta\Lambda u - \gamma)} \int_{-\frac{d}{2}}^{\frac{d}{2}} \int_{-\frac{b}{2}}^{\frac{b}{2}} e^{-j2\pi\xi(u-f)} e^{-j2\pi\eta v} d\xi d\eta \quad (6.1-13)$$

The total first order light amplitude will be (letting N be odd for convenience):

$$G_1(u,v) = \sum_{p=-\left(\frac{N-1}{2}\right)}^{\left(\frac{N-1}{2}\right)} \bar{g}_p(u,v) \quad (6.1-14)$$

Thus making use of the identity:

$$\sum_{n=-\left(\frac{N-1}{2}\right)}^{\left(\frac{N-1}{2}\right)} e^{jnz} = \frac{\sin \frac{Nz}{2}}{\sin \frac{z}{2}} \quad (6.1-15)$$

the positive first order light intensity will be:

$$|G_1(u, v)|^2 = \frac{\psi_m^2}{4} \left(\frac{b \sin \pi b v}{\pi b v} \right)^2 \left(\frac{\sin \pi N(\beta v - \beta \Lambda u - \gamma)}{\sin \pi(\beta v - \beta \Lambda u - \gamma)} \right)^2 \cdot \left(\frac{d \sin \pi d(u - f)}{\pi d(u - f)} \right)^2 \quad (6.1-16)$$

Consider this result in terms of the complex optical transmission function. A separable transmission function has been defined (Lambert 1965) as one which can be written as the product of two completely independent functions of the spatial variables in the aperture. That is, for a separable transmission function:

$$T_1(x, y) e^{j\psi_1(x, y)} = T_1(x) e^{j\psi_1(x)} T_1(y) e^{j\psi_1(y)} \quad (6.1-17)$$

and it is seen that in this case:

$$\begin{aligned} G_1(u, v) &= \int_{-\infty}^{\infty} \int_{-\infty}^{\infty} T_1(x, y) e^{j\psi_1(x, y)} e^{-j2\pi ux} e^{-j2\pi vy} dx dy \\ &= \int_{-\infty}^{\infty} T_1(x) e^{j\psi_1(x)} e^{-j2\pi ux} dx \int_{-\infty}^{\infty} T_1(y) e^{j\psi_1(y)} e^{-j2\pi vy} dy \\ &= G_1(u) G_1(v) \end{aligned} \quad (6.1-18)$$

Thus, under these conditions, the output light distribution can be expressed as the product of two independent functions of the output variables u and v .

This is seen to be true for Eq. (2.2-3) which has been shown to result from a separable transmission function. In

the large aperture bandwidth case however, it is easily shown (using Eqs. 6.1-12 and 6.1-14) that the complex optical transmission function is:

$$T_1(x,y) e^{j\psi_1(x,y)} = \frac{\psi_m}{2} \sum_{p=-\frac{(N-1)}{2}}^{\frac{(N-1)}{2}} \text{rect}\left(\frac{x+p\Lambda\beta}{d}\right) \text{rect}\left(\frac{y-p\beta}{b}\right) \cdot e^{j2\pi[f(x+p\Lambda\beta) + py]} \quad (6.1-19)$$

which cannot be expressed as two completely independent functions of the variables x and y because of interdependence through the index of summation; thus it is not possible to express the resulting output light distribution (Eq. 6.1-16) as the product of two independent functions of the spatial variables of the image plane.

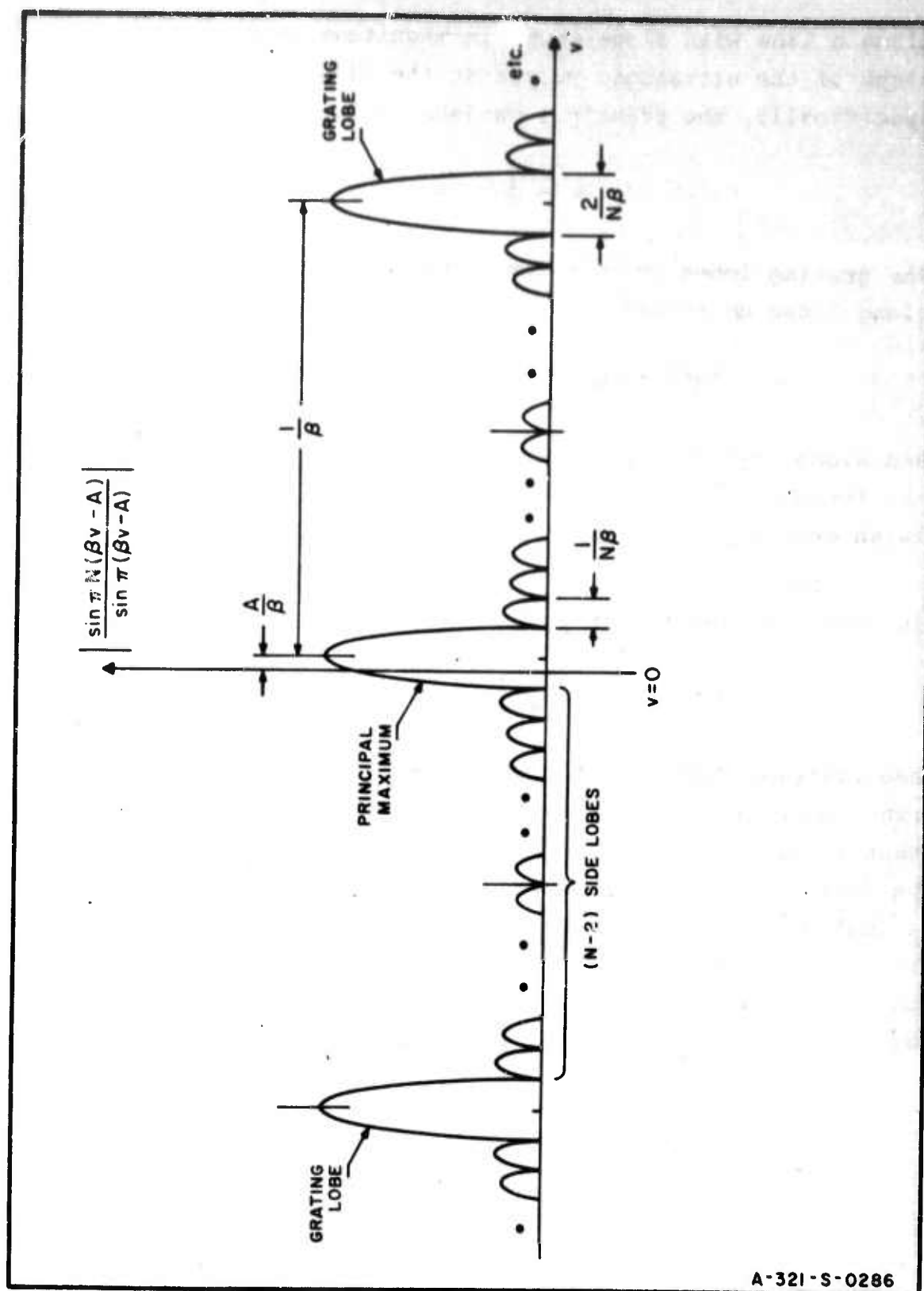
Now consider Eq. (6.1-16) term by term. In general, an expression of the form:

$$\left(\frac{\sin \pi N(\beta v - A)}{\sin \pi(\beta v - A)} \right)^2 \quad (6.1-20)$$

which is seen to be an optical analogue of the radiation pattern of a linear array antenna, has a principal maximum along the line $v = \frac{A}{\beta}$, grating lobes at $v = \frac{n}{\beta} + \frac{A}{\beta}$, where $n =$ integer, and $N-2$ side lobes of width $\frac{1}{N}$ in between each grating lobe (Fig. 6.1-4). Thus the function:

$$\left(\frac{\sin \pi N(\beta v - \beta \Lambda u - \gamma)}{\sin \pi(\beta v - \beta \Lambda u - \gamma)} \right)^2 \quad (6.1-21)$$

is similar to that of Eq. (6.1-20) but its principal maximum, instead of running parallel to the u axis, is skewed



A-321-S-0286

FIG. 6.1-4 GRAPH OF $\left| \frac{\sin \pi N(\beta v - A)}{\sin \pi(\beta v - A)} \right|$

along a line with slope equal in magnitude to that of the slope of the ultrasonic pulses in the light modulator. More specifically, the principal maximum falls along the line:

$$v = \frac{\gamma}{\beta} + \Lambda u \quad (6.1-22)$$

The grating lobes in this case, which are also skewed, run along lines described by

$$v = \frac{n+\gamma}{\beta} + \Lambda u \quad n = \pm 1, \pm 2 \text{ etc.} \quad (6.1-23)$$

and along any cut parallel to the u axis, say at $u = f$, the function has $N-2$ side lobes, each of width $\frac{1}{\beta N}$, between each grating lobe (Fig. 6.1-5).

In considering the remaining terms in Eq. (6.1-6) it is seen that the function

$$\left(\frac{d \sin \pi d(u-f)}{\pi d(u-f)} \right)^2 \quad (6.1-24)$$

has its peak running along the line $u = f$. Thus the diffraction pattern will appear as shown in Fig. 6.1-6. Note that since $\frac{1}{b} \gg \frac{1}{\beta N}$, the main lobe of $\left(\frac{b \sin \pi b v}{\pi b v} \right)^2$ will be relatively broad, and the only effect of this function is a negligible (Lambert 1965) amplitude weighting of the peak first order intensity which, since the observation region of this electro-optical processor excludes the grating lobes of Eq. (6.1-21), occurs at the point:

$$u = f \quad (6.1-25)$$

$$v = \frac{\gamma}{\beta} + \Lambda u \Big|_{u=f} = \frac{\gamma}{\beta} + \Lambda f$$

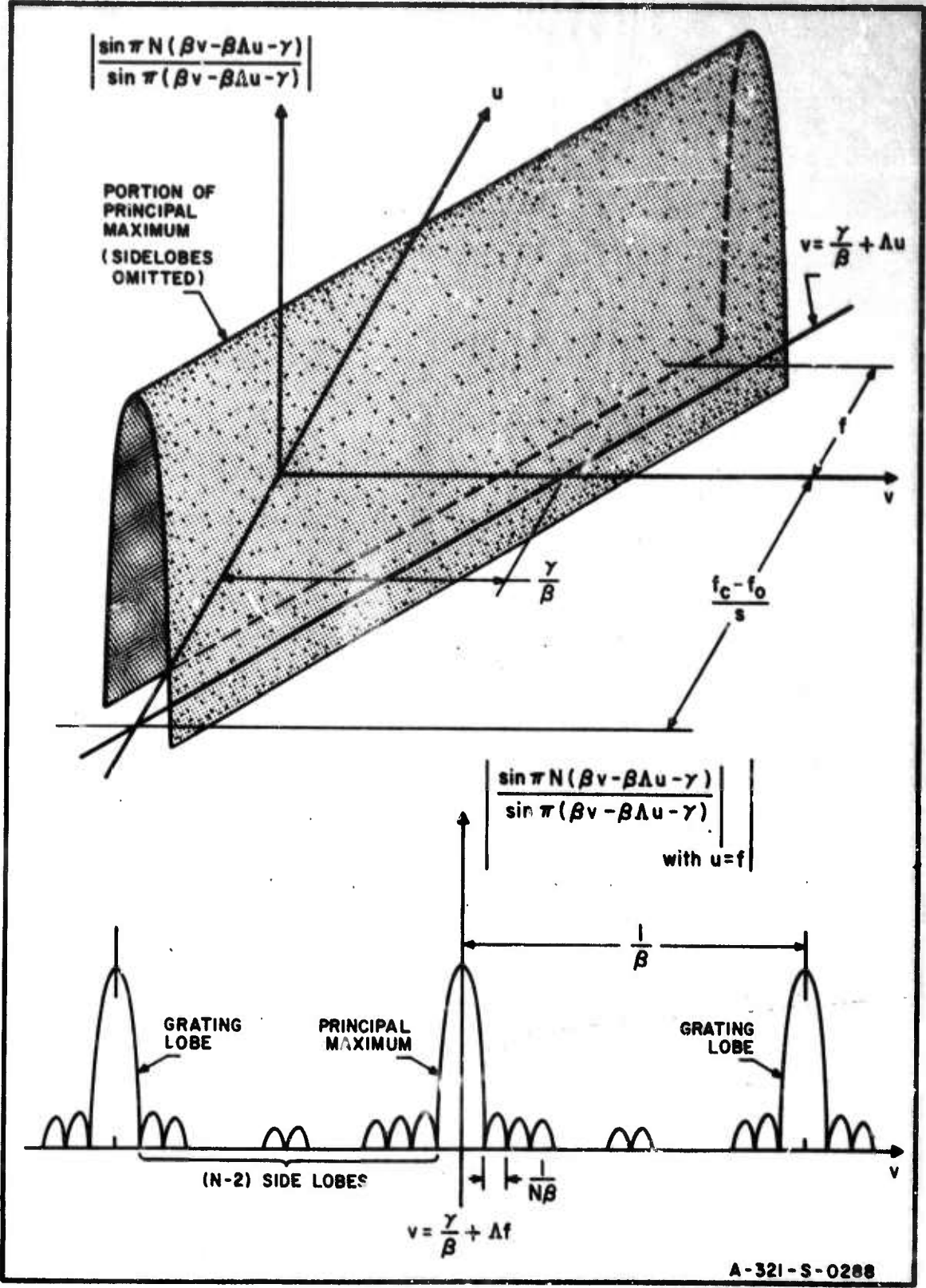


FIG. 6.1-5 GRAPH OF $\left| \frac{\sin \pi N (\beta v - \beta \Delta u - \gamma)}{\sin \pi (\beta v - \beta \Delta u - \gamma)} \right|$

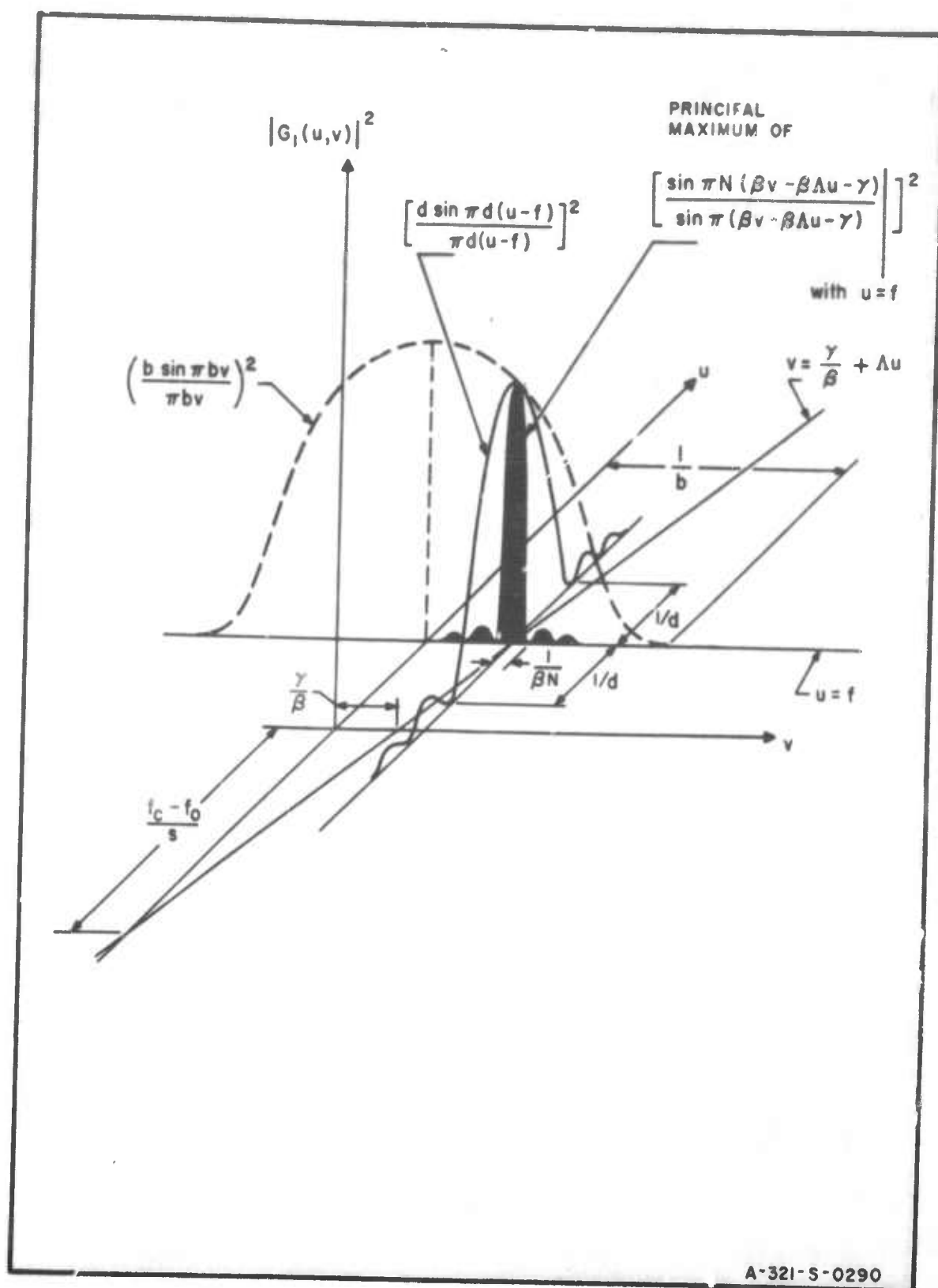


FIG. 6.1-6 POSITIVE FIRST-ORDER LIGHT INTENSITY : SPATIALLY-MULTIPLEXED
LARGE APERTURE - BANDWIDTH LINEAR ARRAY
(N ELEMENTS)

It is evident that the location of peak first order intensity contains information concerning the Doppler frequency and the angle of arrival of the signal at the antenna. The measurement procedure and a comparison between the large and small aperture-bandwidth cases will be discussed in the following section.

6.1.1 INTERPRETATION OF DIFFRACTIONS PATTERNS: LARGE AND SMALL APERTURE-BANDWIDTH LINEAR ARRAYS

For convenience of notation the variables u and v will continue to be used in describing both the output light distribution and the measurement procedures. Actual measurements of course would be obtained in terms of the linear spatial variables, x_1 and y_1 , which are related to the output variables u and v by:

$$\begin{aligned} u &= \frac{x_1}{\lambda F} \\ v &= \frac{y_1}{\lambda F} \end{aligned} \quad (6.1.1-1)$$

where:

λ = light wavelength

F = focal length of integrating lens

In comparing the extraction of information from the diffraction patterns which are produced under large and small aperture-bandwidth conditions it is evident that the signal duration, the number of antenna elements, and the length, width, and spacing of the light modulator channels, would not be the same for both cases; and therefore Eq. (2.2-3)

cannot be compared directly with Eq. (6.1-16). Nevertheless, the form of the results for either case will not be a function of the actual parameter values. Thus the large and small aperture-bandwidth cases will be compared by considering the expressions:

(i) Large Aperture-Bandwidth

$$|G_1(u, v)| = \frac{\psi_m^2}{4} \left(\frac{b \sin \pi b v}{\pi b v} \right)^2 \left(\frac{\sin \pi N(\beta v - \beta \Lambda u - \gamma)}{\sin \pi(\beta v - \beta \Lambda u - \gamma)} \right)^2 \cdot \left(\frac{d \sin \pi d(u - f)}{\pi d(u - f)} \right)^2 \quad (6.1.1-2)$$

(ii) Small Aperture-Bandwidth

$$|G_1(u, v)|^2 = \frac{\psi_m^2}{4} \left(\frac{b \sin \pi b v}{\pi b v} \right)^2 \left(\frac{\sin \pi N(\beta v - \frac{\Delta \phi}{2\pi})}{\sin \pi(\beta v - \frac{\Delta \phi}{2\pi})} \right)^2 \cdot \left(\frac{d \sin \pi d(u - f)}{\pi d(u - f)} \right)^2 \quad (6.1.1-3)$$

where:

$$\Lambda = \frac{\Delta x}{\beta} = \frac{S \Delta \tau}{\beta} \quad (6.1.1-4)$$

$$\gamma = (f_c - f_o) \Delta \tau$$

$$\Delta \phi = 2\pi f_r \Delta \tau$$

f_r = received carrier frequency = $f_c + f_d$

f_c = transmitted carrier frequency

f_d = Doppler frequency

f_o = intermediate frequency

$$f = \frac{f_c + f_d}{s}$$

In both cases, it is seen that the u coordinate of the peak first-order light intensity is located at the point:

$$u = f = \frac{f_o}{s} + \frac{f_d}{s} = \frac{f_o}{s} + u_d \quad (6.1.1-5)$$

where $u_d = \frac{f_d}{s}$ is the displacement, in the u direction, of peak first order intensity from the line $u = \frac{f_o}{s}$. Thus, since f_o is a fixed known frequency, Doppler information is contained in the displacement u_d .

The angle information, in both cases, is contained in the v coordinate of the peak. This displacement, v_a , is given by:

(i) large aperture-bandwidth:

$$v_a = \frac{\gamma}{\beta} + \Lambda u \Big|_{u=f} = \frac{\gamma}{\beta} + \Lambda f \quad (6.1.1-6)$$

(ii) small aperture-bandwidth

$$v_a = \frac{\Delta\phi}{2\pi\beta} \quad (6.1.1-7)$$

Using Eqs. (6.1.1-4) however:

$$\frac{\Delta\phi}{2\pi\beta} = \frac{f_r \Delta\tau}{\beta} = \left(\frac{f_c - f_o + f_o + f_d}{\beta} \right) \frac{\Delta x}{s} = \frac{\gamma}{\beta} + \Lambda f \quad (6.1.1-8)$$

and it is seen that in both cases the peak first order intensity is actually located at exactly the same point in the image plane. Thus, in determining the angle of arrival (using Eqs. (6.1.1-4, 6.1.1-5 and 6.1.1-6):

$$v_a = \left(\frac{f_c + Su_d}{\beta} \right) \frac{\delta \sin \theta}{c} \quad (6.1.1-9)$$

where δ is the antenna element spacing. This distance is generally (Skolnick 1962) one half-wavelength of the transmitted signal, and since $c = \lambda_c f_c$ then Eq. (6.1.1-9) becomes:

$$v_a = \left(\frac{f_c + Su_d}{\beta} \right) \frac{\sin \theta}{2f_c} \quad (6.1.1-10)$$

Hence:

$$\theta = \sin^{-1} \left[\frac{2\beta v_a}{1 + \frac{Su_d}{f_c}} \right] \quad (6.1.1-11)$$

and it is seen that an exact determination of θ requires knowledge of both coordinates of the peak intensity. Since however;

$$Su_d = f_d \ll f_c$$

then Eq. (6.1.1-11) can be written approximately (Lambert, Arm, Aimetie 1965):

$$\theta = \sin^{-1} (2\beta v_a)$$

Although in both the large and small aperture-bandwidth cases the peak first order intensity occurs at the same point, the overall light distribution in the image plane will not be the same. As shown in Fig. 6.1-7, the grid formed by the nulls of the diffraction pattern will be rectangular when the aperture-bandwidth product is small, but will have a rhombic structure because of the skewing of the ultrasonic pulse amplitudes in the large aperture-bandwidth case.

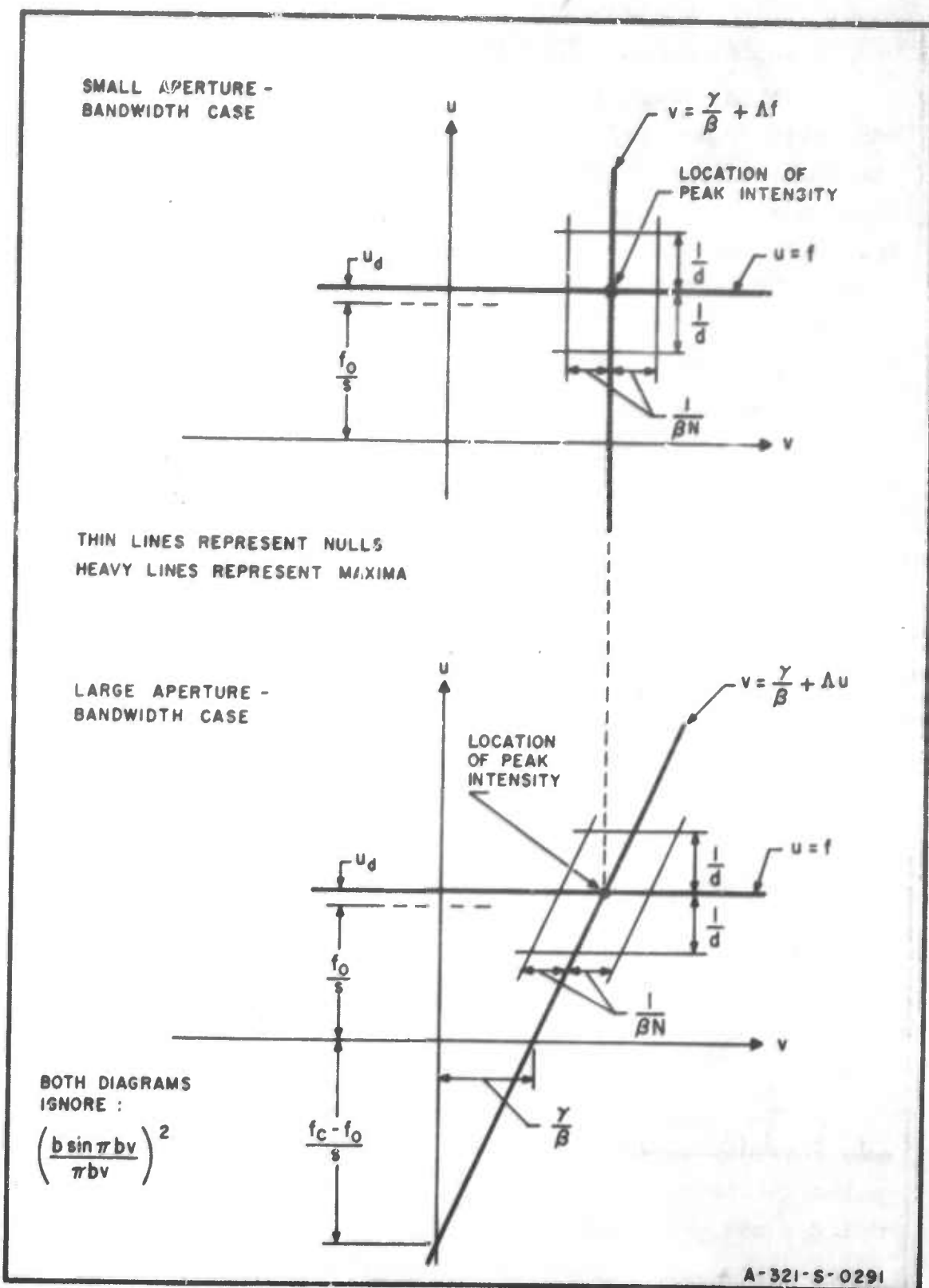


FIG. 6.1-7 NULL PATTERNS AND LOCATION OF PEAK INTENSITIES : LARGE AND SMALL APERTURE-BANDWIDTH SPATIALLY-MULTIPLEXED LINEAR ARRAYS

6.2 LINEAR ARRAY: TIME MULTIPLEXING

In this case the transmission function will always be separable regardless of the aperture-bandwidth product of the antenna, and the diffraction patterns produced in this configuration have already been obtained (Lambert 1965). In Sec. 6.3 however, which deals with the planar array, it will be necessary to consider the time-multiplexing process in some detail. Thus the time-multiplexed linear array will be discussed in this section.

Consider the case shown in Fig. 6.1-1. As shown in Sec. 6.1, (Eq. 6.1-8) after amplification and heterodyning, the output of the n^{th} antenna element will be of the form:

$$V_m P_T(t - n\Delta\tau) \sin 2\pi(f_i(t - n\Delta\tau) - n\gamma) \quad (6.2-1)$$

where the input frequency to the light modulator, f_i , is given by:

$$f_i = f_o + f_d$$

In the time-multiplexing procedure (Fig. 6.2-1) each antenna output is passed through a fixed delay element; the delay for the n^{th} element, T_n , being such that:

$$T_{n+1} - T_n = T_D$$

where T_D is fixed.

The quantity T_D is the time separation between any two adjacent pulses for a boresight signal. Hence, if the pulse duration is T , then it is necessary to choose the delay times such that:

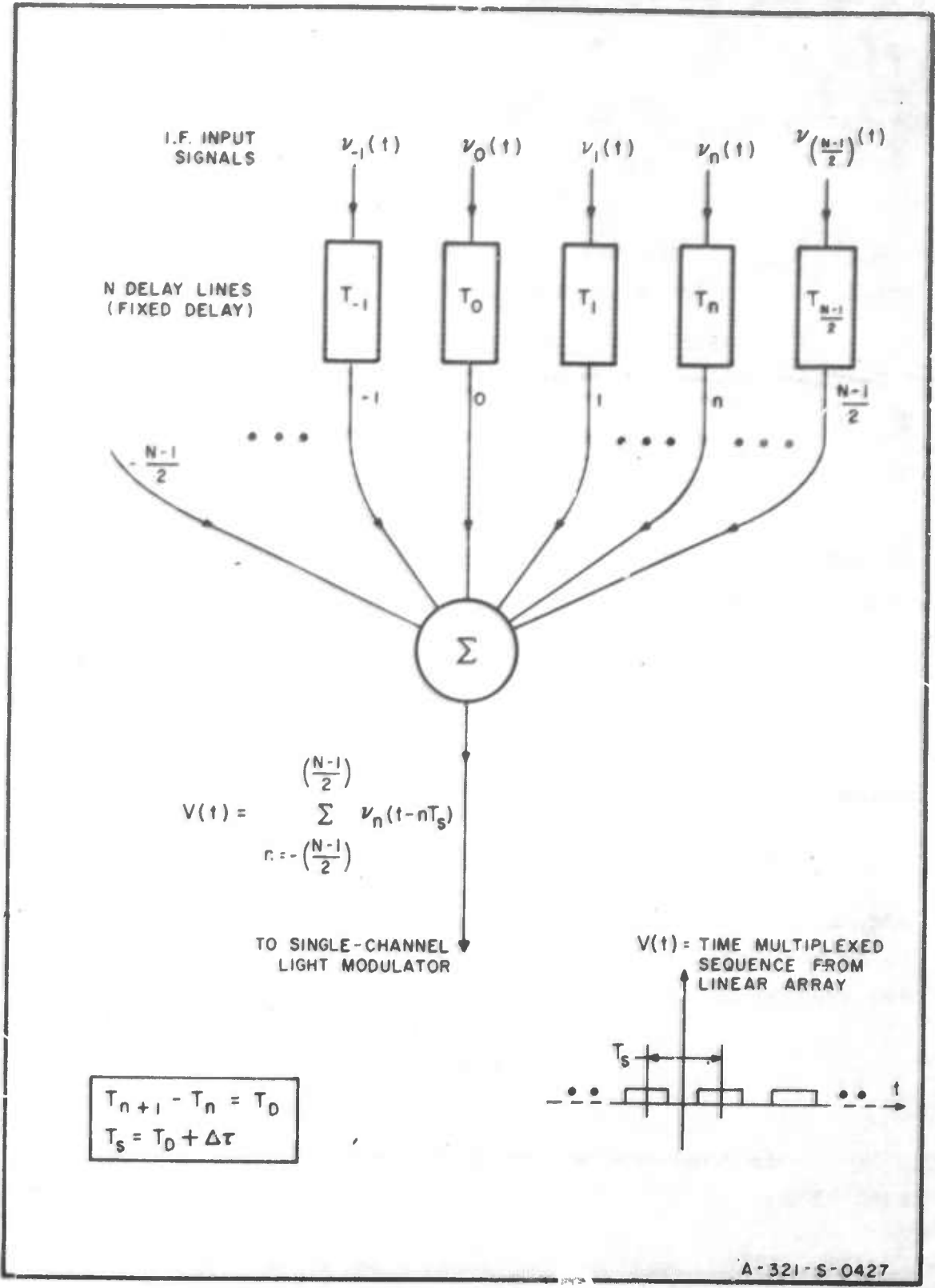


FIG. 6.2-1 TIME MULTIPLEXING . LINEAR ARRAY

$$T_D \geq T + |\Delta\tau|_{\max} \quad (6.2-2)$$

where

$$|\Delta\tau|_{\max} = \frac{\delta \sin |\theta|_{\max}}{c} \quad (6.2-3)$$

and $|\theta|_{\max}$ is the maximum off-boresight angle that the antenna is required to cover.

In general, for some arbitrary value of θ , the time separation between adjacent antenna outputs, T_s , will be given by:

$$T_s = T_D + \Delta\tau \quad (6.2-4)$$

Thus in a manner similar to that of Sec. 6.1 (Eq. 6.1-7 et seq.) the input to the light modulator will be a time function of the form:

$$v(t) = \sum_{n=-\left(\frac{N-1}{2}\right)}^{n=+\left(\frac{N-1}{2}\right)} v_n(t)$$

where

$$v_n(t) = V_m P_T(t - nT_s) \sin 2\pi[f_i(t - nT_s) - n\gamma] \quad (6.2-5)$$

and, at some instant of time, the ultrasonic pulses in the light modulator will appear as shown in Fig. 6.2-2 in which the separation between ultrasonic signals is:

$$d_s = ST_s$$

Note that the length of the light modulator must be such that:

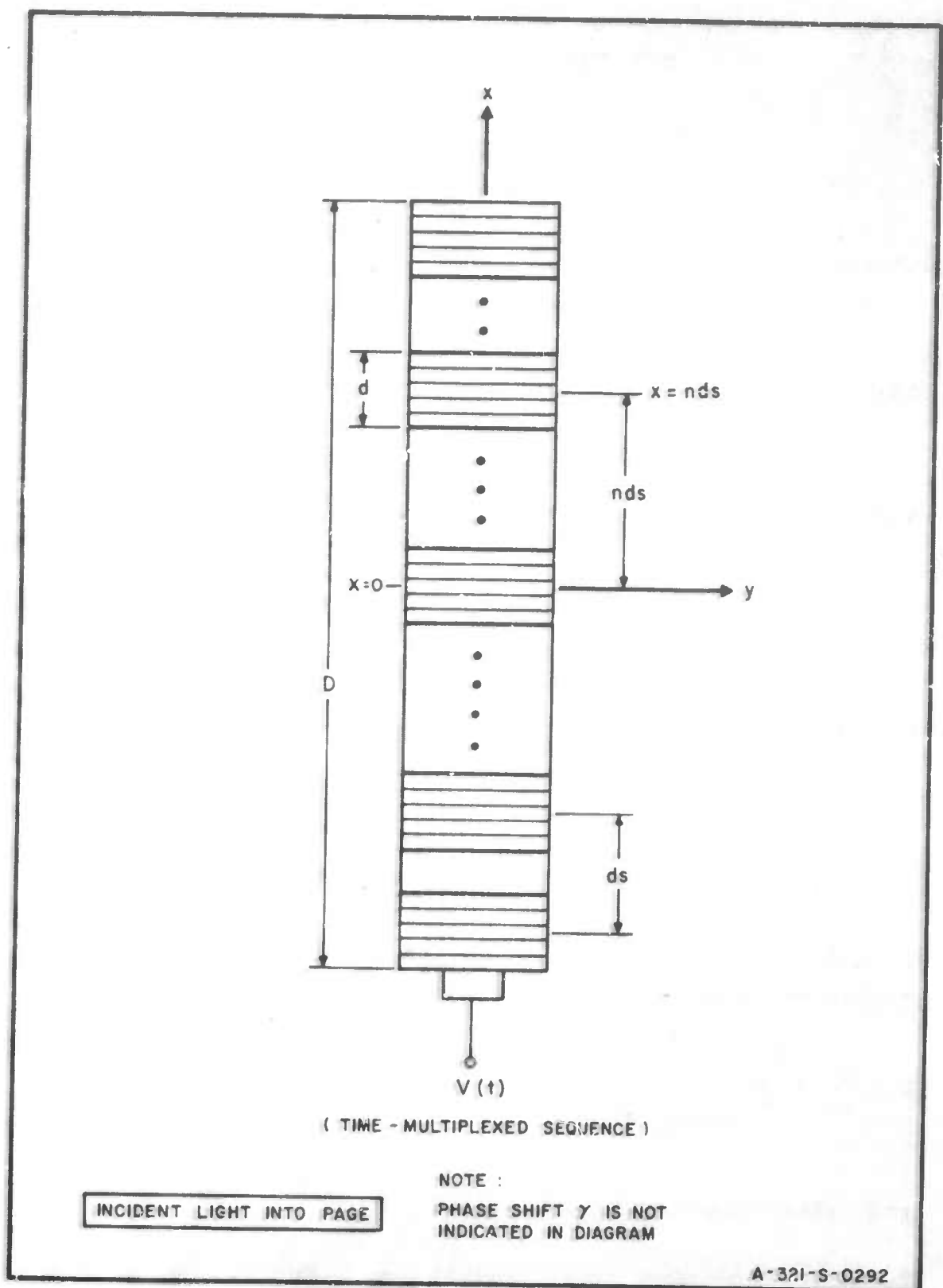


FIG. 6.2-2 SEQUENCE OF TIME-MULTIPLEXED PULSES IN SINGLE-CHANNEL DEBYE-SEARS LIGHT MODULATOR

$$D \geq S(N-1) |T_s|_{\max} + ST.$$

If

$$T_D = T + |\Delta\tau|_{\max}$$

then

$$|T_s|_{\max} = T + 2|\Delta\tau|_{\max}$$

thus

$$D \geq S(NT + 2(N-1)|\Delta\tau|_{\max})$$

and since it will always be true that

$$T \gg |\Delta\tau|_{\max}$$

$$N \gg 1$$

then the aperture length must be approximately:

$$D \approx NST$$

Now, following exactly the same procedure as for Eq. (6.1-12), the contribution to positive first order light amplitude from the light which is diffracted by the ultrasonic signal centered at $x = -nd_s$ is:

$$\bar{g}_p(u,v) = \frac{\psi_m}{2} \int_{x=-nd_s-\frac{d}{2}}^{-nd_s+\frac{d}{2}} \int_{y=-\frac{b}{2}}^{\frac{b}{2}} e^{j2\pi[f(x+nd_s)+ny]} e^{-j2\pi ux} e^{-j2\pi vy} dx dy \quad (6.2-6)$$

and, after changing variables and integrating, the first

order light intensity (using Eqs. 6.1-14, 6.1-15) becomes:

$$|G_1(u, v)|^2 = \frac{\psi_m^2}{4} \left(\frac{b \sin \pi b v}{\pi b v} \right)^2 \left(\frac{\sin \pi N(u d_s + \gamma)}{\sin \pi (u d_s + \gamma)} \right)^2 \cdot \left(\frac{d \sin \pi d(u - f)}{\pi d(u - f)} \right)^2 \quad (6.2-7)$$

The function:

$$\left(\frac{\sin \pi N(u d_s + \gamma)}{\sin \pi (u d_s + \gamma)} \right)^2 \quad (6.2-8)$$

is, once again, an optical analogue of the radiation pattern of a linear array antenna, with maxima occurring at: $(u d_s + \gamma) = 0, \pm 1, \pm 2$ etc, and $N-2$ side lobes of width $\frac{1}{N d_s}$ in between each peak. Since angle information is contained in this function it is necessary to minimize the amplitude weighting imposed by $\left(\frac{d \sin \pi d(u - f)}{\pi d(u - f)} \right)^2$.

This may be done as follows (Lambert 1965):

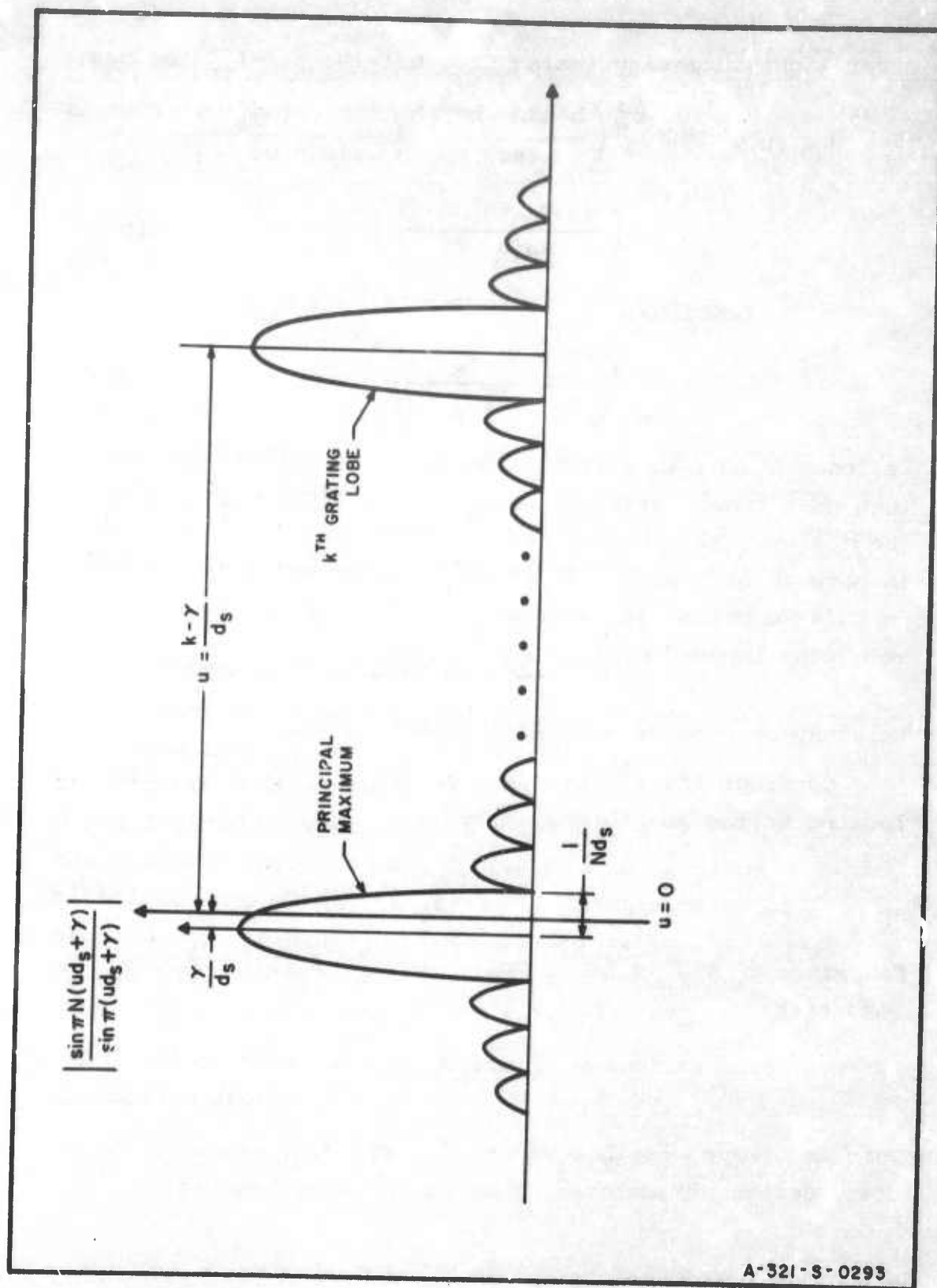
Consider the k^{th} grating lobe of Eq. (6.2-8). This is located at the point (Fig. 6.2-3):

$$u = \frac{k - \gamma}{S T_s} \quad (6.2-9)$$

Now since $T_s = T_D + \Delta\tau$, and $\gamma = (f_c - f_o)\Delta\tau$, choose f_o such that:

$$k = f_o T_D \quad (6.2-10)$$

This is always possible since f_o and T_D are both arbitrary design parameters. Thus Eq. (6.2-9) becomes:



A-321-S-0293

FIG. 6.2-3 GRAPH OF $\left| \frac{\sin \pi N (ud_s + \gamma)}{\sin \pi (ud_s + \gamma)} \right|$

$$u = \frac{f_o T_D - (f_c - f_o) \Delta \tau}{s(T_D + \Delta \tau)} = \frac{f_o}{s} - \left(\frac{\Delta \tau}{T_D + \Delta \tau} \right) \left(\frac{f_c}{s} \right) \quad (6.2-11)$$

and angle information is contained in the quantity:

$$u_a = \left(\frac{\Delta \tau}{T_D + \Delta \tau} \right) \left(\frac{f_c}{s} \right) \quad (6.2-12)$$

which represents the displacement of peak first order intensity from the line $u = \frac{f_o}{s}$. Note that the peak of $\left(\frac{d \sin \pi d(u-f)}{\pi d(u-f)} \right)^2$ actually falls at $u = \frac{f}{s} = \frac{f_o + f_d}{s}$. However, f_d will always be much smaller than f_o so that the amplitude weighting from this function as well as from $\left(\frac{b \sin \pi b v}{\pi b v} \right)^2$ can be ignored (Lambert 1965).

Thus the diffraction pattern appears as is shown in Fig. 6.2-4. It is seen that the location of peak first order intensity is independent of the Doppler frequency and therefore only the angle information can be recovered. In this case the angle θ would be given by (using Eqs. 6.2-12, 6.1-1 and assuming half-wavelength antenna-element spacing):

$$\theta = \sin^{-1} \left[\left(\frac{su_a}{f_c - su_a} \right) (2f_c T_D) \right]$$

6.3 PLANAR ARRAY ANTENNA

Consider a plane wave incident on a planar array antenna with M rows and N columns (Fig. 6.3-1). The angles between the wave normal and the rows and columns of the array will be, respectively, $90-\theta_y$ and $90-\theta_x$ which will result in incremental time delays between adjacent outputs in any of the rows of the array given by:

$$\Delta \tau_y = \frac{\delta_y \sin \theta_y}{c} \quad (6.3-1)$$

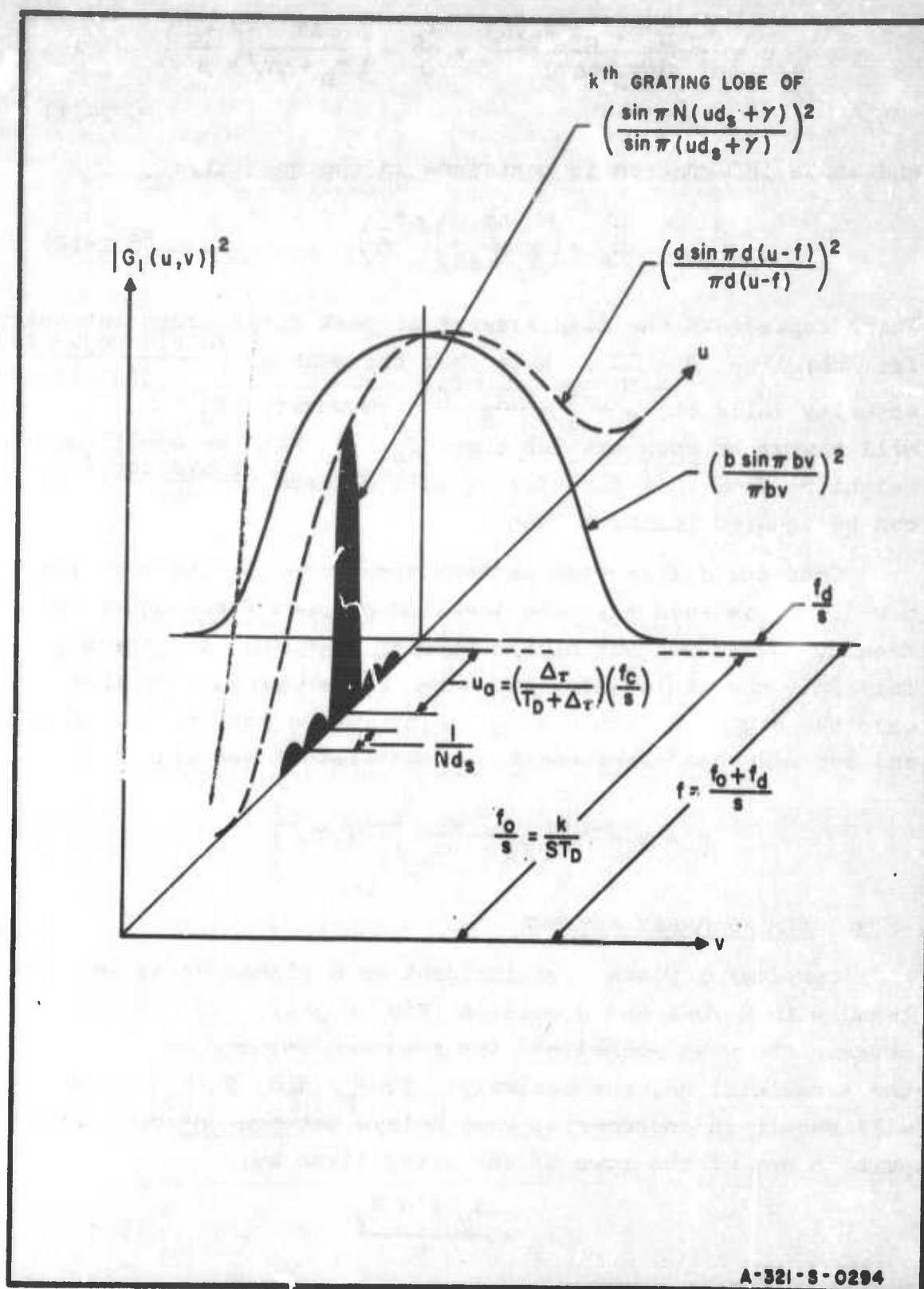


FIG. 6.2-4 DIFFRACTION PATTERN : TIME-MULTIPLEXED LINEAR ARRAY
(N ELEMENTS)

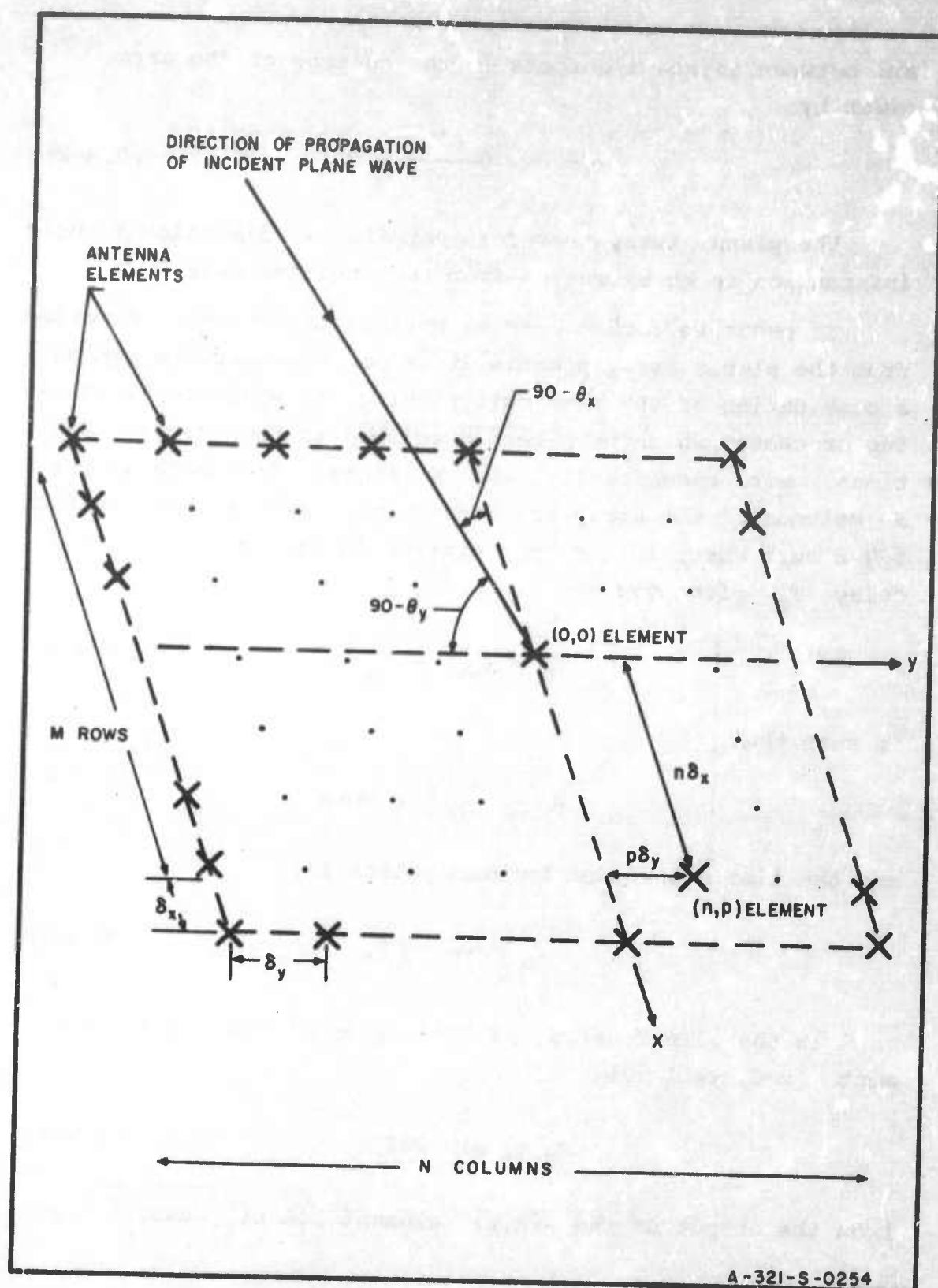


FIG. 6.3-1 PLANAR ARRAY WITH INCIDENT PLANE WAVE

and between adjacent outputs in the columns of the array given by:

$$\Delta\tau_x = \frac{\delta_x \sin \theta_x}{c} \quad (6.3-2)$$

The planar array therefore permits two dimensional angle information to be extracted from the incident wave.

In order to form a complex optical transmission function from the planar array signals, it is now necessary to employ a combination of the time-multiplexing and spatial-multiplexing processes which have been described in the previous sections. More specifically, the M signals from each of the N columns of the array are time-multiplexed as shown in Fig. 6.3-2 such that, in a manner similar to Sec. 6.2, the fixed delay T_D given by:

$$T_D = T_{n+1} - T_n \quad (6.3-3)$$

is such that

$$T_D > T + |\Delta\tau_x|_{\max} \quad (6.3-4)$$

and the time separation between pulses is:

$$T_s = T_D + \Delta\tau_x \quad (6.3-5)$$

In the planar array, if the output of the $(0,0)$ element $(x=0, y=0)$ is:

$$P_T(t) \sin 2\pi f_r t \quad (6.3-6)$$

then the output of the (n,p) element $(x=n\delta_x, y=p\delta_y)$ is:

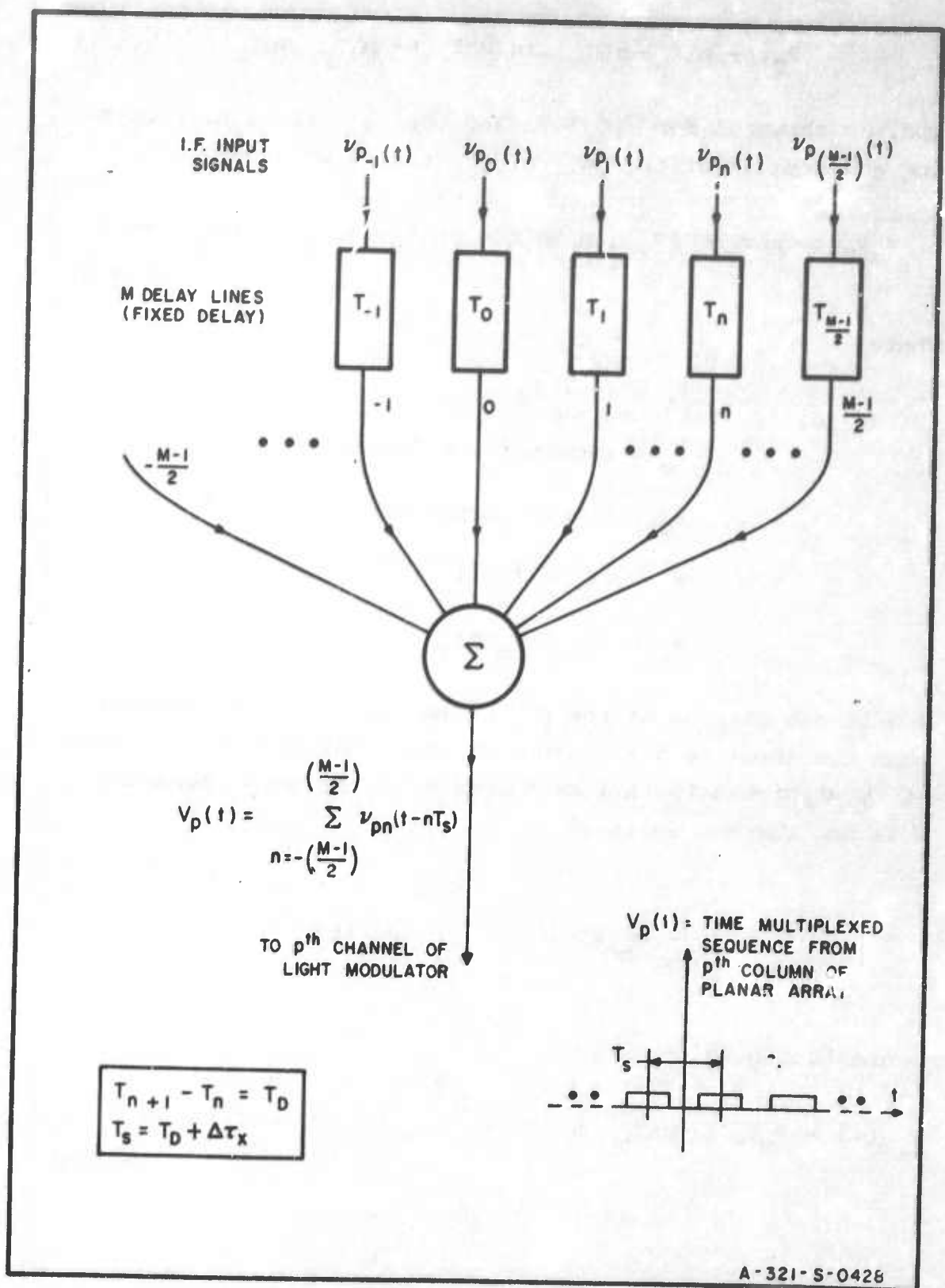


FIG. 6.3-2 TIME MULTIPLEXING SIGNALS FROM p^{th} COLUMN OF PLANAR ARRAY

$$P_T(t - p\Delta\tau_y - n\Delta\tau_x) \sin 2\pi f_r(t - p\Delta\tau_y - n\Delta\tau_x) \quad (6.3-7)$$

and, as shown in Eqs. (6.1-7) and (6.1-8), after heterodyning and amplification, Eq. (6.3-7) can be written:

$$V_m P_T(t - p\Delta\tau_y - n\Delta\tau_x) \sin 2\pi[f_i(t - p\Delta\tau_y - n\Delta\tau_x) - p\gamma_2 - n\gamma_1] \quad (6.3-8)$$

where:

$$f_i = f_o + f_d$$

$$f_o = \text{intermediate frequency}$$

$$f_d = \text{Doppler frequency}$$

$$\gamma_1 = (f_c - f_o)\Delta\tau_x$$

$$\gamma_2 = (f_c - f_o)\Delta\tau_y$$

Now if the outputs of the p^{th} column are time multiplexed, then the input to the channel of the light modulator located at $y = p\beta$ will be a time function of the form (assuming M is odd for convenience):

$$V_p(t) = \sum_{n=-(\frac{M-1}{2})}^{(\frac{M-1}{2})} v_{pn}(t)$$

where (using Eq. 6.3-5):

$$v_{pn}(t) = V_m P_T(t - p\Delta\tau_y - nT_s) \sin 2\pi[f_i(t - p\Delta\tau_y - nT_s) - p\gamma_2 - n\gamma_1] \quad (6.3-9)$$

Thus the complex transmission function will consist of N spatially-multiplexed sequences of M time-multiplexed signals.

When the electrical signal in Eq. (6.3-9) excites the ultrasonic transducer, the ultrasonic signal will be of the form (as shown in Eq. 6.1-9):

$$P_d(x+p\Delta x+nd_s)\sin 2\pi[f(x+p\Delta x+nd_s) + py_2 + ny_1] \quad (6.3-10)$$

and, at some instant of time, the ensemble of ultrasonic signals will appear as shown in Fig. 6.3-3. It is seen that the sequences are skewed along the line:

$$x = -\Delta y \quad (6.3-11)$$

and the incremental displacement between adjacent sequences is given by:

$$\Delta x = S\Delta\tau_y = \Delta\beta \quad (6.3-12)$$

Thus in a manner similar to Sec. 6.2 (Eq. 6.2-6) the contribution to positive first order light amplitude from the light which is diffracted by the signals in the channel at $y = p\beta$ is:

$$\tilde{g}_p(u,v) = \frac{\psi_m}{2} \sum_{n=-(\frac{M-1}{2})}^{(\frac{M-1}{2})} \int_{x=-p\Delta\beta-nd_s-\frac{d}{2}}^{-p\Delta\beta-nd_s+\frac{d}{2}} \int_{y=p\beta-\frac{b}{2}}^{p\beta+\frac{b}{2}} e^{j2\pi[f(x+p\Delta\beta+nd_s) + py_2 + ny_1]} e^{-j2\pi ux} e^{-j2\pi vy} dx dy \quad (6.3-13)$$

Let

$$\xi = x + p\Delta B + nd_s, \quad \eta = y - p\delta$$

and

$$\begin{aligned} \tilde{g}_p(u, v) = & \frac{\psi_m}{2} e^{-j2\pi p[\beta v - \beta \Delta u - \gamma_2]} \sum_{n=-\frac{(M-1)}{2}}^{\frac{(M-1)}{2}} e^{j2\pi n[ud_s + \gamma_1]} \\ & \cdot \left[\int_{-\frac{d}{2}}^{\frac{d}{2}} \int_{-\frac{b}{2}}^{\frac{b}{2}} e^{-j2\pi \xi(u-f)} e^{-j2\pi \eta v} d\xi d\eta \right] \end{aligned} \quad (6.3-14)$$

The total output light amplitude is (assuming, for convenience, that N is odd):

$$G_1(u, v) = \sum_{p=-\frac{(N-1)}{2}}^{\frac{(N-1)}{2}} \tilde{g}_p(u, v) \quad (6.3-15)$$

and, using the identity:

$$\sum_{p=-\frac{(N-1)}{2}}^{\frac{(N-1)}{2}} e^{jnz} = \frac{\sin \frac{Nz}{2}}{\sin \frac{z}{2}} \quad (6.3-16)$$

the first-order light intensity becomes:

$$\begin{aligned} |G_1(u, v)|^2 = & \frac{\psi_m^2}{4} \left(\frac{b \sin \pi b v}{\pi b v} \right)^2 \left(\frac{d \sin \pi d(u-f)}{\pi d(u-f)} \right)^2 \\ & \cdot \left(\frac{\sin \pi N(\beta v - \beta \Delta u - \gamma_2)}{\sin \pi(\beta v - \beta \Delta u - \gamma_2)} \right)^2 \left(\frac{\sin \pi M(ud_s + \gamma_1)}{\sin \pi(ud_s + \gamma_1)} \right)^2 \end{aligned} \quad (6.3-17)$$

In the light of the procedures which have been previously followed in Secs. 6.1 and 6.2, this result, which is essentially a combination of Eqs. (6.1-16) and (6.2-7), is to be expected. In a manner similar to that of Sec. 6.1, it can be shown that the complex optical transmission function is non-separable and Eq. (6.3-17) therefore cannot be expressed as the product of two independent functions of the variables u and v . Thus the principal maximum of:

$$\left(\frac{\sin \pi N(\beta v - \beta \Lambda u - \gamma_2)}{\sin \pi(\beta v - \beta \Lambda u - \gamma_2)} \right)^2 \quad (6.3-17)$$

runs along the line:

$$v = \frac{\gamma_2}{\beta} + \Lambda u \quad (6.3-18)$$

and, choosing $f_0 = kT_D$ (Sec. 6.2), the peak of $|G_1(u, v)|^2$ occurs at the intersection of Eq. (6.3-18) and the k^{th} grating lobe of

$$\left(\frac{\sin \pi M(u d_s + \gamma_1)}{\sin \pi(u d_s + \gamma_1)} \right)^2 \quad (6.3-19)$$

as shown in Fig. 6.3-4.

As before, the amplitude weighting imposed by the functions:

$$\left(\frac{b \sin \pi b v}{\pi b v} \right) \left(\frac{\sin \pi d(u - f)}{\pi d(u - f)} \right)^2 \quad (6.3-20)$$

can be ignored.

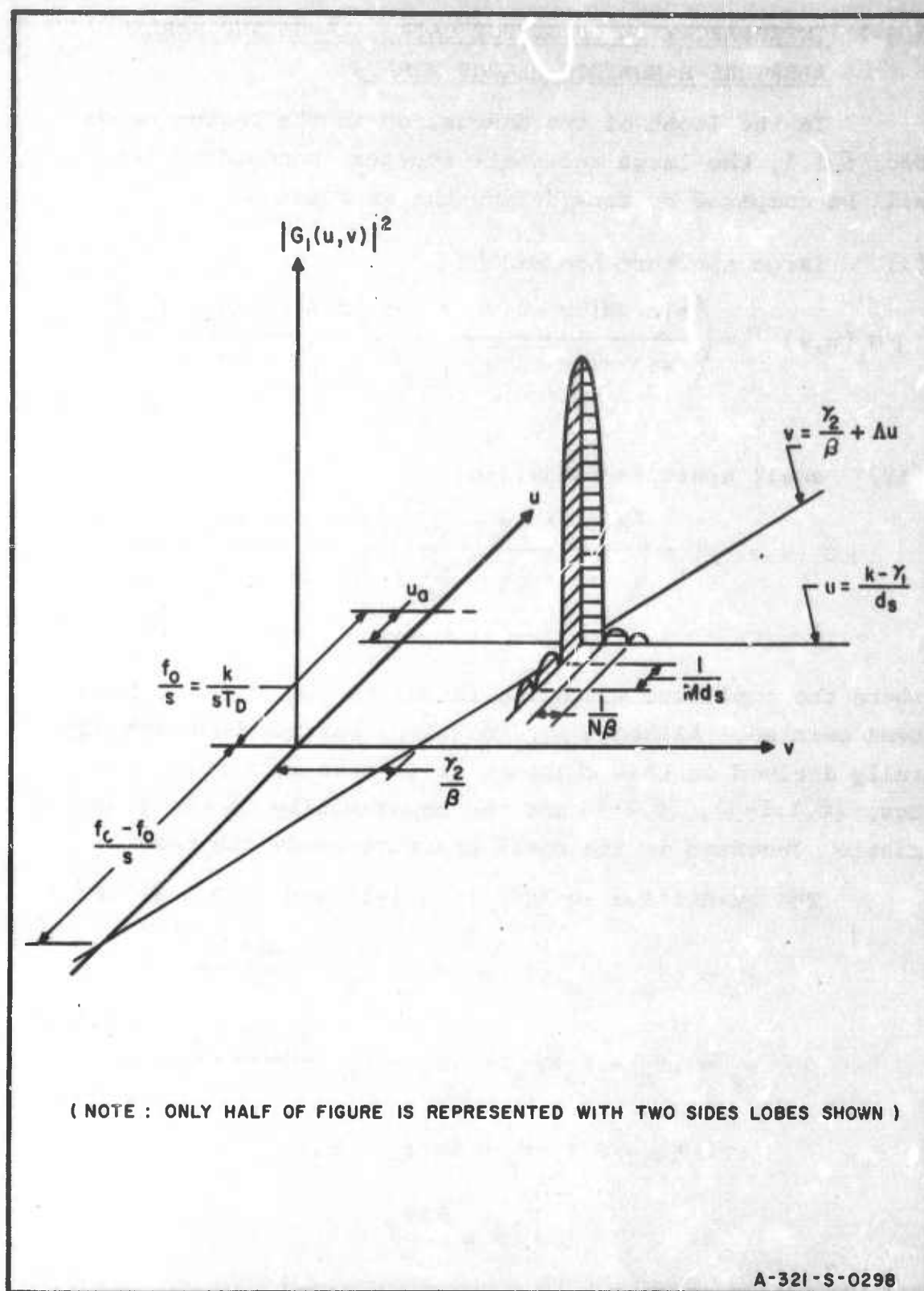


FIG. 6.3-4 POSITIVE FIRST-ORDER PEAK LIGHT INTENSITY : LARGE APERTURE - BANDWIDTH PLANAR ARRAY

6.3-1 INTERPRETATION OF OUTPUT DATA: LARGE AND SMALL APERTURE-BANDWIDTH PLANAR ARRAYS

In the light of the discussion at the beginning of Sec. 6.1.1, the large and small aperture-bandwidth cases will be compared by considering the expressions:

(i) large aperture-bandwidth

$$|G_1(u, v)|^2 = \left(\frac{\sin \pi N(\beta v - \beta \Lambda u - \gamma_2)}{\sin \pi(\beta v - \beta \Lambda u - \gamma_2)} \right)^2 \left(\frac{\sin \pi M(u d_s + \gamma_1)}{\sin \pi(u d_s + \gamma_1)} \right)^2 \quad (6.3.1-1)$$

(ii) small aperture-bandwidth

$$|G_1(u, v)|^2 = \left(\frac{\sin \pi N(\beta v - \frac{\Delta \phi}{2\pi})}{\sin \pi(\beta v - \frac{\Delta \phi}{2\pi})} \right)^2 \left(\frac{\sin \pi M(u d_s + \gamma_1)}{\sin \pi(u d_s + \gamma_1)} \right)^2 \quad (6.3.1-2)$$

where the amplitude weighting functions (Eq. 6.3-20) have been omitted. Although Eq. (6.3.1-2) has not been specifically derived in this chapter, it is seen to result from Eqs. (6.1.1-3), (6.2-7) and the separability of the transmission function in the small aperture-bandwidth case.

The quantities in Eqs. (6.3.1-1) and (6.3.1-2) are

$$\begin{aligned} \gamma_1 &= (f_c - f_o) \Delta \tau_x = (f_c - f_o) \frac{\delta_x \sin \theta_x}{c} \\ \gamma_2 &= (f_c - f_o) \Delta \tau_y = (f_c - f_o) \frac{\delta_y \sin \theta_y}{c} \end{aligned} \quad (6.3.1-3)$$

$$\Delta \phi = 2\pi f_r \Delta \tau_y = 2\pi(f_c + f_d) \Delta \tau_y$$

$$\Lambda = \frac{\Delta x}{\beta} = \frac{s \Delta \tau_y}{\beta}$$

$$d_s = s(T_D + \Delta\tau_x)$$

and it will be assumed that: $\frac{\delta x}{c} = \frac{\delta y}{c} = \frac{1}{2f_c}$.

The information concerning θ_x is contained in the u coordinate of peak first-order intensity. In Sec. 6.2 it has been shown that:

$$u_a = \left(\frac{\Delta\tau_x}{T_D + \Delta\tau_x} \right) \left(\frac{f_c}{s} \right) \quad (6.3.1-4)$$

where u_a is the measured displacement, in the u direction, of the peak from the line $u = \frac{f_o}{s}$. Thus, in both the large and small aperture-bandwidth cases:

$$\theta_x = \sin^{-1} \left[\left(\frac{su_a}{f_c - su_a} \right) (2f_c T_D) \right] \quad (6.3.1-5)$$

With regard to the v -coordinate of peak first-order intensity, this occurs at the point, v_a , given by:

(i) large aperture-bandwidth:

$$v_a = \frac{\gamma_2}{\beta} + \frac{\Lambda u}{u = \frac{f_o}{s} - u_a} \quad (6.3.1-6)$$

and since:

$$\gamma_2 = (f_c - f_o)\Delta\tau_y \quad (6.3.1-7)$$

$$\Lambda = \frac{\Delta x}{\beta} = \frac{s\Delta\tau_y}{\beta}$$

then

$$v_a = \left[1 - \frac{su_a}{f_c} \right] \frac{f_c \Delta\tau_y}{\beta} \quad (6.3.1-8)$$

(ii) small aperture-bandwidth

$$v_a = \frac{\Delta\phi}{2\pi\beta} = \left(\frac{f_c + f_d}{\beta} \right) \Delta\tau_y \quad (6.3.1-9)$$

In this configuration the Doppler frequency cannot be measured; since however $f_c \gg f_d$, then the approximate location is:

$$v_a = -\frac{f_c \Delta\tau_y}{\beta} \quad (6.3.1-10)$$

Thus in (i):

$$\theta_y = \sin^{-1} \left[\frac{2\beta v_a}{1 - \frac{\beta u_a}{f_c}} \right] \quad (6.3.1-11)$$

and for (ii)

$$\theta_y = \sin^{-1}(2\beta v_a) \quad (6.3.1-12)$$

To summarize these results, it is seen that the peak intensity will not occur at the same point for both cases. In the large aperture-bandwidth case, although no error is introduced by Doppler frequency, it will be necessary to use two measurements in order to obtain the angle θ_y . This occurs because of the non-separable transmission function; that is, since the output light distribution cannot be represented as the product of two independent functions of u and v , and the v coordinate of peak intensity will be dependent on the u coordinate as is evidenced by Eq. (6.3.1-8). This of course does not occur in the small aperture-bandwidth case since the transmission function is separable.

In order to compare the diffraction patterns for the two cases, let $\frac{f_0}{\beta} = f_s$ and rewrite Eq. (6.3.1-10) as:

$$v_a = \frac{f_c - f_o}{\beta} \Delta\tau_y + \frac{f_o}{s} \frac{s\Delta\tau_y}{\beta} = \frac{\gamma_2}{\beta} + \Delta f_s$$

Thus it is seen that in the small aperture-bandwidth case, the peak intensity occurs at the intersection of the lines:

$$u = \frac{k - \gamma_1}{d_s} = f_s - u_a$$

$$v = \frac{\gamma_2}{\beta} + \Delta f_s$$

and in the large aperture-bandwidth case at the intersection of

$$u = \frac{k - \gamma_1}{d_s} = f_s - u_a$$

$$v = \frac{\gamma_2}{\beta} + \Delta u$$

This is shown in Fig. 6.3.1-1. As indicated in Sec. 6.1.1, the null pattern in the large aperture-bandwidth case is rhombic because of the skewing of the transmission function.

6.4 SIGNAL TO NOISE DEGRADATION IN LARGE APERTURE-BANDWIDTH ELECTRO-OPTICAL ARRAY-ANTENNA PROCESSORS

Random electrical signals exciting the transducers of a Debye-Sears light modulator will cause random ultrasonic signals to propagate in the light modulator medium, and thus cause a randomized diffraction of the incident light. This effect will therefore contribute to the overall output noise level. It is especially necessary to consider this source of output noise in large aperture-bandwidth cases since, under these conditions, there will always be more light which is phase modulated by noise than by signal (Sec. 6.4.2).

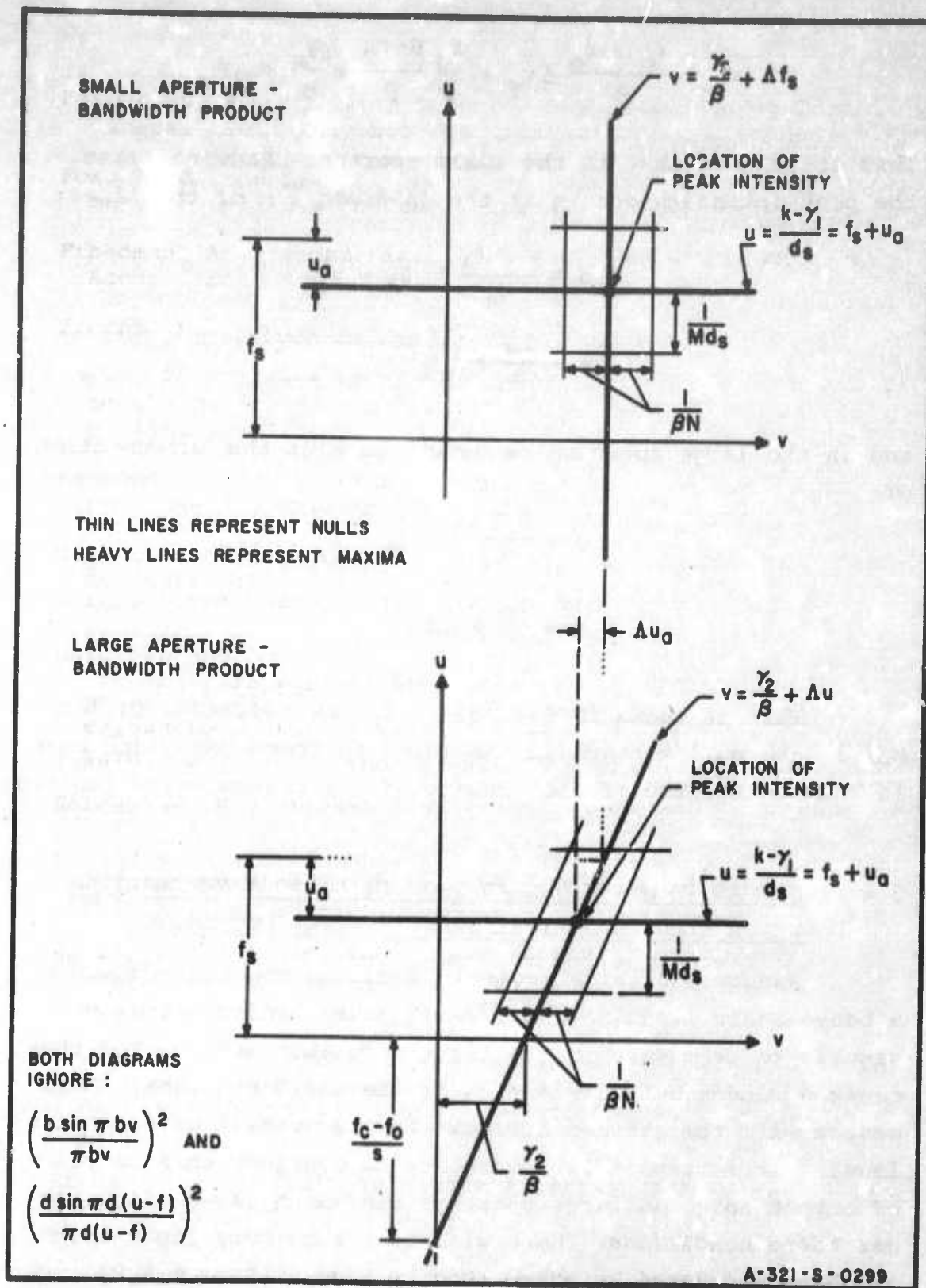


FIG. 6.3.1-1 NULL PATTERN AND LOCATION OF PEAK INTENSITIES : LARGE AND SMALL APERTURE - BANDWIDTH PLANAR ARRAYS.

In what follows, a mathematical model describing the diffraction patterns caused by random ultrasonic disturbances will be derived for a general random process and also for the special case in which the process is assumed to be Gaussian (not necessarily white noise). It will be seen that in the Gaussian case the general expressions derived, which reduce to those obtained for the general case, will be exact. These results will then be used to evaluate the degradation in output signal to noise ratio resulting from large aperture-bandwidth conditions. It will be seen that, using white noise as an example, when the electro-optical processor is used to process signals from a planar array antenna, the degradation due to a large aperture-bandwidth product will be negligible, but may be significant in the case of a linear array if the spatially-multiplexed configuration is employed.

6.4.1 LIGHT DIFFRACTION BY RANDOM SIGNALS

(i) General Random Process

An electrical signal exciting the piezoelectric transducer of a Debye-Sears light modulator causes an ultrasonic wave to propagate through the light modulator medium. Let the ultrasonic disturbance propagating in the x direction, at a given instant of time, be denoted as $\psi(x)$.

It has been shown (Raman and Nath 1936) that, for weak ultrasonic fields, the ultrasonic disturbance will give rise to a pure phase modulation of the light wave front given by:

$$\frac{2\pi L\psi(x)}{\lambda}$$

where

L = length of light path in Debye-Sears light modulator

λ = light wavelength

For convenience of notation, the constant, $\frac{2\pi L}{\lambda}$, will be ignored and it will be assumed that an ultrasonic disturbance $\psi(x)$ gives rise to a spatial phase perturbation of the light wave front also denoted as $\psi(x)$. Thus, if the incident light is a plane wave of constant amplitude, the light amplitude in the output, (u,v) , plane of the optical processor has been shown to be (Cutrona 1960):

$$G'(u,v) = K \int_x \int_y e^{j\psi(x)} e^{-j2\pi ux} e^{-j2\pi vy} dx dy$$

where integration is performed over the entire optical aperture, and K is a constant. Let $G(u,v) = \frac{G'(u,v)}{K}$. Since photo detectors are used to obtain output data, the observed light intensity will be proportional to $|G(u,v)|^2$.

Thus, if the signal at the transducer is a real random time function $n(t)$ giving rise to a real random ultrasonic disturbance, $n(x)$, the normalized output light amplitude at a given instant of time will be:

$$G(u,v) = \int_x \int_y e^{jn(x)} e^{-j2\pi ux} e^{-j2\pi vy} dx dy$$

and in this case let the output intensity be:

$$R_T(u,v) = E[G(u,v) G^*(u,v)]$$

where:

E denotes expected value

* denotes complex conjugate.

Now consider an optical processor using a Debye-Sears light modulator with N channels (Fig. 6.1-2) whose transducers are excited by samples of a random process. Let N be odd for convenience. Since the samples at different transducers arise from noise which has been generated in separate networks and also from random excitations of separate antenna elements, the noise samples are assumed independent; it is also assumed that the samples have zero mean.

Hence the contribution to the total output light amplitude, $G(u,v)$, from the channel located at $y = p\beta$ will be:

$$g_p(u,v) = \int_{-D/2}^{D/2} \int_{p\beta - \frac{b}{2}}^{p\beta + \frac{b}{2}} e^{jn_p(x)} e^{-j2\pi ux} e^{-j2\pi vy} dx dy \quad (6.4.1-1)$$

In this method of signal processing the ultrasonic signals are always assumed to be small (Lambert 1962), thus:

$$g_p(u,v) = \int_{-D/2}^{D/2} \int_{p\beta - \frac{b}{2}}^{p\beta + \frac{b}{2}} [1 + jn_p(x) - \frac{1}{2}n_p^2(x) + O(n^3)] e^{-j2\pi ux} e^{-j2\pi vy} dx dy$$

where $O(n^3)$ denotes the error in the approximation of $e^{jn(x)}$ due to terms of the order of n^3 .

For convenience of notation, let:

$$\int_{-D/2}^{D/2} f(x) e^{-j2\pi ux} dx = I f(x)$$

$$\int_{-D/2}^{D/2} f(x) e^{j2\pi ux} dx = I * f(x)$$

$$\int_{-D/2}^{D/2} (1) e^{-j2\pi ux} dx = \frac{D \sin \pi Du}{\pi Du} = Z(u)$$

$$\int_{-b/2}^{b/2} (1) e^{-j2\pi vy} dy = \frac{b \sin \pi bv}{\pi bv} = Z(v)$$

note that:

$$\begin{aligned} I f(x) I * f(x) &= \int_{-D/2}^{D/2} f(x_1) e^{-j2\pi ux_1} dx_1 \int_{-D/2}^{D/2} f(x_2) e^{j2\pi ux_2} dx_2 \\ &= \int_{-D/2}^{D/2} \int_{-D/2}^{D/2} f(x_1) f(x_2) e^{-j2\pi u(x_1 - x_2)} dx_1 dx_2 \end{aligned}$$

Thus:

$$g_p(u, v) = Z(v) e^{-j2\pi p \delta v} [Z(u) + j I n_p(x) - \frac{1}{2} I n_p^2(x) + I O(n^3)]$$

and the total output light amplitude from all N channels will be:

$$G(u, v) = \sum_{p=-(\frac{N-1}{2})}^{(\frac{N-1}{2})} g_p(u, v)$$

Hence:

$$\begin{aligned} E[|G(u, v)|^2] &= E \left\{ Z^2(v) \sum_p \sum_q e^{-j2\pi(p-q)\delta v} \right. \\ &\quad \left. [Z(u) + j I n_p(x_1) - \frac{1}{2} I n_p^2(x_1) + I O(n^3)] \right\} \end{aligned}$$

$$\cdot [Z(u) - j I^* n_q(x_2) - \frac{1}{2} I^* n_q^2(x_2) + I^* \sigma(n^3)] \}$$

and:

$$\begin{aligned} E[|G(u,v)|^2] &= Z^2(v) \sum_p \sum_q e^{-j2\pi(p-q)\beta v} Z^2(u) \\ &+ Z^2(v) \sum_p \sum_q e^{-j2\pi(p-q)\beta v} Z(u) \left[j I E[n_p(x_1)] - j I^* E[n_q(x_2)] \right. \\ &\quad \left. - \frac{1}{2} I E[n_p^2(x_1)] - \frac{1}{2} I^* E[n_q^2(x_2)] + I \sigma(n^3) + I^* \sigma(n^3) \right] \\ &+ Z^2(v) \sum_p \sum_q e^{-j2\pi(p-q)\beta v} \left[I I^* E[n_p(x_1) n_q(x_2)] + I I^* \sigma(n^3) \right] \end{aligned} \quad (6.4.1-2)$$

Now if $r(t_1, t_2)$ is the autocorrelation function of the electrical signals exciting the transducers, which for a real process is defined as:

$$r(t_1, t_2) = E[n(t_1) n(t_2)]$$

then the autocorrelation function for the random ultrasonic disturbance which arises from these signals will be:

$$r(x_1, x_2) = E[n(x_1) n(x_2)]$$

Hence by assumption of independence and zero mean:

$$E[n_p(x_1) n_q(x_2)] = r(x_1, x_2) \delta_{pq}$$

where

$$\delta_{pq} = \begin{cases} 0 & p \neq q \\ 1 & p = q \end{cases}$$

and

$$E[n_p^2(x)] = E[n_q^2(x)] = r(0) \quad \text{for all } p \text{ and } q.$$

Thus:

$$I E[n_p^2(x_1)] = I^* E[n_q^2(x_2)] = r(0) \int_{-D/2}^{D/2} e^{-j2\pi ux} dx = r(0) Z(u)$$

$$I I^* E[n_p(x_1) n_q(x_2)] = \int_{-D/2}^{D/2} \int_{-D/2}^{D/2} r(x_1, x_2) \delta_{pq} e^{-j2\pi u(x_1 - x_2)} dx_1 dx_2$$

and, within the approximation arising through neglecting the error terms, $O(n^3)$:

$$R_T(u, v) = Z^2(v) \sum_{p=-(\frac{N-1}{2})}^{(\frac{N-1}{2})} \sum_{q=-(\frac{N-1}{2})}^{(\frac{N-1}{2})} e^{-j2\pi(p-q)u}$$

$$\left[Z^2(u)(1 - r(0)) + \int_{-D/2}^{D/2} \int_{-D/2}^{D/2} r(x_1, x_2) \delta_{pq} e^{-j2\pi u(x_1 - x_2)} dx_1 dx_2 \right]$$

Make use of the identity:

$$\sum_{p=-(\frac{N-1}{2})}^{(\frac{N-1}{2})} e^{j p z} = \frac{\sin \frac{Nz}{2}}{\sin \frac{z}{2}}$$

and:

$$R_T(u, v) = Z^2(v) Z^2(u) (1 - r(0)) \left(\frac{\sin \pi N v}{\sin \pi v} \right)^2 + Z^2(v) N \int_{-D/2}^{D/2} \int_{-D/2}^{D/2} r(x_1, x_2) e^{-j2\pi u(x_1 - x_2)} dx_1 dx_2$$

(6.4.1-3)

The first term on the right hand side of Eq. (6.4.1-3) is the zero-order light intensity resulting from diffraction due to the configuration of optical aperture. The term $(1 - r(0))$ takes account of the light which has been diffracted away from the zero order by the random signal, and the contribution from the random process is described by the expression:

$$R(u,v) = Z^2(v)N \int_{-D/2}^{D/2} \int_{-D/2}^{D/2} r(x_1, x_2) e^{-j2\pi u(x_1 - x_2)} dx_1 dx_2 = Z^2(v)R(u)$$

Since the random ultrasonic disturbance is assumed to be a function of x alone, it is seen that only the u variation will depend upon the statistical properties of the random process, the v variation being dependent only upon the width of the ultrasonic wave through the function:

$$Z^2(v) = \left(\frac{b \sin \pi bv}{\pi bv} \right)^2$$

It is also seen that the response to N channels is N times that of a single channel. Thus the light intensity from each channel contributes independently to the total output and all contributions resulting from interference between diffracted light from separate channels tend to be cancelled. This follows from Eq. (6.4.1-2) and the assumption of zero mean and independence of $n_p(x)$ and $n_q(x)$. In the case of deterministic signals, however, this cancellation between outputs from separate channels does not take place and the peak output intensity is proportional to N^2 . Thus, as will be seen, the output signal to noise ratio (ignoring all other noise sources) will tend to be increased as the number of channels increases.

(ii) Gaussian Random Process

In this case let $n(x)$ be a random sample of a Gaussian random process (not necessarily white noise). As before (Eq. 6.4.1-1) the contribution to output light amplitude from the channel located at $y = p\beta$ is:

$$g_p(u, v) = Z(v) e^{-j2\pi p\beta v} \int_{-D/2}^{D/2} e^{jn_q(x)} e^{-j2\pi ux} dx$$

and

$$E[|G(u, v)|^2] = Z^2(v) \sum_p \sum_q e^{-j2\pi(p-q)\beta v} \int_{-D/2}^{D/2} \int_{-D/2}^{D/2} E \left[e^{j[n_p(x_1) - n_q(x_2)]} e^{-j2\pi u(x_1 - x_2)} \right] dx_1 dx_2$$

However, since the process is assumed Gaussian, then for each value of x_1 and x_2 the random variable ζ defined as:

$$\zeta = n(x_1) - n(x_2)$$

is itself a Gaussian random variable.

Recall that the characteristic function of a random variable ζ with probability density $P(\zeta)$ is defined as:

$$M_\zeta(\omega) = E[e^{j\omega\zeta}] = \int_{-\infty}^{\infty} P(\zeta) e^{j\omega\zeta} d\zeta$$

and that if ζ is Gaussian with zero mean and variance $= \sigma^2$, then:

$$M_\zeta(\omega) = e^{\frac{-\omega^2 \sigma^2}{2}}$$

Thus:
$$E \left[e^{j(n(x_1) - n(x_2))} \right] = E \left[e^{j\zeta} \right] = M_\zeta(1) = e^{-\frac{\sigma^2}{2}}$$

where, since $E[n(x)] = 0$:

$$\sigma^2 = E \left[(n(x_1) - n(x_2))^2 \right] = 2 r(0) - 2 r(x_1, x_2)$$

In the case of N channels:

$$E \left[e^{j[n_p(x_1) - n_q(x_2)]} \right] = e^{-r(0)} e^{r(x_1, x_2) \delta_{pq}}$$

and since:

$$\int_{-D/2}^{D/2} \int_{-D/2}^{D/2} e^{-j2\pi u(x_1 - x_2)} dx_1 dx_2 = Z^2(u)$$

then:

$$\begin{aligned} E[|G(u, v)|^2] &= R_T(u, v) = Z^2(v) e^{-r(0)} \sum_p \sum_q e^{-j2\pi(p-q)\beta v} \cdot \\ &\int_{-D/2}^{D/2} \int_{-D/2}^{D/2} e^{r(x_1, x_2) \delta_{pq}} e^{-j2\pi u(x_1 - x_2)} dx_1 dx_2 \\ &= e^{-r(0)} Z^2(v) Z^2(u) \left[\left(\frac{\sin \pi N \beta v}{\sin \pi \beta v} \right)^2 - N \right] \\ &+ e^{-r(0)} Z^2(v) N \int_{-D/2}^{D/2} \int_{-D/2}^{D/2} e^{r(x_1, x_2)} e^{-j\pi u(x_1 - x_2)} dx_1 dx_2 \quad (6.4.1-4) \end{aligned}$$

which is exact. Thus the contribution from the random process in the Gaussian case occurs through the expression:

$$Z^2(v) N \int_{-D/2}^{D/2} \int_{-D/2}^{D/2} e^{r(x_1, x_2)} e^{-j2\pi u(x_1 - x_2)} dx_1 dx_2$$

Equation (6.4.1-4) can now be reduced to that of the general case, since:

$$e^{-r(0)} = 1 - r(0) + O(n^4)$$

$$e^{r(x_1, x_2)} = 1 + r(x_1, x_2) + O(n^4)$$

and, within the approximation resulting from ignoring error terms of the order of n^4 :

$$R_T(u, v) = [1 - r(0)] Z^2(v) \left[Z^2(u) \left(\frac{\sin \pi N \beta v}{\sin \pi \beta v} \right)^2 - Z^2(u) N \right. \\ \left. + Z^2(u) N + N \int_{-D/2}^{D/2} \int_{-D/2}^{D/2} r(x_1, x_2) e^{-j2\pi u(x_1 - x_2)} dx_1 dx_2 \right] \\ = Z^2(v) Z^2(u) \left(\frac{\sin \pi N \beta v}{\sin \pi \beta v} \right)^2 [1 - r(0)] \\ + Z^2(v) N \int_{-D/2}^{D/2} \int_{-D/2}^{D/2} r(x_1, x_2) e^{-j2\pi u(x_1 - x_2)} dx_1 dx_2$$

which is identical with Eq. (6.4.1-3)

Consider some specific examples:

(i) Stationary White Noise: Infinite Bandwidth

Let the random electrical signals $n(t)$ be samples of stationary white noise with power spectral density W_0 . Then, ignoring the finite bandwidth of the light modulator, the power spectral density of the random ultrasonic disturbance will be KW_0 where K is a constant representing a possible attenuation in noise power, and also incorporates any necessary changes of units. Then:

$$r(x_1, x_2) = r(x_1 - x_2) = KW_0 \delta(x_1 - x_2)$$

and

$$R(u,v) = Z^2(v) K W_0 N \int_{-D/2}^{D/2} \int_{-D/2}^{D/2} \delta(x_1 - x_2) e^{-j2\pi u(x_1 - x_2)} dx_1 dx_2 = Z^2(v) K W_0 N D$$

This result is consistent with this optical processor's behavior as a spectrum analyzer. It has been shown (Eq. 2.1-6) that a sinusoidal signal of frequency f_i applied to a single-channel light modulator of length D and width b will result in first-order output light amplitude of the form:

$$Z(v) \left[\frac{D \sin \pi D(u + \frac{f_i}{S})}{\pi D(u + \frac{f_i}{S})} + \frac{D \sin \pi D(u - \frac{f_i}{S})}{\pi D(u - \frac{f_i}{S})} \right] \quad (6.4.1-5)$$

where S is the sonic velocity.

The distance of these "spectral lines" from the line $u = 0$ is a function of the frequency of the electrical signal at the transducer. Thus, under assumption of infinite bandwidth, white noise, having power at all frequencies, results in a constant light intensity for all values of the spatial-frequency variable " u ".

(ii) Stationary White Noise: Band Limited

The band-pass characteristics of the light modulator used in this method of electro-optical processing are determined by the bandwidth of the piezoelectric transducers. This may be written (Mason, 1948, Liben 1960):

$$B = k f_t$$

where:

B = electrical bandwidth of light modulator

f_t = resonant frequency of piezoelectric transducer

and k is a constant equal to $\frac{1}{2}$ in the ideal case (Mason 1948, Liben 1960).

In terms of the upper and lower 3 db frequencies the bandwidth can also be written as:

$$B = f_2 - f_1$$

Thus, since an electrical signal of frequency f_i will result in an ultrasonic signal with spatial frequency: $f = \frac{f_i}{s}$, then it is possible to define the spatial bandwidth as:

$$B_s = \frac{f_2 - f_1}{s} = \frac{B}{s} \quad (\text{units of cycles per meter})$$

If the resonant frequency of the piezoelectric transducer is f_t , then the resonant spatial frequency will be:*

$$f_o = \frac{f_t}{s}$$

and, in the band-limited case, the power spectral density of the ultrasonic disturbance due to white noise can be written as (considering for convenience positive frequencies only):

$$KW_o \text{ rect} \left(\frac{f - f_o}{B_s} \right)$$

where

$$\text{rect} \left(\frac{f}{B_s} \right) = \begin{cases} 1 & |f| \leq \frac{B_s}{2} \\ 0 & \text{otherwise} \end{cases}$$

* This is a change in notation; f_o is not to be confused with the intermediate frequency of Secs. 6.1, 6.2 and 6.3.

Therefore by stationarity of the random process:

$$r(x_1 - x_2) = KW_0 \int_{f_0 - \frac{B_s}{2}}^{f_0 + \frac{B_s}{2}} e^{j2\pi f(x_1 - x_2)} df = KW_0 e^{j2\pi f_0(x_1 - x_2)} \frac{\sin \pi B_s(x_1 - x_2)}{\pi B_s(x_1 - x_2)}$$

and (Eq. 6.4.1-3):

$$R(u, v) = Z^2(v) NKW_0 B_s \int_{-D/2}^{D/2} \int_{-D/2}^{D/2} \frac{\sin \pi B_s(x_1 - x_2)}{\pi B_s(x_1 - x_2)} e^{-j2\pi(u-f_0)(x_1 - x_2)} dx_1 dx_2$$

In order to evaluate the integral, let $\phi = u - f_0$ and observe that:

$$\int_{-D/2}^{D/2} \frac{\sin \pi B_s(x_1 - x_2)}{\pi B_s(x_1 - x_2)} e^{-j2\pi\phi x_1} dx_1$$

is the Fourier transform, with respect to the variable ϕ , of:

$$\text{rect}\left(\frac{x_1}{D}\right) \cdot \frac{\sin \pi B_s(x_1 - x_2)}{\pi B_s(x_1 - x_2)}$$

and is therefore the convolution of

$$\left[\frac{D \sin \pi D\phi}{\pi D\phi} \right] \text{ with } \left[\frac{e^{-j2\pi\phi x_2}}{B_s} \text{rect}\left(\frac{\phi}{B_s}\right) \right]$$

Hence:

$$R(u, v) = Z^2(v) NKW_0 B_s \int_{-D/2}^{D/2} \left[\frac{1}{B_s} \int_{-\frac{B_s}{2}}^{\frac{B_s}{2}} \frac{D \sin \pi D(\phi - \lambda)}{\pi D(\phi - \lambda)} e^{-j2\pi\lambda x_2} d\lambda \right] e^{j2\pi\phi x_2} dx_2$$

By interchanging the order of integration:

$$R(u,v) = Z^2(v)NKW_0 \int_{-\frac{B_s}{2}}^{\frac{B_s}{2}} \frac{\sin \pi D(\phi-\lambda)}{\pi D(\phi-\lambda)} \left[\int_{-D/2}^{D/2} e^{j2\pi x_2(\phi-\lambda)} dx_2 \right] d\lambda$$

and:

$$R(u,v) = Z^2(v)NKW_0 D^2 \int_{-\frac{B_s}{2}}^{\frac{B_s}{2}} \left[\frac{\sin \pi D(\phi-\lambda)}{\pi D(\phi-\lambda)} \right]^2 d\lambda.$$

Since:

$$\int_{-\infty}^{\infty} \left(\frac{\sin \pi D(\phi-\lambda)}{\pi D(\phi-\lambda)} \right)^2 d\lambda = \frac{1}{D}$$

Then allowing the bandwidth to become infinite results in $R(u,v) = Z^2(v)NKW_0 D$ as before.

In order to evaluate:

$$\int_{-\frac{B_s}{2}}^{\frac{B_s}{2}} \left(\frac{\sin \pi D(\phi-\lambda)}{\pi D(\phi-\lambda)} \right)^2 d\lambda$$

recall that, in the most general case, this electro-optical processor is used to process signals from a planar array antenna with M rows and N columns, that the M signals from each of the N columns are time multiplexed to form time sequences of M pulses, and that the N time sequences are fed into separate channels of the light modulator. Thus the value of D , the length of the light modulator channels, must be chosen so that, at a given instant of time, all of the M time-multiplexed pulses will be able to fit into the optical aperture.

Hence (Eq. 6.2-5 et. seq.):

$$D \approx MTS$$

where

M = number of rows in the array

T = pulse duration $\approx \frac{1}{B}$

S = sonic velocity

and
$$D \approx \frac{MS}{B} = \frac{M}{B_s}$$

In a large aperture-bandwidth case, say: $M > 100$ and therefore $B_s \gg \frac{2}{D}$. Thus (see Fig. 6.4.1-1) since over 90 percent of the total area under the curve $(\frac{\sin \pi Dx}{\pi Dx})^2$ falls under the main lobe $(-\frac{1}{D} \leq x \leq +\frac{1}{D})$, the value of the integral should be very nearly constant and approximately equal to $\frac{1}{D}$ for values of u in the range:

$$f_o - \frac{B_s}{2} + \frac{1}{D} \leq u \leq f_o + \frac{B_s}{2} - \frac{1}{D}$$

and for values of u such that:

$$f_o + \frac{B_s}{2} + \frac{1}{D} \leq u \leq f_o - \frac{B_s}{2} - \frac{1}{D}$$

the integral should be very nearly zero since only the side lobes of the integrand will fall into the region of integration (Fig. 6.4.1-2). As a result, since the observation region in this signal processor encompasses the region:

$$f_o - \frac{B_s}{2} \leq u \leq f_o + \frac{B_s}{2}$$

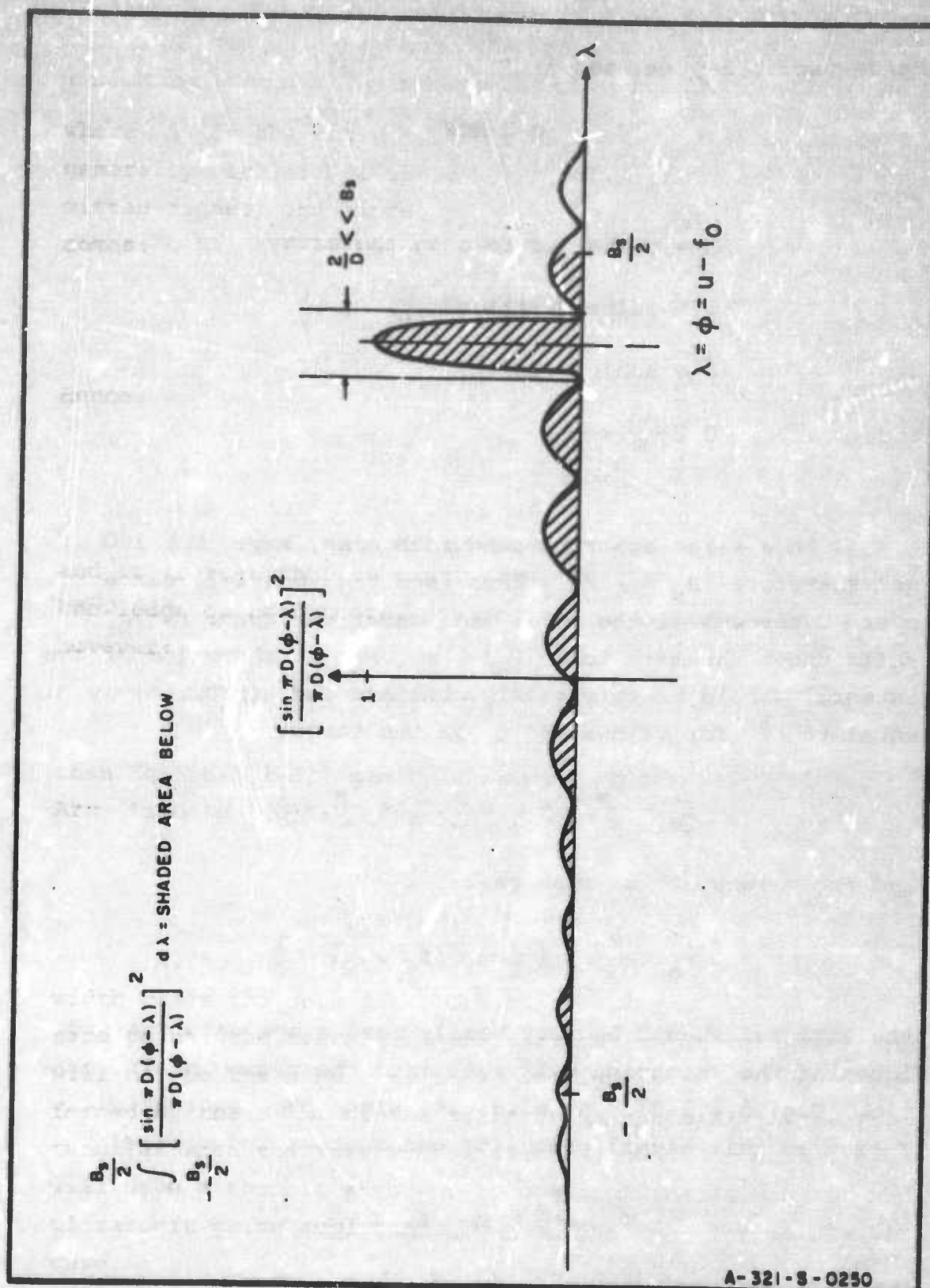


FIG. 6.4.1-1

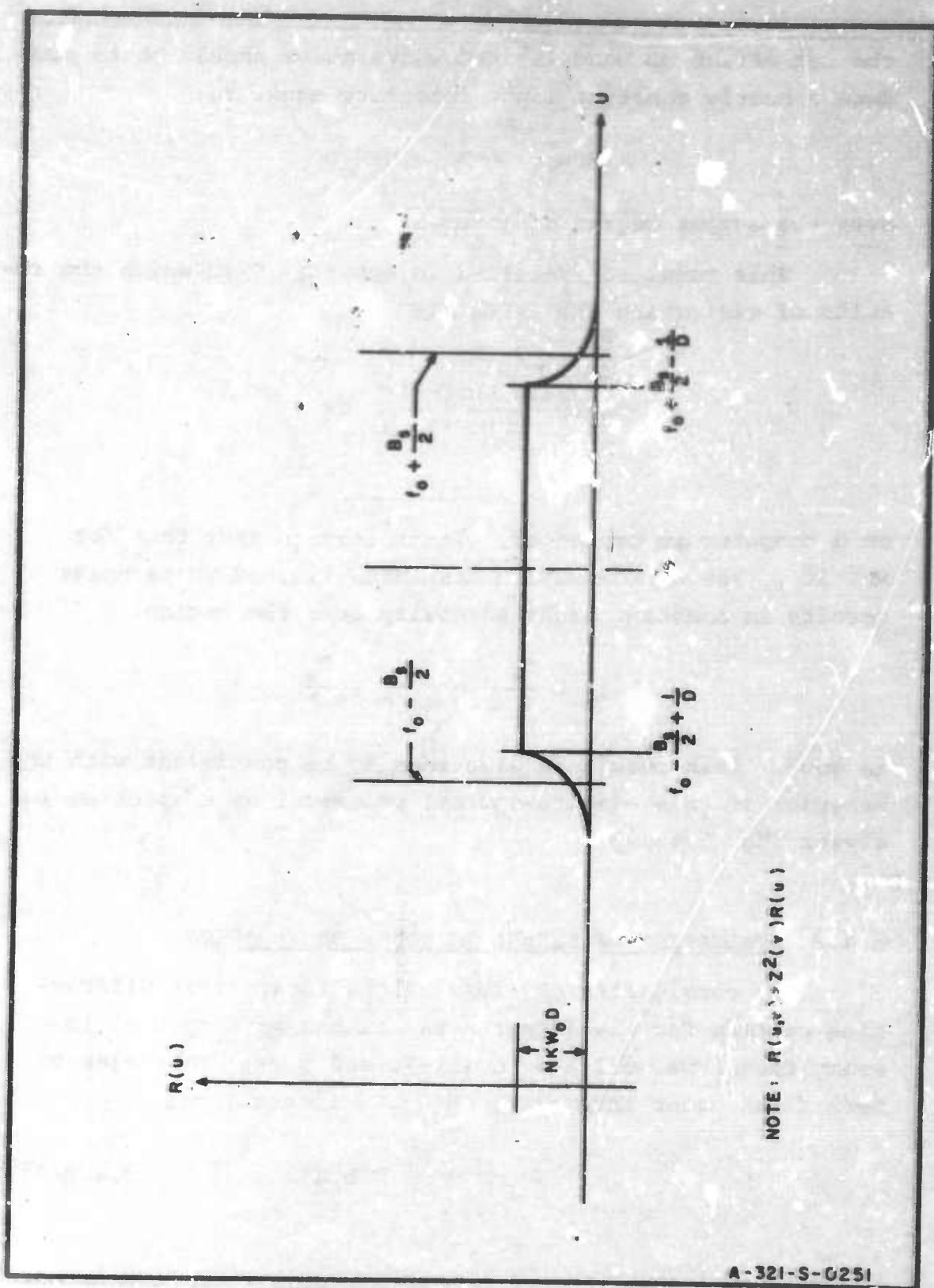


FIG. 6.4.1-2

the net effect of band-limited white noise should be to produce a nearly constant light intensity equal to:

$$R(u,v) = 2^2(v)NKW_0D$$

over the output region of interest.

This result is verified in Appendix C in which the results of evaluating the integral:

$$\int_{-\frac{B_s}{2}}^{+\frac{B_s}{2}} \left(\frac{\sin \pi D(\phi - \lambda)}{\pi D(\phi - \lambda)} \right)^2 d\lambda$$

on a computer are presented. It is seen in fact that for $M > 10$, the approximation that band-limited white noise results in constant light intensity over the region:

$$f_0 - \frac{B_s}{2} \leq u \leq f_0 + \frac{B_s}{2}$$

is good. This result is also seen to be consistent with the behavior of this electro-optical processor as a spectrum analyzer (Eq. 6.4.1-5).

6.4.2 EVALUATION OF SIGNAL TO NOISE DEGRADATION

In considering the form of the first-order diffraction pattern for the linear array it can be seen that in every case (Eqs. 6.1.1-2, 6.1.1-3, and 6.2-7) the relative peak first order intensity, $|G_{1p}|^2$, is equal to:

$$|G_{1p}|^2 = \frac{\psi_m^2}{4} N^2 b^2 d^2 \quad (6.4.2-1)$$

and for the planar array the peak first-order intensity is (Eqs. 6.3-20, 6.3.1-1 and 6.3.1-2):

$$|G_{1P}|^2 = \frac{\psi_m^2}{4} N^2 b^2 M^2 d^2 \quad (6.4.2-2)$$

It is evident therefore that for both the linear and the planar array:

$$|G_{1P}|^2 = \frac{\psi_m^2}{4} [\text{area covered by ultrasonic signal}]^2 \quad (6.4.2-3)$$

The actual value of output light intensity is of course dependent on the power in the light incident on the optical aperture. Regardless of the actual value, however, it is seen that in all cases (i.e., large and small aperture-bandwidth product and linear and planar array antennas) the peak output light intensity which has been diffracted by the ultrasonic signals must be proportional to the square of the area covered by the signals in the optical aperture.

When the piezoelectric transducers are excited by stationary white noise, the output intensity in the region of interest has been shown to be proportional to (Sec. 6.4.1 examples (i) and (ii)):

$$R(u,v) = Z^2(v) NKW_0 D \quad (6.4.2-4)$$

from which:

$$R(u,v) \leq \frac{KW_0}{ND} [\text{area covered by random ultrasonic disturbance}]^2$$

Thus let:

A_s = maximum area in optical aperture covered by signal

A_n = area in optical aperture covered by noise

and the peak signal to peak noise ratio in the output plane is:

$$\rho = \frac{\psi_m^2}{4} \frac{ND}{KW_o} \frac{A_s^2}{A_n^2} \quad (6.4.2-5)$$

Now the fact that large aperture-bandwidth processing will lead to a degradation in signal to noise ratio can be seen by comparing Figs. 6.1-3 and 6.3-3 with Figs. 2.2-3 and 2.4-3.

In the case of small aperture-bandwidth product the displacement in the received signal envelopes can be ignored (Sec. 6.1); then, at some instant of time, the ensemble of ultrasonic signals can be assumed to completely fill the aperture (Lambert 1965, see Figs. 2.2-3 and 2.4-3). Thus since $A_s^2 \approx A_n^2$, then, for both linear and planar small aperture-bandwidth arrays, the signal to noise ratio assuming stationary white noise becomes:

$$\rho = \frac{\psi_m^2}{4} \frac{ND}{KW_o} \quad (6.4.2-6)$$

When the aperture-bandwidth product is large, however, the time delays between received signals cannot be ignored and the ultrasonic signals become skewed across the width of the optical aperture (Figs. 6.1-3, 6.3-3). Thus, since the aperture must be large enough to contain all the pulses, at no time will it be completely filled with signal; hence the area occupied by noise will always exceed that which is occupied by signal and a degradation in signal to noise ratio, over that which is expressed in Eq. (6.4.2-6), will result.

Therefore in order to evaluate this effect, let the degradation be defined as:

$$\text{Degr.} = -10 \log \left(\frac{A_n}{A_s} \right)^2 \quad (6.4.2-7)$$

This quantity will now be obtained for the linear and planar large aperture-bandwidth arrays.

(i) Degradation in Large Aperture-Bandwidth Linear Arrays: Spatial Multiplexing

Since $\Delta x = \frac{S \delta \sin \theta}{c}$, it is seen in Fig. 6.4.2-2 that the skewing of the ensemble of ultrasonic pulses will become more pronounced as $|\theta|$ increases. The length of the aperture must be large enough to accommodate the maximum off-bore-sight signal which the antenna is required to cover; therefore if the pulse duration is T the length of each ultrasonic pulse will be $d = ST$, and (assuming $\frac{\delta}{c} = \frac{1}{2f_c}$):

$$D = d + \frac{S(N-1) \sin |\theta|_{\max}}{2f_c} \quad (6.4.2-8)$$

In this case:

$$A_s = Nbd, \quad A_n = NbD, \quad \text{and} \quad \frac{A_n}{A_s} = \frac{D}{d}$$

but:

$$\frac{D}{d} = 1 + \frac{S(N-1) \sin |\theta|_{\max}}{d2f_c}$$

and since:

$$d = ST \approx \frac{S}{B}$$

then (letting $|\theta|_{\max} = 90 \text{ deg}$):

$$\text{Degr.} = -10 \log \left[1 + \frac{B(N-1)}{2f_c} \right]^2 = -20 \log \left[1 + \frac{B(N-1)}{2f_c} \right] \quad (6.4.2-9)$$

Thus it is seen that, in the spatially multiplexing of large aperture-bandwidth product linear-array signals, a significant degradation in signal to noise ratio, over the small aperture-bandwidth case, can take place. The actual amount of degradation will depend upon the number of elements, N , and the quantity $\frac{B}{f_c}$ which is the fractional bandwidth of the transmitted signal. Some representative values will be given at the end of this section.

(ii) Degradation in Large Aperture-Bandwidth Planar Arrays

In this case:

$$\Delta x = S \Delta \tau_y = \frac{S \delta_y \sin \theta_y}{c}$$

and, in order that the aperture be large enough to accommodate all the pulses, the length of the light modulator channels, D , must be such that (Fig. 6.4.2-4):

$$D = S(M-1) |T_s|_{\max} + ST + S(N-1) |\Delta \tau_y|_{\max}$$

Let

$$|\theta_x|_{\max} = |\theta_y|_{\max} = 90 \text{ deg}$$

then:

$$|\Delta \tau_x| = |\Delta \tau_y|_{\max} = \frac{1}{2f_c} \left(\text{assuming } \frac{\delta_x}{c} = \frac{\delta_y}{c} = \frac{1}{2f_c} \right)$$

Thus (Eq. 6.2-5 et. seq.)

$$|d_s|_{\max} = S |T_s|_{\max} = S \left(T + \frac{1}{f_c} \right)$$

and:

$$D = S(M-1) \left[T + \frac{1}{f_c} \right] + ST + \frac{S(N-1)}{2f_c}$$

$$D = MST + \frac{2M + N - 3}{2f_c} s$$

$$D = Md + \frac{2M + N - 3}{2f_c} s$$

where, as before, d = length of single ultrasonic pulse = ST .

In the case of the planar array:

$$A_s = MdNb$$

$$A_n = NbD$$

hence:

$$\frac{A_n}{A_s} = \frac{D}{Md} = 1 + \frac{2M + N - 3}{2f_c} \frac{s}{Md}$$

and since

$$d = ST \approx \frac{S}{B},$$

then:

$$\text{Degr.} = -10 \log \left[1 + \frac{2M + N - 3}{M} \frac{B}{2f_c} \right]^2 \quad (6.4.2-10)$$

Therefore it can be seen at once that, in the case of the planar array, the degradation will not be as large as it is for the linear array since:

$$M \approx N \gg 3$$

and thus:

$$\text{Degr.} \approx -20 \log \left[1 + \frac{3}{2} \frac{B}{f_c} \right] \quad (6.4.2-11)$$

This follows from the fact that, with the planar array, the skewing of each sequence of time-multiplexed pulses is no greater than that which occurred on each single pulse in the

case of the spatially-multiplexed linear array. Thus planar array processing makes more efficient use of the area of the optical aperture and the degradation will be less. Note that Degr. for the time-multiplexed linear array can be obtained from Eq. (6.4.2-10) by setting $N=1$. It is seen that in this case:

$$\text{Degr.} \approx -20 \log \left[1 + \frac{B}{f_c} \right] \qquad (6.4.2-12)$$

which is less than for the planar array.

Values of Degr. for different size antennas and different fractional bandwidths are presented below.

<u>Linear Array</u>				
$\frac{B}{f_c}$ = fractional bandwidth of transmitted signal	.05	.10	.15	.2
N = 24	3.9	6.4	8.7	10.4
N = 100	10.7	15.4	18.5	20.6
N = 300	18.6	24.0	27.4	30.

Planar Array

$\frac{B}{f_c}$ = fractional bandwidth of transmitted signal	.05	.10	.15	.2
N = M = 24	.6	1.2	1.7	2.2
N = M = 100	.62	1.2	1.7	2.3
N = M = 300	.63	1.2	1.8	2.3

The entries in the above tables are the amounts of degradation, in decibels, for different size linear and planar arrays and for different values of fractional bandwidth, $\frac{B}{f_c}$. For convenience the planar array has been assumed square ($M = N$).

6.5 SUMMARY AND CONCLUSIONS

This section has considered the extraction of information from the diffraction patterns which would occur in electro-optical processing of large aperture-bandwidth array antennas. It has been shown that under these conditions the complex optical transmission function would be non-separable and the resulting diffraction patterns have been obtained here for the first time.

The effects of non-separability have been analyzed and the necessary interpretation of the location of peak first-order light intensity, in terms of the angle information contained in the optical transmission function, has

been obtained. It has been shown that, in the case of the planar array, this interpretation will not be the same as it is when the transmission function is separable.

The effects of the non-separable transmission function on the output signal to noise ratio have also been evaluated. The results of this analysis indicate that, in the case of the large aperture-bandwidth planar array, the degradation in signal to noise ratio would not be significant. In electro-optical processing of large aperture-bandwidth linear arrays it has been shown that the spatially-multiplexed configuration could introduce a serious signal to noise degradation which, however, could be avoided with the use of time multiplexing.

7. EXPERIMENTAL INVESTIGATIONS

The results of the preceding chapters indicate, from theoretical considerations, that Debye-Sears light modulators employing fused-silica as the light-modulator medium will be applicable to electro-optical array-antenna processing, and will provide significant gains in signal-processing capacity over that which can be achieved with liquid light modulators. The purpose of this chapter is to present experimental verification of these theoretical conclusions.

The specific experimental investigations which are relevant to the above results have been indicated in the preceding chapters. They fall into two categories. It is first of all necessary to demonstrate the suitability of the fused-silica light-modulator medium for electro-optical processing and then to verify the theoretical evaluation of its signal-processing capacity. With regard to the former, the important considerations are: the linearity of the electro-acoustic transfer characteristics and the ability of a fused-silica light-modulator to produce diffraction patterns without introducing optical distortion. In evaluating the processing capacity it has been assumed: that the light-modulator bandwidth will be approximately 50 per cent of the resonant transducer frequency; that internal-refraction effects can be controlled by proper choice of transducer depth; and that adjacent channels in the spatially-multiplexed configuration can be spaced by one transducer width. Thus the experimental work followed this outline, and the results were found to support the conclusions concerning the use of fused-silica light modulators in electro-optical array-antenna processing. The following sections present some of the data resulting from these experiments.

7.1 DESCRIPTION OF MEASUREMENT APPARATUS

The experiments with the fused-silica light-modulators were performed on the coherent optical configuration shown schematically in Fig. 7.1-1.

All the optical components and the collimated regions, in which the experimental modulators were placed, were shielded against extraneous light, dust, and the motion of the air, by cylindrical-bellows light shields and light-tight boxes. The complete operating system is shown in Fig. 7.1-2.

The optical table was a 16 ft. \times 18 in. \times 16 in. granite block mounted on an 18 in. steel channel fabricated to form a T-shaped support (Fig. 7.1-3), and the steel base was supported, in tripod fashion, by air-operated, self-regulating damping mounts. The top surface of the table was ground to a flatness of ± 0.0001 in. and a T-shaped slot, 1 in. wide by 14 ft. long, was machined into it, along the center line, to accommodate the optical components. To provide a reference surface for these components, one side of the slot was hand finished to a flatness of 0.001 in.

In these experiments, the laser light source produced a 1.8 mm diameter linearly-polarized beam with a wavelength of $.6328\mu$. The polarization in this case was verified by means of a Nichol prism to be vertical (perpendicular to the surface of the optical bench). The light beam emerging from the laser was adapted to the requirements of the experiments by means of the spreading-lens assembly shown in Fig. 7.1-4. The assembly consisted of a microscope objective lens, fixed to a flat plate supported by a lens mount, and a pinhole subassembly attached to a microscope barrel. The actual size of the pinhole as well as the focal length

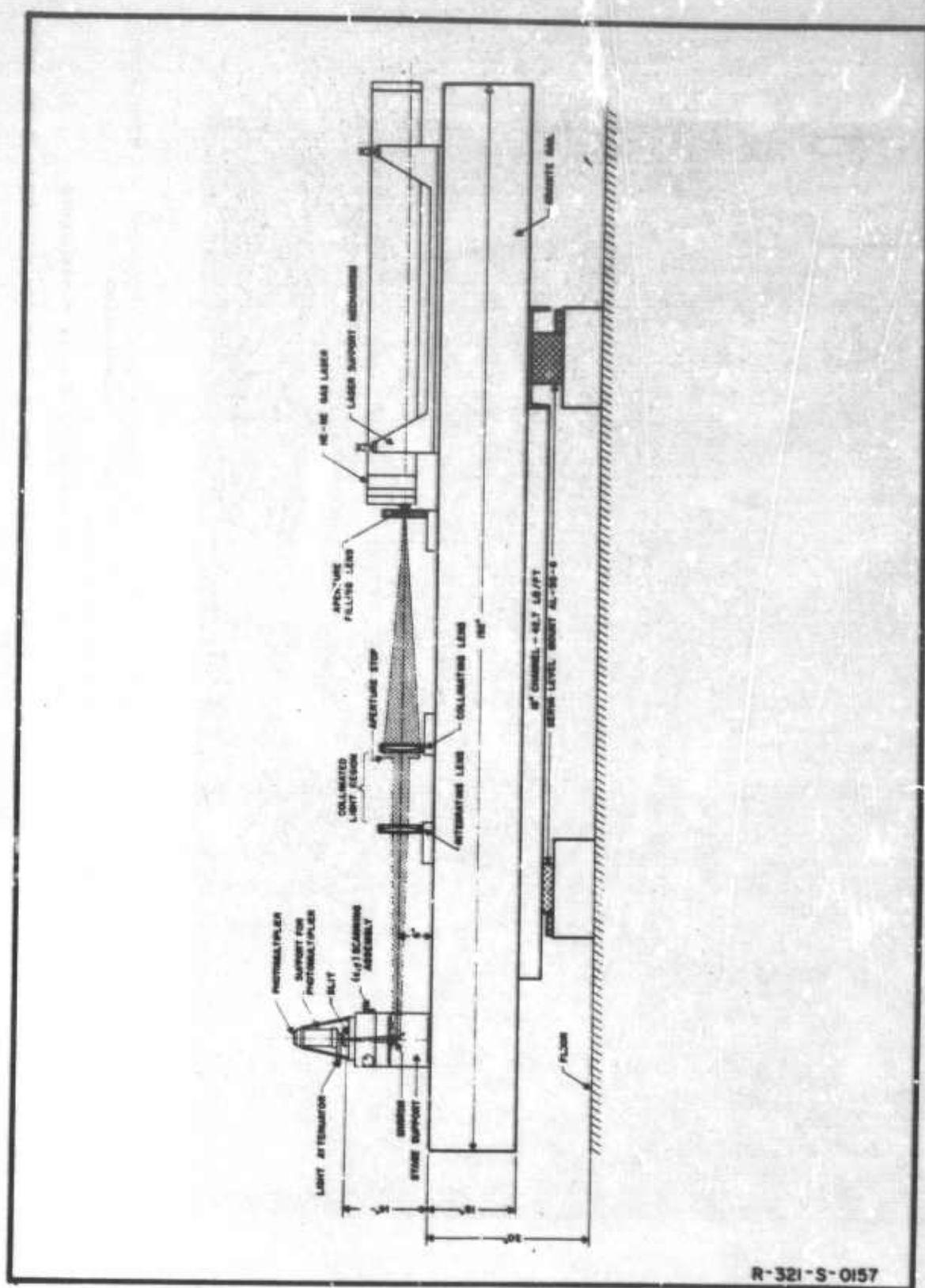
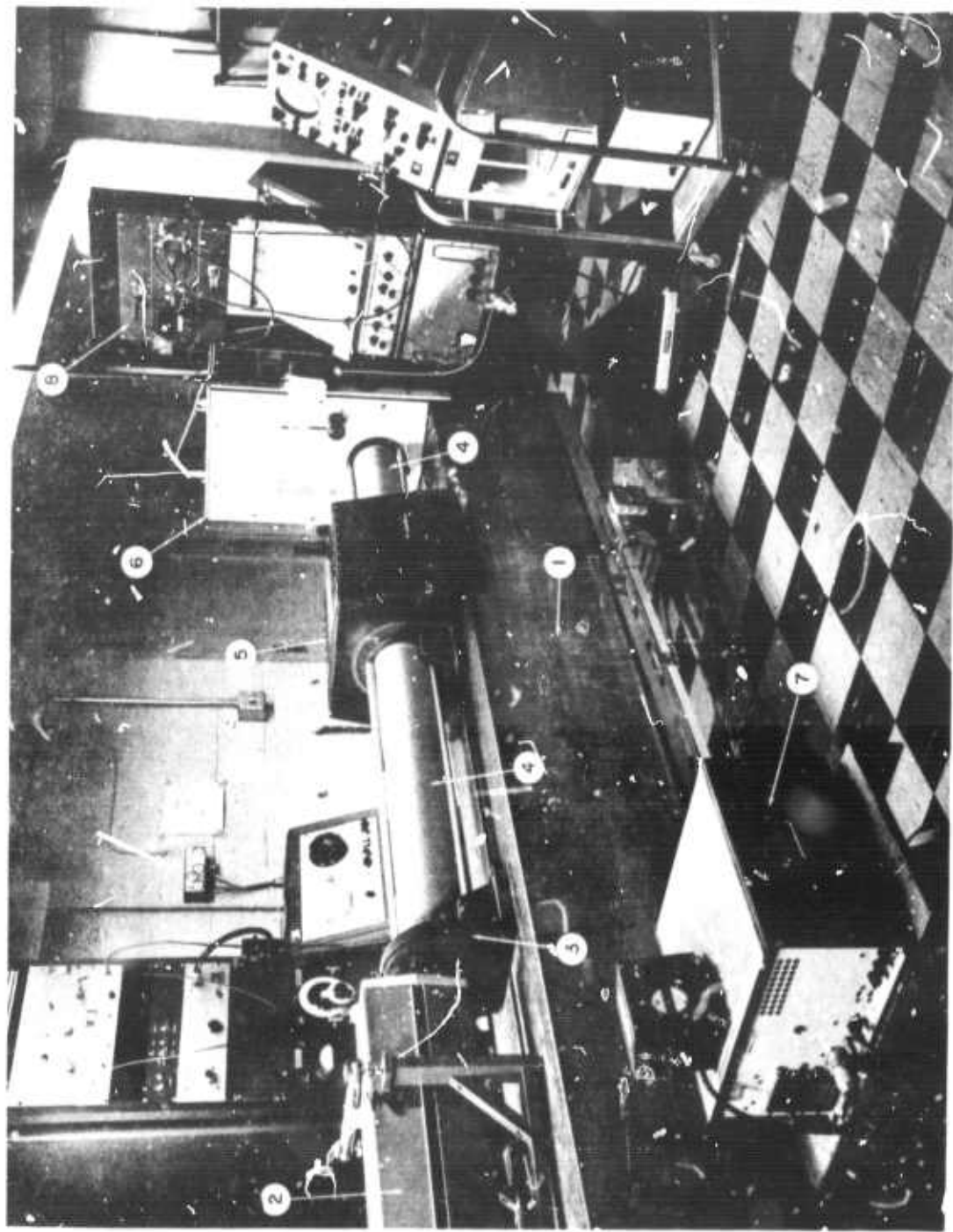
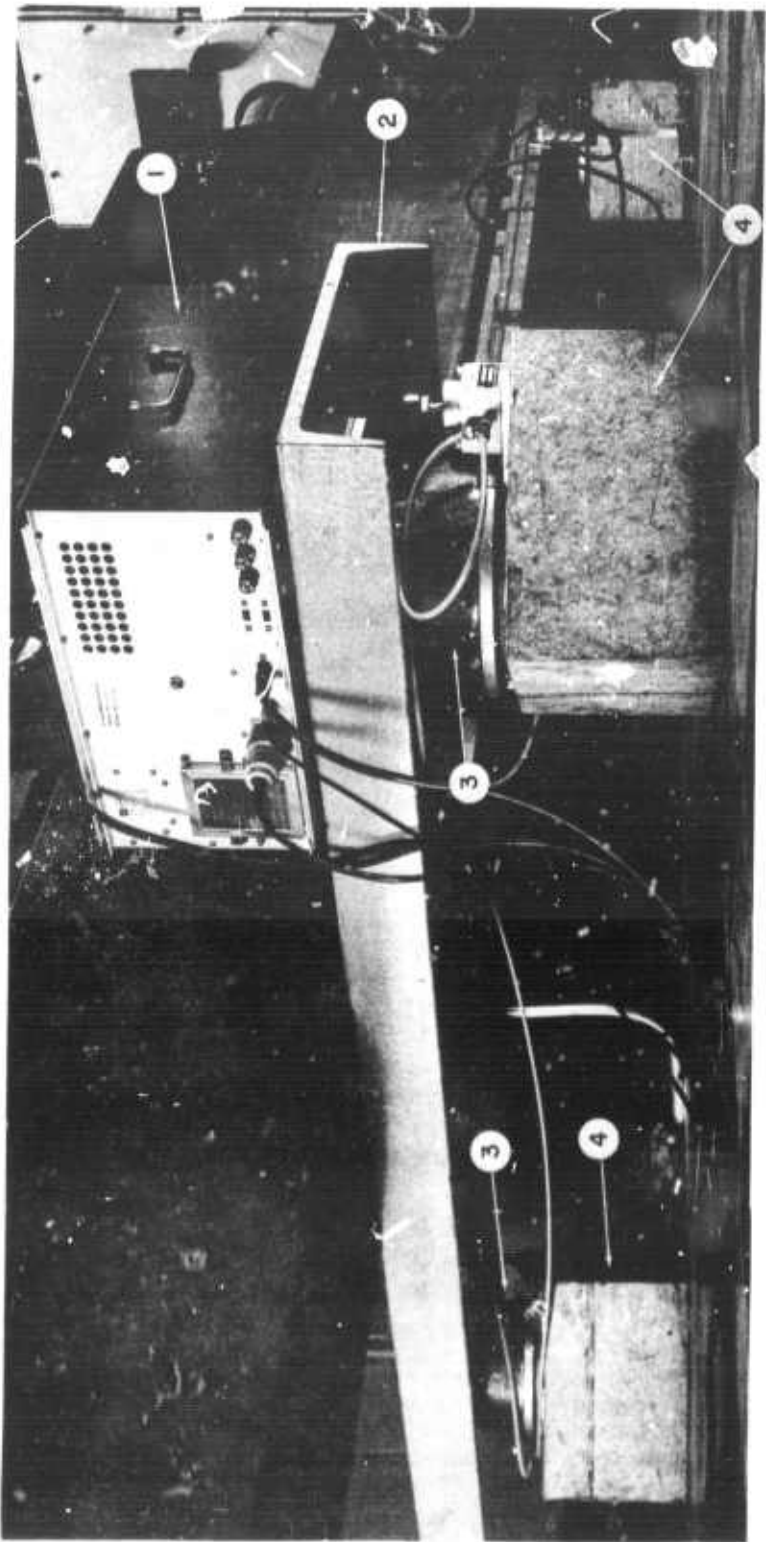


FIG. 7.1-1 SCHEMATIC DIAGRAM OF COHERENT OPTICAL SYSTEM



- 810H-321-0097
- | | |
|-------------------------------------|--|
| 1. Granite Optical Table | 5. Light-Shield over Collimated Region (Location of Modulator) |
| 2. Laser Light Source | 6. Light-Shield for XY-Scanning Mechanism |
| 3. Mount for Spreader-Lens Assembly | 7. Laser Power-Supply |
| 4. Bellows Light-Shields | 8. Readout and Photomultiplier-Supply Electronics |

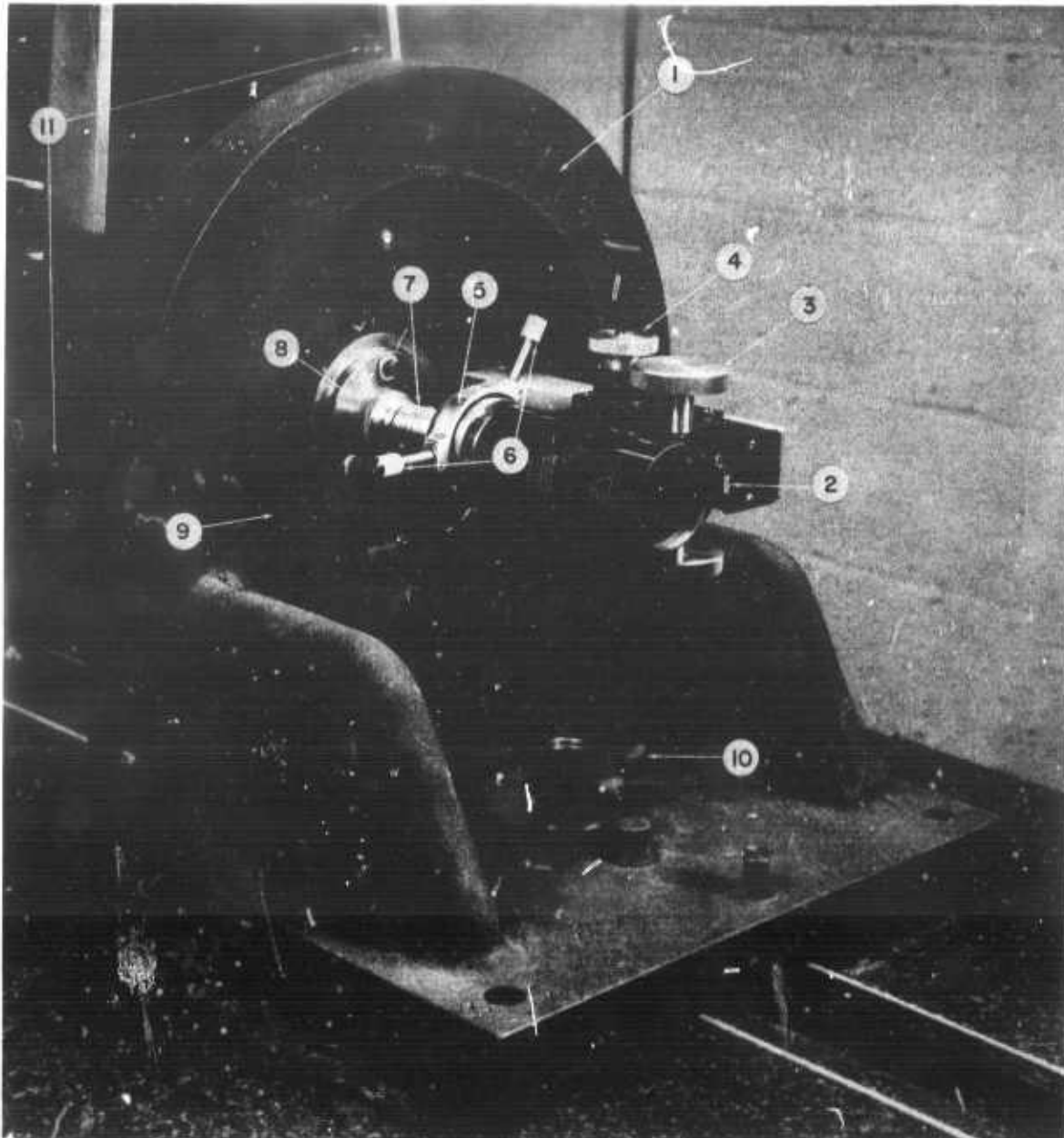
Fig. 7.1-2 Coherent Optical System



810H-321-0095

- 1. Laser Power-Supply
- 2. Steel-Channel T-Support for Optical Table
- 3. Serva-Level Air-Cushion Damping Mounts
- 4. Granite Foundation Blocks

Fig. 7.1-3 T-Support for Optical Table and Damping Mounts



810H-321-0098

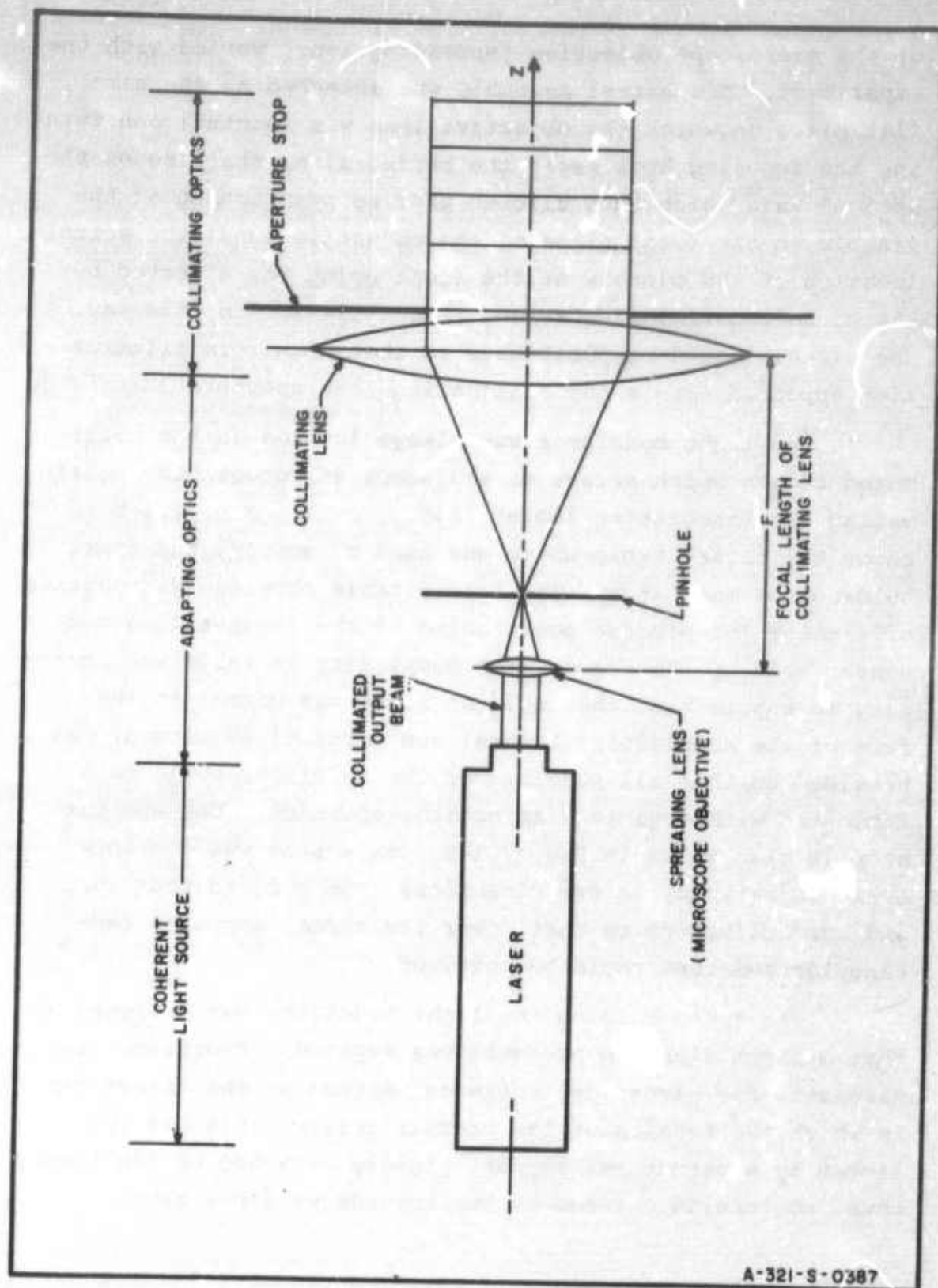
1. Lens Mount
2. Microscope-Barrel Assembly
3. Coarse Focusing Adjustment
4. Fine Focusing Adjustment
5. Pinhole Assembly
6. Pinhole Positioning Screws
7. Microscope Objective Lens
8. Objective-Lens Holder
9. Spreader-Lens-Assembly Mounting Plate
10. Lens-Mount Locking Knob
11. Mounting-Plate Adjustment Screws

Fig. 7.1-4 Spreader-Lens Assembly

of the microscope objective (spreading lens) varied with the experiment. The barrel assembly was attached to the same flat plate on which the objective lens was mounted; and turning the focusing knob moved the barrel along the line of the optical axis which thus allowed precise positioning of the pinhole in the focal plane of the objective lens; the actual location of the pinhole at the focal point was affected by the pinhole-positioning screws (Fig. 7.1-4). In this way, the pinhole could be positioned so that a uniform illumination appeared across the collimating-lens aperture (Fig. 7.1-5).

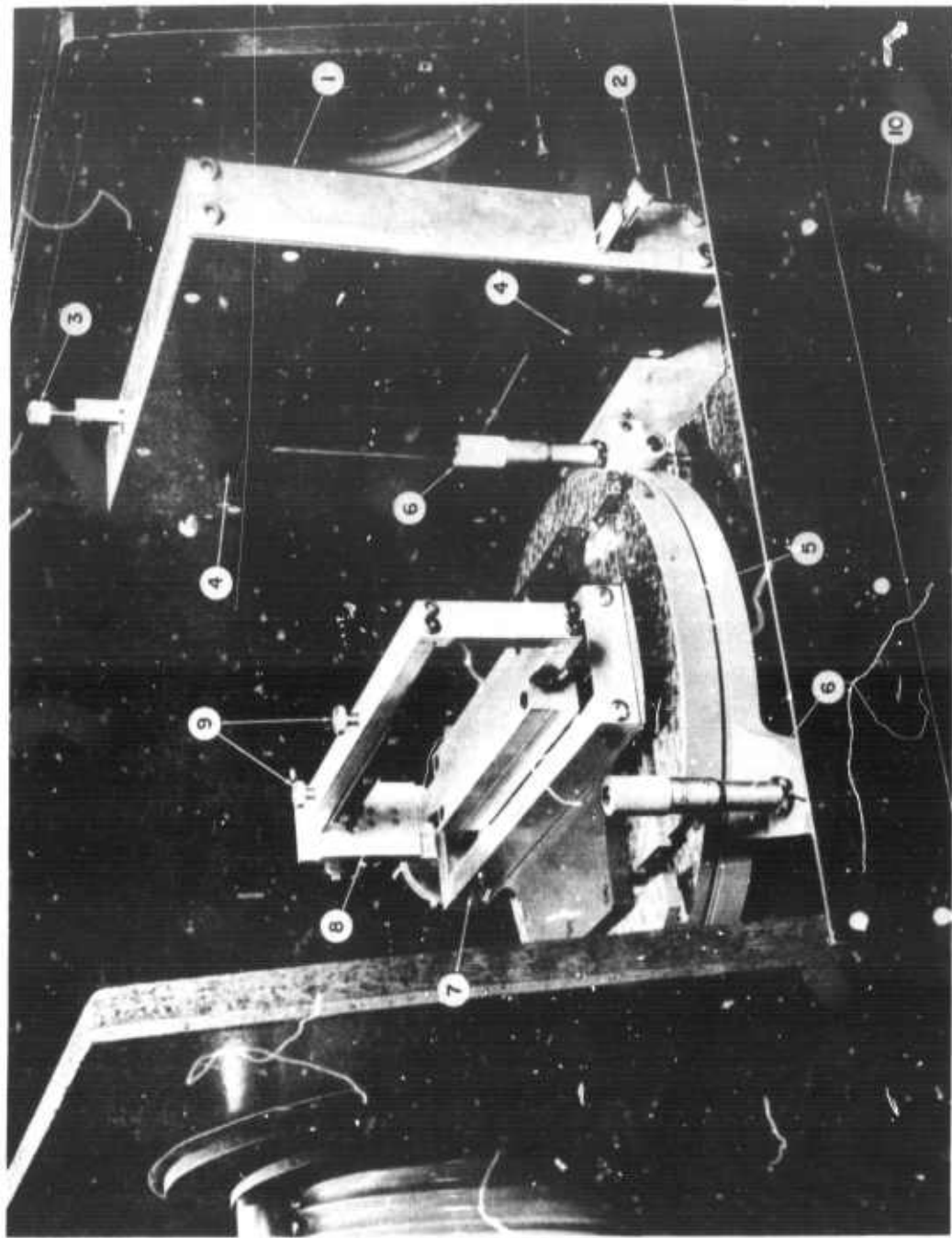
The light modulator was always located in the collimated region which refers to the space in between the collimating and integrating lenses (Fig. 7.1-1). Fig. 7.1-6 shows the rotary table which was used to support the frame holding the modulator. The rotary table provided six degrees of freedom for precise positioning of the fused-silica modulator held by the frame. The complexity of table was necessary to ensure that the incident light was normal to the face of the modulator. Lateral and vertical adjustment was provided so that all portions of the modulator could be illuminated with a given size optical aperture. The aperture stop is also shown in Fig. 7.1-6. This stop was continuously adjustable, in two dimensions from zero to four in., and was calibrated so that, over its range, any size rectangular aperture could be obtained.

The frame holding the light modulator was designed so that minimum clamping pressure was applied. Provision was also made for electrical cable connection to the transducer in which the tension of the coaxial driver cable was relieved by a structural support rigidly attached to the frame; thus, no tension existed at the transducer connection.



A-321-S-0387

FIG. 7.1-5 COLLIMATION OF LASER BEAM



810H-321-0096

- | | |
|-------------------------------------|---------------------------------|
| 1. Adjustable Aperture Stop | 6. Table-Adjustment Micrometers |
| 2. Horizontal Aperture-Size Control | 7. Traversing Assembly |
| 3. Vertical Aperture-Size Control | 8. Modulator Holding-Frame |
| 4. Aperture-Size Indicator | 9. Clamping Screws |
| 5. Rotary Table | 10. Light Shield |

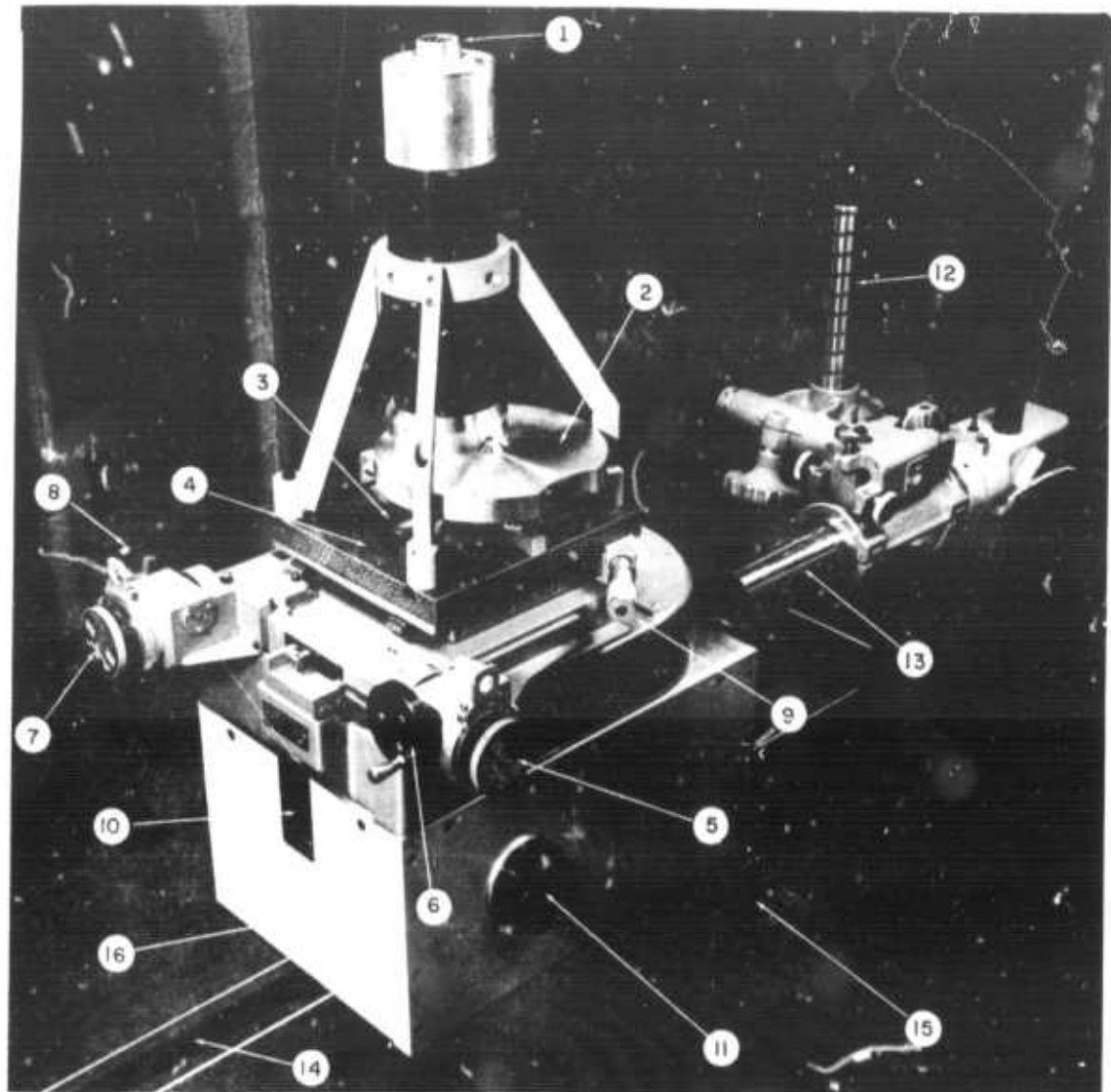
Fig. 7.1-6 Details of Collimated Light Region

Detection of the light-modulator output was made with the scanning mechanism shown in Figs. 7.1-7 and 7.1-8. In this device a precision xy-table was mounted above the optical axis of the system rather than normal to it and the converging beam from the integrating lens was folded, within the table support, by a precision flat mirror set at 45 deg to the optic axis. Provision was made to rotate this mirror out of the system to permit the light beam to fall on the auto-collimator telescope for alignment purposes.

The image plane of the integrating lens was coincident with the plane of the xy-table, in which an adjustable slit was mounted, and the table was positioned by means of the manually-operated traversing knobs. Electrical readout of the table position was continuously given by two potentiometers directly coupled to the table-control shafts.

Above the slit assembly was a continuously variable neutral-density filter used to limit the peak intensity of light entering the photomultiplier. The combination of filter and photomultiplier was rigidly attached to the xy-table and moved with the table so that this unit was always in the correct position with regard to the slit. The entire scanner mechanism was enclosed in a light-tight box (Figs. 7.1-2 and 7.1-8), with access to controls and adjustment provided by magnetically-held access panels and through-wall connections.

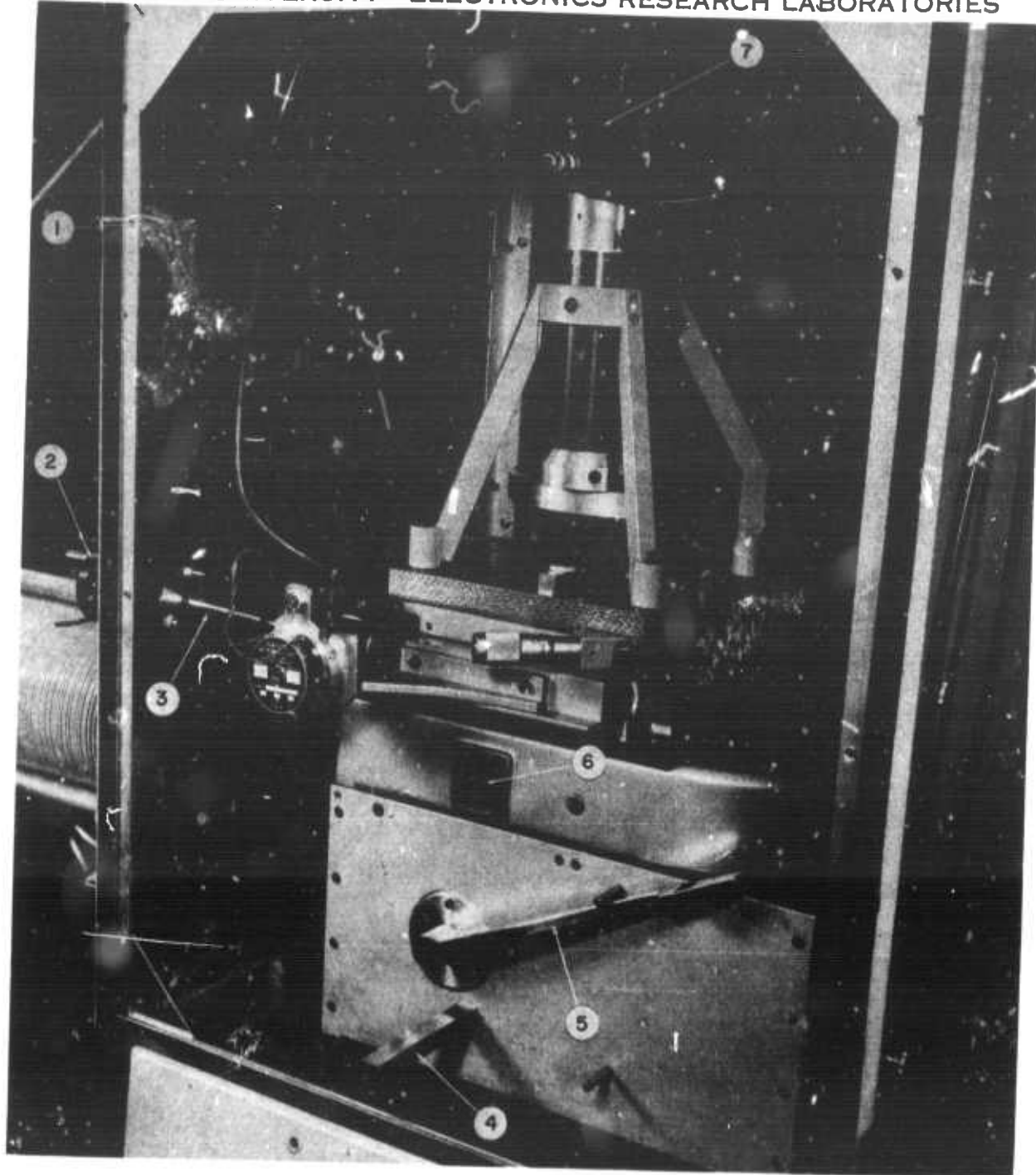
* Note: The linear output variables in this system are actually referred to as x_1 and y_1 .



810H-321-0074

- | | |
|-------------------------------------|------------------------------------|
| 1. Photomultiplier Output Connector | 9. Table-Rotation Control |
| 2. Variable Density Filter | 10. Light-Input Slot |
| 3. Slit Mount | 11. Mirror-Position Control |
| 4. x,y-Table | 12. Autocollimator-Telescope Mount |
| 5. y-Axis Analog Potentiometer | 13. Autocollimator Telescope |
| 6. y-Traverse Mechanisms | 14. T-Slot Guide |
| 7. x-Axis Analog Potentiometer | 15. Granite Optical Table |
| 8. x-Traverse Mechanisms | 16. x,y-Table Support |

Fig. 7.1-7 x,y-Stage: Scanning-Mechanism Details



1. Light Shield
2. Slit-Traversing Knob
3. Traversing-Mechanism Connecting Shaft
4. Pellicle-Assembly Support Bar
5. Mirror-Position Lever
6. Window for Pellicle Assembly
7. Photomultiplier Voltage Divider Unit

810H-321-0094

Fig. 7.1-8 Scanning-Mechanism Assembly

7.2 BASIC SYSTEMS MEASUREMENTS

7.2.1 MEASUREMENT OF LIGHT-INTENSITY DISTRIBUTION IN IMAGE PLANE

Consider the zero-order light diffraction pattern produced by a rectangular optical aperture of length D (x dimension) and width b (y dimension); the relative light intensity in the image plane will be given by (Eq. 2.1-2):

$$|G(u,v)|^2 = \left(\frac{b \sin \pi bv}{\pi bv} \right)^2 \left(\frac{D \sin \pi Du}{\pi Du} \right)^2 = Z^2(v) Z^2(u) \quad (7.2.1-1)$$

The ideal pattern produced by the peaks and nulls of $|G(u,v)|^2$ is shown in Fig. 7.2.1-1.

The actual value of light intensity can be measured by the scanning apparatus (Figs. 7.1-7 and 7.1-8), which is represented schematically in Fig. 7.2.1-2. In making such a measurement the slit is positioned at some fixed value of u or v and is scanned in the orthogonal dimension; thus in Fig. 7.2.1-1 the slit is shown to be positioned at $v = 0$ and the resulting measured relative light intensity would be:

$$|G(u,0)|^2 = b^2 Z^2(u) \quad (7.2.1-2)$$

The orthogonal scan could of course be obtained by rotating the slit by 90 deg and positioning it at $u = 0$. In this case the relative measured light intensity would be:

$$|G(0,v)|^2 = D^2 Z^2(v) \quad (7.2.1-3)$$

Some representative measurements of this kind are presented in Figs. 7.2.1-3 and 7.2.1-4. It is seen that zero-order intensities can be obtained which are close to ideal.

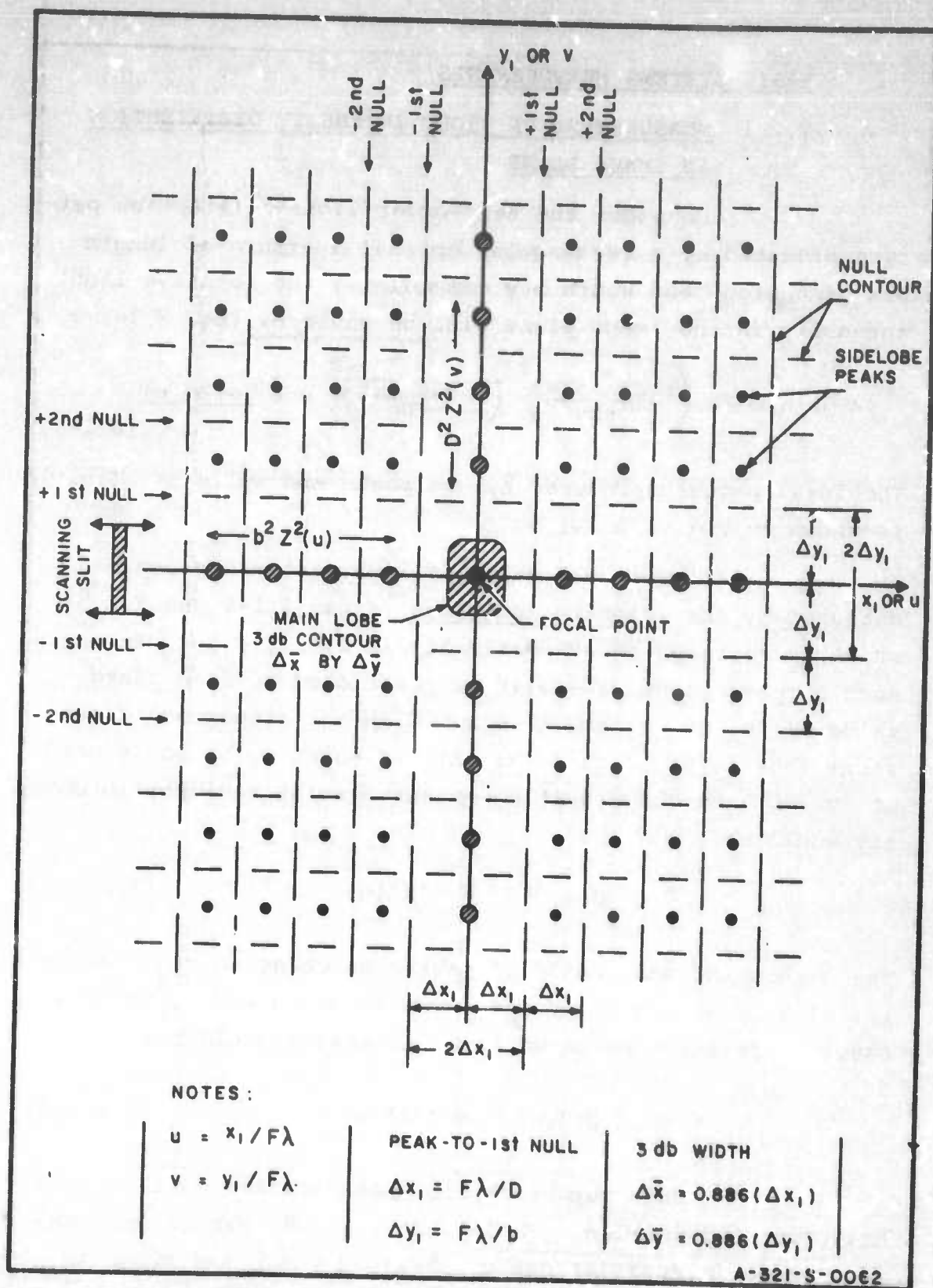


FIG. 7.2.1-1 SCHEMATIC REPRESENTATION OF FINE STRUCTURE FOR IDEAL ZERO-ORDER LIGHT DISTRIBUTION

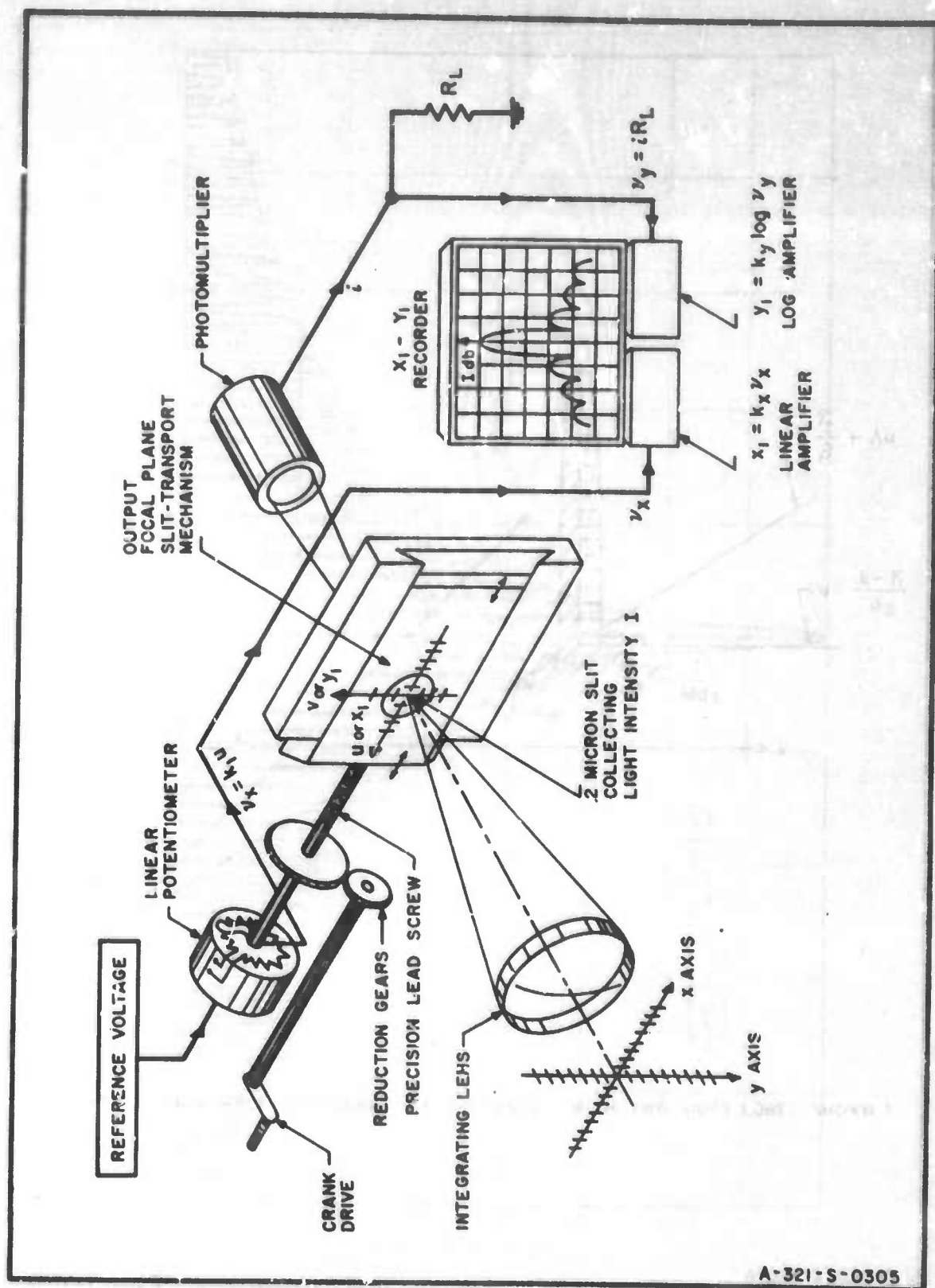


FIG. 7.2.1-2 SCHEMATIC DIAGRAM OF APPARATUS FOR MEASURING SPATIAL LIGHT-INTENSITY DISTRIBUTION

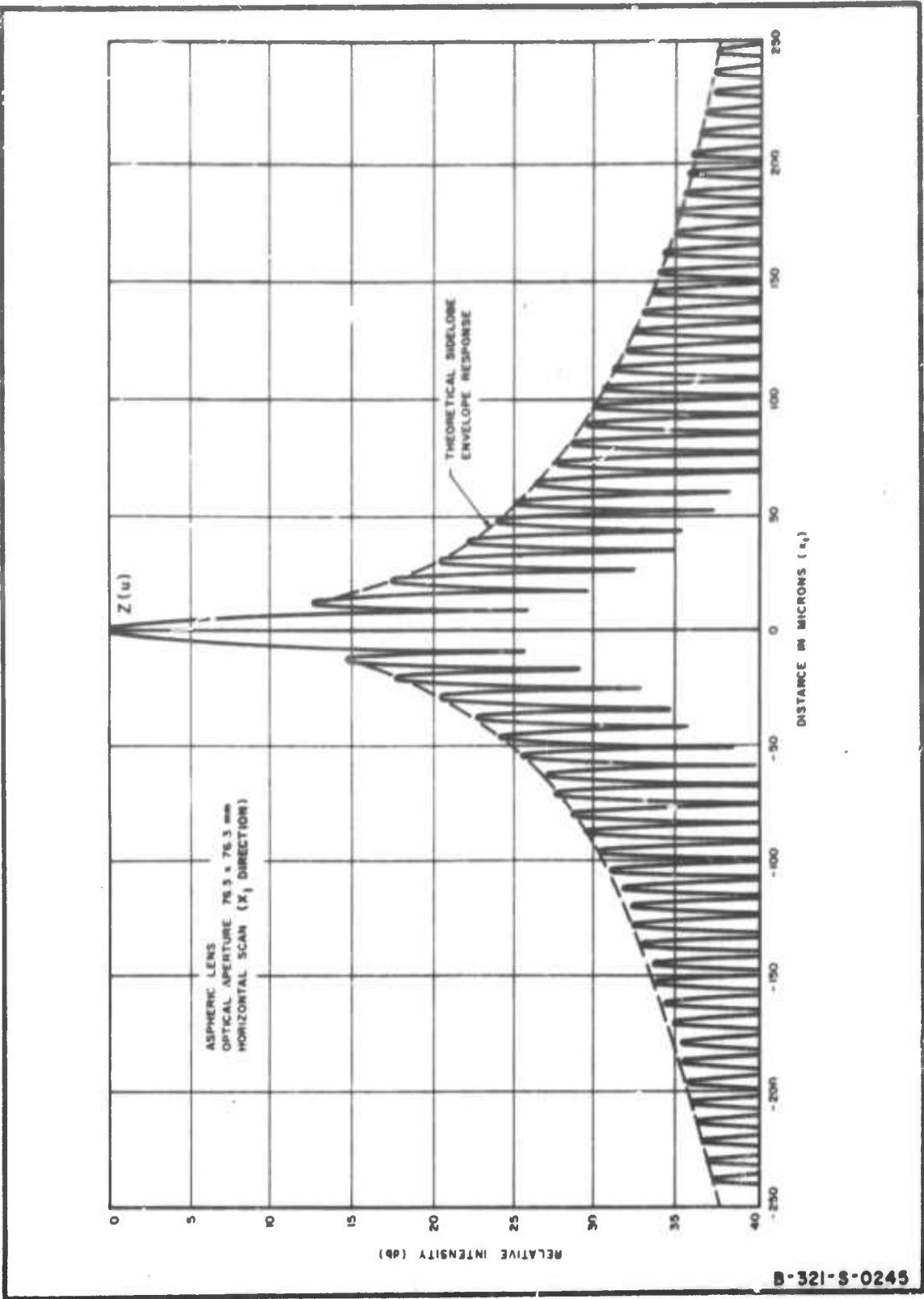


FIG. 7.2.1-3 OUTPUT FOCAL-PLANE LIGHT-INTENSITY DISTRIBUTION ALONG x_1 COORDINATE WITH 3"x3" APERTURE

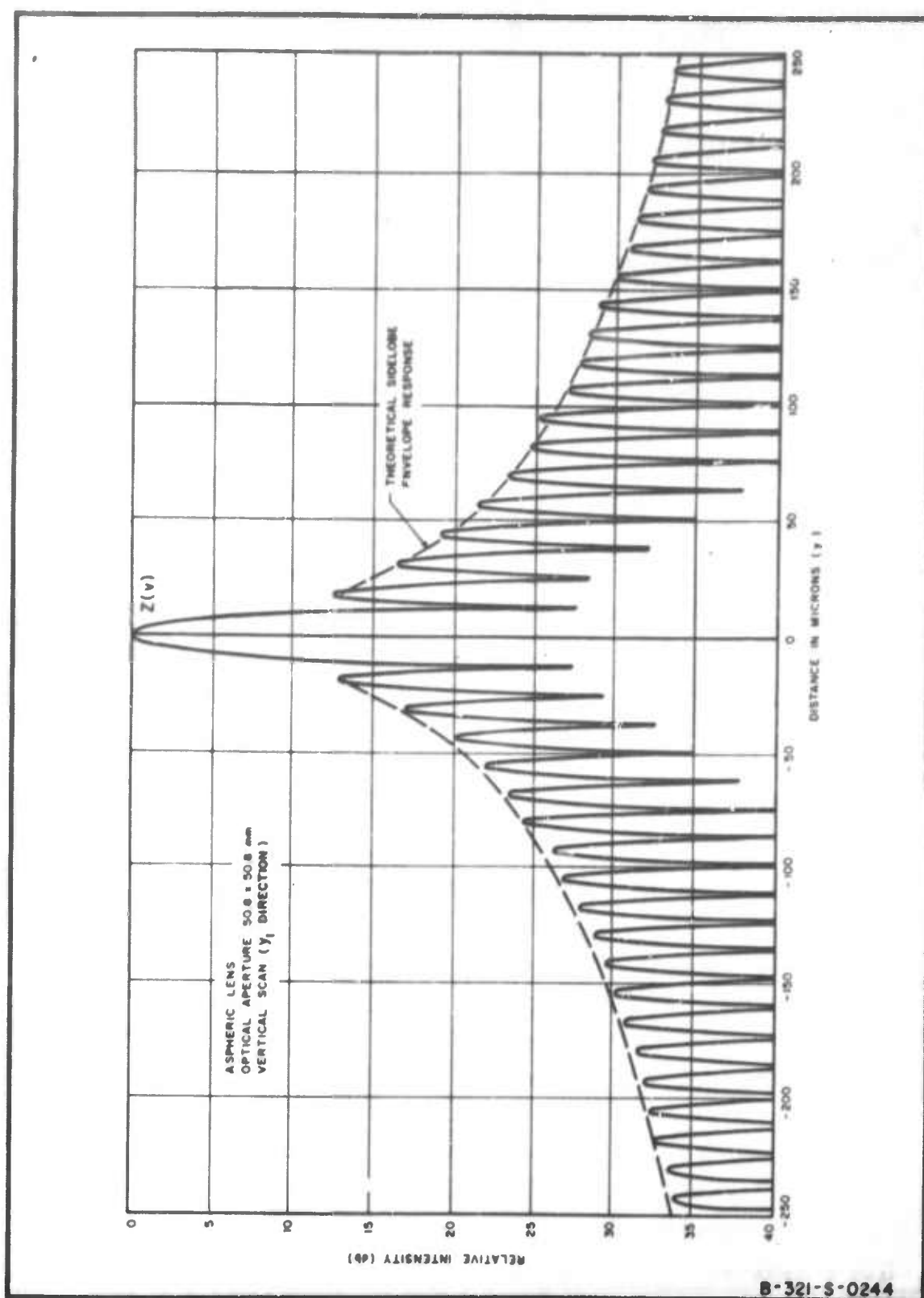


FIG. 7.2.1-4 OUTPUT FOCAL-PLANE LIGHT-INTENSITY DISTRIBUTION ALONG y_1 COORDINATE WITH 2"x2" APERTURE

Data of this kind provide indications of misalignment of the optical system, focusing errors, lens errors, and non-uniformity in the amplitude and phase front of the light distribution in the collimated region. The optical quality of a transparent medium can also be tested by these zero-order measurements and, in this way, all the fused-silica blanks used in these experiments were verified to be free of significant residual stresses and surface irregularities.

In measuring the first-order diffracted light intensity it is of course necessary to consider regions of the image plane which are removed from the origin (Ch. 2). Since the direction of ultrasonic propagation in these experiments was always in the x direction, the region of interest lay along the u axis (where $Z^2(v) = b^2$) at a distance from the origin which was consistent with the frequency of the acoustic wave. In considering the zero-order intensity in these regions the ideal light level can be defined as:

$$L(u) = \left(\frac{1}{\pi Du}\right)^2 \quad (7.2.1-4)$$

It is seen that $L(u)$ is the envelope of the side lobes of $Z^2(u)$ (Fig. 7.2.1-5).

In general, the measured light level will be somewhat higher than that given by $L(u)$ resulting from light which is scattered because of imperfections in the lens surfaces. Since scattered light tends to obscure the location of peak first-order intensity, thus decreasing the dynamic range of the system, it is of course desirable to keep the light level as close as is possible to the ideal in the output region of interest. A measurement of the scattered light in this optical system is presented in Fig. 7.2.1-6 along with the theoretical level. The output region of interest is noted in Fig. 7.2.1-6. It is seen that the

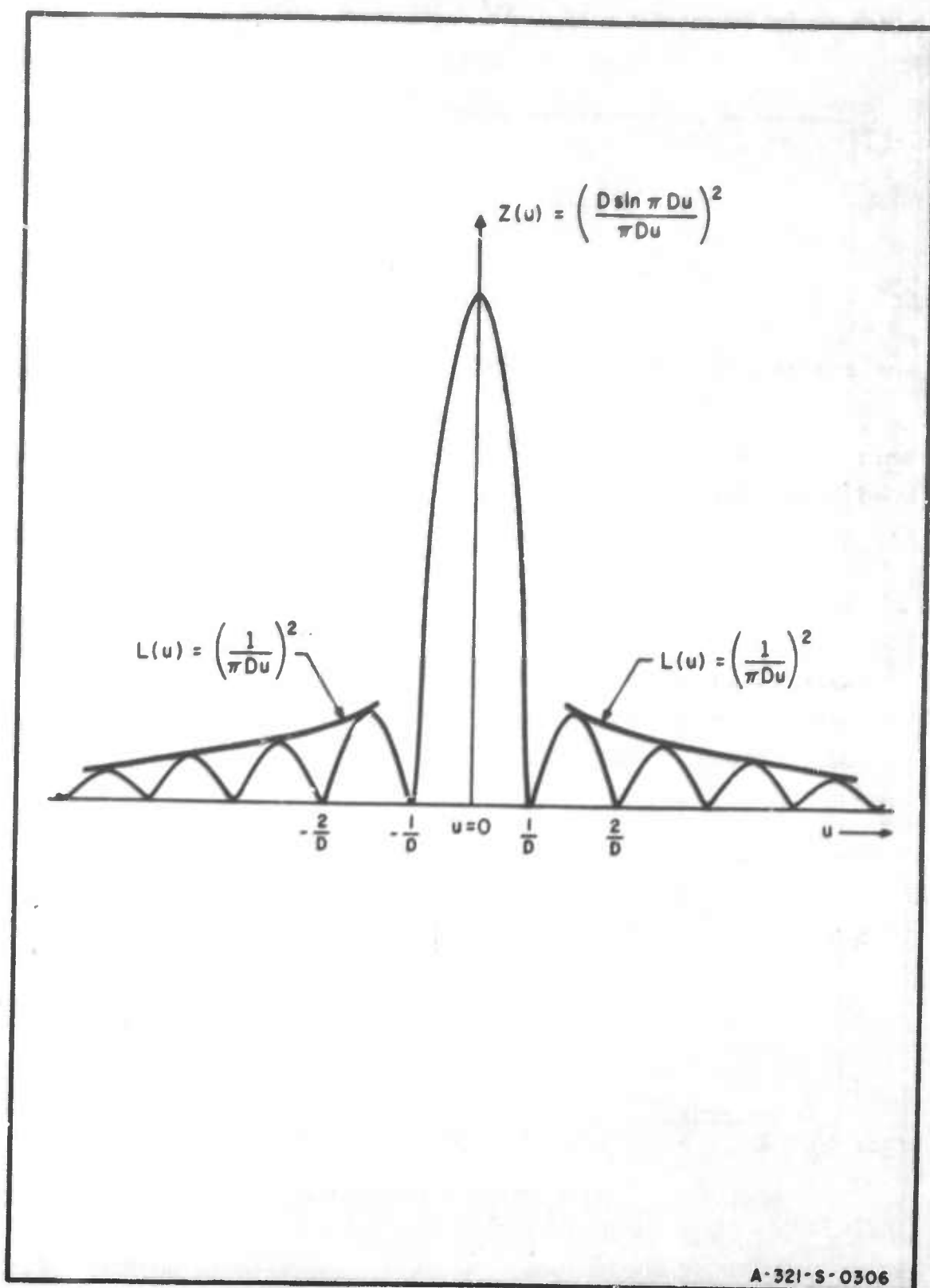


FIG. 7.2.1-5 IDEAL ZERO-ORDER LIGHT-INTENSITY DISTRIBUTION FOR APERTURE OF LENGTH D . (SCAN ALONG u AXIS)

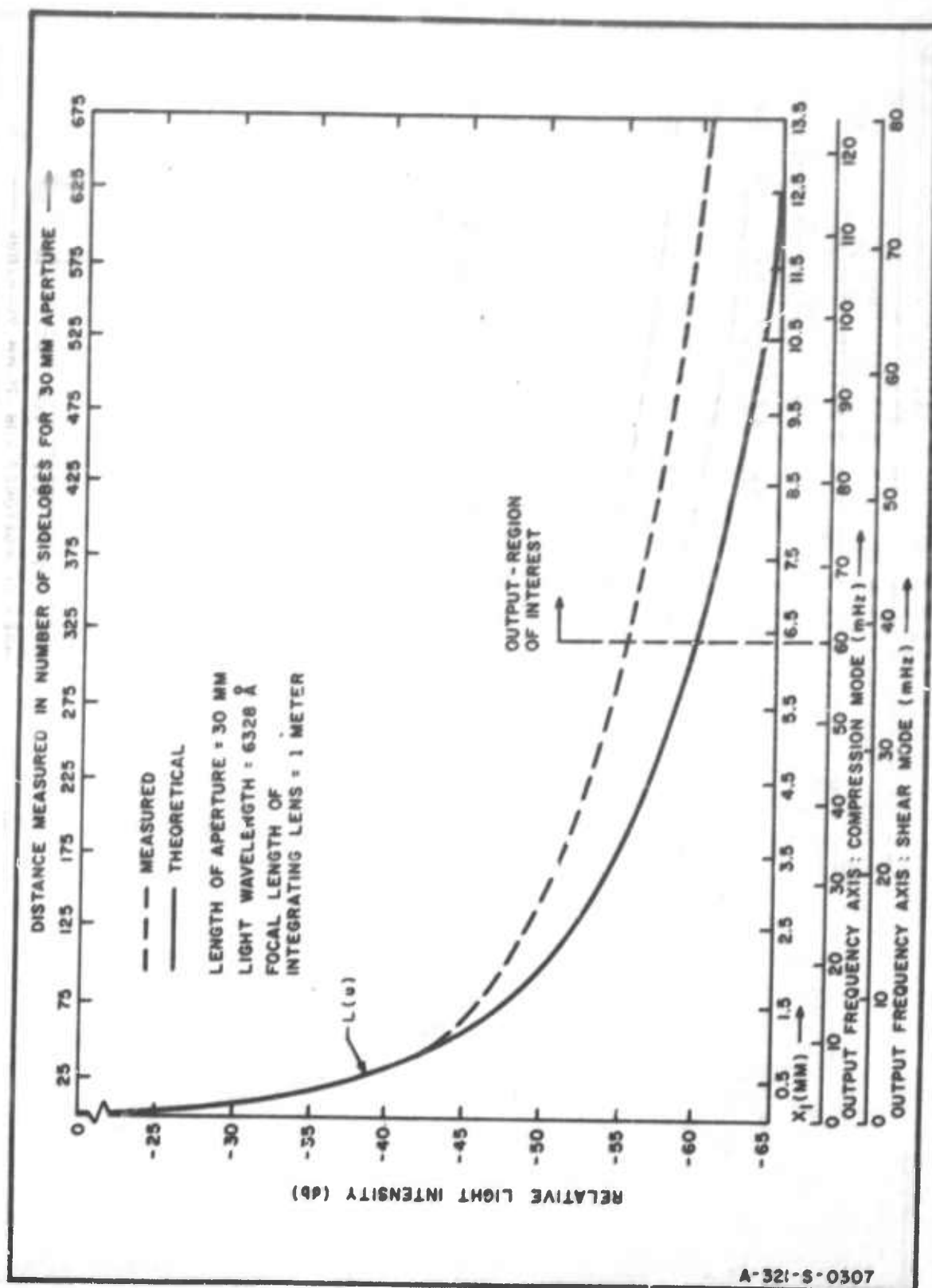


FIG. 7.2.1-6 SCATTERED LIGHT LEVEL OF OPTICAL SYSTEM

scattered light level in this region was approximately 5 db above the theoretical value.

7.2.2 MEASUREMENTS USING SCHLIEREN TECHNIQUES

The Schlieren configuration is diagrammed in Fig. 7.2.2-1. The integrating lens produces, in the (u,v) plane, the Fourier transform of the light distribution in the optical aperture, and the imaging lens performs a second Fourier-transform operation on this light distribution and thus reproduces an image of the original distribution which can be observed on a ground-glass screen or recorded on film. Since the perturbations of the aperture light distributions caused by the ultrasonic wave are small, they are swamped out by the D.C. light and, ordinarily, cannot be observed. If, however, a spatial filter is employed as shown, then the D.C. or zero-order light is blocked out and the imaging lens operates only on the light which has been diffracted by the acoustic wave. As a result the perturbations in the aperture light distribution can now be observed and the resulting image will be that of the ultrasonic beam only. Since the ultrasonic beam is a traveling wave its image is smeared in time and the fine (sinusoidal) structure is obliterated. Its spatial configuration in the light modulator, however, is generally what is of interest and this will be reproduced by the imaging lens.

As is seen in Fig. 7.2.2-1, the two first-order fringes caused by diffraction of light by a sinusoidal acoustic wave in the x direction lie on the u axis at the points $u = \pm \frac{f_1}{S}$:

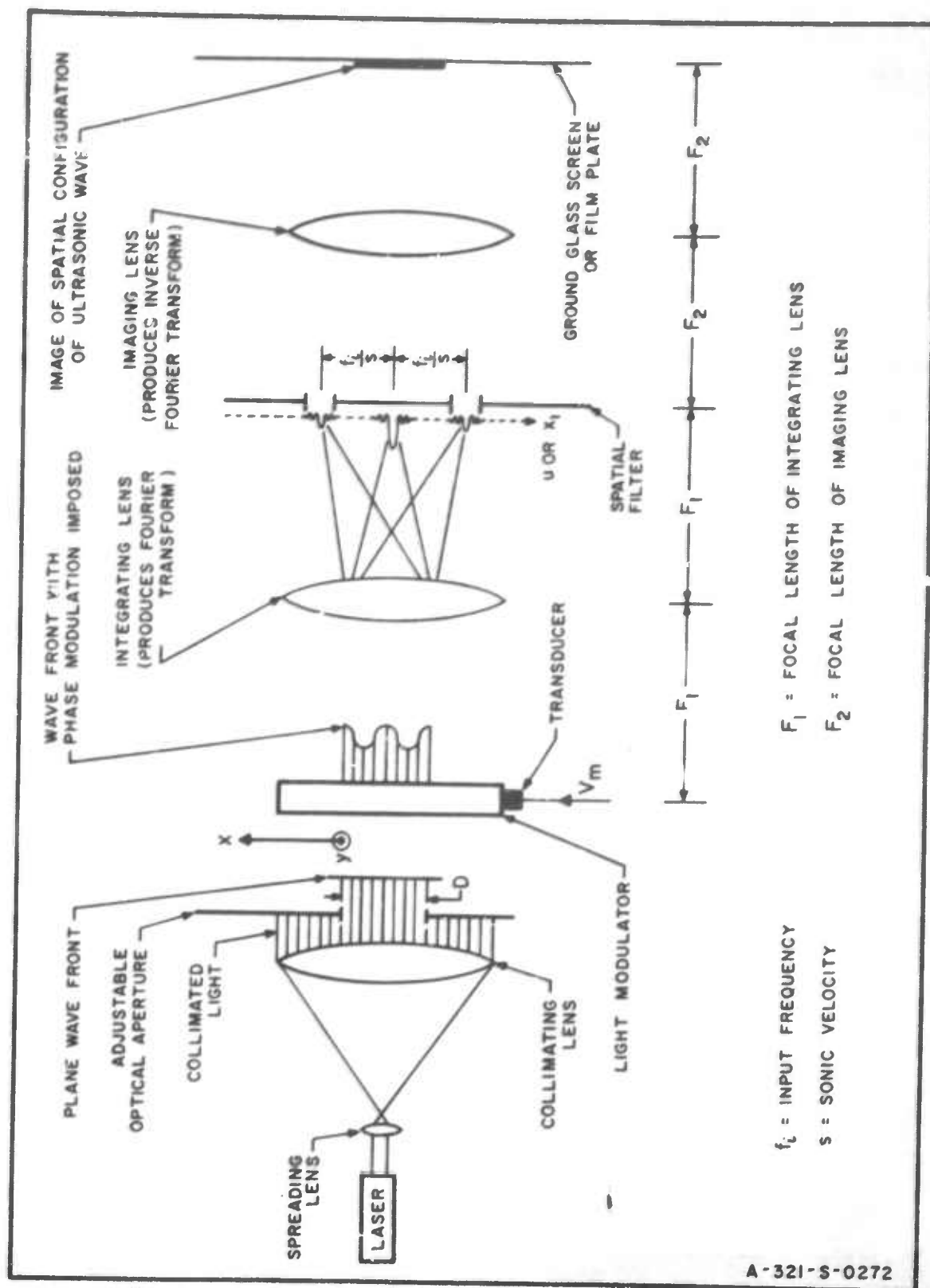


FIG. 7.2.2-1 SCHLIEREN CONFIGURATION

where:

f_i = frequency of electrical signal exciting piezoelectric transducer

S = sonic velocity

and similarly, an acoustic wave of the same frequency along the y axis would result in fringes appearing on the (orthogonal) v axis at the points $v = \pm \frac{f_i}{S}$. It is evident therefore that the circle in the (u,v) plane of radius $r = \left| \frac{f_i}{S} \right|$ is the locus of all first-order fringes resulting from ultrasonic diffraction by a signal with spatial frequency $f = \frac{f_i}{S}$, and that the angles projected along the vertical by both the line drawn through the two fringes and the direction of ultrasonic propagation are equal (Fig. 7.2.2-2).

Consider a specific example. A rectangular blank of fused silica has a 36 deg wedge cut on the inactive end as shown in Fig. 7.2.2-3. Thus the initial ultrasonic wave lies along the x axis, the first reflection makes an angle of 108 deg with positive x direction, the second reflection makes an angle of 72 deg etc. The fact that the reflections are not centered at the origin of the (x,y) plane will cause a phase shift in the diffracted light, but will not effect its position in the (u,v) plane. Thus, considering the first two reflections only, (all higher reflections were too weak to be observed) the fringes should appear along lines $\theta_0 = 0$, $\theta_1 = 108$ deg, $\theta_2 = 72$ deg as shown in Fig. 7.2.2-4. This in fact was observed experimentally, and the resulting Schlieren photograph (Fig. 7.2.2-5) was recorded by using the spatial filter shown in Fig. 7.2.2-4. This technique will be referred to again in Secs. 7.3.1 and 7.4.3.

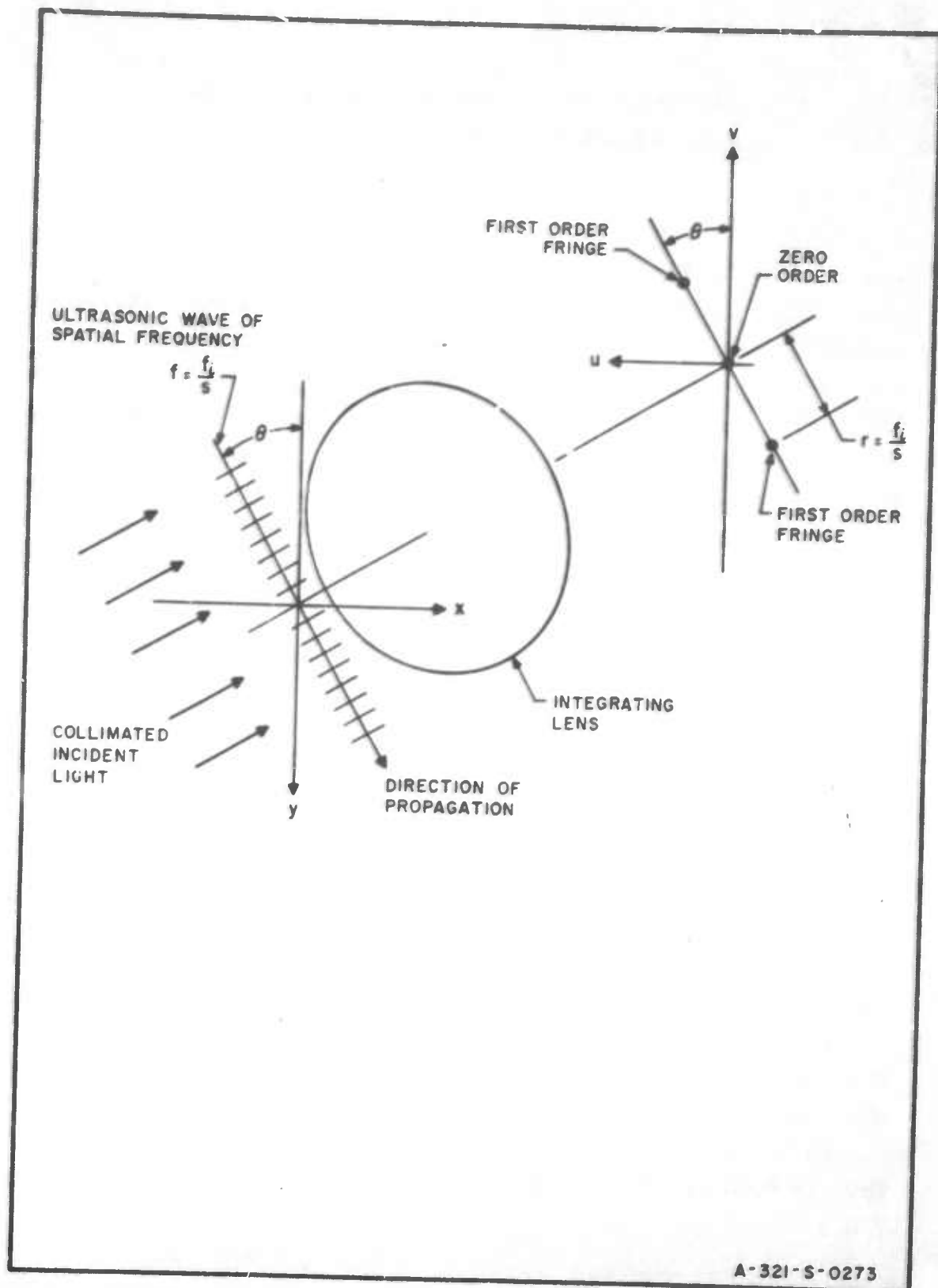


FIG. 7.2.2-2 FIRST-ORDER DIFFRACTION FRINGES FOR ULTRASONIC WAVE WITH ARBITRARY DIRECTION OF PROPAGATION.

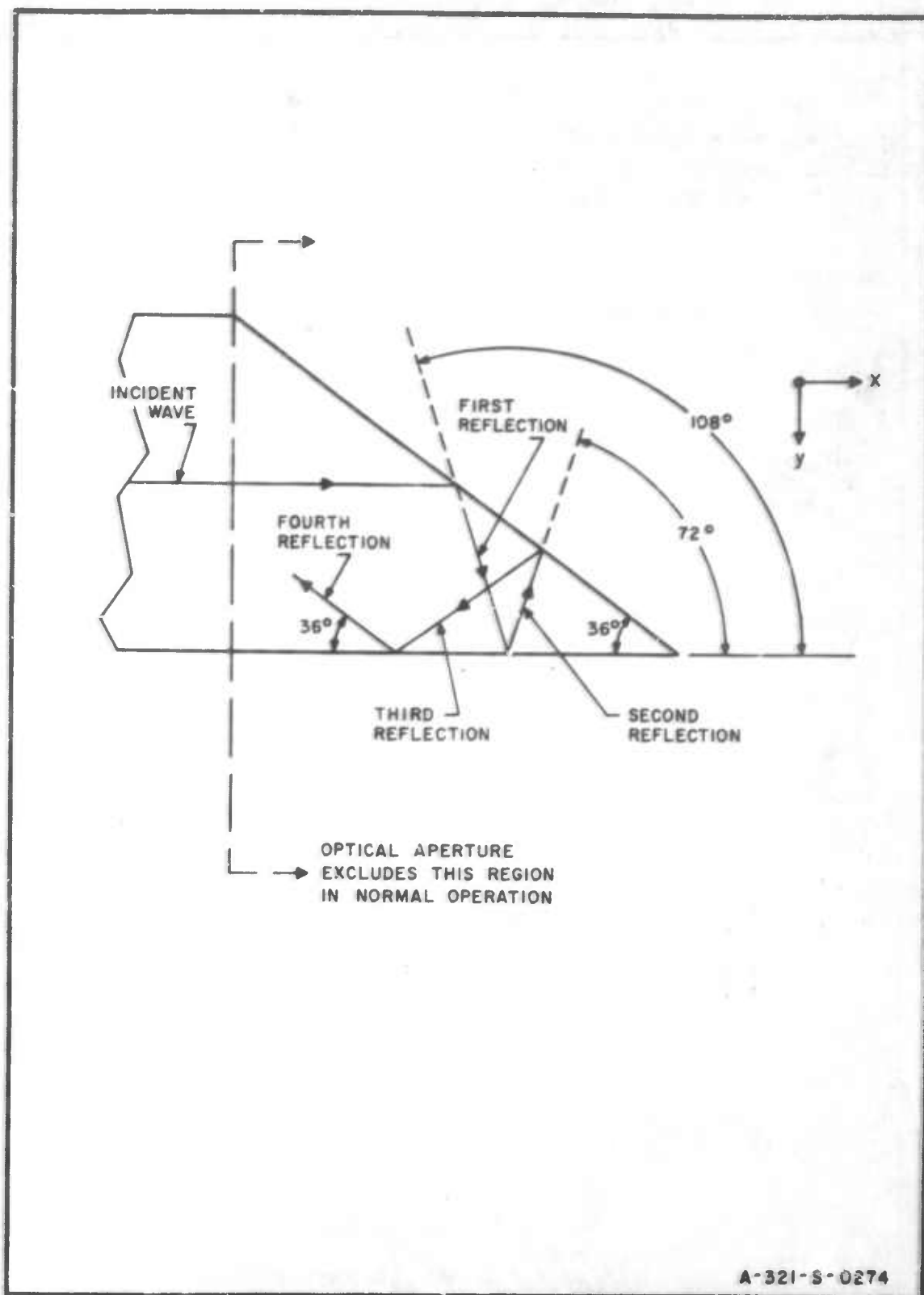


FIG. 7.2.2-3 OPERATION OF WEDGE

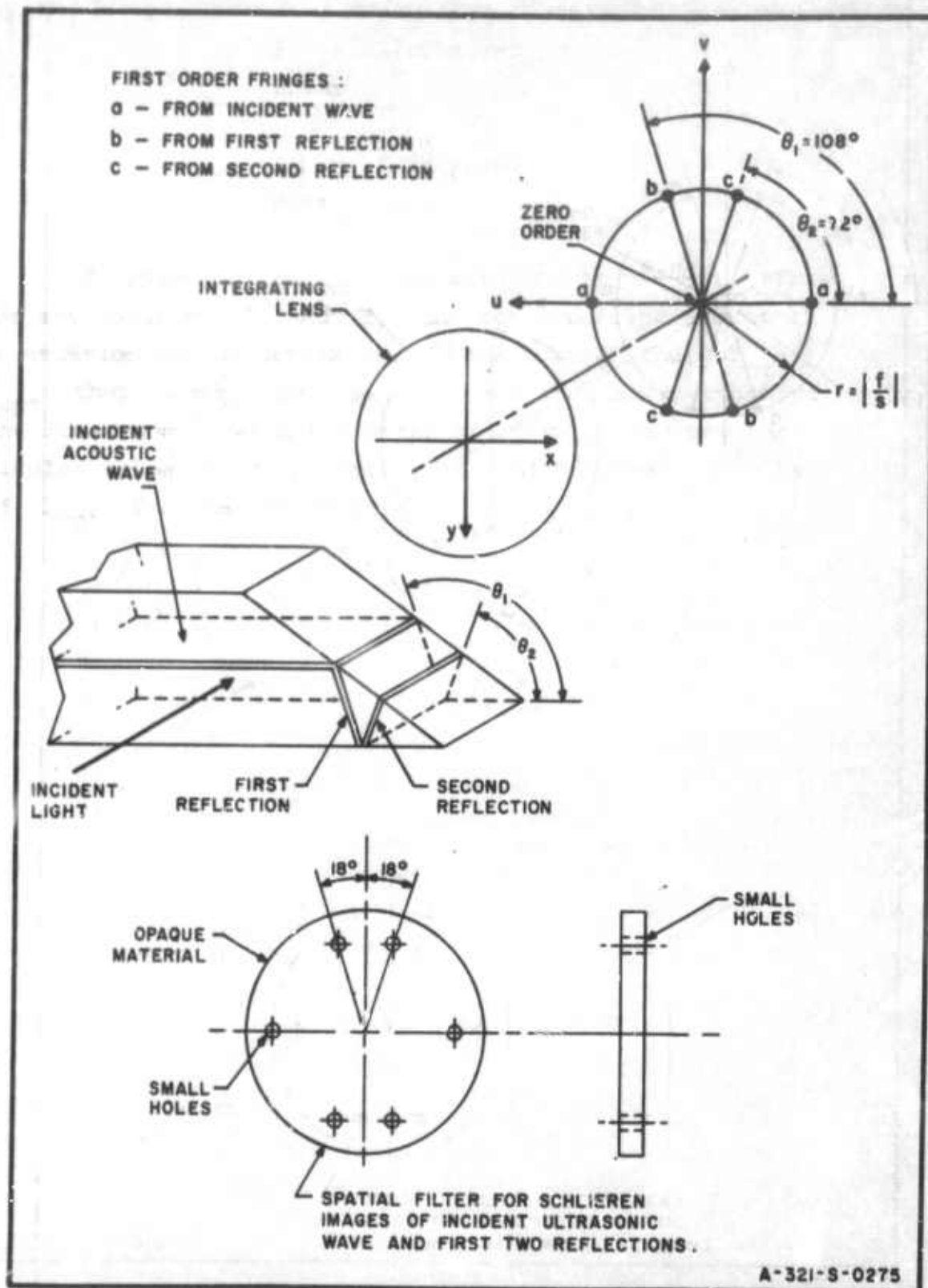


FIG. 7.2.2-4 DIFFRACTION PATTERN CAUSED BY INCIDENT WAVE AND FIRST TWO REFLECTIONS FROM 36° WEDGE

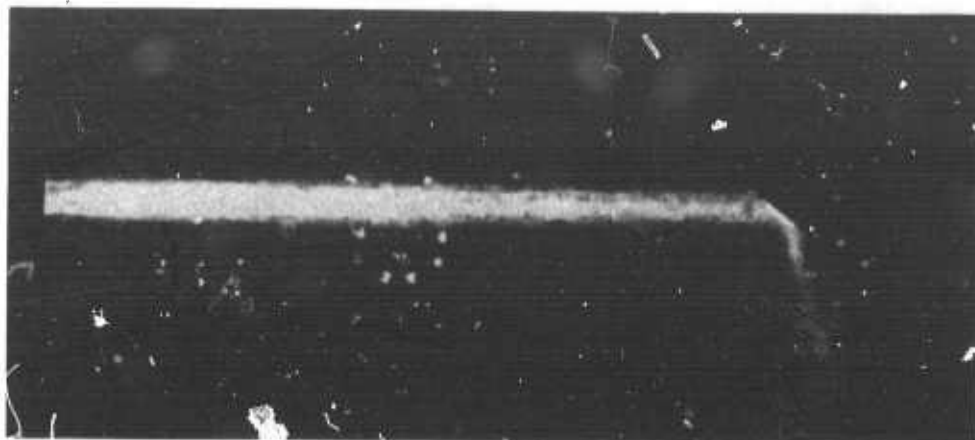


Fig. 7.2.2-5

Schlieren Photographs of Incident Beam
and Observable Reflections From 36° Wedge

7.3 ULTRASONIC LIGHT-DIFFRACTION EXPERIMENTS IN AN AMORPHOUS SOLID MEDIUM

The basic light-modulator configuration used in these experiments is shown in Fig. 7.3-1. When excitation is applied the electric field is essentially located in the area defined by the back electrode, hence the dimensions of this electrode determine the cross section of the acoustic wave; electrical contact in this case was obtained by direct spring contact with a miniature phosphor-bronze bellows (Fig. 7.3-2).

7.3.1 ELIMINATION OF STANDING WAVES

If the inactive end of the light modulator is parallel to the end on which the piezoelectric transducer is bonded then, if no method of absorption is provided for, the reflected ultrasonic energy (assuming C.W. operation) can be of sufficient strength to result in standing waves in the light modulator provided the following relationship holds:

$$\frac{2f_i l}{S} = n$$

where

n = integer = number of half cycles in the
light modulator

l = length of light modulator

f_i = frequency of electrical signal exciting
transducer

S = sonic velocity

and the incremental change in frequency for which standing waves will reoccur will be given by:

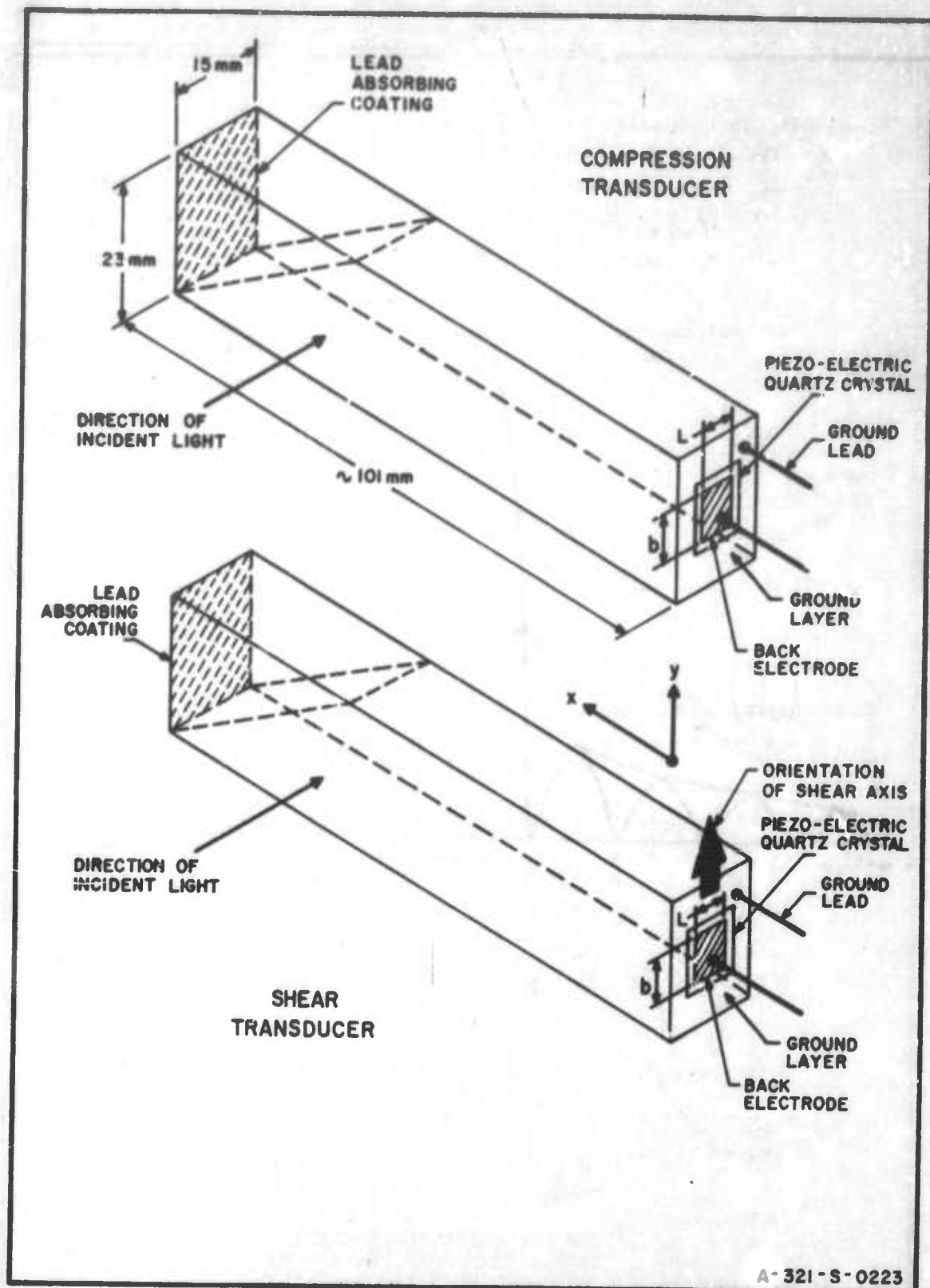


FIG. 7.3-1 EXPERIMENTAL SOLID LIGHT MODULATOR

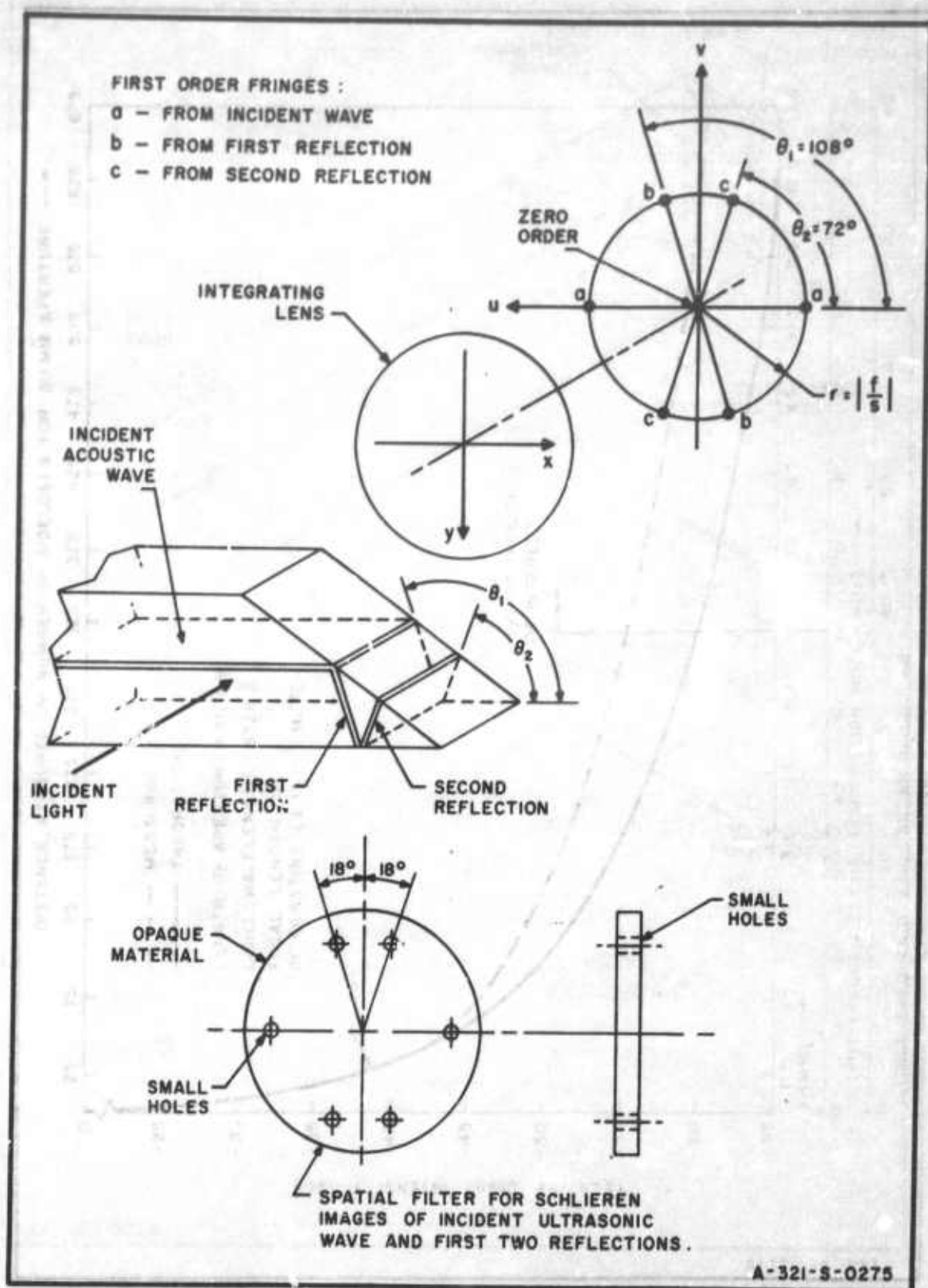


FIG. 7.2.2-4. DIFFRACTION PATTERN CAUSED BY INCIDENT WAVE AND FIRST TWO REFLECTIONS FROM 36° WEDGE

$$\Delta f_i = \frac{s}{2l}$$

In the particular cases under consideration:

$$l \approx .101 \text{ m}$$

$$s = 3760 \text{ m/sec for shear waves}$$

$$s = 5968 \text{ m/sec for compression waves}$$

From which:

$$\Delta f_i |_{\text{shear}} \approx 19 \text{ khz}$$

$$\Delta f_i |_{\text{compression}} \approx 30 \text{ khz}$$

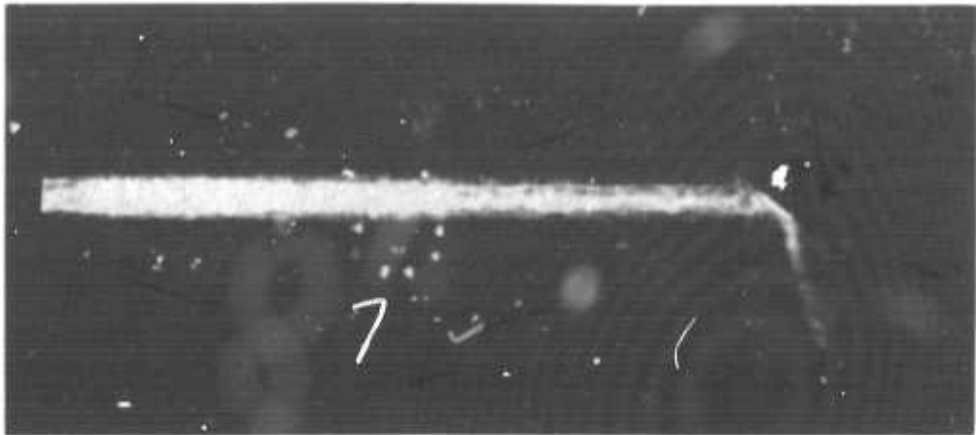
This phenomenon was observed in the initial experiments. In the experiments a 5μ slit was used in the measurement of the photodetector current resulting from the diffracted first-order peak light intensity (Sec. 7.3-2 See Fig. 7.3.2-1). This slit width, however, permitted the first-order fringes for the shear and compression modes to shift along the u axis by amounts corresponding to approximately 30 khz and 47 khz respectively, without causing the peak intensities to fall outside the region in the image plane covered by the slit. Thus for any given position of the scanning slit, it was possible to obtain at least two "peaks" in first-order light intensity by making relatively slight (i.e., 19 khz and 30 khz) changes in the oscillator frequency which was always in the 50 MHz to 100 MHz range.

Since the electro-optical array-antenna processor assumes the existence of progressive waves in the light modulator, it was necessary to eliminate the standing waves in

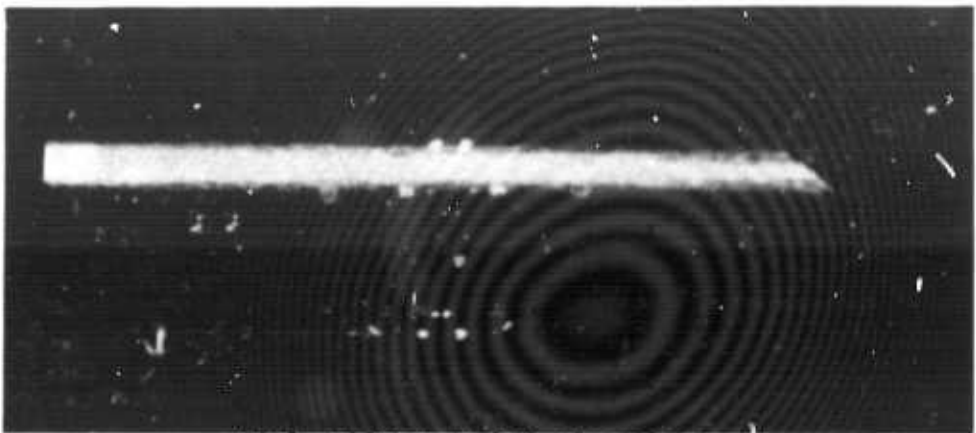
order to obtain relevant experimental data. One method of achieving this was to provide for absorption of ultrasonic energy by covering the inactive end with a cerroseal coating. A second method, however, was found to eliminate the possibility of standing waves completely. In this case a 36 deg wedge was cut on the inactive end of the light modulator, the choice of angle being selected to provide for four reflections (assuming no ultrasonic mode conversion) to take place in the "wedge region" before the beam can escape and enter the portion of the light modulator which is exposed to the incident light (Fig. 7.2.2-3). It was found that, without providing for any additional absorption, this deflection procedure was sufficient to eliminate standing wave phenomena.

Although this method was sufficient for these experiments, in an electro-optical array-antenna processor it would also be necessary to eliminate spurious signals resulting from the reflected ultrasonic energy. This might be done by employing the wedge and then coating its surfaces with some form of absorption medium to provide for additional attenuation on each reflection. One absorbing material which was tried was silver paint, and some qualitative results are shown in Fig. 7.3.1-1 which were obtained with the spatial filter described in Sec. 7.2.2. It is seen that without the absorber two full reflections are strong enough to be observed, but with the silver-paint coating the first reflection is attenuated and the second is not strong enough to be visible.

The results of a more quantitative experiment are shown in Fig. 7.3.1-2a and b. The light modulator in this case was operating in the compression mode and the wedge, which was coated with silver paint, was cut at an angle of $43^{\circ}18'$ to provide for ultrasonic mode conversion (Mason 1964).



Without Silver-Paint Absorber

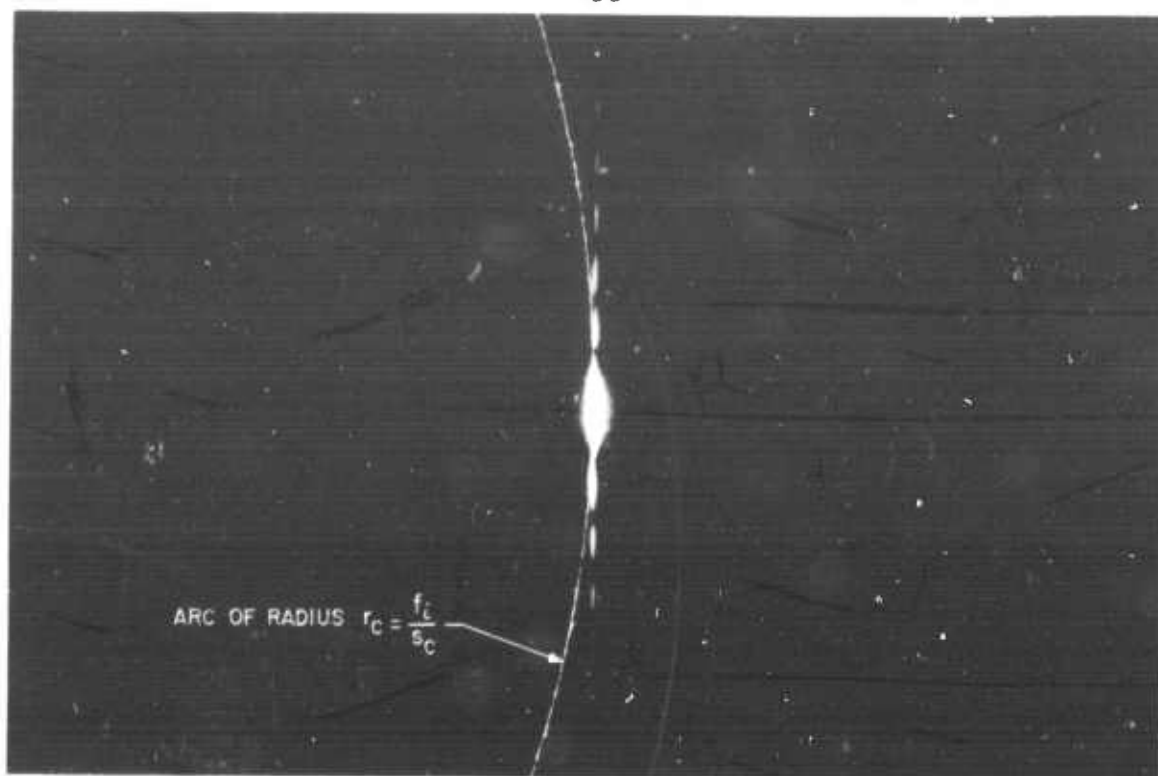


With Silver-Paint Absorber

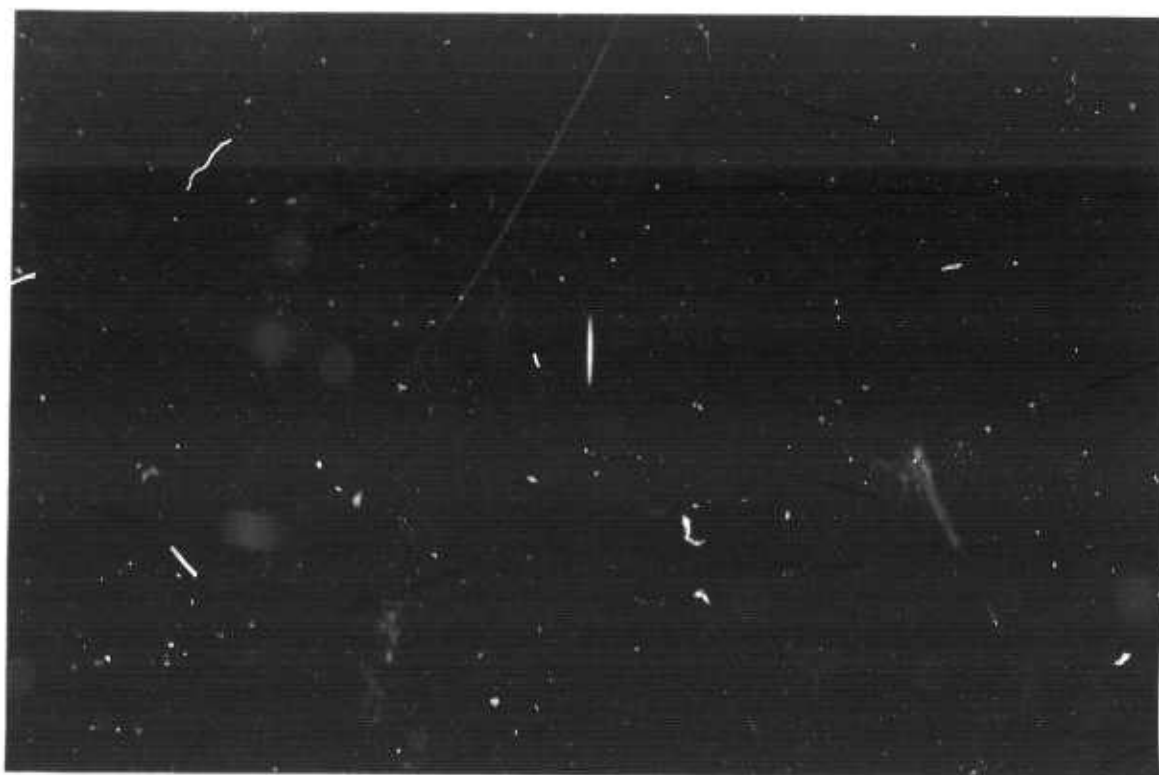
Fig. 7.3.1-1

Schlieren Photographs of Reflections from
36° Wedge Showing Effects of Silver Paint Absorber

Peak light intensity in "b" is approx. 26 db below that of "a"



- a -



- b -

Fig. 7.3.1-2

Photograph of First-Order Diffraction Pattern
Showing Absence of Reflections From Observation Region

These photographs show a region around the peak first-order intensity which is considerably larger than that which would correspond to the observation region of the electro-optical array-antenna processor. In the "a" photograph the diffracted light intensity is strong enough to exhibit its side lobe structure; in the "b" photograph the peak light intensity was measured to be approximately 26 db below that of "a" and only the peak of the first order is visible. Now, as shown in Sec. 7.2.2, any reflections of longitudinal waves would lie on a circle of radius: $r_c = \frac{f_i}{s_c}$ where f_i is the input frequency and s_c is the velocity of compression waves; and those of transverse waves would lie on a circle of radius $r_s = \frac{f_i}{s_s}$ where s_s is the shear velocity. In fused silica however, s_s is smaller than s_c and the extent of this difference is such that shear reflections lie outside the observation region of interest; this in fact was the reason for the choice of wedge angle. Thus since the exposure time for both photographs was the same, it is seen (by Fig. 7.3.1-2b) that, in the region of interest, any reflections in Fig. 7.3.1-2a must be more than 26 db below the peak intensity, otherwise they would be observable. From this it may be concluded that the use of a wedge and an absorption coating can effectively eliminate spurious reflected ultrasonic signals which would correspond to false targets in electro-optical array-antenna processors using fused-silica light modulators.

7.3.2 MEASUREMENT OF TRANSFER CHARACTERISTICS

It has been shown in Ch. 4 that for both shear and compression modes:

$$\psi_m = KV_m$$

where:

ψ_m = peak phase deviation of light wave front

V_m = peak input voltage

K = constant (K_s for shear mode, K_c for compression mode)

The constant K will depend on the mode of propagation and, for the compression mode, on the light polarization (See Eqs. 4.5-2 and 4.5-3). In this case the laser beam was polarized perpendicular to the direction of ultrasonic propagation which, in the case of the compression mode, will generally be optimal (Sec. 4.4-2).

The experimental arrangement for measuring ψ_m as a function of V_m is shown in Fig. 7.3.2-1. The photomultiplier produces a current, proportional to the output light intensity at the location of the 5μ scanning slit, which is passed through a load resistor R_L . Thus, in the actual measurement procedure, a voltage V was measured across R_L which was proportional to the light intensity at the position of the scanning slit.

In determining the relationship between V_m and ψ_m use is made of the fact that, under the condition that $\psi_m < 0.2$ radians, the ratio of first order to zero order light intensity is $\frac{\psi_m^2}{4} : 1$ (Raman and Nath 1936, Lambert 1962). Thus if the detector output voltages which are measured when the scanning slit is positioned at the center of the zero-order and first-order diffraction fringes are respectively, V_0 and V_1 , then:

$$\frac{\psi_m^2}{4} = \frac{V_1}{V_0} \quad (7.3.2-1)$$

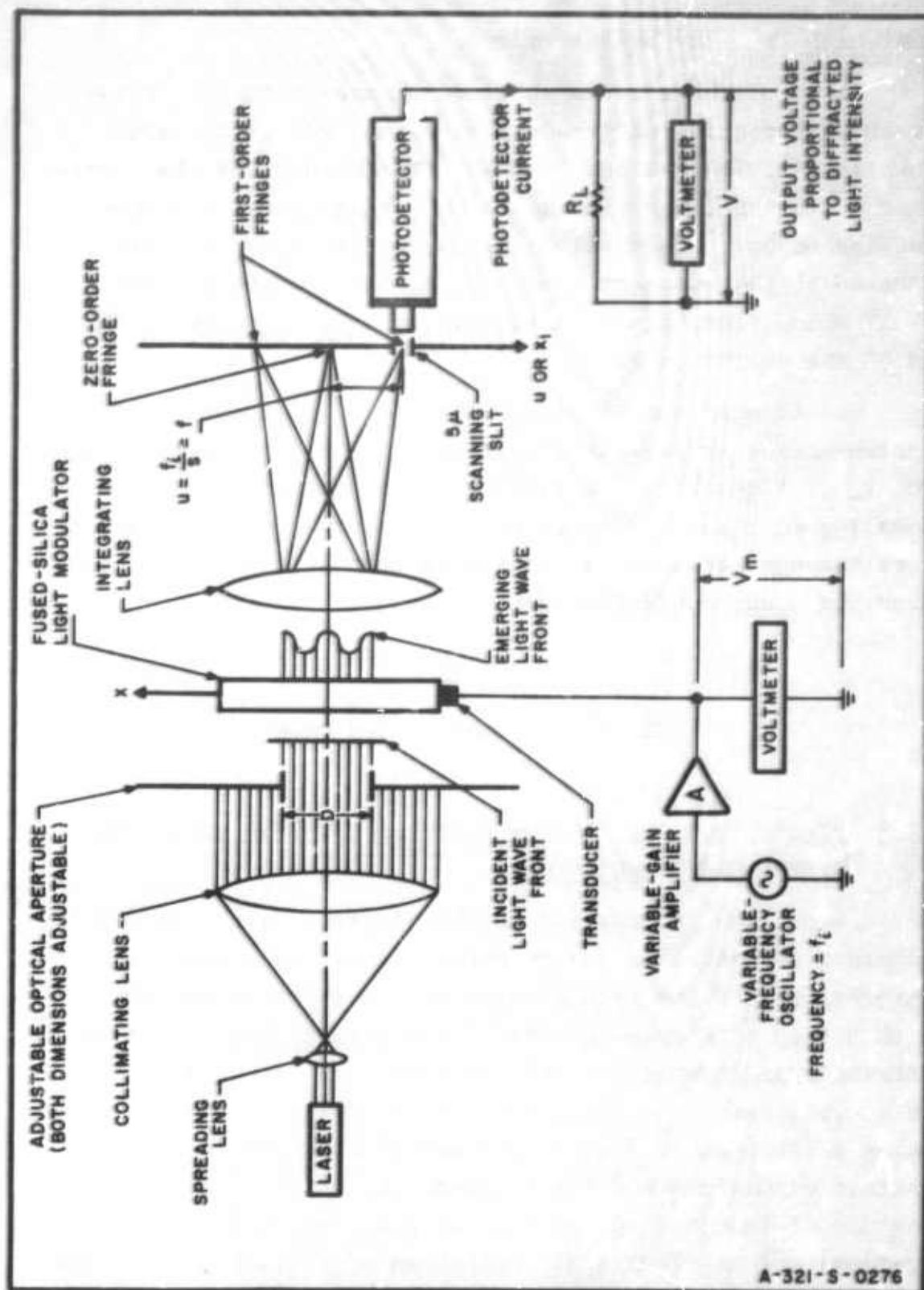


FIG. 7.3.2-1 SYSTEM FOR MEASURING DIFFRACTED LIGHT INTENSITY.

from which ψ_m may be determined.

Some of the results obtained in measuring the transfer characteristics of fused-silica light modulators are shown in Fig. 7.3.2-2 and 7.3.2-3. The values for the transducer depth, L , was 4 mm and 5 mm for the shear and compression modes respectively; the input frequency f_i was adjusted to the resonant frequency of the transducer (Sec. 7.4.1) which, for these transducers, was found to be 75 MHz and 85 MHz as indicated.

It is seen that a linear relationship, necessary for electro-optical array-antenna processing, exists between ψ_m and V_m . A quantitative measure of the constant of proportionality in these cases can be obtained by drawing straight lines through the data, as indicated in the figures, and from which for these configurations:

$$\psi_m = .00116 V_m \quad \text{shear mode}$$

$$\psi_m = .0024 V_m \quad \text{compression mode}$$

7.3.3 FIRST-ORDER DIFFRACTION PATTERNS OBTAINED WITH FUSED-SILICA LIGHT MODULATOR

Since the information in the electro-optical signal processor is contained in the structure of the diffraction patterns, one of the requirements of the light modulators is that they introduce no optical distortion resulting from ultrasonic propagation in the light modulator medium; i.e., the acoustic wave must act as a pure diffraction grating producing a first-order diffraction pattern consistent with the aperture dimensions and the frequency of excitation. For an aperture of length D (dimension along direction of sonic propagation) and an electrical excitation of frequency f_a , the

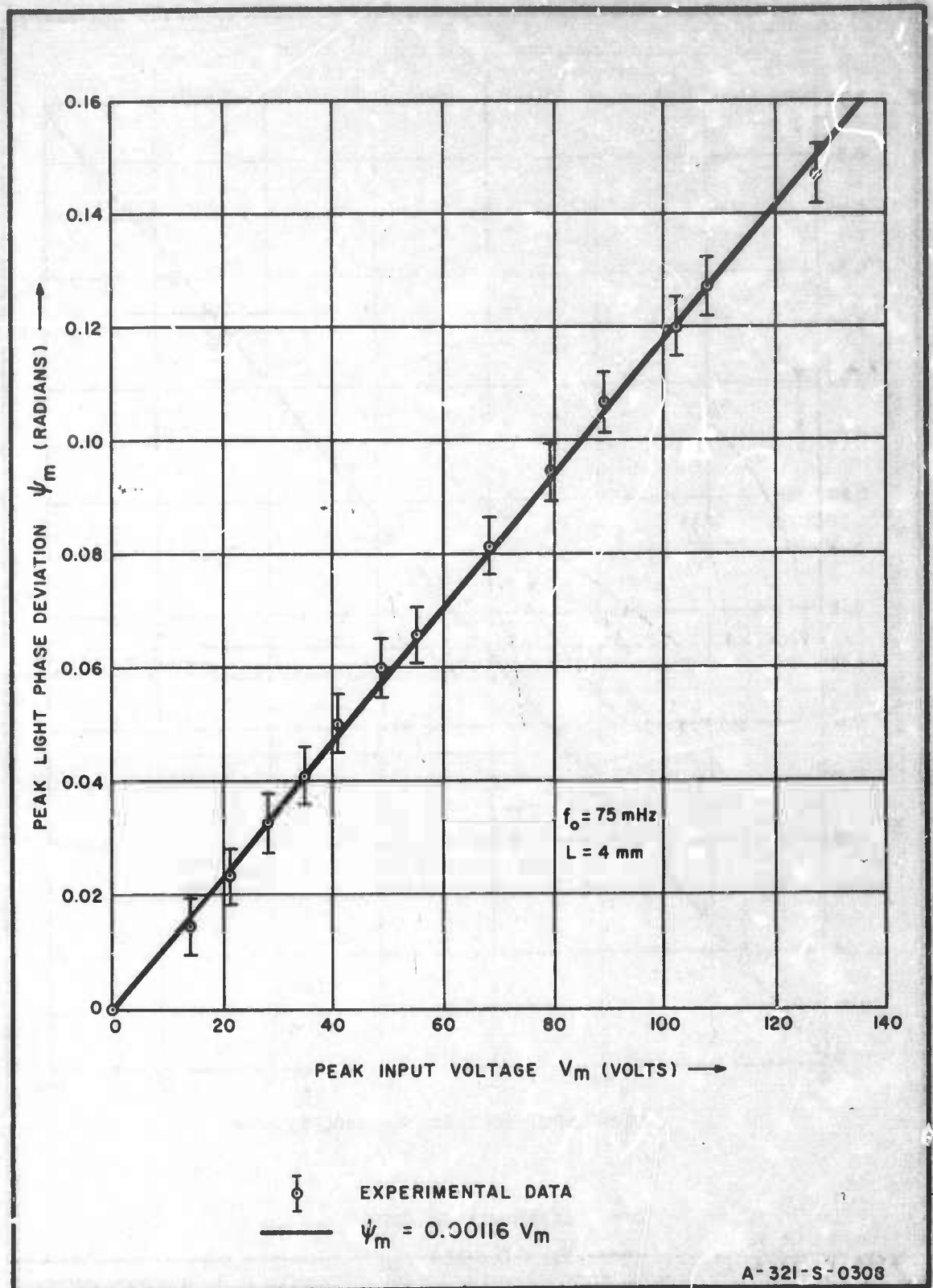


FIG. 7.3.2-2 PEAK PHASE MODULATION vs PEAK INPUT VOLTAGE FOR A FUSED-SILICA LIGHT-MODULATOR EMPLOYING SHEAR-MODE TRANSDUCER

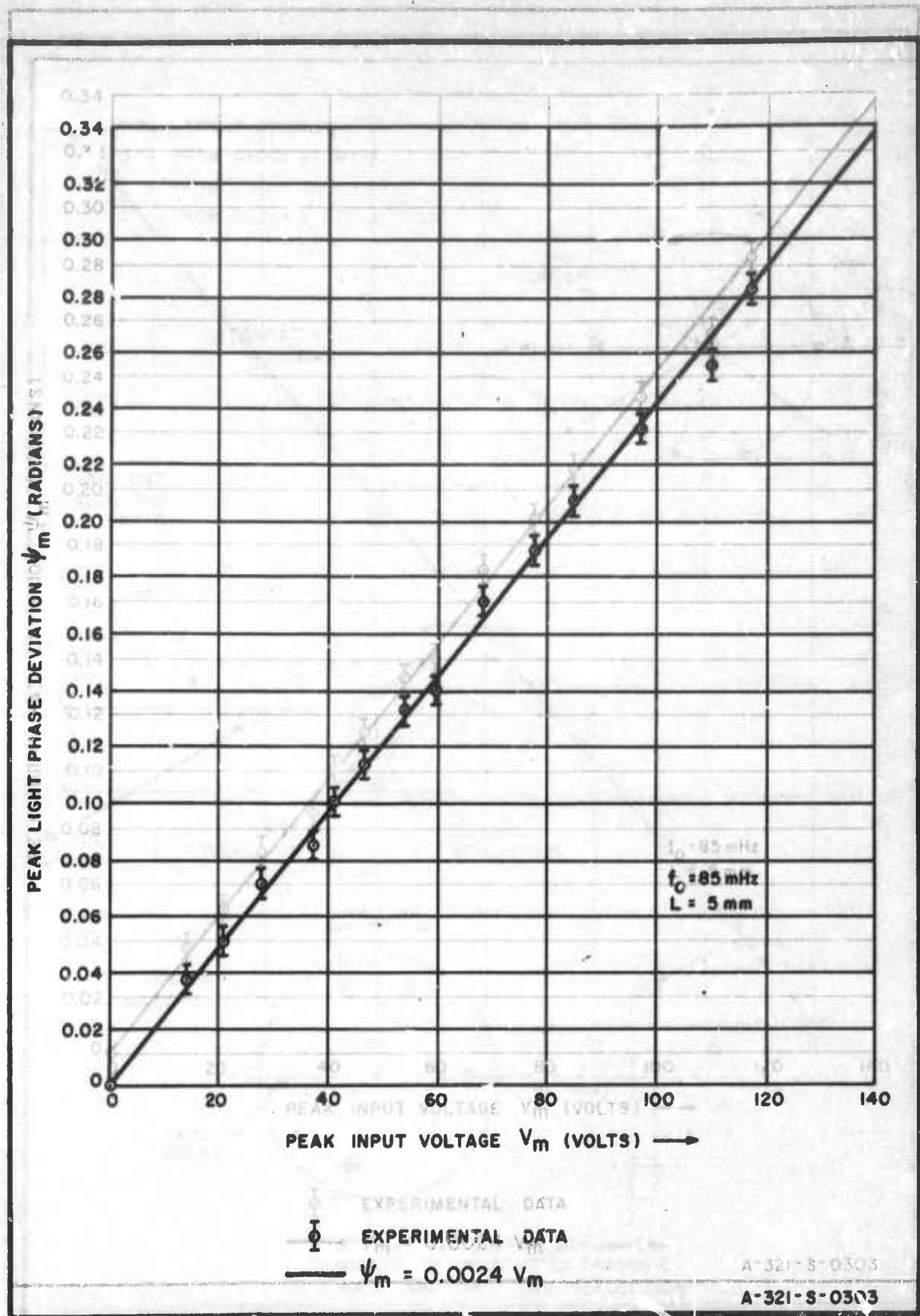


FIG. 7.3.2-3 PEAK PHASE MODULATION vs PEAK INPUT VOLTAGE FOR A FUSED-SILICA LIGHT-MODULATOR EMPLOYING COMPRESSION-MODE TRANSDUCER

first-order diffracted light intensity as a function of the output variable u should be proportional to:

$$\left(\frac{\sin \pi D(u - f)}{\pi D(u - f)} \right)^2$$

where:

$$f = \frac{f_i}{S} = \text{spatial frequency} \\ \text{(cycles per meter)}$$

S = sonic velocity .

The first-order intensity therefore is, theoretically, a replica of the zero-order pattern, with its peak occurring at the point:

$$u = f$$

The output variable u is given by:

$$u = \frac{f_i}{S} = \frac{x_1}{\lambda F}$$

where:

x_1 = linear displacement of first-order peak intensity

λ = light wavelength

F = focal length of integrating lens

In these experiments: $\lambda = 6328 \times 10^{-10}$ m , $F = 1$ m , and since this measurement employed a light modulator with a compression transducer for which:

$$f_i = 70 \text{ MHz}$$

S = sonic velocity 5968 m/sec

then theoretical displacement of peak first-order intensity would be:

$$x_1 = 7.42 \text{ mm} .$$

Using the scanning apparatus shown schematically in Fig. 7.2.1-2, the first-order light intensity distribution was recorded (Fig. 7.3.3-1) using a phase deviation of $\psi_m = 0.2$ radians. The aperture dimensions in this case were:

$D = 30 \text{ mm}$ (length of aperture along dimension of sonic propagation)

$b = 4 \text{ mm}$ (width of aperture = width of transducer).

Since the direction of sonic propagation is in the x direction, only the output distribution as a function of the output variable u is of interest. The location of peak first-order intensity was found experimentally to be:

$$x_1 = 7.50 \text{ mm} .$$

This distribution may be compared with that of the zero order as shown in Fig. 7.3.3-2. It is seen that the light intensity at the first nulls is 26 db below the peak in the zero-order pattern as compared with approximately 23 db below peak intensity in the first order. This may be due to errors introduced by the integrating lens which must operate off its optic axis in producing the first-order light distribution. In general, however, it is seen that the first-

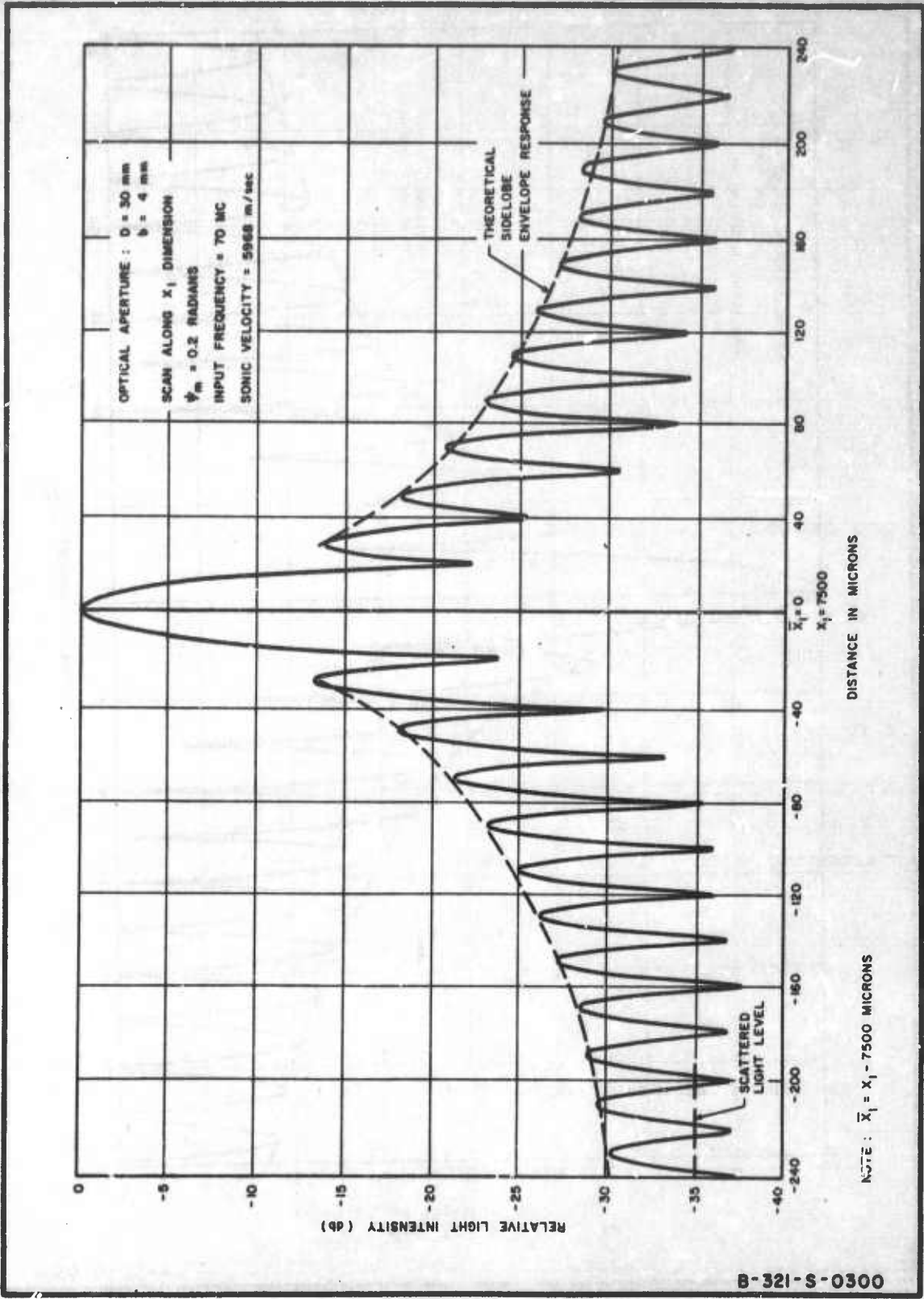


FIG. 7.3.3-1 POSITIVE FIRST-ORDER LIGHT INTENSITY
(COMPRESSION MODE)

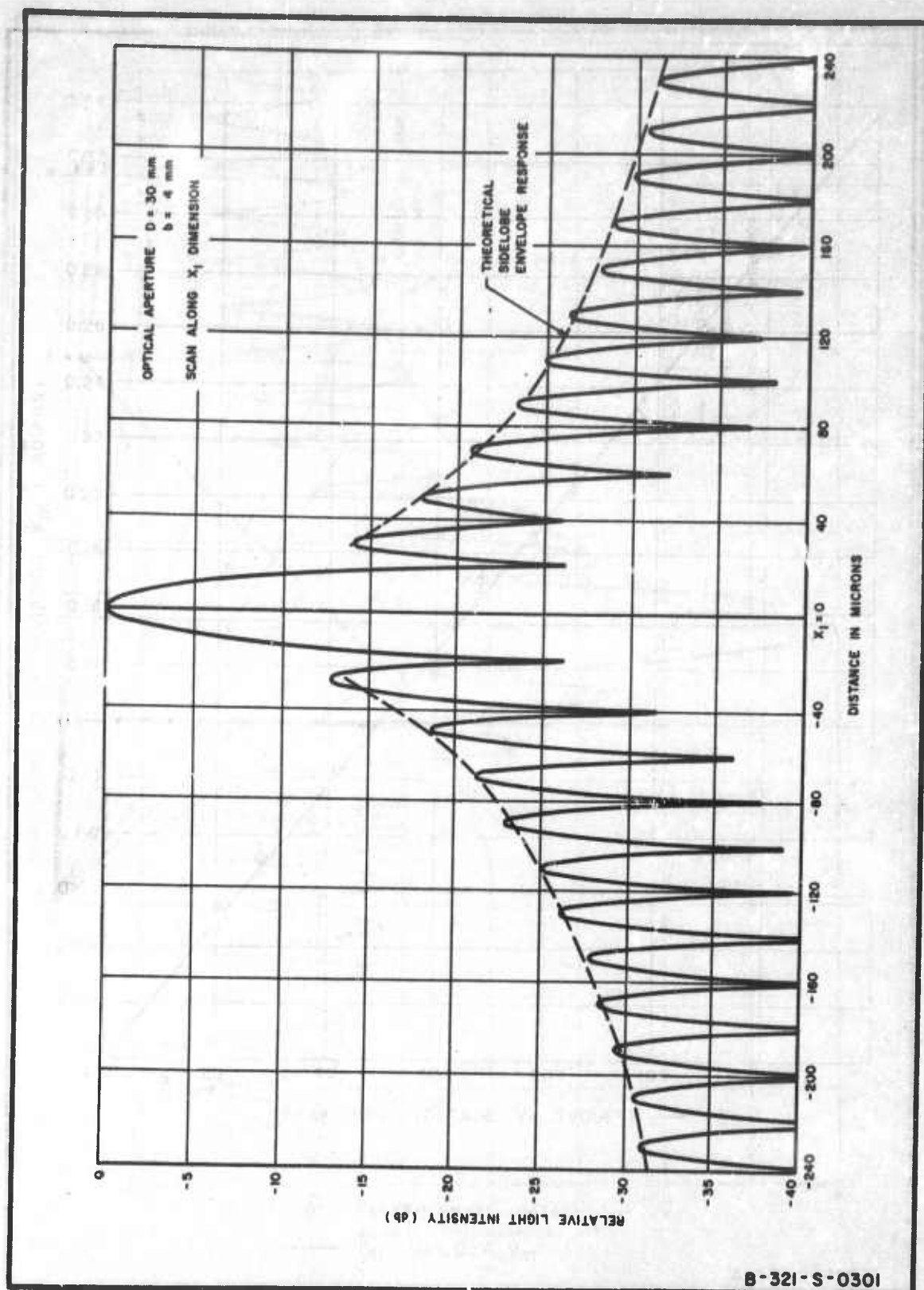


FIG. 7.3.3-2 ZERO-ORDER LIGHT INTENSITY

order diffraction pattern is a nearly ideal replica of the zero order, and that no distortion is introduced by ultrasonic propagation in the medium.

This measurement is also seen to be consistent with the scattered light level of the optical system. That is, from Fig. 7.3.3-1 the background level is seen to be approximately 35 db below the first-order peak. This peak however, for a peak phase deviation of .2 radians, is easily shown to be 20 db below that of the zero order. Thus the scattered light level at $x_1 = 7500\mu$ is approximately 55 db below the peak of the zero order which agrees with results shown in Fig. 7.2.1-6.

7.4 FUSED-SILICA LIGHT-MODULATOR EXPERIMENTS RELATED TO EVALUATION OF SIGNAL-PROCESSING CAPACITY

7.4.1 MEASUREMENT OF LIGHT-MODULATOR BANDWIDTH

This measurement employed the arrangement shown in Fig. 7.3.2-1. In this case the value of V_m was held fixed while the input frequency was varied. For each frequency setting the slit position was readjusted in order to correspond to the location of peak first-order intensity and the resulting photodetector current produced a voltage, proportional to $(\psi_m)^2$, across the load resistor R_L . Thus the measured output voltage was a function of the input frequency f_i and the experimentally measured relative peak phase deviation of the light modulator, as a function of input frequency, can be described by the expression:

$$10 \log \left| \frac{V(f_i)}{V(f_o)} \right|$$

where f_o is the resonant frequency of the light modulator.

Figures 7.4.1-1 and 7.4.1-2 present the bandpass characteristics of the two light modulators whose experimentally determined transfer characteristics were presented in Sec. 7.3.2. It is seen that the bandwidths are approximately 44 per cent and 64 per cent of the resonant frequency for the shear and compression modes respectively, which justifies, experimentally, the assumption of a 50 per cent light-modulator bandwidth in the evaluation (Ch. 5) of the signal processing capacity of fused-silica light modulators.

7.4.2 INTERNAL-REFRACTION EFFECTS: DETERMINATION OF LOWER BOUND ON TRANSDUCER DEPTH

In Sec. 5.2.2 it has been shown that, in this electro-optical processor, the minimum transducer depth which would be necessary because of internal-refraction considerations is given by:

$$L = \frac{n_o S^2}{\lambda f_i^2} \quad (7.4.2-1)$$

where

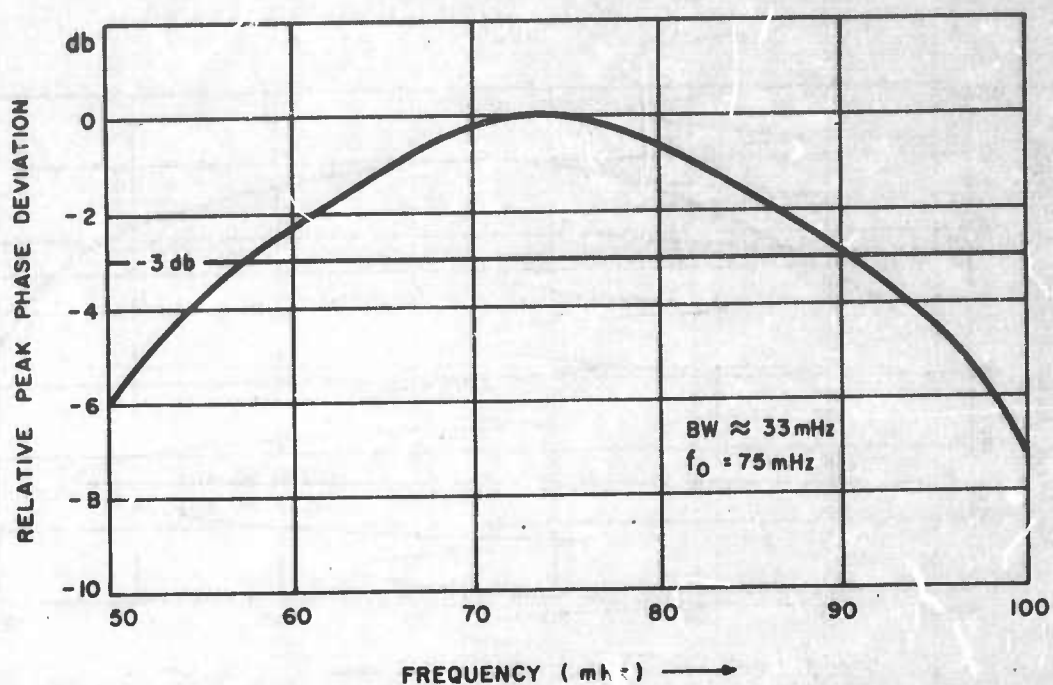
n_o = equilibrium value of refractive index

S = sonic velocity

f_i = input frequency

λ = light wavelength

That is, for any given value of V_m (assuming that Willard's criterion and the assumptions of Rao and Murty are not violated) this value of transducer depth theoretically maximizes the effective phase modulation which has been defined as:



A-321-S-0311

FIG. 7.4.1-1 BANDPASS CHARACTERISTICS OF FUSED-SILICA LIGHT-MODULATOR EMPLOYING ULTRASONIC SHEAR MODE

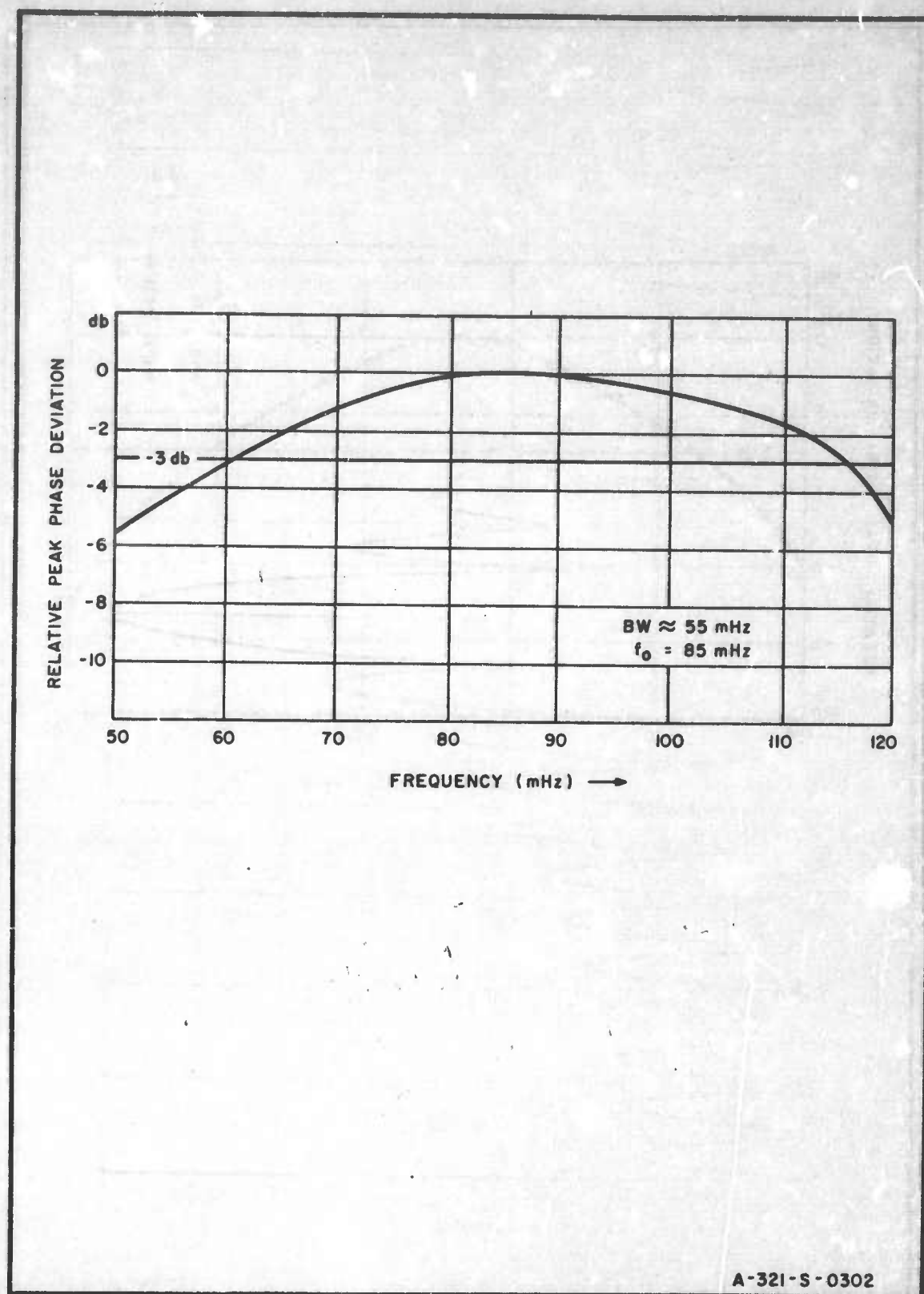


FIG. 7.4.1-2 BANDPASS CHARACTERISTICS OF FUSED-SILICA LIGHT-MODULATOR EMPLOYING ULTRASONIC COMPRESSION MODE

$$\bar{\psi}_m = \psi_m \frac{\sin \gamma}{\gamma} \quad (7.4.2-2)$$

where $\frac{\sin \gamma}{\gamma}$ is the attenuation factor due to internal-refraction effects, $\psi_m = \frac{2\pi n L}{\lambda}$, and $\gamma = \frac{\pi \lambda L f_i^2}{2n_0 S^2}$.

The experimental verification of this relationship (eq. 7.4.2-1) utilized the arrangement shown in Fig. 7.3.2-1. In this case a fused-silica light modulator with a compression transducer was used, the amplitude of the input signal was held at a fixed value, and the input frequency was 100 MHz. The peak first-order intensity was then measured as a function of transducer depth, L , which was varied from 11 mm to 5 mm in steps of 1 mm. It was found that the peak first-order light intensity was a maximum for $L = 8$ mm. This result agrees with the theory developed in Sec. 5.2.2 since the value of L_{opt} (Eq. 5.2.2-11) for the compression mode at 100 MHz in fused silica is approximately 8 mm as may be seen in Fig. 5.2.2-4.

The results are presented, normalized to $\bar{\psi}_m(8)$, in Fig. 7.4.2-1. It is seen that:

$$\frac{\bar{\psi}_m(L)}{\bar{\psi}_m(8)} = \frac{k_1 L \frac{\sin k_2 L}{k_2 L}}{k_1 8 \frac{\sin k_2 8}{k_2 8}}$$

where k_1 and k_2 are constants, and since

$$\gamma = k_2 L \bigg|_{L=8} \approx \frac{\pi}{2} \Rightarrow k_2 \approx \frac{\pi}{16}$$

then:

$$\frac{\bar{\psi}_m(L)}{\bar{\psi}_m(8)} \approx \sin \frac{\pi L}{16}$$

and this curve is included in Fig. 7.4.2-1.

Thus although internal-refraction effects will decrease with the transducer depth, these results provide experimental verification that there will always be practical lower bound on this dimension (Eq. 7.4.2-1), and that, in this electro-optical processor, the transducer depth need not be any smaller.

7.4.3 EXPERIMENTAL STUDIES OF ULTRASONIC BEAM BROADENING AND CROSS-CHANNEL COUPLING

In Sec. 5.2.4 it is shown that the maximum number of light-modulator channels which may be fitted into an optical aperture of a given size is limited by cross talk between adjacent channels due to spreading of the ultrasonic wave in propagation, and possible electromechanical cross coupling between adjacent transducers. It is easily shown that the relationship of Eq. (5.2.4-1) is equivalent to a light-modulator configuration in which adjacent light-modulator channels are separated by one transducer width, and the length of the light modulator is given by:

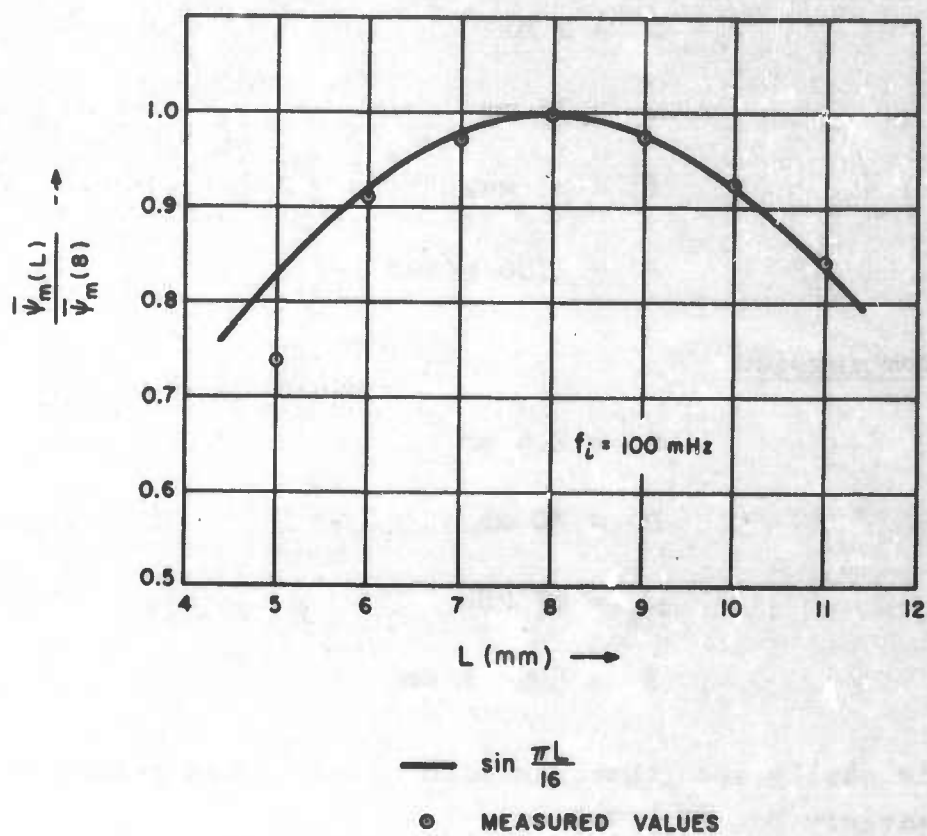
$$D = \frac{b^2}{\lambda_s} \quad (7.4.3-1)$$

where

b = transducer width

λ_s = sonic wavelength = $\frac{s}{f_i}$

Note that in this configuration the ultrasonic beams are allowed to spread out into, but not beyond, the opaque region in between the light-modulator channels.



A-321-S-0312

FIG. 7.4.2-1 NORMALIZED EFFECTIVE PHASE MODULATION vs TRANSDUCER DEPTH

COLUMBIA UNIVERSITY—ELECTRONICS RESEARCH LABORATORIES

The experimental investigation of the effects of beam broadening employed a multiple-transducer configuration in which two back electrodes were simultaneously excited, and the resulting pair of acoustic waves was photographed by means of Schlieren techniques. This was done for both the shear and compression modes under the following conditions:

(i) Shear

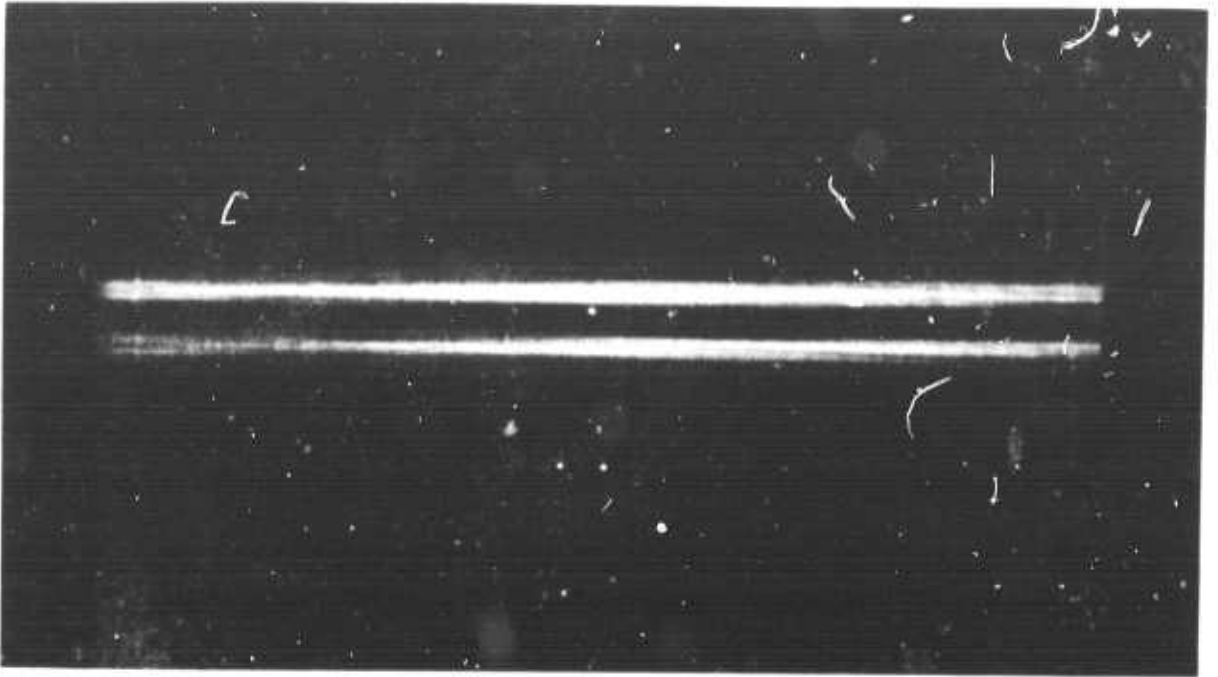
$$\begin{aligned}b &= 2 \text{ mm} \\D &= 75 \text{ mm} \\f_1 &= 70 \text{ MHz} \\S &= 3760 \text{ m/sec}\end{aligned}$$

(ii) Compression

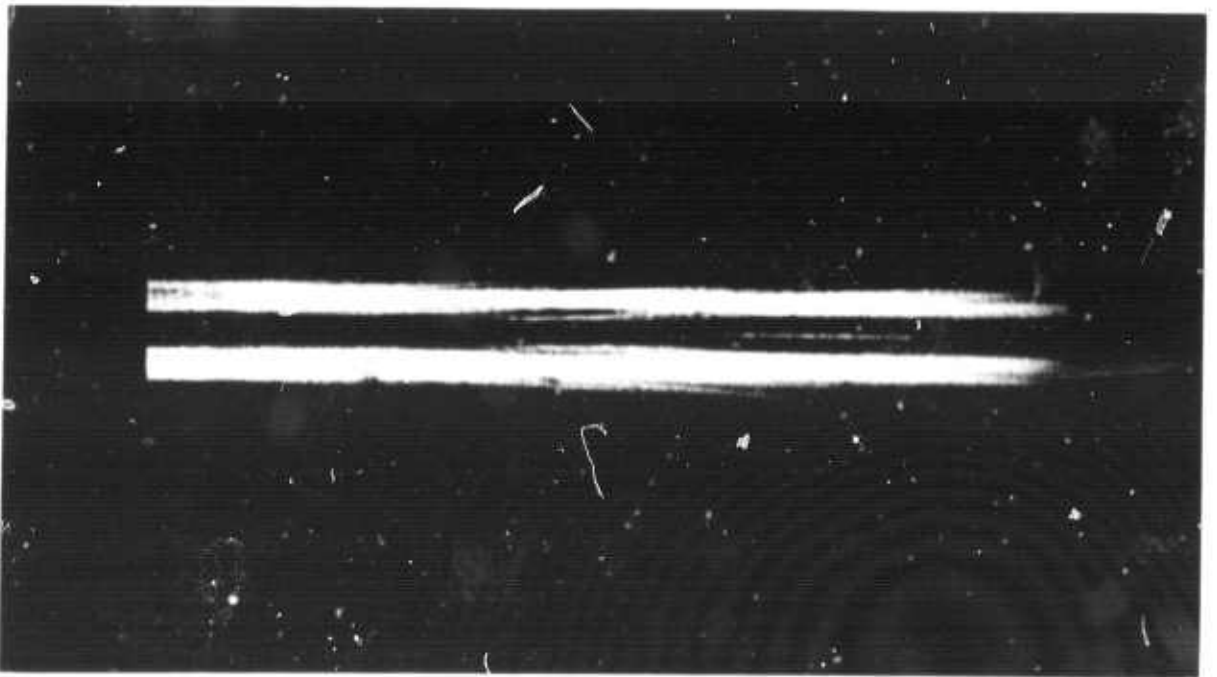
$$\begin{aligned}b &= 2.5 \text{ mm} \\D &= 70 \text{ mm} \\f_1 &= 67 \text{ MHz} \\S &= 5968 \text{ m/sec}\end{aligned}$$

and it is easily seen that, in both cases, these parameter values satisfy Eq. (7.4.3-1).

Some examples of the photographs which were obtained are presented in Fig. 7.4.3-1. It is seen that, for both modes of propagation, although the aperture length permits some broadening to take place, the ultrasonic beam does not spread out into the adjacent channel. This verifies Eq. (5.2.4-1) for fused-silica light modulators with regard to the effects of ultrasonic diffraction.



Shear Mode

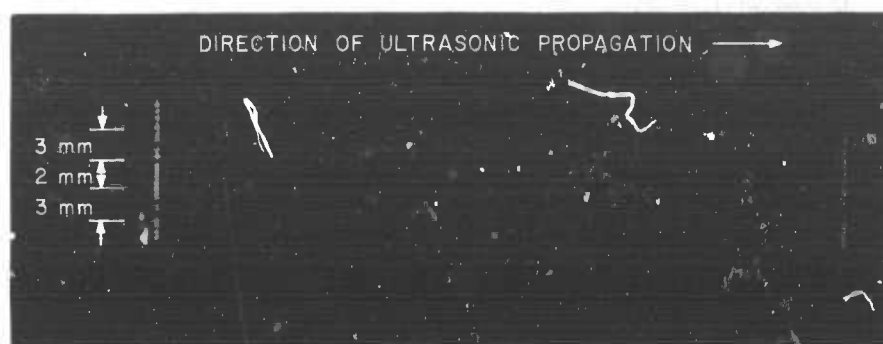


Compression Mode

Fig. 7.4.3-1 Schlieren Photographic-Study Showing
Extent of Beam Broadening

In order to investigate other possible sources of cross-channel coupling, additional multiple-transducer experiments were performed. In one experiment, for both the shear and compression modes, the experimental configuration employed two electrodes 3 mm wide with a separation of 2 mm; the input frequency in this case was 75 MHz. In the Schlieren photographs of Figs. 7.4.3-2a and 7.4.3-3a, both electrodes were excited by a low voltage and the exposure time was approximately 1 sec. One electrical connector was then removed, the back electrode was left in place, and a similar photograph was taken using an electrical excitation 10 times as large (Fig. 7.4.3-2b and 3b). Now it is evident that any deleterious electromechanical cross coupling would cause a spurious signal to be generated at the unexcited electrode. No such signal, however, was visible. Thus since it is possible to observe an acoustic wave resulting from an excitation one tenth of that which produced these photographs then, by linearity of ψ_m and V_m , any diffracted light intensity resulting from electromechanical cross coupling is verified to be suppressed by more than 20 db for this configuration.

A second similar experiment was performed in which, for each mode, a single electrode (Figs. 7.4.3-4a and 7.4.3-5a) 7 mm wide was excited by a low voltage signal. This experiment used different transducers from above and the frequency was 70 MHz. The electrode was then divided in half by a scratch, which effectively produced two 3.5 mm electrodes separated by less than .5 mm, and a photograph was taken (using the same exposure as before) of the beams produced by exciting one of the halves by a signal 10 times as large (Figs. 7.4.4-4b and 5b). In the case of the shear transducer the excited electrode happened to be located equidis-



a - Both Transducers Excited

Input Voltage = V_{in}

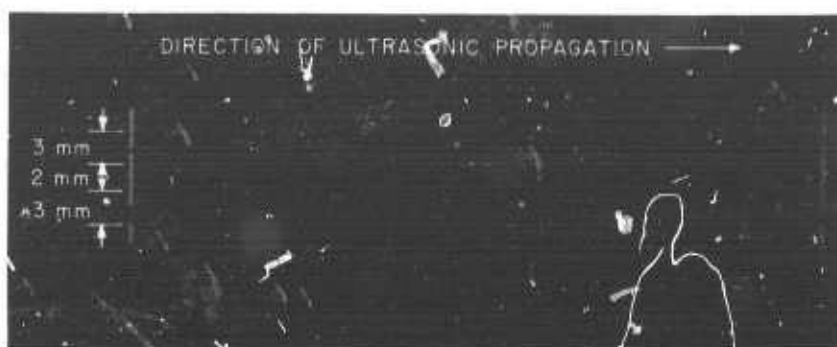


b - One Transducer Excited

Input Voltage = $10 V_{in}$

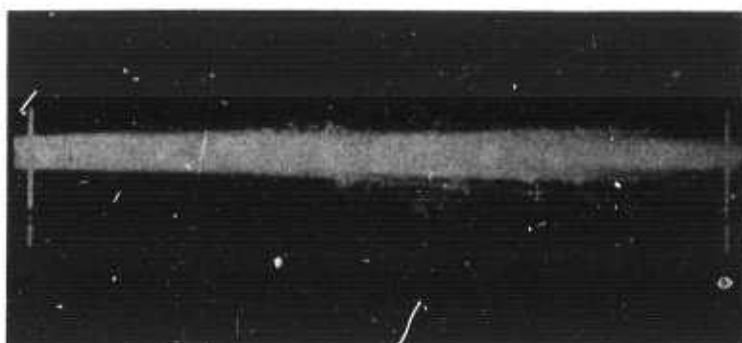
Fig. 7.4.3-2

Shear-Mode Transducer : Schlieren
Photographic-Study of Cross Coupling



a - Both Transducers Excited

Input Voltage = V_{in}



b - One Transducer Excited

Input Voltage = $10 V_{in}$

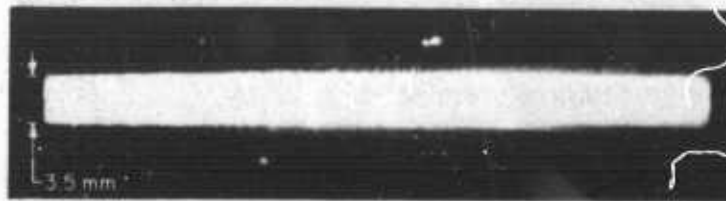
Fig. 7.4.3-3

Compression-Mode Transducer : Schlieren
Photographic-Study of Cross Coupling



a - 7 mm Electrode

Input Voltage = V_{in}

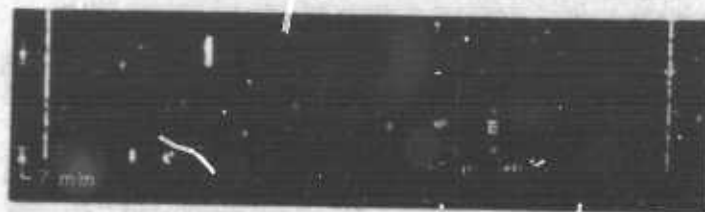


b - Divided 7 mm Electrode

Input Voltage = $10 V_{in}$

Fig. 7.4.3-4

Shear-Mode Transducer : Schlieren
Photographic-Study of Cross Coupling



a - 7 mm Electrode

Input Voltage = V_{in}



b - Divided 7 mm Electrode

Input Voltage = $10 V_{in}$

Fig. 7.4.3-5 Compression-Mode Transducer : Schlieren
Photographic Study of Cross Coupling

tantly from the unexcited 3.5 mm half and a second electrode which was in place from a previous experiment.

It is seen that, for the compression mode, no spurious signal is visible which, by the same argument used for the results of Figs. 7.4.3-2 and 7.4.3-3, verifies that very closely spaced compression transducers will be isolated by at least 20 db. For the shear mode, however, this might not be the case. Although it may not be readily apparent from the reproduction of Fig. 7.4.3-4b, the original photograph for the case of the shear transducer showed faint traces at the locations of the passive electrodes on both sides of the active region which could represent a spurious excitation arising from the extremely narrow separations in this experiment. Thus the results of these experiments verify that the choice of the compression mode for the optimal processor configuration, as defined in Ch. 5, is also consistent with its characteristics with regard to cross-coupling effects.

7.5 SUMMARY AND CONCLUSIONS OF EXPERIMENTAL WORK

It has been the purpose of this chapter to present some of the results of the experimental investigations into the possible use of fused-silica light modulators for electro-optical array-antenna processing.

The electro-acoustic transfer characteristics have been investigated experimentally and been found to be linear, which has been shown to be necessary for electro-optical array antenna processing, and it has also been established that fused-silica light modulators can produce first-order diffraction patterns free of optical distortion. These investigations illustrate, in general, the applicability of this light-modulator medium to electro-optical signal processing.

Other experiments relating to the light-modulator bandwidth, internal-refraction effects, and the minimum spacing of spatially-multiplexed light modulator channels have also been performed in order to provide experimental verification of the results of Chap. 5, which state the significant gains in signal-processing capacity could be achieved with the use of fused-silica light modulators. It has been shown experimentally that:

(i) Light-modulator bandwidths which are 50 per cent of the resonant transducer frequency are easily obtained.

(ii) The effects of internal refraction on the minimum necessary transducer depth can be precisely determined. This verifies that the transducer dimensions stated in Ch. 5 for the optimal configuration are realistic.

(iii) The relationship between the maximum possible number of spatially-multiplexed light-modulator channels and the dimensions of the optical aperture, which have been obtained for the electro-optical processors which have been synthesized (Lambert 1965), is valid for the optimal mode of sonic propagation in fused silica.

As a result of these investigations the evaluation of the signal-processing capacity of the fused-silica Debye-Sears light-modulator (Ch. 5) is experimentally justified.

APPENDIX ABEHAVIOR OF ELECTROMAGNETIC PLANE WAVES
IN HOMOGENEOUS ANISOTROPIC MEDIA

The following describes how light is affected in passing through an anisotropic medium such as a crystal. It will be seen that:

(i) In a crystal there is a set of principal dielectric axes and three principal dielectric constants ϵ_x , ϵ_y and ϵ_z .

(ii) For a given energy density $w = 2w_e$, where w_e equals electric energy density, at each point in the crystal the \vec{D} field of a propagating electromagnetic wave will obey the relationship:

$$\frac{D_x^2}{\epsilon_x} + \frac{D_y^2}{\epsilon_y} + \frac{D_z^2}{\epsilon_z} = 8\pi w_e$$

where x , y and z are the principal dielectric axes.

(iii) This relationship for the \vec{D} field defines the "ellipsoid of wave normals,"

$$\frac{x^2}{\epsilon_x} + \frac{y^2}{\epsilon_y} + \frac{z^2}{\epsilon_z} = 1$$

in the coordinate system defined by the principal axes. When light propagates through the crystal it is in general split into separate beams. The characteristics of these two beams are functions of the direction of the unit wave normal, and can be described by the following geometrical construction:

Through the origin construct a plane perpendicular to the direction of propagation. The intersection of this plane

with the ellipsoid of wave normals is an ellipse \hat{C} . Each of the two beams will be linearly polarized with mutually perpendicular directions of polarization along the major and minor axes of \hat{C} , and with velocities of propagation which are inversely proportional to the lengths of the semi-major and minor axes. If the lengths of the semi-major and minor axes are r' and r'' , then the indices of refraction for light which is linearly polarized along these axes will be given by:

$$r' = \frac{n'}{\sqrt{\mu}}, \quad r'' = \frac{n''}{\sqrt{\mu}}.$$

A-1 \vec{D} AND \vec{E} FIELDS IN HOMOGENEOUS ANISOTROPIC MEDIA

In a material which is electrically anisotropic* the simple relationship $\vec{D} = \epsilon \vec{E}$ no longer holds, and it is necessary to write:

$$D_x = \epsilon_{xx} E_x + \epsilon_{xy} E_y + \epsilon_{xz} E_z$$

$$D_y = \epsilon_{yz} E_x + \epsilon_{yy} E_y + \epsilon_{yz} E_z$$

$$D_z = \epsilon_{zx} E_x + \epsilon_{zy} E_y + \epsilon_{zz} E_z$$

That is, the dielectric properties are described by the nine quantities: $\epsilon_{xx}, \epsilon_{xy}, \dots$; which constitute the dielectric tensor of the material.

The electric energy density in the medium is given by:

$$4\pi w_e = \int_0^{\vec{D}} \vec{E} \cdot d\vec{D}$$

* It is assumed that the media under consideration are magnetically isotropic, that is: $\vec{B} = \mu \vec{H}$ throughout.

Therefore:

$$4\pi dw_e = E_x dD_x + E_y dD_y + E_z dD_z$$

and

$$E_x dD_x + E_y dD_y + E_z dD_z$$

is an exact differential, and may be written as:

$$E_x dD_x + E_y dD_y + E_z dD_z = d(\vec{E} \cdot \vec{D}) - (D_x dE_x + D_y dE_y + D_z dE_z)$$

Thus the second term on the right, being the difference of two exact differentials is also an exact differential. Therefore:

$$\frac{\partial D_x}{\partial E_y} = \epsilon_{xy} = \frac{\partial D_y}{\partial E_x} = \epsilon_{yx} \dots \text{etc.}$$

and the dielectric tensor is symmetric.

The electric energy density in the medium may now be written:

$$8\pi w_e = \vec{E} \cdot \vec{D} = \epsilon_{xx} E_x^2 + \epsilon_{yy} E_y^2 + \epsilon_{zz} E_z^2 + 2\epsilon_{yz} E_y E_z + 2\epsilon_{xz} E_x E_z + 2\epsilon_{xy} E_x E_y$$

This quadratic form is positive definite since energy density is nonnegative; hence the right hand side defines an ellipsoid. Since, for rotation of axes, E_x , E_y and E_z obey the same laws of transformation as do the coordinate directions (x , y and z), there exists a coordinate system, referred to as the principal dielectric axes of the material, and in which the equation of the ellipsoid is:

$$\epsilon_x E_x^2 + \epsilon_y E_y^2 + \epsilon_z E_z^2 = 8\pi w_e$$

In this principal coordinate system the material equations take the form:

$$D_x = \epsilon_x E_x, \quad D_y = \epsilon_y E_y, \quad D_z = \epsilon_z E_z$$

and

$$8\pi w_e = \epsilon_x E_x^2 + \epsilon_y E_y^2 + \epsilon_z E_z^2 = \frac{D_x^2}{\epsilon_x} + \frac{D_y^2}{\epsilon_y} + \frac{D_z^2}{\epsilon_z} \quad (1.1)$$

where ϵ_x , ϵ_y and ϵ_z are the principal dielectric constants. Thus \vec{D} and \vec{E} will have different directions unless \vec{E} lies along one of the principal axes, or unless $\epsilon_x = \epsilon_y = \epsilon_z$, in which case the ellipsoid degenerates into a sphere. It will be seen that this will be the case for cubic crystals and for unstrained amorphous media.

A-2 PLANE WAVES IN ANISOTROPIC MEDIA

Consider a monochromatic plane electromagnetic wave with frequency f and velocity $\frac{c}{n}$ propagating in a uniform anisotropic medium. Let the unit wave normal be given by \vec{s} , and a radius vector by $\vec{r} = x\vec{i} + y\vec{j} + z\vec{k}$. Then each of the vector quantities \vec{E} , \vec{D} , \vec{H} and \vec{B} will be proportional to $\exp j2\pi f \left[\frac{n}{c}(\vec{r} \cdot \vec{s}) - t \right]$. In this notation, the operation $\frac{\partial}{\partial t}$ is equivalent to multiplication by $-j2\pi f$, and $\frac{\partial}{\partial x}$ is equivalent to multiplication by $j2\pi f \frac{n}{c} s_x$. Therefore: $\frac{\partial \vec{E}}{\partial t} = -j2\pi f \vec{E}$ and $\nabla \times \vec{E} = j2\pi f \frac{n}{c} \vec{s} \times \vec{E}$.

Since there are no currents, Maxwell's equations for the medium are:

$$\nabla \times \vec{H} = \frac{1}{c} \frac{\partial \vec{D}}{\partial t} \qquad \nabla \times \vec{E} = -\frac{1}{c} \frac{\partial \vec{B}}{\partial t}$$

which may be written as:

$$\vec{n}\vec{s} \times \vec{H} = -\vec{D} \quad \vec{n}\vec{s} \times \vec{E} = \vec{B} = \mu\vec{H} \quad (2.1)$$

by direct substitution:

$$\vec{D} = -\frac{n^2}{\mu} \vec{s} \times (\vec{s} \times \vec{E}) \quad (2.2)$$

and since in general

$$\vec{A} \times (\vec{B} \times \vec{C}) = \vec{B}(\vec{A} \cdot \vec{C}) - \vec{C}(\vec{A} \cdot \vec{B})$$

then

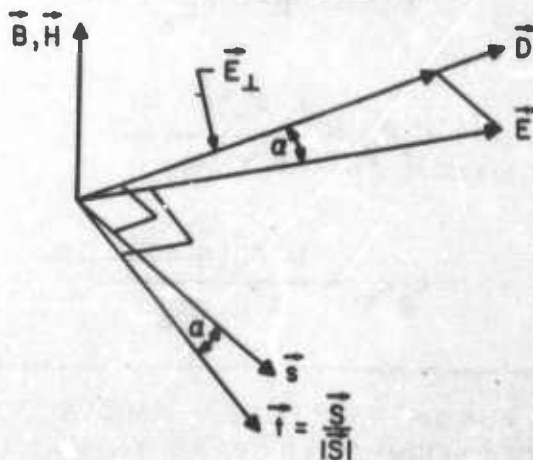
$$\vec{D} = \frac{n^2}{\mu} \left[\vec{E} - \vec{s}(\vec{s} \cdot \vec{E}) \right] = \frac{n^2}{\mu} \vec{E}_\perp \quad (2.3)$$

where \vec{E}_\perp is the component of \vec{E} along the direction of \vec{D} and can be written:

$$\vec{E}_\perp = \left(\vec{E} \cdot \frac{\vec{D}}{|\vec{D}|} \right) \frac{\vec{D}}{|\vec{D}|} \quad (2.4)$$

It is seen from Eq. (2.1) that \vec{H} (and \vec{B}) are at right angles to \vec{s} , \vec{E} and \vec{D} ; hence \vec{s} , \vec{E} and \vec{D} are co-planar. Further, since the vector $\vec{H} \times \vec{s}$ is in the direction of propagation of \vec{D} , then \vec{s} is collinear with $\vec{D} \times \vec{H}$.

Consider the following sketch:



It was seen in the preceding section that, in an anisotropic medium, \vec{D} and \vec{E} are, in general, not collinear. Let the angle between \vec{D} and \vec{E} be denoted by α . The Poynting vector, $\vec{S} = \frac{c}{4\pi} \vec{E} \times \vec{H}$, defines the direction of flow of energy, which is denoted by the unit ray vector $\vec{t} = \frac{\vec{S}}{|\vec{S}|}$. Thus, in anisotropic media there are, in general, two sets of orthogonal vector triplets; \vec{D} , \vec{H} and \vec{s} , and \vec{E} , \vec{H} and \vec{t} . The angle between \vec{t} and \vec{s} is equal to that between \vec{D} and \vec{E} . Hence the direction of the unit wave normal and the direction of energy flow will, in general, not be the same.

A-3 FRESNEL'S FORMULAE FOR PROPAGATION OF LIGHT IN CRYSTALS

It will now be seen that any plane wave incident on an anisotropic medium will be split into two separate linearly polarized waves, each with its own phase velocity.

In a coordinate system coincident with the principal dielectric axes, Eq. (2.3) may be written:

$$\mu\epsilon_k E_k = n^2 \left[E_k - s_k (\vec{s} \cdot \vec{E}) \right] \quad k = x, y, z \quad (3.1)$$

then

$$s_x E_x = \frac{n^2 s_x^2 (\vec{s} \cdot \vec{E})}{n^2 - \mu\epsilon_x}$$

$$s_y E_y = \frac{n^2 s_y^2 (\vec{s} \cdot \vec{E})}{n^2 - \mu\epsilon_y}$$

$$s_z E_z = \frac{n^2 s_z^2 (\vec{s} \cdot \vec{E})}{n^2 - \mu\epsilon_z}$$

Adding the three equations and dividing both sides by $(\vec{s} \cdot \vec{E})$ yields:

$$\frac{s_x^2}{n^2 - \mu\epsilon_x} + \frac{s_y^2}{n^2 - \mu\epsilon_y} + \frac{s_z^2}{n^2 - \mu\epsilon_z} = \frac{1}{n^2}$$

After some algebraic manipulation (i.e., multiply both sides by n^2 , then subtract $s_x^2 + s_y^2 + s_z^2 = 1$ from both sides) this equation may be expressed as:

$$\frac{s_x^2}{\frac{1}{n^2} - \frac{1}{\mu\epsilon_x}} + \frac{s_y^2}{\frac{1}{n^2} - \frac{1}{\mu\epsilon_y}} + \frac{s_z^2}{\frac{1}{n^2} - \frac{1}{\mu\epsilon_z}} = 0 \quad (3.2)$$

The three principal velocities of propagation, related to the three principal dielectric constants, are defined as:

$$v_x = \frac{c}{\sqrt{\mu\epsilon_x}}, \quad v_y = \frac{c}{\sqrt{\mu\epsilon_y}}, \quad v_z = \frac{c}{\sqrt{\mu\epsilon_z}}$$

where

c = speed of light

Recall that the phase velocity is given by: $v_p = \frac{c}{n}$ then Eqs. (3.1) become:

$$E_k = \frac{\frac{1}{v_p^2}}{\frac{1}{v_p^2} - \frac{1}{v_k^2}} s_k (\vec{s} \cdot \vec{E}) \quad k = x, y, z \quad (3.3)$$

and Eq. (3.2) becomes:

$$\frac{s_x^2}{v_p^2 - v_x^2} + \frac{s_y^2}{v_p^2 - v_y^2} + \frac{s_z^2}{v_p^2 - v_z^2} = 0$$

V_x , V_y and V_z are constants depending on the physical constants: ϵ_x , ϵ_y , ϵ_z and μ , of the medium. Hence, for every direction \vec{s} , the above expression becomes a quadratic equation yielding two solutions for the variable V_p^2 . For each value of V_p^2 there are two values, $\pm V_p$. However, $-V_p$ evidently corresponds to the direction $-\vec{s}$, and only two separate values, V_p' and V_p'' , are actually obtained. These values of V_p may now be used in Eqs. (3.3) to obtain the ratios $E_x:E_y:E_z$. It is seen that these ratios are real. Therefore the quantities E_x , E_y and E_z , which in general are complex, and which are the x , y and z components of the vector which describes the direction of vibration of \vec{E} , are all in phase. Thus the light must be linearly polarized.

To summarize, it is seen that an electrically anisotropic medium permits two monochromatic plane waves, with two different phase velocities, and two different linear polarizations, to propagate in any given direction. It will be seen in the next section that these directions of polarization are mutually perpendicular.

A-4 EXACT DETERMINATION OF VELOCITIES OF PROPAGATION AND DIRECTIONS OF POLARIZATION BY GEOMETRICAL CONSTRUCTION

An ellipsoid given by:

$$\frac{x^2}{\epsilon_x} + \frac{y^2}{\epsilon_y} + \frac{z^2}{\epsilon_z} = 1$$

referred to as the ellipsoid of wave normals (Born and Wolf 1964), may be obtained from Eq. (1.1). x , y and z refer to the principal dielectric axes. A procedure for determining the two phase velocities V_p' and V_p'' , and the directions of polarization for an electromagnetic wave with arbitrary direction of propagation is given in the next section.

trary unit wave normal \vec{s} , can be defined in terms of the ellipsoid of wave normals. It is as follows: construct a plane through the origin perpendicular to \vec{s} . The intersection of this plane with the ellipsoid of wave normals will be an ellipse, \mathcal{E} . The directions of polarization for the two waves will lie along the directions of the major and minor axes of \mathcal{E} , and the velocities of propagation for these two waves will be inversely proportional to the lengths of these semi-major and minor axes. More precisely, if the lengths of the semi-major and semi-minor axes are r' and r'' , then the indices of refraction, n' and n'' , for light which is linearly polarized along these axes will be given by:
 $r' = \frac{n'}{\sqrt{\mu}}$, $r'' = \frac{n''}{\sqrt{\mu}}$. This will now be shown.

By Eq. (1.1), the components of the vector \vec{D} , for a given energy density $w = 2w_e$, satisfy the relationship:

$$\frac{D_x^2}{\epsilon_x} + \frac{D_y^2}{\epsilon_y} + \frac{D_z^2}{\epsilon_z} = 8\pi w_e = K$$

make the change of variables:

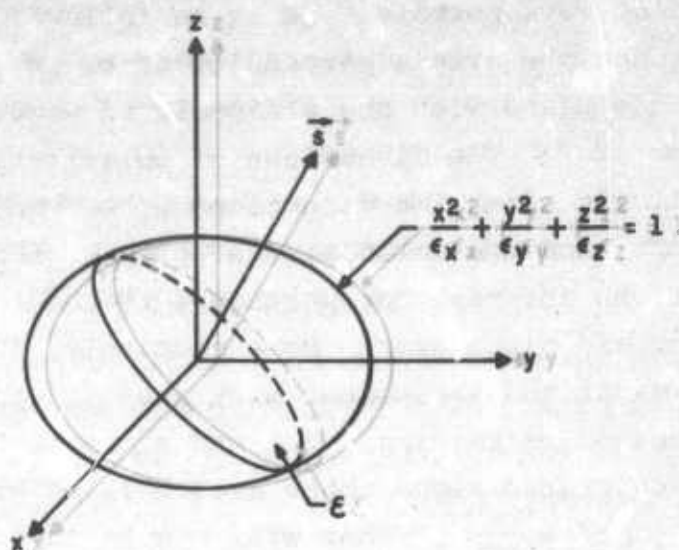
$$x = \frac{D_x}{\sqrt{K}}, \quad y = \frac{D_y}{\sqrt{K}}, \quad z = \frac{D_z}{\sqrt{K}}$$

As a result we obtain the ellipsoid of wave normals:

$$\frac{x^2}{\epsilon_x} + \frac{y^2}{\epsilon_y} + \frac{z^2}{\epsilon_z} = 1$$

whose semi-axes are equal to the square roots of the principal dielectric constants.

Consider the following sketch:



\vec{s} denotes the unit wave normal of a plane wave propagating through the medium. The plane through the origin perpendicular to \vec{s} is the locus of points $\vec{r} = x\vec{i} + y\vec{j} + z\vec{k}$ such that $\vec{r} \cdot \vec{s} = 0$. The intersection of this plane with the ellipsoid of wave normals is an ellipse, \mathcal{E} .

It is evident that of all the points on the intersection of the plane $\vec{r} \cdot \vec{s}$ with the ellipsoid of wave normals, the end points of the major and minor semi-axes of \mathcal{E} are, respectively, farthest from and closest to the origin. Hence finding the semi-axes of \mathcal{E} is equivalent to finding the extrema of $r^2 = x^2 + y^2 + z^2$, with the constraints:

$$\vec{r} \cdot \vec{s} = xs_x + ys_y + zs_z = 0 \quad (4.1)$$

and

$$\frac{x^2}{\epsilon_x} + \frac{y^2}{\epsilon_y} + \frac{z^2}{\epsilon_z} = 1 \quad (4.2)$$

These extrema may be found by the method of La-Grange's multipliers. It involves finding the extrema of:

$$F = x^2 + y^2 + z^2 + 2\lambda_1(xs_x + ys_y + zs_z) + \lambda_2\left(\frac{x^2}{\epsilon_x} + \frac{y^2}{\epsilon_y} + \frac{z^2}{\epsilon_z} - 1\right)$$

where $2\lambda_1$, and λ_2 are undetermined multipliers.

The extrema of F are points at which the partial derivatives of F with respect to x , y and z all vanish. Hence these extrema must have coordinates x, y and z such that:

$$\begin{aligned} x + \lambda_1 s_x + \lambda_2 \frac{x}{\epsilon_x} &= 0, & y + \lambda_1 s_y + \lambda_2 \frac{y}{\epsilon_y} &= 0, \\ z + \lambda_1 s_z + \lambda_2 \frac{z}{\epsilon_z} &= 0 \end{aligned} \quad (4.3)$$

Because of the constraints (Eqs. (4.1) and (4.2)), multiplying these expressions by x , y and z , respectively, and adding gives:

$$r^2 + \lambda_2 = 0$$

Next multiply each expression by s_x , s_y and s_z , respectively, and add. We then obtain, because of Eq. (4.1):

$$\lambda_1 + \lambda_2 \left(\frac{xs_x}{\epsilon_x} + \frac{ys_y}{\epsilon_y} + \frac{zs_z}{\epsilon_z} \right) = 0$$

Finally, by direct substitution of λ_1 and λ_2 into Eq. (4.3) we have:

$$x \left(1 - \frac{r^2}{\epsilon_x} \right) + s_x r^2 \left(\frac{xs_x}{\epsilon_x} + \frac{ys_y}{\epsilon_y} + \frac{zs_z}{\epsilon_z} \right) = 0 \quad (4.4)$$

and two more similar expressions for y and z .

Thus there are three homogeneous equations in terms of the variables x , y and z . A nontrivial solution will exist only if the determinant vanishes; a condition which gives an algebraic expression for r^2 and the extrema may be obtained.

To obtain the desired results recall that, with respect to the principal axes:

$$x = \frac{D_x}{\sqrt{K}}, \quad D_x = \epsilon_x E_y$$

and by Eqs. (2.3) and (2.4):

$$r^2 = x^2 + y^2 + z^2 = \frac{|D|^2}{K} = \frac{|D|^2}{8\pi w_e} = \frac{|D|^2}{\vec{E} \cdot \vec{D}} = \frac{n^2}{\mu}$$

then Eq. (4.4) becomes:

$$\frac{D_x}{\sqrt{K}} \left(1 - \frac{n^2}{\mu \epsilon_x} \right) + \frac{s_x n^2}{\mu \sqrt{K}} (\vec{s} \cdot \vec{E}) = 0$$

and

$$\mu D_k = n^2 [E_k - s_k (\vec{s} \cdot \vec{E})] \quad k = x, y, z \quad (4.5)$$

It is seen, therefore, that the two roots of r from the determinantal equation defined by (4.4), and which are the lengths of the semi-major and minor axes of \mathcal{E} , determine the two values of V_p and n , since:

$$r' = \frac{n'}{\sqrt{\mu}} = \frac{c}{V_p' \sqrt{\mu}}, \quad \text{and} \quad r'' = \frac{n''}{\sqrt{\mu}} = \frac{c}{V_p'' \sqrt{\mu}}$$

Further, note that Eqs. (4.5), which are equivalent to Eq. (4.4), are identical to Eqs. (3.1) from which it was originally shown that two values of phase velocity V_p will oc-

cur. Therefore, the two sets of solutions of Eq. (4.4), say (x', y', z') and (x'', y'', z'') , which determine the coordinate of the major and minor semi-axes of \hat{C} , equivalently determine two vectors $\vec{D}' = (D'_x, D'_y, D'_z)$ and $\vec{D}'' = (D''_x, D''_y, D''_z)$ which must also lie along the major and minor axes of \hat{C} . Thus the directions of polarization and the corresponding velocities are completely determined by the orientation and lengths of the semi-major and minor axes.

APPENDIX B

THE PHOTOELASTIC MATRIX FOR AMORPHOUS MEDIA

B-1 CUBIC SYSTEM

The photoelastic matrix for an amorphous medium will be determined by first considering a cubic system. In a cubic system the three principal axes are mutually equivalent and the three principal dielectric constants are therefore equal. Thus the ellipsoid of wave normals degenerates to a sphere given by:

$$\frac{x^2}{\epsilon} + \frac{y^2}{\epsilon} + \frac{z^2}{\epsilon} = 1$$

where

$$\epsilon_x = \epsilon_y = \epsilon_z = \epsilon$$

When the medium is subjected to a set of stresses and strains the ellipsoid of wave normals becomes (Coker and Filon 1957, Mueller 1938):

$a_{xx}x^2 + a_{yy}y^2 + a_{zz}z^2 + 2a_{yz}yz + 2a_{xz}xz + 2a_{xy}xy = 1$,
and the a_{ij} 's are obtained from Eq. (4.2-2) in Ch. 4 which is written in matrix form as:

$$\bar{a} = P\bar{s}$$

where

$$\bar{a} = \begin{bmatrix} a_{xx} - \frac{1}{\epsilon} \\ a_{yy} - \frac{1}{\epsilon} \\ a_{zz} - \frac{1}{\epsilon} \\ a_{yz} \\ a_{xz} \\ a_{xy} \end{bmatrix}, \quad \bar{s} = \begin{bmatrix} s_{xx} \\ s_{yy} \\ s_{zz} \\ s_{yz} \\ s_{xz} \\ s_{xy} \end{bmatrix}, \quad P = [p_{ij}]$$

Now consider a new set of principal axes, x' , y' , and z' , obtained by reversing some of the original coordinate directions (i.e., $x' = -x$, $y' = -y$, and $z' = z$, etc.). Because of the equivalence of the principal directions the P matrix must be invariant under any such transformation of coordinates and:

$$\bar{a}' = P\bar{S}'$$

where the elements of the tensors,

$$\begin{bmatrix} a'_{xx} & a'_{xy} & a'_{xz} \\ a'_{xy} & a'_{yy} & a'_{yz} \\ a'_{xz} & a'_{yz} & a'_{zz} \end{bmatrix}$$

and

$$\begin{bmatrix} s'_{xx} & \frac{s'_{xy}}{2} & \frac{s'_{xz}}{2} \\ \frac{s'_{xy}}{2} & s'_{yy} & \frac{s'_{yz}}{2} \\ \frac{s'_{xz}}{2} & \frac{s'_{yz}}{2} & s'_{zz} \end{bmatrix}$$

are obtained from the quantities in the unprimed system by the laws of tensor transformation.* In cases of coordinate transformations of the form: $x' = -x$, $y' = -y$, and $z' = z$, however, the primed quantities can be written down by inspection, i.e.,

* The (x,y) component of shear strain is defined as $s_{xy} = s_{yx}$. When the strain components are represented tensor form, however, it is necessary to include the factor of $\frac{1}{2}$ in the off-diagonal terms (Sokolnikoff 1956).

$$\bar{a}' = \begin{bmatrix} a'_{xx} - \frac{1}{\epsilon} \\ a'_{yy} - \frac{1}{\epsilon} \\ a'_{zz} - \frac{1}{\epsilon} \\ a'_{yz} \\ a'_{xz} \\ a'_{xy} \end{bmatrix} = M\bar{a}, \text{ where } M = \begin{bmatrix} 1 & 0 & 0 & 0 & 0 & 0 \\ 0 & 1 & 0 & 0 & 0 & 0 \\ 0 & 0 & 1 & 0 & 0 & 0 \\ 0 & 0 & 0 & -1 & 0 & 0 \\ 0 & 0 & 0 & 0 & -1 & 0 \\ 0 & 0 & 0 & 0 & 0 & 1 \end{bmatrix}$$

The S_{ij} 's will have the same transformation matrix and:

$$\bar{a}' = P\bar{s}' = M\bar{a} = PM\bar{s}.$$

but since

$$\bar{a} = P\bar{s},$$

then

$$M\bar{a} = MP\bar{s}.$$

Thus

$$MP\bar{s} = PM\bar{s}; \quad (MP - PM)\bar{s} = 0 \quad \text{for all } \bar{s},$$

and therefore $MP = PM$ for all such transformations of principal axes. It will now be seen that successive applications of this rule for various transformations will result in the P matrix of the form as shown in Sec. 4.2 of Ch. 4.

For the above

$$MP = \begin{bmatrix} . & . & . & p_{14} & p_{15} & . \\ . & . & . & p_{24} & p_{25} & . \\ . & . & . & p_{34} & p_{35} & . \\ -p_{41} & -p_{42} & -p_{43} & -p_{44} & -p_{45} & -p_{46} \\ -p_{51} & -p_{52} & -p_{53} & -p_{54} & -p_{55} & -p_{56} \\ . & . & . & p_{64} & p_{65} & . \end{bmatrix} = PM$$

$$PM = \begin{bmatrix} \cdot & \cdot & \cdot & -p_{14} & -p_{15} & \cdot \\ \cdot & \cdot & \cdot & -p_{24} & -p_{25} & \cdot \\ \cdot & \cdot & \cdot & -p_{34} & -p_{35} & \cdot \\ p_{41} & p_{42} & p_{43} & -p_{44} & -p_{45} & p_{46} \\ p_{51} & p_{52} & p_{53} & -p_{54} & -p_{55} & p_{56} \\ \cdot & \cdot & \cdot & -p_{64} & -p_{65} & \cdot \end{bmatrix}$$

hence

$$p_{14} = -p_{14} \Rightarrow p_{14} = 0 \quad \text{etc.}$$

Next consider the transformation: $x' = x$, $y' = -y$, $z' = -z$, for which

$$M = \begin{bmatrix} 1 & 0 & 0 & 0 & 0 & 0 \\ 0 & 1 & 0 & 0 & 0 & 0 \\ 0 & 0 & 1 & 0 & 0 & 0 \\ 0 & 0 & 0 & 1 & 0 & 0 \\ 0 & 0 & 0 & 0 & -1 & 0 \\ 0 & 0 & 0 & 0 & 0 & -1 \end{bmatrix}$$

and:

$$\begin{bmatrix} \cdot & \cdot & \cdot & \cdot & 0 & p_{16} \\ \cdot & \cdot & \cdot & \cdot & 0 & p_{26} \\ \cdot & \cdot & \cdot & \cdot & 0 & p_{36} \\ \cdot & \cdot & \cdot & \cdot & p_{45} & 0 \\ 0 & 0 & 0 & -p_{54} & -p_{55} & 0 \\ -p_{61} & -p_{62} & -p_{63} & 0 & 0 & -p_{66} \end{bmatrix} =$$

$$= \begin{bmatrix} \cdot & \cdot & \cdot & \cdot & \cdot & -p_{16} \\ \cdot & \cdot & \cdot & \cdot & \cdot & -p_{26} \\ \cdot & \cdot & \cdot & \cdot & \cdot & -p_{36} \\ \cdot & \cdot & \cdot & \cdot & -p_{45} & 0 \\ 0 & 0 & 0 & p_{54} & -p_{55} & 0 \\ p_{61} & p_{62} & p_{63} & 0 & 0 & -p_{66} \end{bmatrix}$$

Hence, thus far:

$$P = \begin{bmatrix} p_{11} & p_{12} & p_{13} & 0 & 0 & 0 \\ p_{21} & p_{22} & p_{23} & 0 & 0 & 0 \\ p_{31} & p_{32} & p_{33} & 0 & 0 & 0 \\ 0 & 0 & 0 & p_{44} & 0 & 0 \\ 0 & 0 & 0 & 0 & p_{55} & 0 \\ 0 & 0 & 0 & 0 & 0 & p_{66} \end{bmatrix}$$

In order to obtain symmetry, consider the permutation $x' = z$, $y' = x$, $z' = y$ for which

$$M = \begin{bmatrix} 0 & 0 & 1 & 0 & 0 & 0 \\ 1 & 0 & 0 & 0 & 0 & 0 \\ 0 & 1 & 0 & 0 & 0 & 0 \\ 0 & 0 & 0 & 0 & 0 & 1 \\ 0 & 0 & 0 & 1 & 0 & 0 \\ 0 & 0 & 0 & 0 & 1 & 0 \end{bmatrix}$$

thus

$$\begin{bmatrix} p_{31} & p_{32} & p_{33} & 0 & 0 & 0 \\ p_{11} & p_{12} & p_{13} & 0 & 0 & 0 \\ p_{21} & p_{22} & p_{23} & 0 & 0 & 0 \\ 0 & 0 & 0 & 0 & 0 & p_{66} \\ 0 & 0 & 0 & p_{44} & 0 & 0 \\ 0 & 0 & 0 & 0 & p_{55} & 0 \end{bmatrix} =$$

$$\begin{bmatrix} p_{12} & p_{13} & p_{11} & 0 & 0 & 0 \\ p_{22} & p_{23} & p_{21} & 0 & 0 & 0 \\ p_{32} & p_{33} & p_{31} & 0 & 0 & 0 \\ 0 & 0 & 0 & 0 & 0 & p_{44} \\ 0 & 0 & 0 & p_{55} & 0 & 0 \\ 0 & 0 & 0 & 0 & p_{66} & 0 \end{bmatrix}$$

and

$$P = \begin{bmatrix} p_{11} & p_{12} & p_{13} & 0 & 0 & 0 \\ p_{13} & p_{11} & p_{12} & 0 & 0 & 0 \\ p_{12} & p_{13} & p_{11} & 0 & 0 & 0 \\ 0 & 0 & 0 & p_{44} & 0 & 0 \\ 0 & 0 & 0 & 0 & p_{44} & 0 \\ 0 & 0 & 0 & 0 & 0 & p_{44} \end{bmatrix}$$

Finally, if $x' = y$, $y' = x$, $z' = z$, then

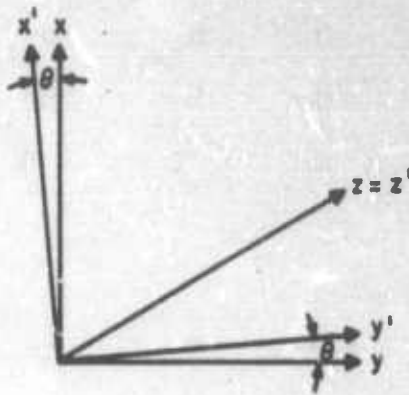
$$M = \begin{bmatrix} 0 & 1 & 0 & 0 & 0 & 0 \\ 1 & 0 & 0 & 0 & 0 & 0 \\ 0 & 0 & 1 & 0 & 0 & 0 \\ 0 & 0 & 0 & 0 & 1 & 0 \\ 0 & 0 & 0 & 1 & 0 & 0 \\ 0 & 0 & 0 & 0 & 0 & 1 \end{bmatrix}$$

from which $p_{13} = p_{12}$.

B-2 AMORPHOUS MEDIA

For the cubic system all transformations of the principal axes involved 90 deg or 180 deg rotations. In the case of an amorphous medium the P matrix must be invariant for all angles of rotation. This rule could have been

applied immediately, but is simpler to apply at this stage since many of the p_{ij} 's have vanished. Consider the following sketch:



If

$$x' = b_{11}x + b_{12}y$$

$$y' = b_{21}x + b_{22}y$$

$$z' = z$$

where

$$b_{11} = b_{22} = \cos \theta$$

$$b_{21} = -b_{12} = \sin \theta$$

then, by the rule of transformation of tensors,

$$a'_{ij} = \sum_k \sum_l b_{ik} b_{jl} a_{kl} \quad i, j, k, l = 1, 2, 3$$

where

$$x \rightarrow 1, \quad y \rightarrow 2, \quad z \rightarrow 3$$

Using this rule it is seen that:

$$\bar{a}' = \begin{bmatrix} b_{11}^2 & b_{12}^2 & 0 & 0 & 0 & 2b_{11}b_{12} \\ b_{21}^2 & b_{22}^2 & 0 & 0 & 0 & 2b_{22}b_{21} \\ 0 & 0 & 1 & 0 & 0 & 0 \\ 0 & 0 & 0 & b_{22} & b_{21} & 0 \\ 0 & 0 & 0 & b_{12} & b_{11} & 0 \\ b_{11}b_{21} & b_{12}b_{22} & 0 & 0 & 0 & (b_{11}^2 - b_{12}^2) \end{bmatrix} \quad \bar{a} = M_1 \bar{a}$$

and

$$\bar{s}' = \begin{bmatrix} b_{11}^2 & b_{12}^2 & 0 & 0 & 0 & b_{11}b_{12} \\ b_{21}^2 & b_{22}^2 & 0 & 0 & 0 & b_{21}b_{22} \\ 0 & 0 & 1 & 0 & 0 & 0 \\ 0 & 0 & 0 & b_{22} & b_{21} & 0 \\ 0 & 0 & 0 & b_{12} & b_{11} & 0 \\ 2b_{11}b_{21} & 2b_{12}b_{22} & 0 & 0 & 0 & (b_{11}^2 - b_{12}^2) \end{bmatrix} \quad \bar{s} = M_2 \bar{s}$$

Note that the factor of $\frac{1}{2}$ in the formulation of the strain tensor has modified this transformation somewhat. In this case, $M_1 P = P M_2$; hence the elements of:

$$\begin{bmatrix} b_{11}^2 p_{11} + b_{12}^2 p_{12} & b_{11}^2 p_{12} + b_{12}^2 p_{11} & p_{12} & 0 & 0 & 2b_{11}b_{12}p_{44} \\ b_{21}^2 p_{11} + b_{22}^2 p_{12} & b_{21}^2 p_{12} + b_{22}^2 p_{11} & p_{12} & 0 & 0 & 2b_{22}b_{21}p_{44} \\ p_{12} & p_{12} & p_{11} & 0 & 0 & 0 \\ 0 & 0 & 0 & b_{22}p_{44} & b_{21}p_{44} & 0 \\ 0 & 0 & 0 & b_{12}p_{44} & b_{11}p_{44} & 0 \\ b_{11}b_{21}p_{11} + b_{12}b_{22}p_{12} & b_{11}b_{21}p_{12} + b_{12}b_{22}p_{11} & 0 & 0 & 0 & (b_{11}^2 - b_{12}^2)p_{44} \end{bmatrix}$$

COLUMBIA UNIVERSITY—ELECTRONICS RESEARCH LABORATORIES

are equal to those of:

$$\left[\begin{array}{cc|cc|c|c|c|c|c} b_{11}^2 p_{11} + b_{21}^2 p_{12} & b_{12}^2 p_{11} + b_{22}^2 p_{12} & p_{12} & 0 & 0 & b_{11} b_{12} p_{11} + b_{21} b_{22} p_{12} \\ b_{11}^2 p_{12} + b_{21}^2 p_{11} & b_{12}^2 p_{12} + b_{22}^2 p_{11} & p_{12} & 0 & 0 & b_{11} b_{12} p_{12} + b_{21} b_{22} p_{11} \\ p_{12} & p_{12} & p_{11} & 0 & 0 & 0 \\ 0 & 0 & 0 & b_{22} p_{44} & b_{21} p_{44} & 0 \\ 0 & 0 & 0 & b_{12} p_{44} & b_{11} p_{44} & 0 \\ 2b_{11} b_{21} p_{44} & 2b_{12} b_{22} p_{44} & 0 & 0 & 0 & (b_{11}^2 - b_{12}^2) p_{44} \end{array} \right]$$

and since $b_{11} = b_{22}$, $b_{12} = -b_{21}$, then $p_{44} = \frac{p_{11} - p_{12}}{2}$.

APPENDIX CDETERMINATION OF $R(u,v)$; BAND-LIMITED CASE

Using white noise as an example it has been shown in Sec. 6.4.1 that the output light intensity, in the band-limited case, is given by:

$$R(u,v) = Z^2(v) NKW_0 D^2 \int_{-\frac{B_s}{2}}^{\frac{B_s}{2}} \left[\frac{\sin \pi D(\lambda - \phi)}{\pi D(\lambda - \phi)} \right]^2 d\lambda$$

The value of the integral is equal to the shaded area in Fig. 6.4.1-1. It is seen that this value is a function of $\phi = u - f_0$ which specifies the position of the main lobe of

$$\left[\frac{\sin \pi D(\lambda - \phi)}{\pi D(\lambda - \phi)} \right]^2.$$

It is convenient for computation to express ϕ as:

$$\phi = \frac{k B_s}{2} \quad k = \text{constant}$$

Thus for $k=0$ the main lobe will fall at the center of the integration region. The integral is an even function of k , and as $|k|$ varies from 0 to 1 the main lobe travels towards the edge of the region; for $|k| > 1$ the main lobe falls outside, etc. Hence letting $x = D(\lambda - \phi)$:

$$\int_{-\frac{B_s}{2}}^{\frac{B_s}{2}} \left[\frac{\sin \pi D(\lambda - \phi)}{\pi D(\lambda - \phi)} \right]^2 d\lambda = \frac{1}{D} \int_{D(-\frac{B_s}{2} - \phi)}^{D(\frac{B_s}{2} - \phi)} \left(\frac{\sin \pi x}{\pi x} \right)^2 dx = \frac{1}{D} \int_{\frac{B_s}{2}(-1-k)}^{\frac{B_s}{2}(1-k)} \left(\frac{\sin \pi x}{\pi x} \right)^2 dx$$

and since, as is shown in Sec. 6.4.1, $DB_g = M$, then:

$$R(u,v) = Z^2(v)NKW_0 D \int_{\frac{M}{2}(-1-k)}^{\frac{M}{2}(1-k)} \left(\frac{\sin \pi x}{\pi x} \right)^2 dx$$

The results of evaluating the integral (denoted as \mathcal{J}) on a computer, for various values of M and k , are shown below:

$M = 2$		$M = 5$	
$ k $	\mathcal{J}	$ k $	\mathcal{J}
0.00	.9028	0.00	.9591
.25	.8991	.25	.9580
.50	.8523	.50	.9417
.75	.7072	.75	.9316
1.00	.4749	$1 - \frac{2}{5}$.9387
1.20	.3527	1.00	.4898
1.40	.2617	$1 + \frac{3}{5}$.0401
etc.		$1 + \frac{4}{5}$.0266
		etc.	

COLUMBIA UNIVERSITY—ELECTRONICS RESEARCH LABORATORIES

M = 10

$ k $	J
0.00	.9797
.25	.9787
.50	.9728
.75	.9490
$1 - \frac{1}{10}$.9457
1.00	.4949
$1 + \frac{2}{10}$.0439
$1 + \frac{3}{10}$.0300
etc.	

M = 50

$ k $	J
0.00	.9959
.25	.9956
.50	.9945
.75	.9905
$1 - \frac{2}{50}$.9503
1.00	.4989
$1 + \frac{2}{50}$.0475
$1 + \frac{3}{50}$.0334
etc.	

M = 100

$ k $	J
0.00	.9979
.25	.9978
.50	.9972
.75	.9953
$1 - \frac{2}{100}$.9509
1.00	.4994
$1 + \frac{2}{100}$.0480
$1 + \frac{3}{100}$.0339
etc.	

For $M = 2$ the width of the main lobe exactly fills the integration region. Thus the value of J for $k = 0$ shows that approximately 90 per cent of the area under $(\frac{\sin \pi x}{\pi x})^2$ falls under the main lobe and, in this case, $|k|$ cannot vary too far from zero before a relatively large portion of the integrand will fall outside the region $|\phi| < \frac{B_s}{2}$. As M becomes larger, however, it is seen that the range of values of $|k| < 1$ for which J remains approximately constant will increase. Since $\phi = \frac{kB_s}{2}$, then $|k| = 1 - \frac{2}{M}$ ($M > 2$) places the peak of the integrand one half of a main-lobe-width inside the integration region, and is the largest value of $|k|$ for which the main lobe falls entirely inside $|\phi| < \frac{B_s}{2}$. For convenience, values of $|k| > 1$ were expressed as $k = (1 + \frac{n}{M})$ $n = 2, 3, 4, \dots$, where n gives the number of half main-lobe widths that the peak of the integrand is outside the region $|\phi| < \frac{B_s}{2}$. Thus it is seen from Fig. C-1 that, for $M > 10$, the integral will be approximately constant when $|k| < 1$ and, as a result, band-limited white noise can be assumed to cause a uniform intensity over the observation region:

$$f_o - \frac{B_s}{2} \leq u \leq f_o + \frac{B_s}{2}$$

and a negligible contribution outside this range of values.

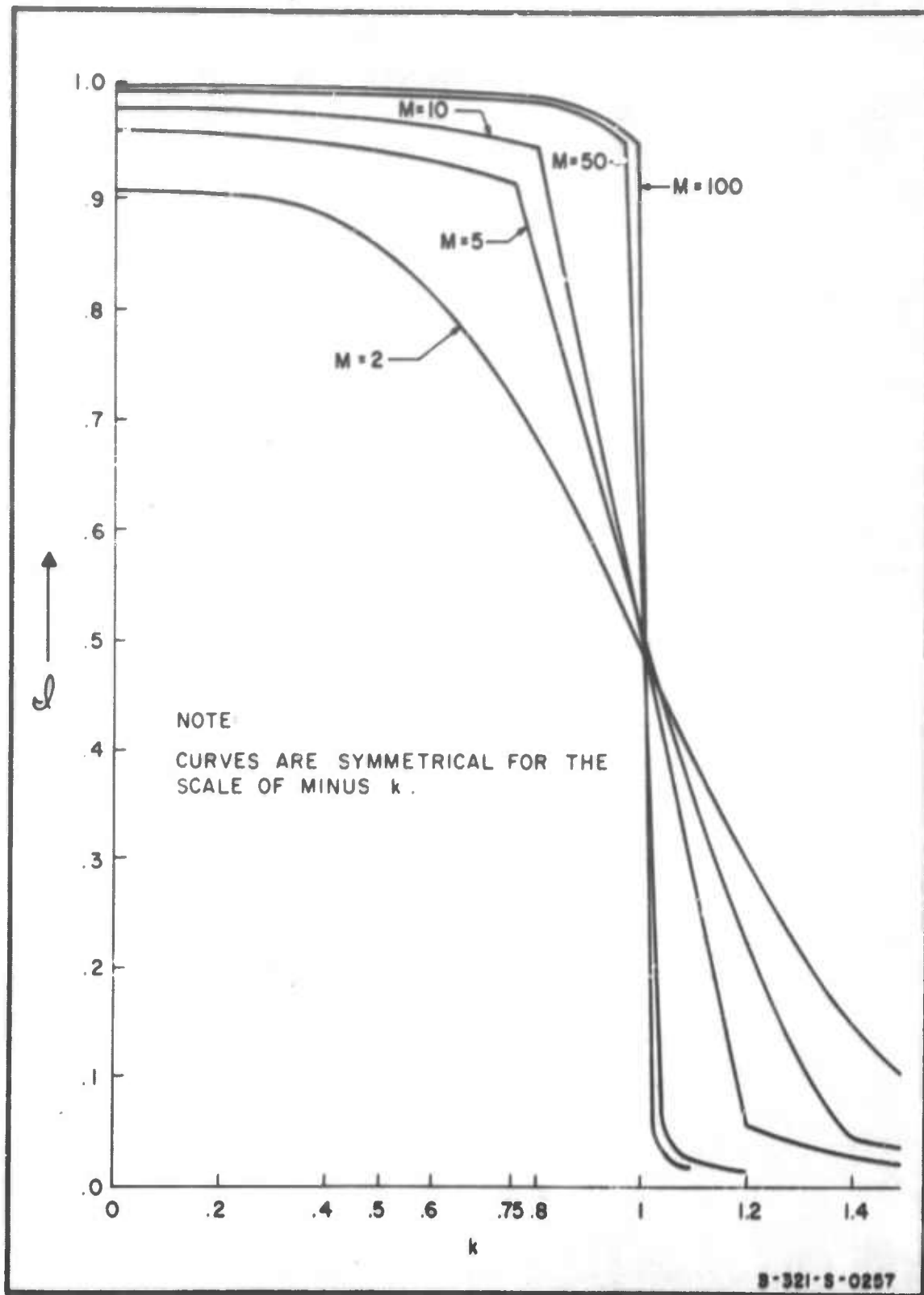


FIG. C-1 VALUES OF Q AS A FUNCTION OF M AND k

APPENDIX DOPTIMIZATION OF DESIGN OF FUSED-SILICA LIGHT MODULATOR:SUMMARY OF RESULTS

This appendix presents a summary of the results of Chap. 5. As before, it is assumed that the electro-optical processor is to be applied to a square planar array antenna.

It has been shown that signal processing capacity is a function of the operating frequency, the sonic velocity, and the size of the optical aperture. With regard to the latter, the nature of the spatial-multiplexing and time-multiplexing processes cause the width of the aperture, rather than its length, to be the limiting dimension. This was shown in Chap. 5 in which the maximum aperture width was assumed to be 6 in., and for which, in each case which was considered, the required aperture length was less than 1 cm. Thus the expressions relevant to this discussion may be expressed in the following form (Eqs. 5.1-3, 5.1-5 and 5.3-1):

$$N = \frac{W^{2/3}}{2} \frac{f_i^{2/3}}{S^{2/3}} \quad (D-1)$$

$$P = \frac{W^{4/3}}{8} \frac{f_i^{7/3}}{S^{4/3}} \quad (D-2)$$

where:

N = number of elements in each row
(and column) of the array

S = sonic velocity

f_1 = frequency of electrical signal
exciting ultrasonic transducers

W = width of optical aperture

Recall that in the derivation of these expressions the bandwidth, B , has been assumed to be given by:

$$B = \frac{f_1}{2} \quad (D-3)$$

Equations (D-1) and (D-2) are plotted in Figs. D-1 and D-2. It is seen that, because of the difference in sonic velocities, if the value of $f_1|_{\max}$ were the same for both modes, then the shear mode would be optimal. As is shown in Secs. 5.3 and 5.4 however, the high frequency capability of the compression mode more than compensates for its greater sonic velocity and, in fact, the compression mode is optimal. This is also shown in Figs. D-1 and D-2. Note that in case (I) the maximum value of N for the shear mode is slightly larger than it is for the compression mode, and in case (II) the two quantities are equal. Thus the optimality of the compression mode arises from the greater bandwidths which are possible rather than from the maximum possible antenna size.

Other important parameters are the dimensions of the ultrasonic transducer. The transducer width does not directly affect processing capacity but must be physically realizable. This dimension is given by:

$$b = \frac{W}{2N}$$

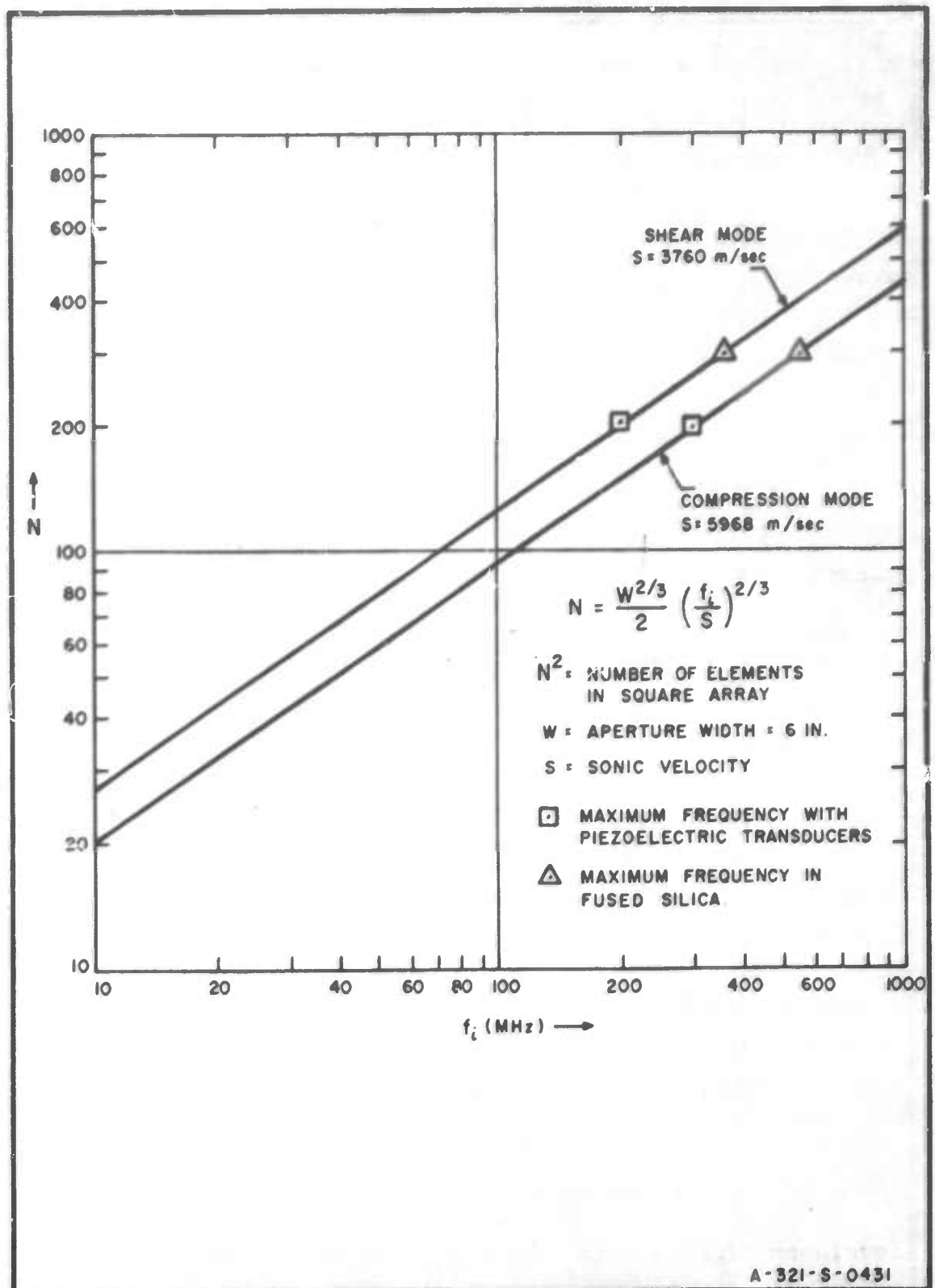


FIG. D-1 NUMBER OF ANTENNA ELEMENTS IN ROW (OR COLUMN) OF SQUARE ARRAY vs. FREQUENCY FOR SHEAR AND COMPRESSION MODES : FUSED-SILICA LIGHT MODULATOR.

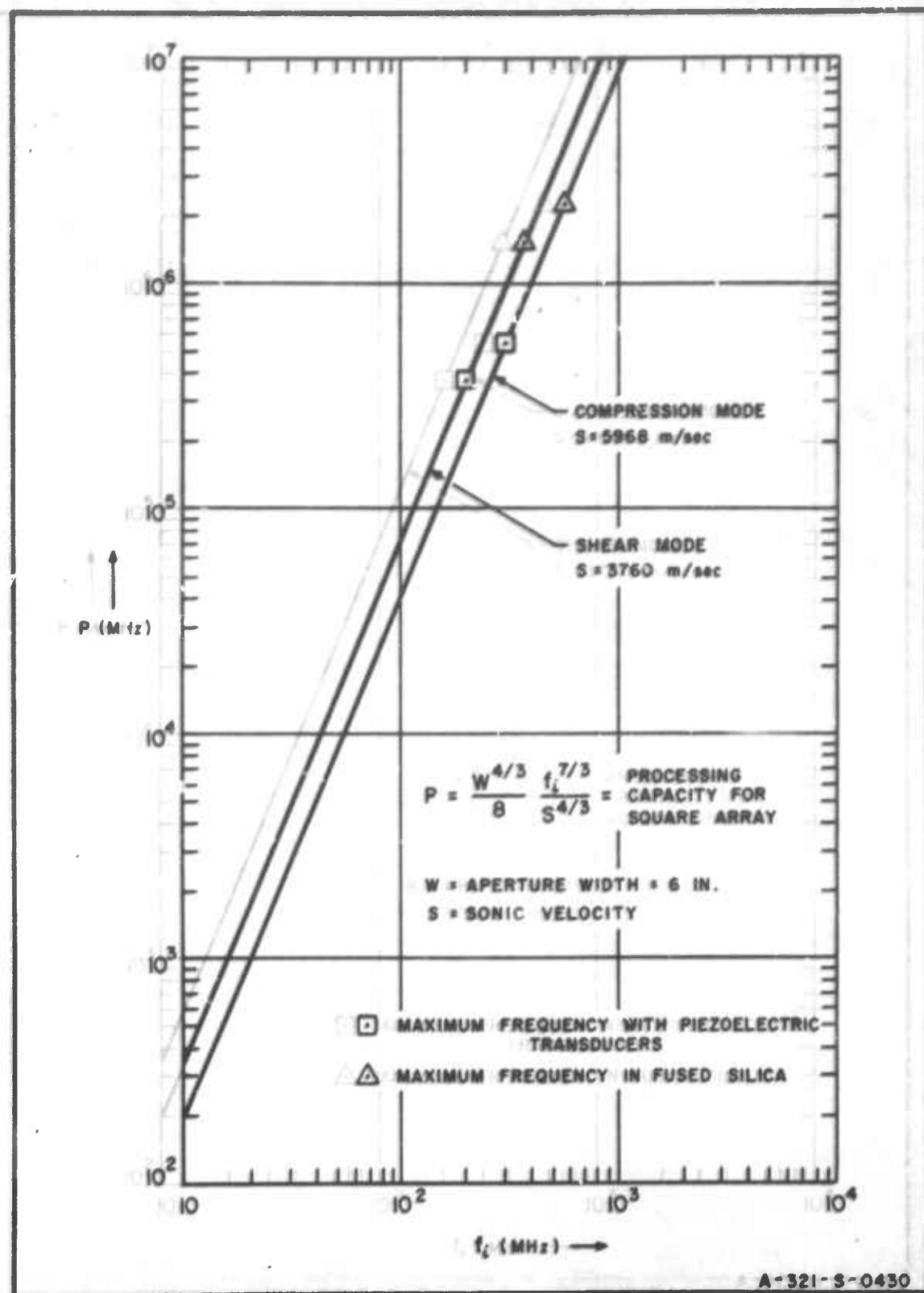


FIG. D-2 PROCESSING CAPACITY vs. FREQUENCY FOR SHEAR AND COMPRESSION MODES: FUSED-SILICA LIGHT MODULATOR

The transducer depth, L , has been shown to have an effect on the operating frequency because of internal refraction. That is, the first order light amplitude will be attenuated by the factor:

$$\frac{\sin \gamma}{\gamma}$$

where

$$\gamma = \frac{\pi \lambda f_i^2}{2n_o S^2} L$$

and consequently, in order to avoid excessive attenuation, a restriction is imposed on the product $f_i^2 L$.

It has been shown in Sec. 5.2.2 however, that the smallest value of L which would be necessary is given by:

$$L_{\text{opt}} = \frac{n_o S^2}{\lambda f_i^2} \quad (\text{D-4})$$

Figures D-3 and D-4 present plots of γ vs L for both shear and compression modes, with f_i as a parameter, according to the relationship:

$$\gamma = \frac{\pi \lambda f_i^2}{2n_o S^2} L \quad (\text{D-5})$$

The nominal values of the constants have been assumed to be:

$$n_o = 1.46$$

$$\lambda = 6328 \times 10^{-10} \text{ m}$$

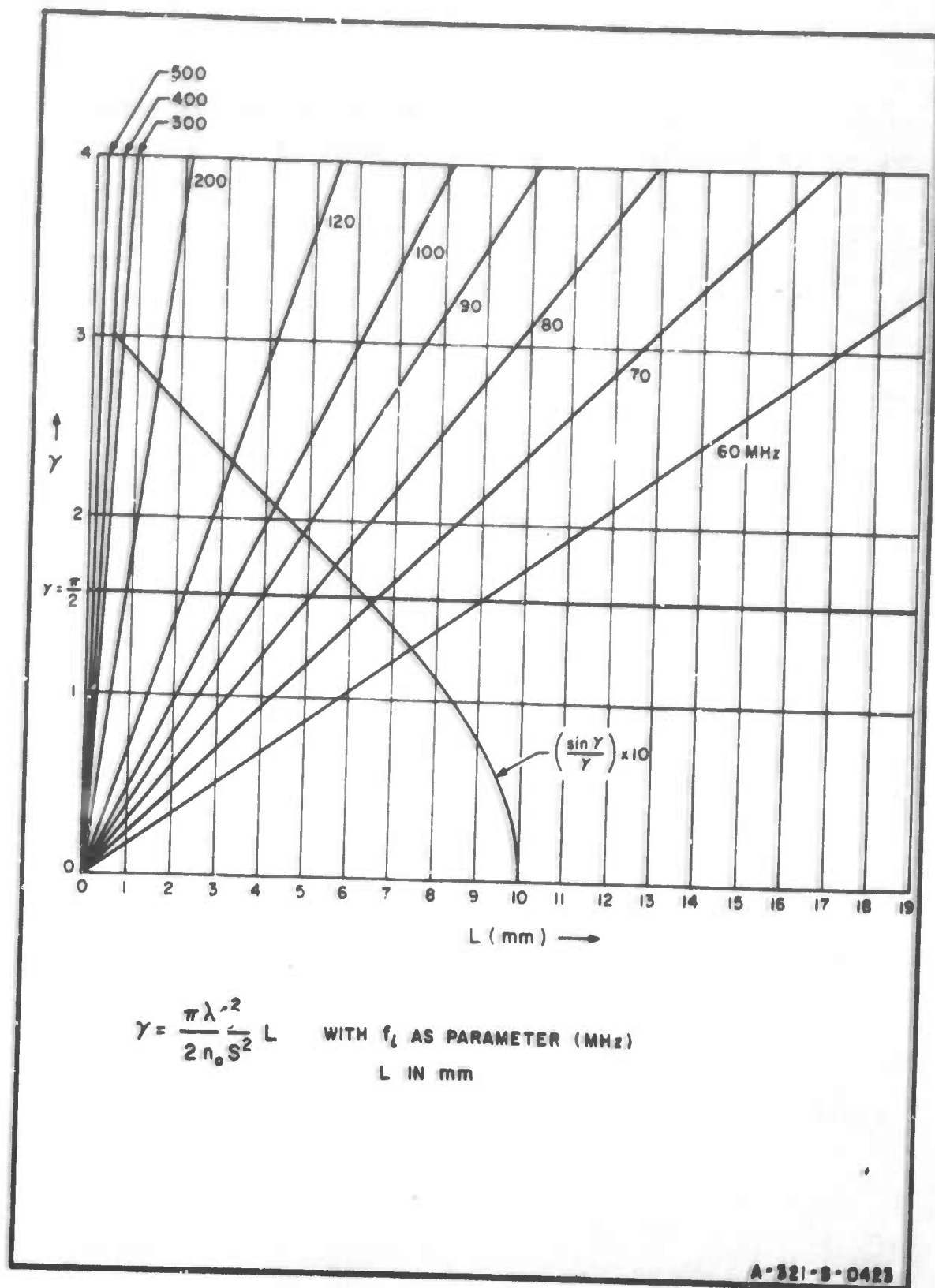
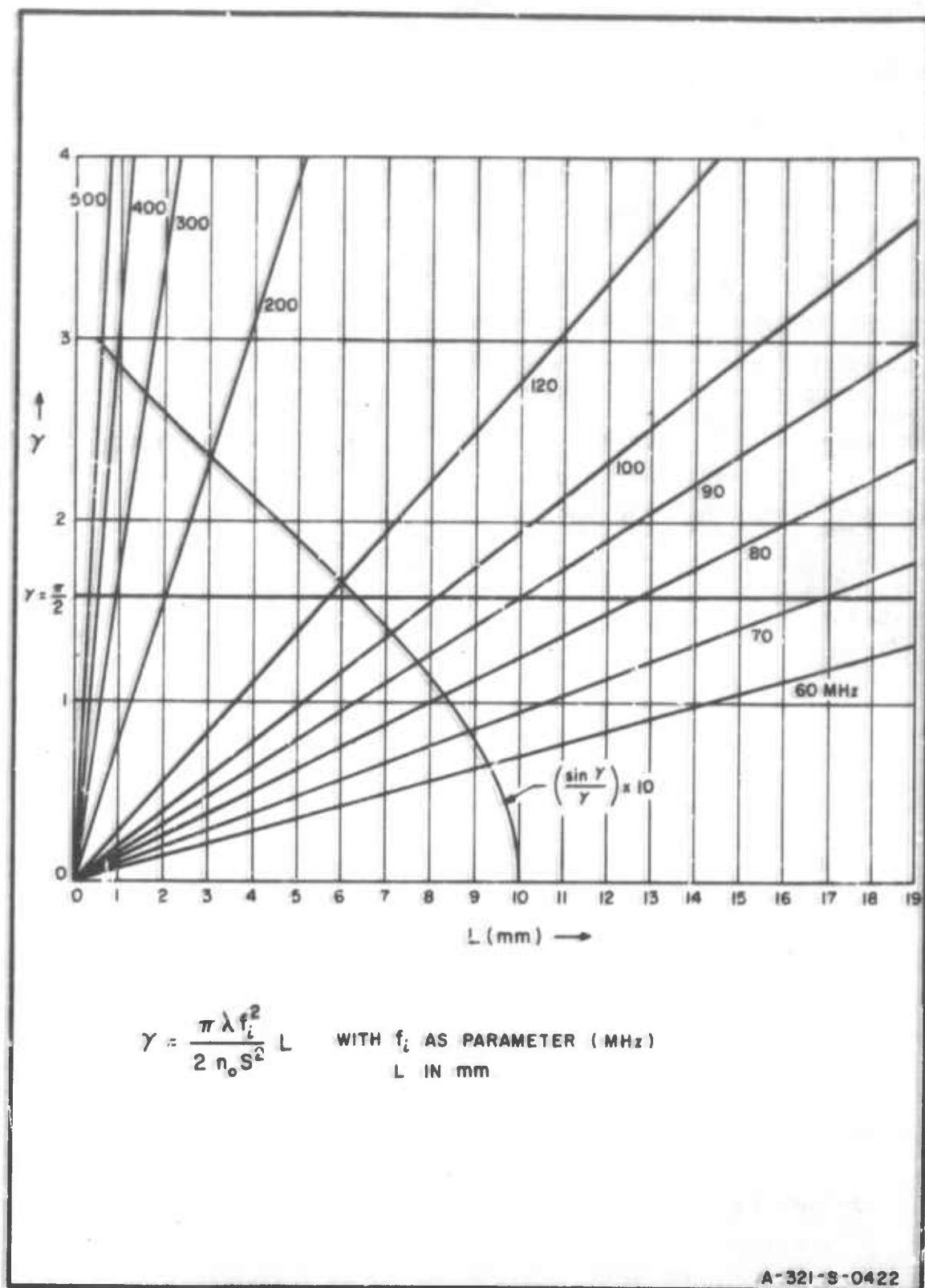


FIG. D-3 TRANSDUCER DEPTH (L) vs. γ FOR SHEAR MODE

FIG. D-4 TRANSDUCER DEPTH (L) vs. γ FOR COMPRESSION MODE

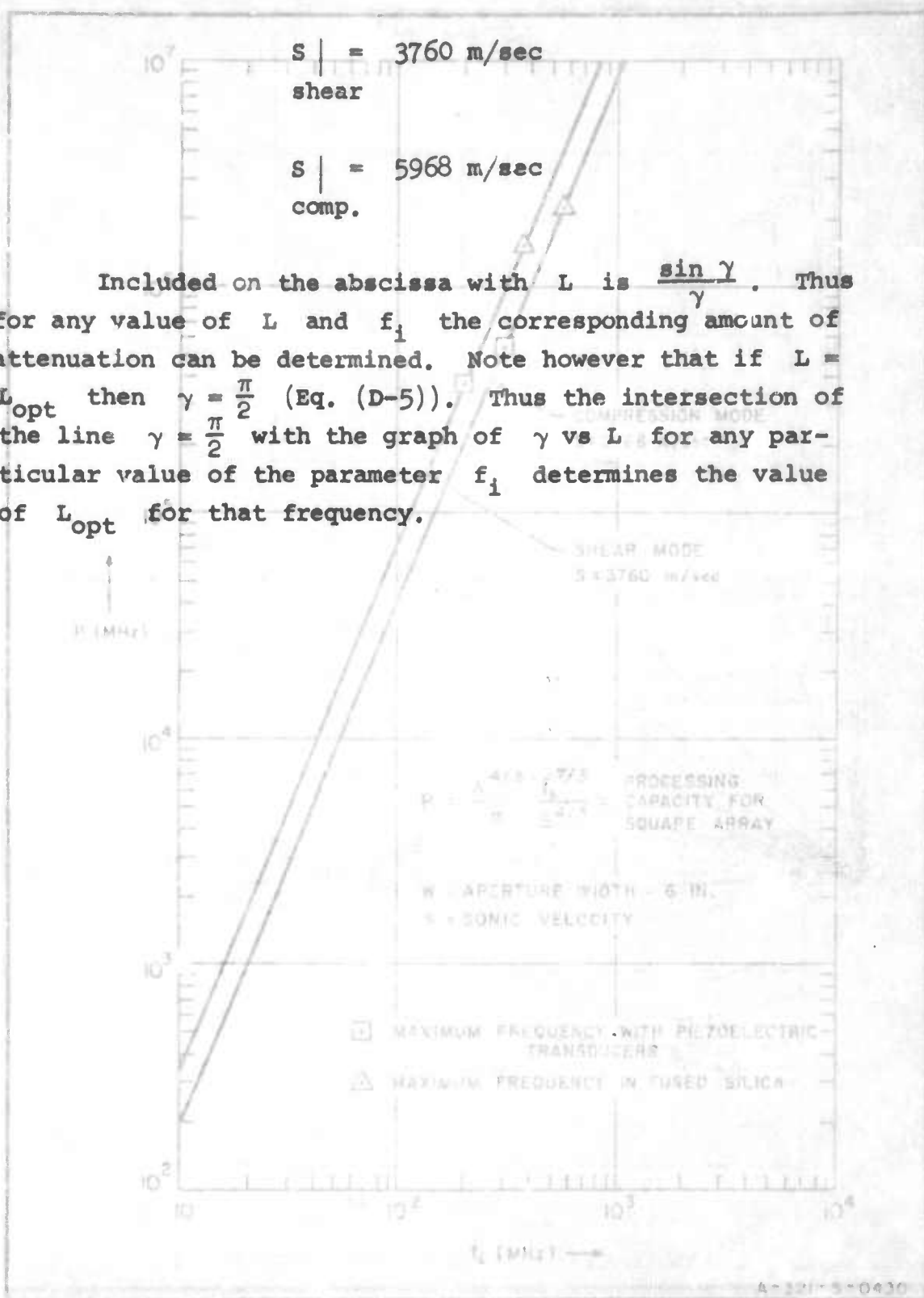


FIG D-2 PROCESSING CAPACITY vs. FREQUENCY FOR SHEAR AND COMPRESSION MODES FUSED-SILICA LIGHT MODULATOR.

REFERENCES

- Allen, J. L., "Phased Array Studies July 1, 1959 to July 1, 1960," MIT Tech. Report No. 228, pp. 147-232.
- Allen, J. L., "Array Radars - A Survey of Their Potential and Their Limitations," Microwave Journal, May, 1962.
- Allen, J. L., "Array Antennas - New Applications for an Old Technique," IEEE Spectrum, p. 115, November 1964.
- Allen, J. L., "Phased Arrays - There is a Future," Microwave Journal, June 1965.
- Arm, M., Konig, W., Lambert, L. and Weissman, I., "Two-Dimensional Filtering," Progress Report P-2/179, July, 1962, Confidential, Columbia University Electronics Research Laboratories, New York, New York.
- Bhagavantam, S. and Rao, B. R., Nature 158,484 (1946); 159,267 (1947); 161,927 (1948).
- Bhatia, A. B., Noble, W. J., "Diffraction of Light by Ultrasonic Waves," I: General Theory; Proc. Royal Soc. A 200, 356-368, December 8, 1953; II: Approximate Expressions for the Intensities and Comparison with Experiment; A 200, 369-385, December 8, 1953 (Also see Ch. 12 of text by Born and Wolf).
- Born, M., and Wolf, E., Principles of Optics, Pergamon, New York, 1965.
- Cheatham, T. P. and Kohlenberg, A., "Optical Filters - Their Equivalence to and Differences from Electrical Networks," Conv. Rec. IRE Nat'l. Conv., 954.
- Coker and Filon, Photoelasticity, University Press, Cambridge, England, 1957.
- Cutrona, et al., "Optical Data Processing and Filtering Systems," IRE Trans. on Inf. Theory, Vol. IT-6, No. 3, June 1960.
- Debye, P. and Sears, F. W., "On the Scattering of Light by Supersonic Waves," Proc. Nat. Acad. of Sci., Vol. 18, No. 6, June 15, 1932, Washington, D.C.

- Foster, N. F., "Cadmium Sulphide Evaporated Layer Transducers," Bell Telephone Labs., Pre-publication Memo, 1965.
- Fox, A. G. and Li, T., "Resonant Modes in a Maser Interferometer," Bell System Tech. Journal, p. 453, March 1961.
- Freedman, A., "Sound Field of a Rectangular Piston," Jour. Acoust. Soc. Amer., Vol. 32, No. 2, p. 197, February 1962.
- Frocht, M., Photoelasticity, John Wiley, New York, 1941.
- Gopal, R., "Effect of the Attenuation of the Ultrasonic Wave on the Diffraction of Light by It," Acoustica, Vol. 13, p. 114, 1963.
- Hammond, V. J., British Communications and Electronics, pp. 104-110, February 1962.
- Hargrove, L. E., "Optical Effects of Ultrasonic Waves Producing Phase and Amplitude Modulation," Jour. Acoust. Soc. Amer., Vol. 34, No. 10, October 1962.
- Hargrove and Achyuthan, "Use of Light Diffraction in Measuring the Parameter of Non-Linearity of Liquids and the Photo-Elastic Constants of Solids," Physical Acoustics, Edited by W. Mason, Vol. 2, Part B, Academic Press, New York, 1965.
- Heidemann, E., Nature, Vol. 136, p. 337, 1935.
- Klein, W. R., Heidemann, E., "An Investigation of Light Diffracted by Wide, High Frequency Ultrasonic Beams," Physica, Vol. 29, pp. 981-986, 1963.
- de Klerk, J. and Kelly, E. F., "Vapor-Deposited Thin-Film Piezoelectric Transducers," Review of Scientific Instruments, Vol. 36, No. 4, April 1965.
- Konig, W. F., Lambert, L. B., Schilling, D. L., "The Effects of Bonding and Backing Materials on the Characteristics of Ultrasonic Delay lines," Wescon Proceedings, August 1961.
- Kraus, J. G., "Radio Telescope Antennas of Large Aperture," Proc. IRE, Vol. 46, No. 1, p. 92, January 1958.

COLUMBIA UNIVERSITY—ELECTRONICS RESEARCH LABORATORIES

- Lamb, J., Redwood, M. and Shteinshleifer, Z., "Absorption of Compressional Waves in Solids from 100 to 1000 Mc," Physical Review Letters, Vol. 3, No. 1, July 1, 1959.
- Lambert, L. B., "Wide-Band Instantaneous Spectrum Analyzer, Employing Delay-Line Light Modulators," IRE International Convention Record, Part 6, 1962.
- Lambert, L. B., "Electro-Optical Signal Processors for Array Antenna," Eng. Sc. D. Thesis, Technical Report T-1/321, May, 1965, Unclassified, Columbia University Electronics Research Laboratories, New York, New York.
- Lambert, L., Aimetie, A., Arm, A., "Electro-Optical Signal Processors for Phased Array Antennas," Optical and Electro-Optical Information Processing, Edited by J. T. Tippett, D. A. Berkowitz et al., MIT Press, Cambridge Mass., and London, England, 1965.
- Liben, W., "Some Applications of an Ultrasonic Light Modulator," Jour. Acoust. Soc. Amer., Vol. 34, No. 6, p. 860, June 1960.
- Lucas, R. and Biquard, P., "Propriétés Optiques des Milieux et Liquides Soumis aux Vibrations Élastiques Ultra Sonores," J. De Phys. Vol. 3, No. 7, 1932.
- Mason, W. P., Electro-Mechanical Transducers and Wave Filters, D. Van Nostrand and Co. Inc., Princeton, N. J., pp. 230, 413, Second Edition, 1948.
- Mason, W. P., Physical Acoustics, Principles and Methods, Vol. 1, Part A, Academic Press, New York, 1964.
- McSkimin, H. J., "Ultrasonic Pulse Technique for Measuring Acoustic Losses and Velocities of Propagation in Liquids as a Function of Temperature and Hydrostatic Pressure," Jour. Acoust. Soc. Amer., Vol. 29, No. 11, pp. 1185-1192, November 1957.
- McSkimin, H. J., "Measurement of Ultrasonic Wave Velocities for Solids in the Frequency Range 100 to 500 Mc," Jour. Acoust. Soc. Amer., Vol. 34, No. 4, p. 404, April 1962.
- Mertens, R., "On the Theory of Diffraction of Light by Supersonic Waves: Part I: Progressive Supersonic Waves," Simon Steven Vol. 27, pp. 212-230, 1949/50.

- Mueller, H., "Theory of Photoelasticity in Amorphous Solids," *Physics*, Vol. 6, No. 6, p. 179, June 1935.
- Mueller, H., "The Intensity and Polarization of the Light Diffracted by Supersonic Waves in Solids," *Physical Review*, Vol. 52, p. 223, August 1, 1937.
- Mueller, H., "Theory of Photoelasticity," *Jour. Amer. Ceramic Soc.* Vol. 21, p. 27, 1938.
- Neuman, F. E., *Abhandl. Kön. Acad. Wiss., Berlin*, Part II, pp. 1-254, 1841.
- Ogg, F., "Steerable Array Radars," *IRE Trans. on Military Electronics*, Vol. MIL-S, p. 80, April 1961.
- Parthasarathy, S. and Panchaly, M., "Ultrasonic Absorption Constant in Liquids by an Improved Optical Method," *Zeitschrift Fur Physik*, Bd. 138, pp. 635-639, 1954.
- Parthasarathy, S. and Mahendroo, P. P., "Relation Between Efficiency of Quartz Transducers and Ultrasonic Absorption Coefficients of Liquids," Parts I and II, *Zeitschrift Fur Physik*, Vol. 147, pp. 573-581, 1957.
- Payne, J. B., "Wideband, High Gain, Variable Time Delay Techniques for Array Antennas," *Proc. of Symposium on Electronically Scanned Array Techniques and Applications*, Vol. 1, p. 200, July 1964, Unclassified.
- Phariseau, P., "On the Diffraction of Light by Progressive Supersonic Waves," *Proc. Indian Acad. Sci.*, Vol. 44A, pp. 165-170, 1956.
- Phariseau, P., "Diffraction of Light by an Amplitude Modulated Ultrasonic Beam," *Physica*, Vol. 25, No. 10, pp. 917-934, October 1959.
- Primak, W. and Post, D., "Photoelastic Constants of Vitreous Silica and its Elastic Coefficient of Refractive Index," *Jour. of Applied Physics*, Vol. 30, No. 5, May 1959.
- Raman, C. V., Nath, N. S., "Diffraction of Light by High Frequency Sound Waves," *Proc. Indian Acad. Sci.*, Part I, Normal Incidence, Sec. A, Vol. 2, p. 406, 1935; Part II, Oblique Incidence, Sec. A, Vol. 2, p. 413, 1935; Part III, Time Variations, Sec. A, Vol. 3, p. 75, 1936; Part IV,

- General Periodic Wave, Sec. A, Vol. 3, p. 119, 1936;
Part V, Oblique Incidence, Sec. A, Vol. 3, p. 459, 1936;
Part VI, Oblique Incidence, Sec. A, Vol. 4, p. 222, 1936.
- Rao, B. R. and Murty, J. S., "Diffraction of Light by Weak Ultrasonic Fields," Zeit. Fur Physik, Bd. 152, p. 440, 1958.
- Richardson, E. G. and Tait, R. I., "Ratios of Specific Heat and High Frequency Viscosities in Organic Liquids Under Pressure, Derived from Ultrasonic Propagation," Philo. Mag., Ser. 8, Vol. 2, No. 16, April 1957.
- Schachter, H., Ph.D. Thesis, Brooklyn Polytech. Inst., Brooklyn, New York, 1964.
- Schaefer, C. and Bergman, L., Naturwiss, Vol. 22, p. 685, 1934.
- Schelkunoff, S. and Friis, H., Antennas: Theory and Practice, Wiley, New York, 1962.
- Schnitkin, H., "Survey of Electronically Scanned Antennas," Part I, The Microwave Journal, December 1960; Part II, The Microwave Journal, January 1961.
- Seki, H., Granato, A., Truell, R., "Diffraction Effects in the Ultrasonic Field of a Piston Source," Jour. Acoust. Soc. Amer., Vol. 28, No. 2, March 1956.
- Silver, S., Microwave Antennas, Theory and Design, MIT Rad. Lab. Series, Vol. 12, 1949.
- Sklar, J. R., "Short-Pulse Limitation of Phased Arrays," Phased Array Studies, July 1, 1960 to July 1, 1961, MIT Linc. Lab. Tech. Report No. 236, pp. 243-258.
- Skolnick, M. J., Introduction to Radar Systems, McGraw-Hill Book Co., Inc., New York, 1962.
- Sokolnikoff, I., Mathematical Theory of Elasticity, McGraw-Hill Book Co., Inc., New York, 1956.
- Vigoureux, P., Ultrasonics, John Wiley and Sons, 1951.
- Willard, G. W., "Criteria for Normal and Abnormal Ultrasonic Light Diffraction Effects," Jour. Acoust. Soc. Amer., Vol. 21, No. 2, March 19, 1949.
- Woodward, P. M., Probability and Information Theory with Applications to Radar, McGraw-Hill, 1953.

Unclassified

Security Classification

DOCUMENT CONTROL DATA - R&D

(Security classification of title, body of abstract and indexing annotation must be entered when the overall report is classified)

1. ORIGINATING ACTIVITY (Corporate author) Electronics Research Laboratories Columbia University New York, New York 10027		2a. REPORT SECURITY CLASSIFICATION Unclassified	
		2b. GROUP	
3. REPORT TITLE Wideband Amorphous-Solid Debye-Sears Light Modulators for Array-Antenna Processors			
4. DESCRIPTIVE NOTES (Type of report and inclusive dates) Technical Report			
5. AUTHOR(S) (Last name, first name, initial) J. Minkoff			
6. REPORT DATE March 1, 1967		7a. TOTAL NO. OF PAGES 285	7b. NO. OF REFS 62
8a. CONTRACT OR GRANT NO. AF 49(638)-1478		8a. ORIGINATOR'S REPORT NUMBER(S) T-7/321	
b. PROJECT NO. ARPA Order No. 279 Amend 5			
c. Project 7300-2837		8b. OTHER REPORT NO(S) (Any other numbers that may be assigned this report)	
d.			
10. AVAILABILITY/LIMITATION NOTICES (1) (2)			
11. SUPPLEMENTARY NOTES		12. SPONSORING MILITARY ACTIVITY Advanced Research Projects Agency Air Force Office of Scientific Research	
13. ABSTRACT <p>The use of fused-silica Debye-Sears light modulators in electro-optical array-antenna processing is investigated theoretically and experimentally, with the result that a significant gain in signal-processing capacity, over that which can be achieved with liquid light-modulators, is shown to be possible. It is shown that fused-silica light-modulators would enable electro-optical processors to be applied to square arrays consisting of more than 30,000 elements receiving signals with bandwidths in excess of 150 MHz.</p> <p>The operation of the fused-silica light-modulator in the neighborhood of 80 MHz is investigated. Transfer characteristics between electrical excitation and spatial modulation of light wave front are found to be linear, first-order light-intensity distributions are measured and found to be nearly ideal, and measurements of bandpass characteristics show that light-modulator bandwidths which are 50 per cent of resonant transducer frequency are easily achieved. The effects of internal refraction on the electro-optical processor are determined. For any given set of operating conditions, a unique lower bound on transducer depth is established which minimizes these effects. The effects of cross coupling on closely spaced light-modulator channels are also investigated experimentally and results are found to be consistent with evaluations of signal-processing capacity.</p>			

DD FORM 1473
1 JAN 64

Unclassified
Security Classification

UNCLASSIFIED

CONTINUATION OF ABSTRACT FOR T-7/321

Large aperture-bandwidth array-antenna processing is shown to result in non-separable optical transmission functions for which the diffraction patterns are determined here for the first time. Evaluation is also made of signal to noise degradation which would occur in this case. It is shown that this degradation would not be a limiting factor in the electro-optical processor.

14. KEY WORDS	LINK A		LINK B		LINK C	
	ROLE	WT	ROLE	WT	ROLE	WT

INSTRUCTIONS

1. ORIGINATING ACTIVITY: Enter the name and address of the contractor, subcontractor, grantee, Department of Defense activity or other organization (corporate author) issuing the report.

2a. REPORT SECURITY CLASSIFICATION: Enter the overall security classification of the report. Indicate whether "Restricted Data" is included. Marking is to be in accordance with appropriate security regulations.

2b. GROUP: Automatic downgrading is specified in DoD Directive 5200.10 and Armed Forces Industrial Manual. Enter the group number. Also, when applicable, show that optional markings have been used for Group 3 and Group 4 as authorized.

3. REPORT TITLE: Enter the complete report title in all capital letters. Titles in all cases should be unclassified. If a meaningful title cannot be selected without classification, show title classification in all capitals in parenthesis immediately following the title.

4. DESCRIPTIVE NOTES: If appropriate, enter the type of report, e.g., interim, progress, summary, annual, or final. Give the inclusive dates when a specific reporting period is covered.

5. AUTHOR(S): Enter the name(s) of author(s) as shown on or in the report. Enter last name, first name, middle initial. If military, show rank and branch of service. The name of the principal author is an absolute minimum requirement.

6. REPORT DATE: Enter the date of the report as day, month, year, or month, year. If more than one date appears on the report, use date of publication.

7a. TOTAL NUMBER OF PAGES: The total page count should follow normal pagination procedures, i.e., enter the number of pages containing information.

7b. NUMBER OF REFERENCES: Enter the total number of references cited in the report.

8a. CONTRACT OR GRANT NUMBER: If appropriate, enter the applicable number of the contract or grant under which the report was written.

8b, 8c, & 8d. PROJECT NUMBER: Enter the appropriate military department identification, such as project number, subproject number, system numbers, task number, etc.

9a. ORIGINATOR'S REPORT NUMBER(S): Enter the official report number by which the document will be identified and controlled by the originating activity. This number must be unique to this report.

9b. OTHER REPORT NUMBER(S): If the report has been assigned any other report numbers (either by the originator or by the sponsor), also enter this number(s).

10. AVAILABILITY/LIMITATION NOTICES: Enter any limitations on further dissemination of the report, other than those

imposed by security classification, using standard statements such as:

- (1) "Qualified requesters may obtain copies of this report from DDC."
- (2) "Foreign announcement and dissemination of this report by DDC is not authorized."
- (3) "U. S. Government agencies may obtain copies of this report directly from DDC. Other qualified DDC users shall request through _____."
- (4) "U. S. military agencies may obtain copies of this report directly from DDC. Other qualified users shall request through _____."
- (5) "All distribution of this report is controlled. Qualified DDC users shall request through _____."

If the report has been furnished to the Office of Technical Services, Department of Commerce, for sale to the public, indicate this fact and enter the price, if known.

11. SUPPLEMENTARY NOTES: Use for additional explanatory notes.

12. SPONSORING MILITARY ACTIVITY: Enter the name of the departmental project office or laboratory sponsoring (paying for) the research and development. Include address.

13. ABSTRACT: Enter an abstract giving a brief and factual summary of the document indicative of the report, even though it may also appear elsewhere in the body of the technical report. If additional space is required, a continuation sheet shall be attached.

It is highly desirable that the abstract of classified reports be unclassified. Each paragraph of the abstract shall end with an indication of the military security classification of the information in the paragraph, represented as (TS), (S), (C), or (U).

There is no limitation on the length of the abstract. However, the suggested length is from 150 to 225 words.

14. KEY WORDS: Key words are technically meaningful terms or short phrases that characterize a report and may be used as index entries for cataloging the report. Key words must be selected so that no security classification is required. Identifiers, such as equipment model designation, trade name, military project code name, geographic location, may be used as key words but will be followed by an indication of technical context. The assignment of links, rules, and weights is optional.